

VU Research Portal

Studies of cell identity factors reveal their role in cell differentiation, polar growth and DNA segregation

Robalino Espinosa, Jose Sebastian

2022

document version

Publisher's PDF, also known as Version of record

[Link to publication in VU Research Portal](#)

citation for published version (APA)

Robalino Espinosa, J. S. (2022). *Studies of cell identity factors reveal their role in cell differentiation, polar growth and DNA segregation*. [PhD-Thesis - Research and graduation internal, Vrije Universiteit Amsterdam].

General rights

Copyright and moral rights for the publications made accessible in the public portal are retained by the authors and/or other copyright owners and it is a condition of accessing publications that users recognise and abide by the legal requirements associated with these rights.

- Users may download and print one copy of any publication from the public portal for the purpose of private study or research.
- You may not further distribute the material or use it for any profit-making activity or commercial gain
- You may freely distribute the URL identifying the publication in the public portal ?

Take down policy

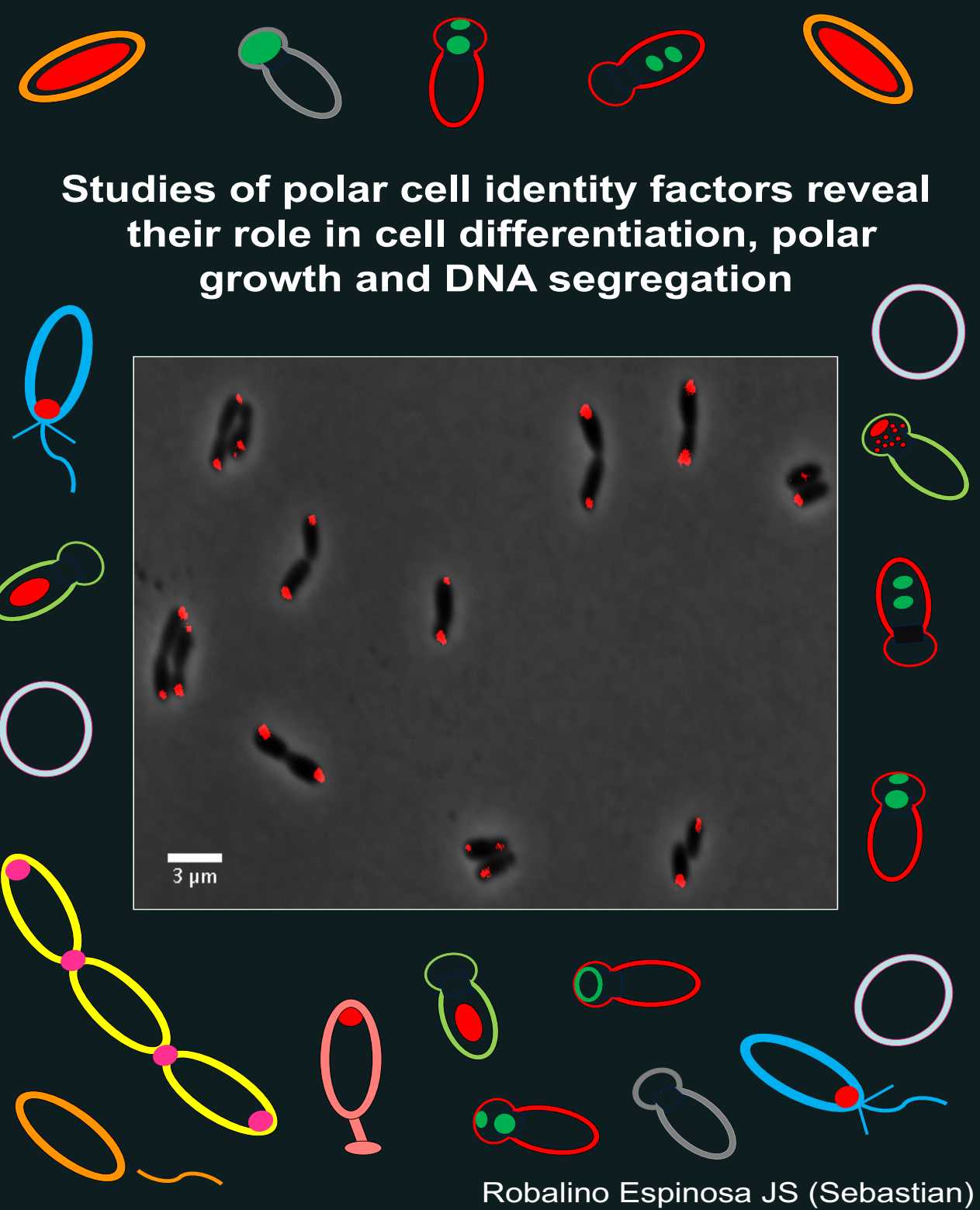
If you believe that this document breaches copyright please contact us providing details, and we will remove access to the work immediately and investigate your claim.

E-mail address:

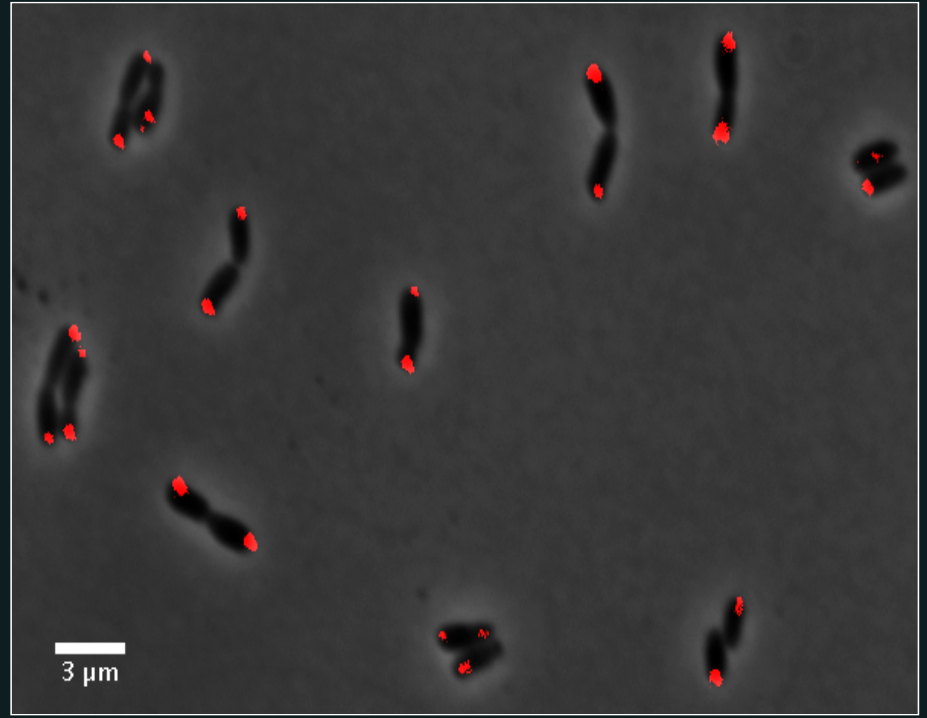
vuresearchportal.ub@vu.nl



Studies of cell identity factors reveal their role in cell differentiation, polar growth and DNA segregation



Studies of polar cell identity factors reveal their role in cell differentiation, polar growth and DNA segregation



Cover description. The ParB protein binds to sequences adjacent to the origin of replication, therefore, a fluorescent fusion to this protein make it possible to follow the dynamics of the bacterial chromosome during the cell cycle. In short cells (early in the cell cycle) the *Agrobacterium tumefaciens* ParB (fused to mCherry) is visible as a distinct focus at the old cell pole. As cell grow, two foci are visible indicating the chromosome has been replicated. One of the foci migrates across the cell to the other pole to ensure that each sibling cell has a copy of the chromosome. This image was taken using a Zeis Axio Observer microscope and was selected the image of the month at UC Berkeley. (Scale bar 3 μ m).

Image contributed by Jose Sebastian Robalino Espinosa and John Zupan of the
Zambryski lab

**Studies of polar cell identity factors
reveal their role in cell differentiation,
polar growth and DNA segregation**

Robalino Espinosa JS (Sebastian)

VRIJE UNIVERSITEIT

**STUDIES OF CELL IDENTITY FACTORS REVEAL THEIR ROLE IN CELL
DIFFERENTIATION, POLAR GROWTH AND DNA SEGREGATION**

ACADEMISCH PROEFSCHRIFT

ter verkrijging van de graad Doctor of Philosophy aan
de Vrije Universiteit Amsterdam,
op gezag van de rector magnificus
prof.dr. J.J.G. Geurts,
in het openbaar te verdedigen
ten overstaan van de promotiecommissie
van de Faculteit der Bètawetenschappen
op woensdag 16 november 2022 om 15.45 uur
in een bijeenkomst van de universiteit,
De Boelelaan 1105

door

Jose Sebastian Robalino Espinosa

geboren te Quito, Ecuador

promotoren: prof.dr. H. Lill
 prof.dr. L. Shapiro

copromotor: dr. D. Bald

promotiecommissie: prof.dr. W. Bitter
 dr. S. Luirink
 dr. D.J. Scheffers
 prof.dr. C. Baron
 dr. T.L. Lenstra

Table of contents

Chapter 1	1
General introduction	
Chapter 2	33
Studies to be continued: Subcellular distribution of the self-assembling protein PodJ is regulated by cell fate determinants in <i>Caulobacter crescentus</i> .	
Chapter 3	90
GROWTH POLE RING protein forms a 200-nm diameter ring structure essential for polar growth and rod shape in <i>Agrobacterium tumefaciens</i>	
Chapter 4	135
Segregation of four <i>Agrobacterium tumefaciens</i> replicons during polar growth: PopZ and PodJ control segregation of essential replicons	
Chapter 5	171
Studies to be continued: Cell shape dependent on GPR and PopZ is required for the subcellular distribution of ParA; and, PodJ and PopZ are required for the partitioning of the pAt replicon	
Chapter 6	196
General discussion, suggested additional experiments and future perspectives	

Chapter 1

General introduction

1

François Jacob once said “*The dream of every cell is to become two*” (1). In order to fulfil this “dream”, the cell must add growth precursors [e.g. peptidoglycan (PG) subunits] to ultimately create two compartments, that will eventually separate from each other to produce two independent sibling cells (2). To accomplish this task, bacteria developed two different ways of growing: dispersed and zonal growth (2). Dispersed growth adds growth precursors across the entire cell envelope; in contrast, zonal growth inserts the growth precursors to a specific cell area (2). Insights into the fundamental mechanisms underlying dispersed growth have come from studies on the α -proteobacterium *Caulobacter crescentus* and on the γ -proteobacterium *Escherichia coli* (3). Unlike dispersed growth, relatively little is known about the mechanisms required for zonal growth, particularly the one that allows bacteria to elongate from a single or both poles of the cell (2). The α -proteobacteria exhibit a conserved cell cycle, but their way of elongating can be either dispersed growth or zonal growth (2). In contrast to *Caulobacter*, cells belonging to Rhizobiales order, including the animal pathogen *Brucella abortus*, the nitrogen-fixing symbiont *Sinorhizobium meliloti* and the plant pathogen/genetic engineer *Agrobacterium tumefaciens*, elongate from single growth pole (GP, Fig. 1a) (2, 4). I studied cell pole identity proteins of *Caulobacter* and their homologues in *Agrobacterium*, which strikingly lacks most of the components required for dispersed growth (Supplemental table) (2, 5).

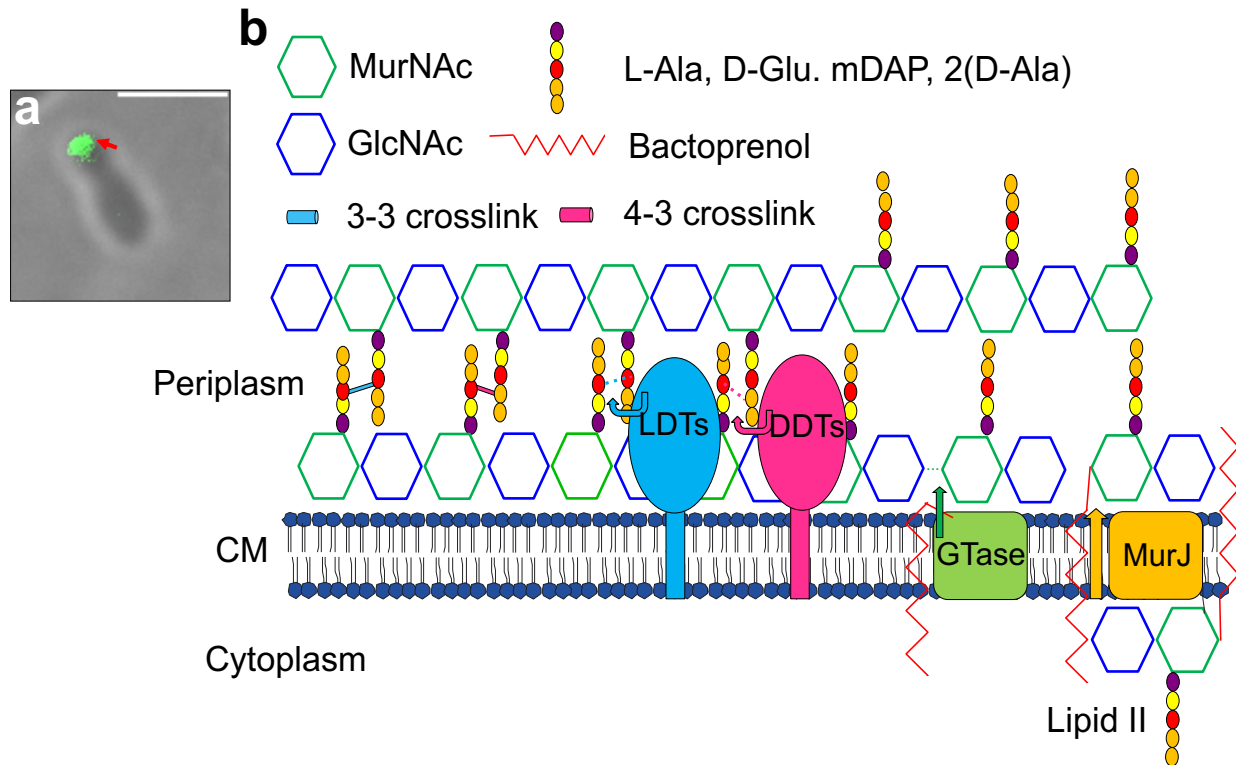


Fig 1. Peptidoglycan synthesis. (a) *Agrobacterium* elongates from the GP. New PG incorporation (read arrow) at the GP is observed after a short-pulse labeling (~5.6% of the cell cycle) with 250 μ M of nitrobenzofurazanyl-amino-D-alanine (NADA). Scale bar 2 μ m. (b) First, The flippase MurJ protein (orange square) translocases (orange arrow) lipid II from the cytoplasm to the periplasm. A GTase (green square) adds (green arrow) the disaccharide-pentapeptide from lipid II to a nascent glycan strand. Penta-peptides from the glycan strands are crosslinked to each other by LDTs (oval with a stick in blue) and DDTs (oval with a stick in magenta). LDTs and DDTs insert 3-3 cross-links (blue line) and 4-4 cross-links (magenta line), respectively. MurNAc and GlcNAc are represented with hexagons in green and blue. Amino-acids, L-Ala, D-Glu, mDAP and 2(D-Ala) are exemplified with purple, yellow, red, and orange circles. The bactoprenol tail is represented with a wavy red line. CM: cytoplasmic membrane (6-13). Figure 1b was adapted from Daitch AK and Goley ED (2020) (6).

***Agrobacterium* cell cycle.** Early in the cell cycle (Fig. 2), *Agrobacterium* secretes a unipolar polysaccharide (UPP) that mediates the attachment of the cell to a substrate (14). UPP marks the non-growing cell end, the old pole (OP, the pole that is not generated by the last cell division) (4, 14). Opposite to the OP emerges the GP displaying a diameter

30% narrower than the old cell compartment (4-5). As the cell matures, the GP proportionally increases in width and length to roughly match its parental OP cell (5). Just before cell division, the GP is converted to an inert cell end, the new OP [(N)OP] (4-5). Following the GP-to-(N)OP transition, septation produces two sibling cells, each containing a new pole (NP, generated by cell division) from where a GP emerges (Fig. 2) (4, 15).

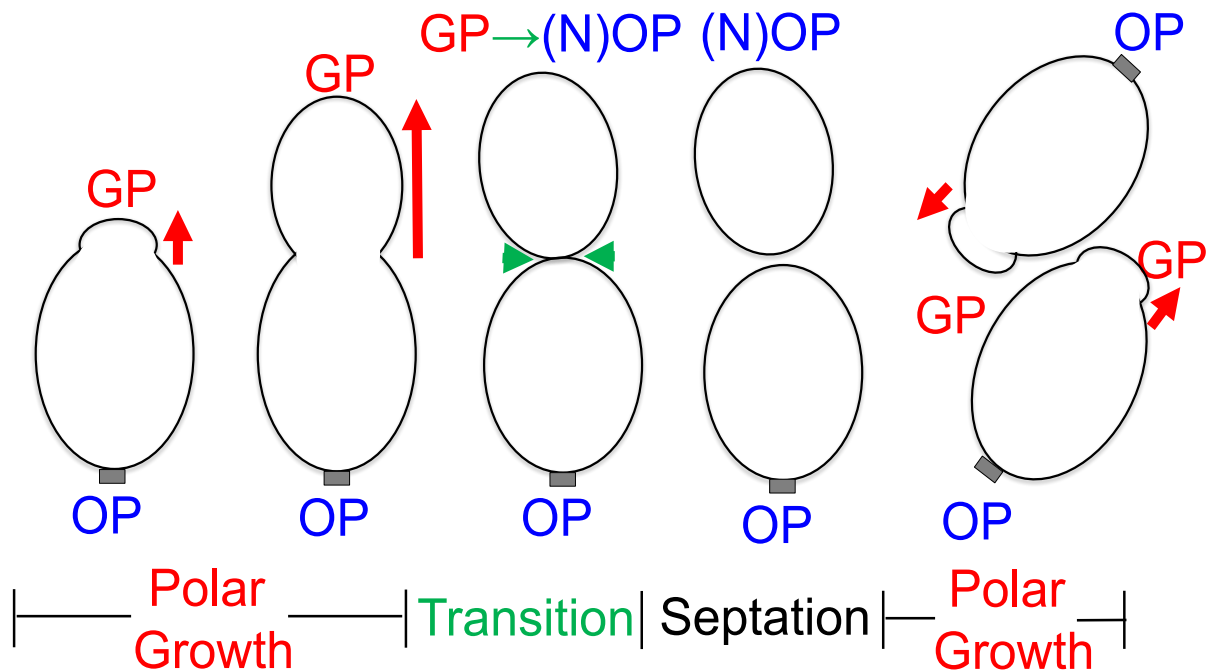


Fig. 2. Polar growth in *Agrobacterium*. First, UPP (grey square) and the GP bud are visible. The GP increases in width and length (red arrows), while the OP does not grow. When the new cell compartment reaches its final size, the GP transitions into a (N)OP (green arrow) and PG synthesis is redirected to the septation site (green arrow heads). Finally, cell division produces two sibling cells, which restart polar growth from their new poles (4-5, 12, 14-15).

Peptidoglycan synthesis. Cell growth relies to a great extent on synthesis of PG, an interconnected mesh composed of several glycan strands linked to each other by peptide bridges (Fig. 1b) (2, 3, 6). In the cytoplasm, lipid II acts as the main precursor of PG and is composed of a disaccharide, penta-peptide and bactoprenol tail (7-9). The disaccharide

contains N-acetylglucosamine (GlcNAc) and N-acetylmuramic acid (MurNAc) sugars (7-9). MurNAc is linked to the bactoprenol tail and penta-peptide, containing L-Ala, D-Glu, mDAP, and 2(D-Ala) amino-acids (aa) (7-9). The flippase MurJ protein translocates lipid II across the membrane to the periplasm, where a glycosyltransferase (GTase) links the disaccharide-pentapeptide to a nascent glycan strand through a β -(1-4) glycosidic bond (10-11). Peptides of different glycan strands are linked to each other by D,D-transpeptidases (DDTs) and L,D-transpeptidases (LDTs) that introduce D-Ala-mDAP (4-3) and mDAP-mDAP (3-3) bonds, respectively (6, 9).

The elongasome and dispersed growth. Dispersed growth in *E. coli* is mediated by the elongasome, a multiprotein complex that contains the bifunctional transglycosylase/transpeptidase PBP1a protein, several accessory proteins (MreC, MreD, RodA, RodZ, MreB) and the DD-transpeptidase PBP2 enzyme (3, 16, 17). The elongasome is organized by short filaments of the bacterial actin homolog MreB (18-19). Notably, *Agrobacterium* lacks MreB and most of the other components of the elongasome (Supplemental table), probably indicating the existence of a polar growth machinery capable to mediate PG synthesis at the GP (Fig. 1a) (5). In agreement with this hypothesis, *Agrobacterium* PG is enriched with 3-3 peptide bonds (50% in *Agrobacterium* versus 10% in *E. coli*) (4, 9). Further, the genome of *Agrobacterium* contains an unusual abundance of open reading frames (ORF) for LDTs. One these putative LDT enzymes, Atu0845 localizes at the GP with *Agrobacterium* PBP1a (5).

The divisome and zonal growth. In *E. coli*, zonal growth at the septation site is mediated by the divisome, a multiprotein complex composed by the bifunctional transglycosylase/transpeptidase PBP1b, PG-remodeling enzymes, the DD-transpeptidase PBP3, and an assortment of regulatory and structural proteins (FtsZ, FtsX, FtsE, ZipA, FtsZ, ZapA, ZapB, FtsA, FtsK, FtsL, FtsB, FtsQ, FtsW, and YhcB) (3, 16, 20-21). The genome of *Agrobacterium* encodes for PBP1b and two PBP3 proteins, PBP3a and PBP3b (Supplemental table) (5). Although PBP3b is not essential, it localizes at the septum with PBP3a (5). Therefore, it is proposed that PBP3a and PBP3b mediate PG synthesis at the septation site of *Agrobacterium* (5).

The polar organizing PopZ protein

Spatiotemporal dynamics of PopZ in *Caulobacter*. One particular protein, designated PopZ, has been identified to play a critical role on cell growth, cell differentiation and DNA segregation (22-30). PopZ is present in nearly all genera of α -proteobacteria (25, 29). However, most of the insights for PopZ function have come from research on *Caulobacter*, whose cell poles undergo to distinct changes in morphology, alternating between a swarmer flagellated cell, incapable to replicate its chromosome, to a sessile stalked cell, capable to replicate its chromosome (Fig. 3a) (25, 29, 31-32).

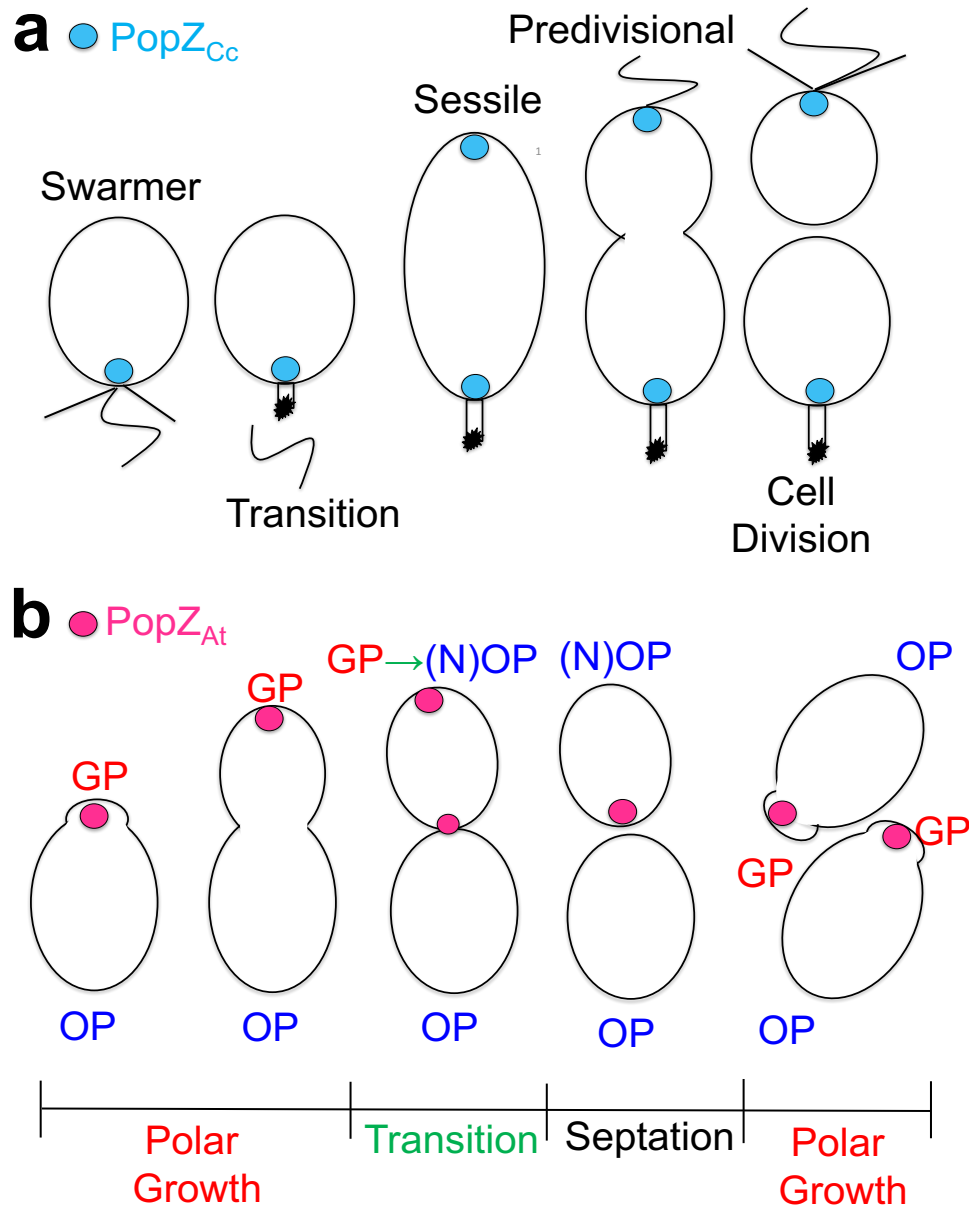


Fig. 3. Spatiotemporal dynamics of PopZ in *Caulobacter* and *Agrobacterium*. (a) Dynamic localization of PopZ_{Cc}. The swarmer cell exhibits a flagellum (wavy line) and pili (straight lines) to a single pole. PopZ_{Cc} (blue circle) is at flagellated pole. During swarmer-to-stalked cell transition, the flagellum and pili are replaced by a stalk (white rectangle) with holdfast material at its distal tip (black star). PopZ_{Cc} remains at the stalked pole for the rest of the cell cycle and accumulates to the new pole. A flagellum appears opposite to the stalk. Asymmetric cell division generates two different sibling cells. In the swarmer sibling cell, PopZ_{Cc} localizes at the flagellated pole, and in the sessile sibling cell, PopZ_{Cc} localizes at the stalked pole. (b) Dynamic localization of PopZ_{At}. PopZ_{At} (magenta circle) is at the GP. During GP-to-(N)OP transition (green arrow) PopZ is mobilized from the (N)OP to the nascent GP of the upper cell at the septation site. Just after septation, PopZ is synthesized and localized to the new GP of the lower sibling cell (25, 29, 31, 33).

During the cell cycle, *Caulobacter* PopZ (PopZ_{CC}) exhibits a dynamic spatial and temporal localization pattern (25,29). In the swarmer cell, PopZ_{CC} localizes to the flagellated pole, whereas in the sessile cell, PopZ_{CC} relocates to both poles of the cell (Fig. 3a) (25, 29, 31-32, 34).

Function of *Caulobacter* PopZ. PopZ_{CC} forms polar micro-domain that interacts with cell fate factors and DNA binding proteins (25-26, 28-29, 35-37). In the swarmer cell, PopZ_{CC} tethers the 4.02-Mbp chromosome to the flagellated pole by directly interacting with ParB, that in turn binds to the *parS* sequence near the origin of replication (25, 38-39). During swarmer-to-stalked cell transition, the PopZ_{CC}-ParB interaction disappears, PopZ_{CC} recruits the scaffolding SpmX protein to the incipient stalked pole, and SpmX activates the cell signaling DivJ protein, leading to the degradation of the master regulator, CtrA (26, 29, 40-41). After DNA replication, one copy of the chromosome remains at the stalked pole, while the other is guided and tethered to the new pole by the DNA binding ParA protein and PopZ_{CC}, respectively (25, 29, 42-43).

Function of *Agrobacterium* PopZ. How does PopZ function in bacteria with multipartite genomes and different in growth modes? The 5.67-Mbp genome of *Agrobacterium* encodes for a single homologue of PopZ_{CC} (Supplemental table) and is distributed into four replicons: circular chromosome (CC, 2.8 Mbp), secondary linear chromosome (LC, 2.0, Mbp), cryptic plasmid (pAt, 0.5 Mbp), and tumor inducing plasmid (pTi, 0.2 Mbp) (22-23, 33, 44-45). A study carried out before it was known that *Agrobacterium* undergoes polar growth, determined that the CC, LC, and pAT replicons exhibit a unipolar and bipolar

localization pattern in short (early in the cell cycle) and longer (later in the cell cycle) cells respectively, whereas the pTi replicon shows a subpolar localization pattern in either short or longer cells (46). A more recent report determined that early in the cell cycle, the CC resides at the OP, and after replication, one copy of the CC migrates to the GP (22).

Agrobacterium PopZ (PopZ_{At}) exhibits an opposite spatial and temporal localization pattern compared to *Caulobacter* (Fig. 3 a-b) (22, 25, 29, 33). PopZ_{At} marks the GP in the cell cycle and, during OP-to-(N)OP transition and cell septation, relocates from the (N)OP to the nascent GP bud of the daughter cell (22, 33). After cell division, *de novo* synthesized PopZ_{At} localizes to the new GP of the mother cell (Fig. 3b) (22, 33). In agreement with this localization pattern, PopZ_{At} was shown to be required for CC partitioning and polar growth (22-24). Indeed, in the absence of PopZ_{At}, the CC is not tethered to the GP and multiple ectopic GPs are produced in the cell (22-24).

Function of *Brucella* PopZ. The 3.3-Mbp genome of *Brucella* encodes for a single homologue of PopZ_{Cc} and is organized into two replicons: chromosome I (ChrI, 2.1 Mbp) and chromosome II (ChrII, 1.2 Mbp) (47-49). In short cells, ChrI and ChrII localize at the OP and between the OP and mid cell, respectively, whereas in longer cells, ChrI exhibits a bipolar localization pattern and ChrII localize near the poles (47). Whether *Brucella* PopZ (PopZ_{Ba}) is required to tether the ChrI and ChrII is unknown. However, PopZ_{Ba} marks the “new pole” (47), suggesting a role for PopZ_{Ba} on chromosome segregation and polar growth.

Mechanisms to localize PopZ. How is the localization of PopZ orchestrated within the cell? Overproduction of PopZ_{Cc} suggests that subcellular accumulation of PopZ_{Cc} occurs by a self-assembling mechanism (29, 36). In agreement with this observation, purified PopZ_{Cc} forms a large oligomeric complex capable to assemble further into filament-like structures (25, 29). A related question is, what localizes PopZ_{Cc} to the new cell pole? Accumulation PopZ_{Cc} at the new pole occurs by several mechanisms that dependent on ParA, PodJ, ZitP and TipN (34, 36, 50-51).

Domain organization of PopZ. How is the structure of PopZ related to its localization and function? PopZ_{Cc} shares no conserved structures with other proteins, but its 178-aa sequence was divided into three functional regions: R1, R2 and R3 (Fig. 4a) (35-36). The N-terminal R1 domain interacts with ParA prompting the bipolar localization of PopZ_{Cc} (35-36). The R2 domain links the R1 with the C-terminal R3 domain, tolerates large amounts of variation and, is highly disordered, proline rich and negatively charged (35-36). The R3 domain is required for the subcellular accumulation and oligomerization of PopZ_{Cc} (35-36).

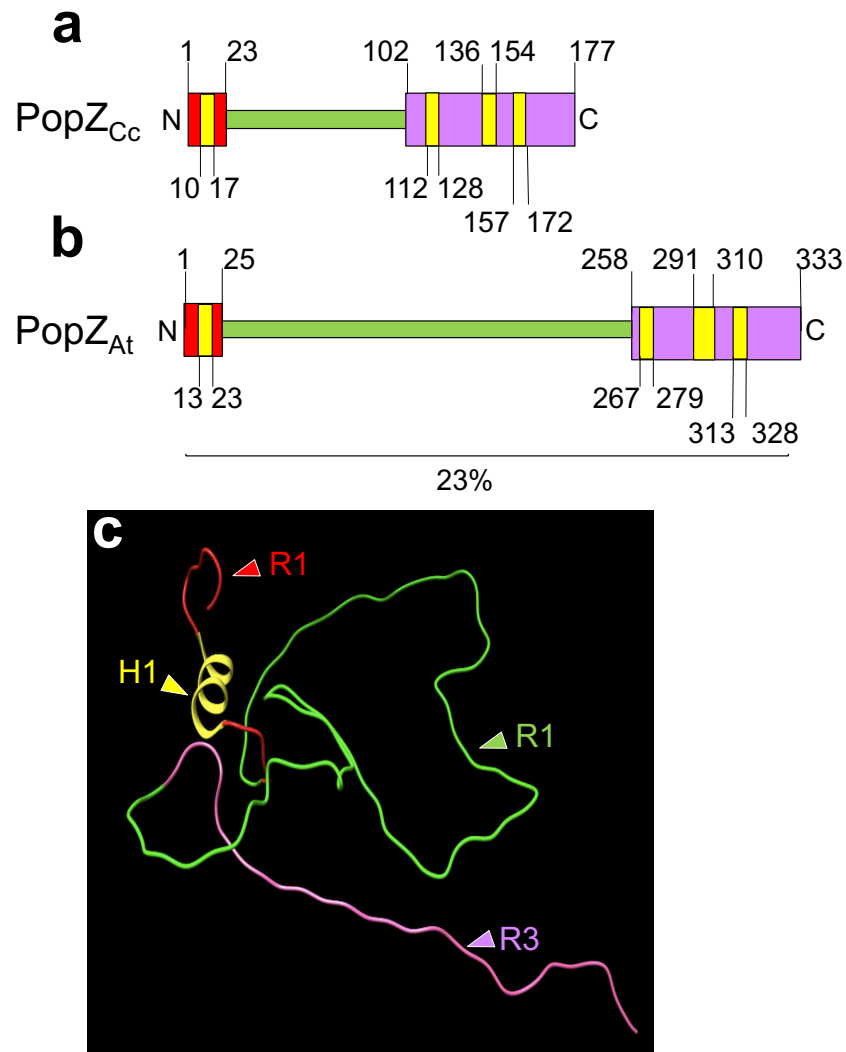


Fig. 4. Domain organization and structure of PopZ. (a) Domain structure of PopZ_{Cc} according to Bowman GR. et al (2013) and Nordyke et al (2020). (b) Domain structure of PopZ_{At} according to Grangeon et al (2017) (3) and Howell et al (2017) (24). PopZ_{At} is 23% identical to PopZ_{Cc}. (a-b) The number of aa is indicated at the top and bottom of each domain. Lengths are approximately to scale. (c) Nuclear magnetic resonance structure of truncated PopZ_{Cc} (residues 1-133). Different domains are indicated with arrowheads. The ribbon diagram was generated using Chimera, PDB number 6XRY. (a-c) R1, R2, R3, and α -helices are indicated in red, green, magenta and yellow respectively (23-24, 35-36, 52-53).

Notably, the structure of PopZ_{Cc} is conserved across its homologues (35-36). As *Caulobacter*, PopZ_{At} contains one α -helix (H1) and three α -helices (H2, H3, and H4) at its N- and C-termini domains, respectively (23, 35-36, 52). Although the R2 linker domain of PopZ_{At} is longer compared to *Caulobacter*, it is also highly disordered, proline rich and negatively charged (23, 35-36). Notably, the R2 and R3 domains are required to localize PopZ_{At} at the GP, likely through homo-oligomerization (23, 24).

The cell division FtsZ protein

The Z-ring. The canonical FtsZ protein plays a critical role on cell division and has been extensively studied in *E. coli* (54). At mid cell and upon binding to GTP, many FtsZ subunits form protofilaments capable to assemble further into a discontinuous ring-like structure, the Z-ring, that treadmills with proteins of the divisome complex and undergoes through several conformational changes creating increasingly smaller concentric rings until the cell is completely bisected (55-62).

Function and spatiotemporal dynamics of *Agrobacterium* FtsZ. The genome of *Agrobacterium* encodes for three homologues of *Escherichia* FtsZ (FtsZ_{Ec}): Atu2086 (FtsZ_{At}), Atu4215 (FtsZ₃), and Atu4673 (FtsZ₁) (Supplemental table) (15, 63). Genetic deletion of either FtsZ₃ or FtsZ₁ does not influence cell growth (63). In contrast, depletion of FtsZ_{At} impacts cell division and the transition of GP-to-N(OP) (63). Consistent with a function on polar growth, FtsZ_{At} localizes at the GP early in the cell cycle and later relocates to the future septation site (Fig. 5) (15, 63-64).

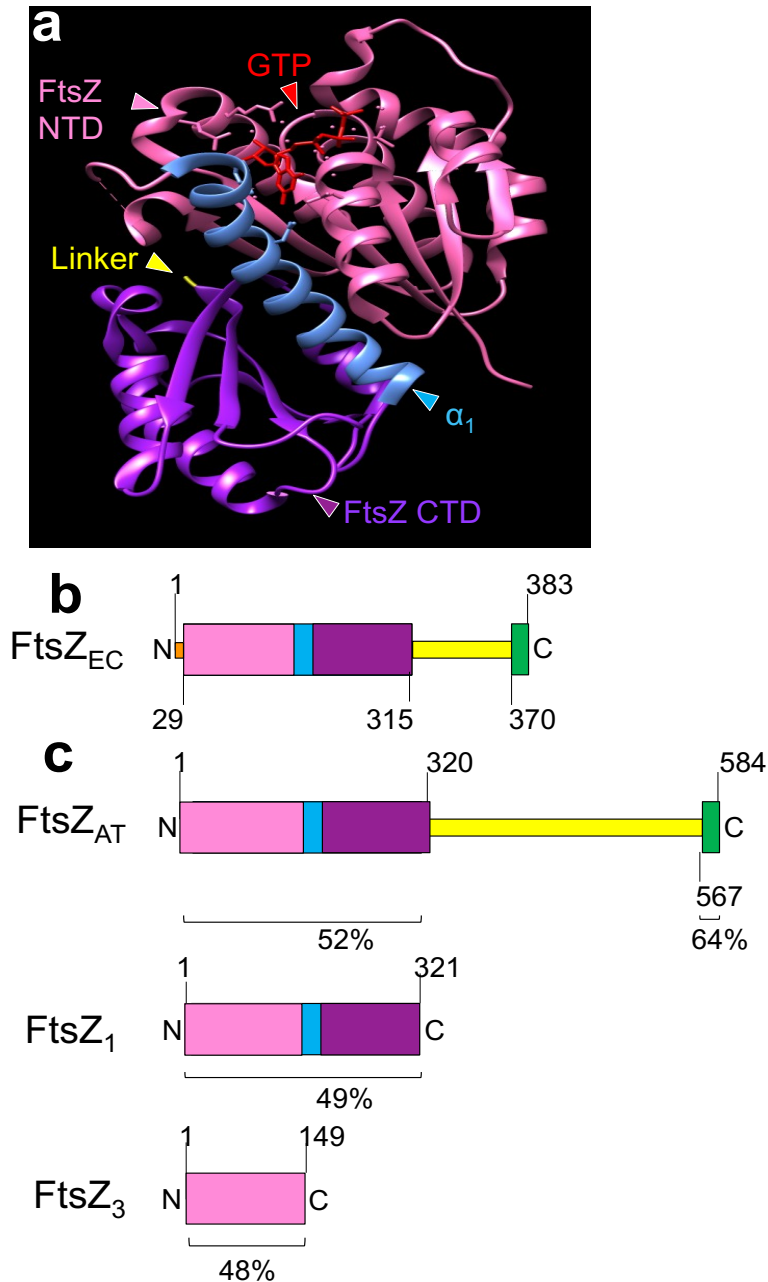


Fig. 6. Structure and domain organization of FtsZ. (a) Crystal structure of a truncated FtsZ_{EC} mutant (residues 10-316, L178E) in a complex with GTP. The different domains of FtsZ_{EC} and GTP are indicated with arrow heads. Only the first residue of the linker is shown in yellow. The ribbon diagram was generated using Chimera, PDB number 6UNX. (b) Domain structure of FtsZ_{EC} according to Zupan et al (2013) (15). (c) Domain structure of FtsZ_{AT}, FtsZ₁ and FtsZ₃ according to Howell et al (2019) (63). The TD and α_2 of FtsZ_{AT} are 52% and 64% to their counterparts in *E. coli*. FtsZ₁ is 49% identical to TD of *E. coli*. FtsZ₃ is 48% identical to FtsZ NTD of *E. coli*. (b-c) The number of aa is indicated at the top or bottom of each protein. Lengths are approximately to scale. (a-c) the FtsZ NTD, α_1 , FtsZ CTD, linker, and α_2 domains are show in magenta, blue, purple, yellow and green, respectively (15, 53, 63, 65).

The N-terminal globular sub-domain (FtsZ NTD) exhibits a GTP binding site and, the C-terminal globular sub-domain (FtsZ CTD) is followed by a disordered linker and a single α -helix (α_2 , Fig. 6b) (15, 65). Notably, FtsZ_{Ec} shares a similar domain architecture with FtsZ_{At} (Fig 6b-c). However, FtsZ_{At} contains a longer linker (15, 63). In contrast to FtsZ_{At}, FtsZ₁ and FtsZ₂ contain only TD and FtsZ NTD, respectively (15, 63).

The polar organelle developmental PodJ protein

Spatiotemporal dynamics of PodJ in *Caulobacter*. *PodJ* is widely spread in the genomes of *Rhizobiales*, *Caulobacterales* and *Rhodobacterales* orders (66). However, like with PopZ, research on *Caulobacter* has provided most of the insights for PodJ function (67-70). *Caulobacter* PodJ (PodJ_{Cc}) exists as two membrane associated isoforms, full length (PodJ_L) and truncated (PodJ_s) (67, 70). In the swarmer cell, PodJ_s localizes at the flagellated pole (67, 70). During the swarmer-to-stalked cell transition, the metalloprotease MmpA protein releases PodJ_s from the incipient stalked pole for its subsequent degradation (Fig. 7a) and, the master regulators DnaA and GcrA activate the transcription of *podJ_{Cc}* (68, 71-72).

In the stalked cell, PodJ_L localizes to the new pole and upon cell compartmentalization the CtrA regulated PerP protease converts PodJ_L to PodJ_S (67, 69-70). Following asymmetric cell division, PodJ_S remains at the flagellated pole of the swarmer sibling cell, while PodJ_L will later localize to the new pole of the stalked cell (Fig. 7a) (67-70).

Function of *Caulobacter* PodJ. PodJ_{Cc} is required for the localization of cell signaling proteins and structural determinants (50, 67, 70, 73-75). Indeed, PodJ_{Cc} localizes the cell signaling PleC and DivL proteins to the new pole leading to the activation of CtrA (67, 70, 75-76). Further, PodJ_{Cc} coordinates the biogenesis of pili and holdfast by providing positional cues to polarly localize the structural determinants, pili secretin CpaE, holdfast attachment Hfa (-A, -B, and -D) and holdfast secretin HfsD proteins (67, 73-74). PodJ_{Cc} is also required for the swarmer pole localization of PopA, a protein essential for the regulation of the flagellar filament length (77-78). Not until recently, except for the interaction of PodJ_{Cc} with DivL (75), it was not known whether these localization dependencies were due to a scaffolding activity of PodJ_{Cc}. However, recent studies report the interaction of PodJ_{Cc} with PleC, CpaE and PopA (50, 76, 77). Therefore, although it remains unknown if PodJ_{Cc} interacts with Hfa (-A, -B, and -D) and HfsD proteins, at least the PleC, DivL, PopA and CpaE proteins are directly recruited to the new pole by PodJ_{Cc}.

Function of *Agrobacterium* PodJ. How does PodJ function in bacteria with obvious differences in growth modes? The genome of *Agrobacterium* encodes for a single homologue of PodJ_{Cc} (Supplemental table) (33). *Agrobacterium* PodJ (PodJ_{At}) localizes at the OP and later relocates to both poles of the cell (Fig. 7b) (33). Consistent with this

localization pattern, PodJ_{At} was shown to be required in the transition of GP-to-N(OP) (79). Further, in the absence of PodJ_{At}, cells exhibit multiple constriction sites and ectopic poles, where PopZ_{At} localizes (79). It is unknown whether PodJ_{At} is required for the localization of cell signaling proteins, however recent observations support the interaction of PodJ_{At} with PleC (76).

Function of *Sinorhizobium* PodJ. The genome of *Sinorhizobium* encodes for two homologues of PodJ_{Cc}, PodJ1 and PodJ2 (80). No biological function or localization pattern was described to PodJ2 (80). In contrast, genetic deletion of PodJ1 produces branched cells with cell division defects (80). Further, PodJ1 is required for the polar localization of the cell signaling DivK protein (80). Consistent with this function, PodJ1 exhibits a unipolar localization pattern (80). Indeed, "*PodJ1 localizes to the "newer" pole just before cell division and persists in only one daughter cell at the OP (80)"*" (33).

Domain organization of PodJ. According to Lawler et al; 2006 (81), PodJ_{Cc} is a 974-aa bitopic protein, with a cytosolic N-terminal domain (PodJ NTD) and periplasmic C-terminal domain (PodJ CTD), both connected by a single transmembrane α -helix (Fig. 8a) (81). PodJ NTD contains three **coiled-coil** regions and is essential for motility and holdfast formation (81). Further, PodJ NTD is required for the interaction of PodJ_{Cc} with cell fate determinants (e.g. PleC) (50,76,34). PodJ CTD contains three consecutive tetratricopeptide repeats, a PG binding sub-domain and is essential for pili formation (81).

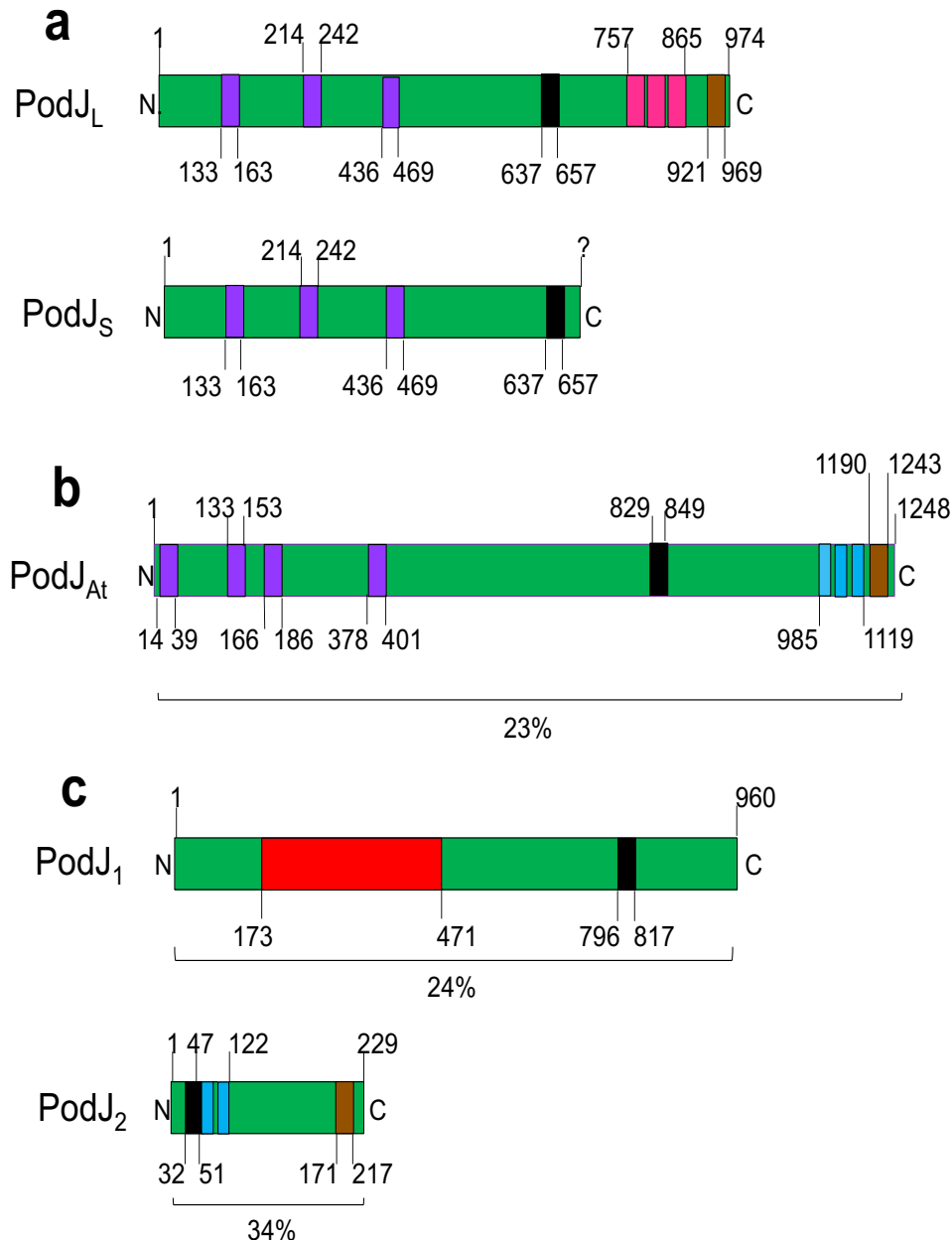


Fig. 8. Domain organization of PodJ. (a) Domain structure of PodJ_L and PodJ_S according to Lawler et al (2006). The PerP recognition site at the C-terminus of PodJ_S is unknown. (b) Domain structure of PodJ_{At} according to Grangeon et al (2015) (33). PodJ_{At} is 23% identical to PodJ_{CC}. (c) Domain structure of PodJ₁ and PodJ₂ according to Fields et al (2012) (80). PodJ₁ and PodJ₂ are 24% and 34% identical to PodJ_{NTD} and PodJ_{CTD} of *Caulobacter*, respectively. (a-c) The number of amino acids is indicated at the top or bottom of each protein. Coiled-coil regions, a SMC sub-domain, transmembrane α -helices, Sel-1 repeats, tetratricopeptide regions, and PG binding sub-domains are shown in purple, red, black, blue, magenta, and brown respectively (33, 80-81). Lengths are approximately to scale. Note: recent studies (34,50,76) include a disordered region and six coiled-coil areas on PodJ NTD of *Caulobacter*.

Is the domain organization of PodJ conserved among α -proteobacteria? PodJ_{At} is longer than PodJ_{Cc} (1248-aa versus 974-aa) and, although it only displays 23% of identity to PodJ_{Cc}, its domain organization and topology resemble to that of *Caulobacter* (33). Indeed, PodJ_{At} contains four **coiled-coil** regions, a single transmembrane α -helix, three consecutive Sel1-like repeats and a PG binding sub-domain (Fig. 8b) (33).

The domain organization of PodJ1 and PodJ2 suggests that *Sinorhizobium* contained a single open reading frame of *podJ* (80). Indeed, PodJ1 is 24% similar to PodJ NTD of *Caulobacter* and, contains an α -helix and a cytosolic SMC domain with **coiled-coil** regions (80). Further, PodJ2 is 34% similar to PodJ CTD of *Caulobacter* and contains a transmembrane α -helix followed by a periplasmic C-terminal domain containing two consecutive Sel1-like repeats and PG binding sub-domain (Fig. 8c) (80).

Mechanisms to localize PodJ. Different experiments in *E. coli* have described that N-terminal fluorescent fusions to PodJ from different α -proteobacteria, including *Agrobacterium* and *Caulobacter*, localize to heterologous poles (33-34, 50,76). Zhao et al; 2018 (50) have suggested that polar accumulation of PodJ_{Cc} is likely mediated by interactions of PodJ_{Cc} with shared cell wall components between *Caulobacter* and *E. coli* such as the Tol-Pal complex, pili and flagellar assemblies (50). The PodJ foci in *E. coli* suggest that subcellular accumulation of PodJ occurs by a self-assembly mechanism (50). Indeed, PodJ_{Cc} NTD forms high molecular weight complexes (50).

Scope of the thesis. The aim of this thesis was to investigate the role of cell identity proteins on cell differentiation, polar growth and DNA segregation.

In **Chapter 2**, the physical connections and factors required to regulate the subcellular accumulation of PodJ_{Cc} were studied. Further, the biochemical properties of PodJ_{Cc} were investigated. PleC, DivL, PopA, SpmX, and PopZ_{Cc} interact with PodJ_{Cc}, which self-associates in *E. coli* and *in vitro*. PleC, PopA, SpmX, PopZ_{Cc}, and the cell signaling DivJ protein are required for the unipolar localization of PodJ_{Cc}. Notably, in the absence of SpmX, PodJ_{Cc} accumulates to the poles and constriction site of the cell. Therefore, SpmX seems to act as a key determinant for the subcellular distribution of PodJ_{Cc}.

Chapter 3 (82) identified an uncharacterized *Agrobacterium* protein (Atu1348) that was named as GROWTH POLE RING, due its striking localization as a hexameric ring at the GP. After cell division, GPR localizes to the new GPs in sibling cells. GPR is an extremely long protein (2,155-aa) containing two N-terminal transmembrane domains with the bulk of the protein in the cytoplasm. GPR also contains two disordered regions (1-80- and 1890-2000-aa) and two apolipoprotein regions (290-1542- and 1583-1878-aa) exhibiting continuous α -helices. Strikingly, depletion or deletion of GPR result in essentially spherical cells that grow poorly. As GPR contains no predicted enzymatic domains and forms a 200-nm-diameter ring, we propose that GPR acts as an organizing center for PG and membrane synthesis during polar growth. Notably, GPR homologs are present in numerous Rhizobiales.

Chapter 4 (30) described the segregation and replication of the four genetic replicons of *Agrobacterium* within the context of polar growth. Early in the cell cycle, the three largest replicons (CC, LC and pAt) reside at the OP. CC replicates first at the OP, while the LC and pAt move away from the OP before replication. Following replication, one copy of the CC, LC and pAt move towards the GP before cell division. In contrast, the pTi replicon does not occupy specific regions in the cell and, after replication, it is randomly distributed throughout the old and new cell compartments. Strikingly, segregation of the two essential replicons (CC and LC) is dependent of PopZ_{At} and PodJ_{At}. In the absence of PopZ_{At}, CC and LC do not effectively segregate resulting in sibling cells without CC and LC. In the absence of PodJ_{At}, the CC and LC abnormally localize to the GP at the beginning of the cell cycle and replicate from this position. Therefore, PodJ_{At} plays an essential role in CC and LC tethering to the OP during early stages of polar growth.

Chapter 5 monitored the localization the Walker A-type ATPase *Agrobacterium* (ParA) ParA_{At}, which alternates from a large dense patch (LDP) located in a large region of the non-growing OP compartment in the shortest cells to gradient with the strongest accumulation of ParA at or near the GP in the longest cells. Notably, this localization pattern, requires rod cell shape morphology dependent on PopZ_{At} and GPR. Further, Chapter 5 describes the localization of CC and LC in the absence of GPR, and the localization pAt in the absence of PopZ_{At} and PodJ_{At}. Rod shape morphology dependent on GPR is required for the segregation of the CC and LC. PopZ_{At} and PodJ_{At} are required for pAt localization as discrete foci to enable segregation following replication.

In **Chapter 6**, “General discussion, suggested additional experiments and future perspectives”, I summarized and discussed the results of this thesis.

Acknowledgments.

I thank Prof. Patricia Zambryski and John Zupan at the Department of Plant and Microbial Biology at University of California, Berkeley, and Steven Ruzin and Denise Schichnes at the College of Natural Resources Biological Imaging Facility at University of California, Berkeley, for assistance with the Delta-Vision microscope. Fig. 1a. was generated in the P.Z. laboratory. Research in the P.Z. laboratory was supported by National Science Foundation Grant MCB-0923840. I thank Prof. Patricia Zambryski at the Department of Plant and Microbial Biology at University of California, Berkeley, Prof. Holger Lill and Dirk Bald at Department of Molecular and Cell Biology at Vrije University Amsterdam, and Conrad Woldringh at Swammerdam Institute for Life Sciences (SILS) at University of Amsterdam, for the insightful and critical reading of this introduction. I received fellowship support from the Secretaría Nacional de Educación Superior, Ciencia, Tecnología, e Innovación, Ecuador.

References:

1. J. Starka, Avant-propos (foreword). *Ann. Microbiol.* **125B**, 133–134 (1974).
2. T. A. Cameron, J. R. Zupan, P. C. Zambryski, The essential features and modes of bacterial polar growth. *Trends Microbiol.* **23**, 347–353 (2015).
3. T. Den Blaauwen, M. A. De Pedro, M. Nguyen-diste, J. A. Ayala, Morphogenesis of Rod-shaped Sacculi. *FEMS Microbiol. Rev* **32**, 321–344 (2008).
4. P. J. B. Brown, *et al.*, Polar growth in the Alphaproteobacterial order Rhizobiales. *PNAS*. **109**, 1697–1701 (2012).
5. T. A. Cameron, J. Anderson-Furgeson, J. R. Zupan, J. J. Zik, P. C. Zambryski, Peptidoglycan synthesis machinery in *Agrobacterium tumefaciens* during unipolar growth and cell division. *mBio*. **5** (2014).
6. A. K. Daitch, E. D. Goley, Uncovering Unappreciated Activities and Niche Functions of Bacterial Cell Wall Enzymes. *Curr Biol* **30**, 1170–1175 (2020).
7. D. Mengin-lecreulx, B. Flouret, J. V. A. N. Heijenoort, Cytoplasmic Steps of Peptidoglycan Synthesis in *Escherichia coli*. *J. Bacteriol.* **151**, 1109–1117 (1982).
8. J. Van Heijenoort, Lipid Intermediates in the Biosynthesis of Bacterial Peptidoglycan. *Microbiol. Mol. Biol. Rev.* **71**, 620–635 (2007).
9. B. Glauner, J. V Höltje, U. Schwarz, The Composition of the Murein of *Escherichia coli*. *J Biol Chem* **263**, 10088–10095 (1988).
10. L.-T. Sham, *et al.*, Bacterial cell wall. MurJ is the flippase of lipid-linked precursors for peptidoglycan biogenesis. *Science* **345**, 220–222 (2014).
11. N. Ruiz, Bioinformatics identification of MurJ (MviN) as the peptidoglycan lipid II flippase in *Escherichia coli*. *PNAS* **105**, 15553–15557 (2008).
12. E. Kuru, *et al.*, In situ probing of newly synthesized peptidoglycan in live bacteria with fluorescent D-amino acids. *Angew. Chem. Int. Ed. Engl.* **51**, 12519–12523 (2012).
13. E. Kuru, S. Tekkam, E. Hall, Y. V Brun, M. S. Van Nieuwenhze, Synthesis of fluorescent d -amino acids and their use for probing peptidoglycan synthesis and bacterial growth in situ. *Nat. Protoc.* **10**, 33–52 (2015).
14. A. D. Tomlinson, C. Fuqua, Mechanisms and regulation of polar surface attachment in *Agrobacterium tumefaciens*. *Curr. Opin. Microbiol.* **12**, 708–714 (2009).
15. J. R. Zupan, T. A. Cameron, J. Anderson-furgeson, P. C. Zambryski, Dynamic FtsA and FtsZ localization and outer membrane alterations during polar growth and cell division in *Agrobacterium tumefaciens*. *PNAS* **110**, 9060–9065 (2013).
16. A. Typas, *et al.*, Regulation of peptidoglycan synthesis by outer-membrane proteins. *Cell* **143**, 1097–1109 (2011).
17. M. Banzhaf, *et al.*, Cooperativity of peptidoglycan synthases active in bacterial cell elongation. *Mol. Microbiol.* **85**, 179–194 (2012).
18. S. Van Teeffelen, S. Wang, L. Furchtgott, K. Casey, N. S. Wingreen, The bacterial actin MreB rotates, and rotation depends on cell-wall assembly. *Proc. Natl. Acad. Sci.* **108**, 15822–15827 (2011).
19. M. T. Swulius, *et al.*, Long helical filaments are not seen encircling cells in electron cryotomograms of rod-shaped bacteria. *Biochem. Biophys. Res. Commun.* **407**, 650–655 (2011).
20. U. Bertsche, *et al.*, Interaction between two murein (peptidoglycan) synthases, PBP3 and PBP1B, in *Escherichia coli*. *Mol. Microbiol.* **61**, 675–690 (2006).
21. J. Mehla, *et al.*, YhcB (DUF1043), a novel cell division protein conserved across gamma-proteobacteria. *BioRxiv* (2021).
22. H. M. Ehrle, *et al.*, Polar Organizing Protein PopZ is required for chromosome segregation in *Agrobacterium tumefaciens*. *J. Bacteriol.* **199** (2017).

23. R. Grangeon, J. Zupan, Y. Jeon, P. C. Zambryski, Loss of PopZ At activity in *Agrobacterium tumefaciens* by deletion or depletion leads to multiple growth poles. *mBio*. **8** (2017).
24. M. Howell, *et al.*, Absence of the Polar Organizing Protein PopZ Results in Reduced and Asymmetric Cell Division in *Agrobacterium tumefaciens*. *J. Bacteriol.* **199** (2017).
25. G. R. Bowman, *et al.*, A Polymeric protein anchors the chromosomal origin/ParB complex at a bacterial cell pole. *Cell* **134**, 945–955 (2008).
26. G. R. Bowman, *et al.*, *Caulobacter* PopZ forms a polar subdomain dictating sequential changes in pole composition and function. *Mol. Microbiol.* **76**, 173–89 (2010).
27. J. L. Ptacin, A. Gahlmann, G. R. Bowman, A. M. Perez, A. R. S. Von Diezmann, Bacterial scaffold directs pole-specific centromere segregation. *PNAS* **111** (2014).
28. K. Lasker, *et al.*, Selective sequestration of signalling proteins in a membraneless organelle reinforces the spatial regulation of asymmetry in *Caulobacter crescentus*. *Nat. Microbiol.* **5**, 418–429 (2020).
29. G. Ebersbach, A. Briegel, G. J. Jensen, C. Jacobs-Wagner, A self-associating protein critical for chromosome attachment, division, and polar organization in *Caulobacter*. *Cell* **134**, 956–968 (2008).
30. J. S. Robalino-Espinosa, J. R. Zupan, A. Chavez-Arroyo, P. Zambryski, Segregation of four *Agrobacterium tumefaciens* replicons during polar growth: PopZ and PodJ control segregation of essential replicons. *PNAS* **117**, 26366–26373 (2020).
31. P. D. Curtis, Y. V Brun, Getting in the loop: regulation of development in *Caulobacter crescentus*. *Microbiol. Mol. Biol. Rev.* **74**, 13–41 (2010).
32. S. K. Govers, C. Jacobs-Wagner, *Caulobacter crescentus*: model system extraordinaire. *Curr. Biol.* **30** (2020).
33. R. Grangeon, J. R. Zupan, J. Anderson-furgeson, P. C. Zambryski, PopZ identifies the new pole, and PodJ identifies the old pole during polar growth in *Agrobacterium tumefaciens*. *PNAS*. **112**, 1166–11671 (2015).
34. W. Zhao, *et al.*, Scaffold-scaffold interactions regulate cell polarity in a bacterium. *BioRxiv.* (2020).
35. G. R. Bowman, *et al.*, Oligomerization and higher-order assembly contribute to sub-cellular localization of a bacterial scaffold. *Mol. Microbiol.* **90**, 776–795 (2013).
36. G. Laloux, C. Jacobs-wagner, Spatiotemporal control of PopZ localization through cell cycle-coupled multimerization. *J. Cell Biol.* **201**, 827–841 (2013).
37. J. A. Holmes, *et al.*, *Caulobacter* PopZ forms an intrinsically disordered hub in organizing bacterial cell poles. *PNAS* **113**, 12490–12495 (2016).
38. D. A. Mohl, J. W. Gober, Cell cycle-dependent polar localization of chromosome partitioning proteins in *Caulobacter crescentus*. *Cell* **88**, 675–684 (1997).
39. V. Tamara, *et al.*, Complete genome sequence of *Caulobacter crescentus*. *PNAS*. **98**, 4136–4141 (2001).
40. A. M. Perez, *et al.*, A localized complex of two protein oligomers controls the orientation of cell polarity. *MBio* **8**, 1–16 (2017).
41. S. K. Radhakrishnan, M. Thanbichler, P. H. Viollier, The dynamic interplay between a cell fate determinant and a lysozyme homolog drives the asymmetric division cycle of *Caulobacter crescentus*. *Genes Dev.* **22**, 212–225 (2008).
42. H. C. Lim, *et al.*, Evidence for a DNA-relay mechanism in ParABS-mediated chromosome segregation. *Elife* (2014).
43. I. V Surovtsev, M. Campos, C. Jacobs-Wagner, DNA-relay mechanism is sufficient to explain ParA-dependent intracellular transport and patterning of single and multiple cargos. *PNAS* **113**, 7268–7276 (2016).
44. G. B, *et al.*, Genome sequence of the plant pathogen and biotechnology agent *Agrobacterium tumefaciens* C58. *Science* **294**, 2323–2328 (2001).
45. D. W. Wood, *et al.*, The genome of the natural genetic engineer *Agrobacterium tumefaciens*

- C58. *Science* **294**, 2317–2324 (2001).
46. L. S. Kahng, L. Shapiro, Polar Localization of Replicon Origins in the Multipartite Genomes of *Agrobacterium tumefaciens* and *Sinorhizobium meliloti*. *J. Bacteriol.* **185**, 3384–3391 (2003).
 47. M. Deghelt, *et al.*, G1-arrested newborn cells are the predominant infectious form of the pathogen *Brucella abortus*. *Nat. Commun.* **5** (2014).
 48. X. De Bolle, S. Crosson, J.-Y. Matroule, J.-J. Letesson, *Brucella abortus* Cell Cycle and Infection Are Coordinated. *Trends Microbiol.* **23**, 812–821 (2015).
 49. S. M. Halling, *et al.*, Completion of the Genome Sequence of *Brucella abortus* and Comparison to the Highly Similar Genomes of *Brucella melitensis* and *Brucella suis*. *J. Bacteriol.* **187**, 2715–2726 (2005).
 50. W. Zhao, *et al.*, A circuit of protein-protein regulatory interactions enables polarity establishment in a bacterium. *BioRxiv.* (2018).
 51. M. Berge, *et al.*, Modularity and determinants of a (bi-) polarization control system from free-living and obligate intracellular bacteria. *Elife* **5** (2016).
 52. C. T. Nordyke, Y. M. Ahmed, R. Z. Puterbaugh, R. Bowman, Grant, K. Varga, Intrinsically disordered bacterial polar organizing protein Z, PopZ, interacts with protein binding partners through an N-terminal Molecular Recognition Feature. *J. Mol. Biol.* **432**, 6092–6107 (2020).
 53. E. F. Pettersen, *et al.*, UCSF Chimera — A Visualization System for Exploratory Research and Analysis. *J Comput Chem* **25**, 1605–1612 (2004).
 54. J. Lutkenhaus, S. Pichoff, S. Du, Bacterial cytokinesis: From Z ring to divisome. *Cytoskeleton* **69**, 778–790 (2012).
 55. A. Mukherjee, J. O. E. Lutkenhaus, Guanine Nucleotide-Dependent Assembly of FtsZ into Filaments. *J. Bacteriol.* **176**, 2754–2758 (1994).
 56. A. Mukherjee, J. Lutkenhaus, Analysis of FtsZ Assembly by Light Scattering and Determination of the Role of Divalent Metal Cations. *J. Bacteriol.* **181**, 823–832 (1999).
 57. G. Fu, *et al.*, In Vivo Structure of the *E. coli* FtsZ-ring Revealed by Photoactivated Localization Microscopy (PALM). *PLoS One* **5** (2010).
 58. Z. Li, M. J. Trimble, Y. V Brun, G. J. Jensen, The structure of FtsZ filaments in vivo suggests a force-generating role in cell division. *EMBO J.* **26**, 4694–4708 (2007).
 59. M. P. Strauss, *et al.*, 3D-SIM Super Resolution Microscopy Reveals a Bead-Like Arrangement for FtsZ and the Division Machinery: Implications for Triggering Cytokinesis. *PLoS Biol.* **10** (2012).
 60. H. P. Erickson, M. Osawa, FtsZ Constriction Force – Curved Protofilaments Bending Membranes. *Subcell. Biochem.* **84**, 139–160 (2017).
 61. A. W. Bisson-Filho, *et al.*, Treadmilling by FtsZ filaments drives peptidoglycan synthesis and bacterial cell division. *Science* **355**, 739–743 (2017).
 62. E. D. Goley, *et al.*, Assembly of the *Caulobacter* cell division machine. *Mol. Microbiol.* **80**, 1680–1698 (2013).
 63. M. Howell, *et al.*, *Agrobacterium tumefaciens* divisome proteins regulate the transition from polar growth to cell division. *Mol. Microbiol.* **111**, 1074–1092 (2019).
 64. S. A. Flores, M. Howell, J. J. Daniel, R. Piccolo, P. J. B. Brown, Absence of the Min System Does Not Cause Major Cell Division Defects in *Agrobacterium tumefaciens*. *FEMS Microbiol. Rev* **9**, 1605–1612 (2018).
 65. M. A. Schumacher, T. Ohashi, L. Corbin, H. P. Erickson, High-resolution crystal structures of *Escherichia coli* FtsZ bound to GDP and GTP research communications. *Acta Crystallogr F Struct Biol Commun* **76**, 94–102 (2020).
 66. M. Brilli, *et al.*, The diversity and evolution of cell cycle regulation in alpha-proteobacteria: a comparative genomic analysis. *BMC Syst. Biol.* **4** (2010).
 67. P. H. Viollier, N. Sternheim, L. Shapiro, Identification of a localization factor for the polar

- positioning of bacterial structural and regulatory proteins. *PNAS* **99**, 13831–13836 (2002).
68. J. C. Chen, P. H. Viollier, L. Shapiro, A membrane metalloprotease participates in the sequential degradation of a *Caulobacter* polarity determinant. *Mol. Microbiol.* **55**, 1085–1103 (2005).
 69. J. C. Chen, *et al.*, Cytokinesis signals truncation of the PodJ polarity factor by a cell cycle-regulated protease. *EMBO J.* **25**, 377–386 (2006).
 70. A. J. Hinz, D. E. Larson, C. S. Smith, Y. V. Brun, The *Caulobacter crescentus* polar organelle development protein PodJ is differentially localized and is required for polar targeting of the PleC development regulator. *Mol. Microbiol.* **47**, 929–941 (2003).
 71. J. Holtzendorff, *et al.*, Oscillating global regulators control the genetic circuit driving a bacterium cell cycle. *Science*. **304**, 983–987 (2004).
 72. A. K. Hottes, L. Shapiro, H. H. Mcadams, DnaA coordinates replication initiation and cell cycle transcription in *Caulobacter crescentus*. *Mol. Microbiol.* **58**, 1340–1353 (2005).
 73. G. G. Hardy, *et al.*, A localized multimeric anchor attaches the *Caulobacter* holdfast to the cell pole. *Mol. Microbiol.* **76**, 409–427 (2010).
 74. J. Javens, Z. Wan, G. G. Hardy, Y. V. Brun, Bypassing the need for subcellular localization of a polysaccharide export-anchor complex by overexpressing its protein subunits. *Mol. Microbiol.* **89**, 350–371 (2013).
 75. P. D. Curtis, *et al.*, The scaffolding and signalling functions of a localization factor impact polar development. *Mol. Microbiol.* **84**, 712–735 (2012).
 76. C. Zhang, W. Zhao, S. W. Duvall, K. A. Kowallis, W. S. Childers, Regulation of a bacterial histidine kinase by a phase separating scaffolding protein. *BioRxiv* (2021).
 77. J. Wang, W. E. Moerner, L. Shapiro, A localized adaptor protein performs distinct functions at the *Caulobacter* cell poles. *PNAS* **118** (2021).
 78. A. Duerig, *et al.*, Second messenger-mediated spatiotemporal control of protein degradation regulates bacterial cell cycle progression. *Genes Dev.* **23**, 93–104 (2009).
 79. J. C. Anderson-furgeson, J. R. Zupan, R. Grangeon, P. C. Zambryski, Loss of PodJ in *Agrobacterium tumefaciens* leads to ectopic polar growth, branching, and reduced cell division. *J. Bacteriol.* **198**, 1883–1891 (2016).
 80. A. T. Fields, *et al.*, The conserved polarity factor PodJ1 impacts multiple cell envelope-associated functions in *Sinorhizobium meliloti*. *Mol. Microbiol.* **84**, 892–920 (2012).
 81. M. L. Lawler, D. E. Larson, A. J. Hinz, D. Klein, Y. V. Brun, Dissection of functional domains of the polar localization factor PodJ in *Caulobacter crescentus*. *Mol. Microbiol.* **59**, 301–316 (2006).
 82. J. R. Zupan, R. Grangeon, J. S. Robalino-Espinosa, N. Garnica, P. Zambryski, GROWTH POLE RING protein forms a 200-nm-diameter ring structure essential for polar growth and rod shape in *Agrobacterium tumefaciens*. *PNAS*. **116**, 10962–10967 (2019).

Supplemental table. Peptidoglycan synthesis and cell division genes in *Agrobacterium*

<i>E. coli</i> / <i>C. crescentus</i> gene	Loci	Name	Notes
Cell elongation scaffold			
MreB	NP		actin scaffold
MreC	NP		associate with MreB & IM
MreD	NP		associate with MreB & IM
RodA	NP		lipid II flippase (PG
RodZ	NP		
Cell division scaffold			
FtsZ	Atu2086	FtsZ	Z-ring scaffold. Full-length α -Proteobacteria version
	Atu4673		lacks extra C-terminal domains typically found in α -Proteobacteria
	Atu4215		partial tubulin domain only
FtsA	Atu2087	FtsA	interact/stabilize Z-ring
ZapA	Atu8191†		interact/stabilize Z-ring
ZapB	NP		
ZapC	NP		
FtsK (SpolIII E)	Atu2759		coordination of division & chromosome segregation
	Atu3210		
FzIA	Atu0293†		interact/stabilize Z-ring
FzIC	Atu2824		
KidO	Atu5198†		may be recruited to z-ring to prevent assembly of adjacent rings
FtsQ (DivIB)	Atu2088		stabilizes divisome interactions
FtsL	NP		stabilizes divisome interactions
FtsB (DivIC)	Atu1428		stabilizes divisome interactions
FtsN	Atu1710†		stabilizes divisome interactions
DamX	NP		PG binding
DedD	NP		PG binding
RlpA	Atu1500		PG binding
	Atu0290		

Peptidoglycan precursor synthesis			
MurA-G	present		PG precursor synthesis
Ddl	Atu2089		PG precursor synthesis
Alr	NP		racemases (synthesis of D-ala & D-Glu)
DadX	Atu3292		racemases (synthesis of D-ala & D-Glu)
Mur	Atu1867		racemases (synthesis of D-ala & D-Glu)
MraY	Atu2097		PG precursor synthesis
FtsW	Atu2095		lipid II flipase (PG precursor)
Peptidoglycan synthesis / hydrolysis / remodeling			
MtgA	Atu2720		transglycosylase only; to division site/PBP3
HMW PBPs			
PBP1a	Atu1341	PBP1a	1° cell elongation transglycosylase
PBP1b	Atu0103	PBP1b1	1° cell division transglycosylase
PBP1c	Atu0931	PBP1b2	
	Atu3694	PBP1c	
PBP2	NP		1° cell elongation transpeptidase in typical bacilli
PBP3	Atu2100	PBP3a	1° cell division transpeptidase
	Atu1067	PBP3b	
LMW PBPs			
PBP5	Atu1499		
PBP4B	Atu3077		
	Atu0933		

Peptidoglycan synthesis / hydrolysis / remodeling		
PBP6	NP	
PBP6B	NP	
	Atu2321†	
	Atu1505†	
	Atu3634†	
PBP4	NP	
PBP7	NP	
LD-transpeptidases		
YcbB	Atu1615	
	Atu1164†	
	Atu1293†	
	Atu2133†	
YbiS	Atu2336†	Rhizobiales/Rhodobacterales LDT
	Atu5196†	Rhizobiales/Rhodobacterales LDT
	Atu0048†	Rhizobiales/Rhodobacterales LDT
	Atu0845†	Rhizobiales/Rhodobacterales LDT
	Atu0669†	Rhizobiales/Rhodobacterales LDT
	Atu3331†	Rhizobiales/Rhodobacterales LDT
	Atu0844†	
	Atu2764†	
YafK	Atu3332	
	Atu3631	
YnhG	NP	
ErfK	NP	
YcfS	NP	

Peptidoglycan synthesis / hydrolysis / remodeling		
DD- & LD-endopeptidases		
MepA	Atu0186	
Lytic transglycosylases		
Slit70	NP	septum cleavage w/ PBP7
MltA	Atu0009	septum cleavage w/ PBP1B
MltB	Atu0092† Atu3779† Atu2122†	septum cleavage
MltC	NP	septum cleavage
MltD	NP	septum cleavage
MltE (EmtA)	Atu2112	
MltF	NP	
Amidases		
AmiA	NP	LytC-type PG amidase
AmiB	NP	LytC-type PG amidase
AmiC	Atu1340	LytC-type PG amidase
AmiD	Atu2113	
Peptidoglycan regulation		
LpoA NP	NP	regulates PBP1a
LpoB NP	NP	regulates PBP1b
FtsE	Atu3606	FtsE/X ABC system interacts with EnvC protein to activate AmiA/B
FtsX	Atu3607†	FtsE/X ABC system interacts with EnvC protein to activate AmiA/B
EnvC	Atu2775 Atu1832†	activates AmiA/B
NlpD / DipM	Atu1700	activates AmiC, LytM factor
YgeR	NP	
YebA	NP	
Ivy	NP	inhibits MltB
OM-PG linkage		
ToIABRQ-Pal	present	OM invagination during septation / PG linkage
Lpp	NP	links PG tightly to OM (in γ-proteobacteria)

Additional proteins		
PopZ	Atu1720†	cell polarity
TipN	NP	cell polarity
PodJ	Atu0499†	cell polarity
MipZ	NP	inhibits FtsZ at pole (Caulobacter)
SlmA	NP	nucleoid occlusion (E coli)
MinCDE	present	z-ring positioning
SulA	NP	inhibits cell division during SOS

† Lower confidence hits, matching primarily by shared domains, or with low sequence similarity, altered domain architecture, or other ambiguities.

NP indicates the corresponding gene was not present in the *Agrobacterium* genome.

From “Peptidoglycan Synthesis Machinery in *Agrobacterium tumefaciens* During Unipolar Growth and Cell Division” by Cameron, T. A., Anderson-Furgeson, J., Zupan, J. R., Zik, J. J. & Zambryski, P. C, 2014, MBio, 5, ([10.1128/mBio.01219-14](https://doi.org/10.1128/mBio.01219-14)) (1).

Supplemental references

1. T. A. Cameron, J. Anderson-Furgeson, J. R. Zupan, J. J. Zik, P. C. Zambryski, Peptidoglycan synthesis machinery in *Agrobacterium tumefaciens* during unipolar growth and cell division. *mBio*. 5 (2014).

Chapter 2

Studies to be continued: Subcellular distribution of the self-assembling PodJ protein is regulated by cell fate determinants in *Caulobacter crescentus*

Robalino Espinosa JS^{a,b}, Kalogeraki V^a, Lourenco R^a, Saurabh S^a,
Pathak D^a, Chen JC^c, Shapiro L^{a,1}

^aDepartment of Developmental Biology, Stanford University School of Medicine;

^bPresent Address: Department of Molecular Cell Biology, Amsterdam Institute for Molecules, Medicines and Systems, Faculty of Earth- and Life Sciences, Vrije Universiteit Amsterdam; ^cDepartment of Biology, San Francisco State University.

2

Abstract

Cell differentiation relies on the sub-cellular accumulation of cell signaling and scaffold proteins. In the dimorphic and asymmetrically dividing bacterium *Caulobacter crescentus*, the global response regulator CtrA controls the expression of least 95 developmental genes. Notably, the polar organizing PodJ protein accumulates to the new pole, where it localizes the CtrA activation pathway, by providing positional cues to the cell signaling PleC and DivL proteins. Yet, the physical connections and required factors that regulate the sub-cellular accumulation of PodJ are just being explored. Here, by coimmunoprecipitation of crosslinked proteins followed by mass spectrometry, we obtained a putative interactome of PodJ that was systematically studied using a library into a bacterial to hybrid system. Notably, the cell fate factors PleC, DivL, PopA, SpmX, and PopZ physically associated with PodJ, which exhibited polymeric protein behavior, as self-associated when heterologously expressed in *Escherichia coli* and its cytosolic domain formed high-molecular-weight complexes *in vitro*. We also monitored the subcellular distribution of PodJ. PleC, PopA, SpmX, PopZ, and the cell signaling DivJ protein were required for the unipolar localization of PodJ. In the absence of SpmX, PodJ accumulated to both poles and the constriction site of the cell. Therefore, we propose that SpmX acts as a key determinant for the subcellular distribution of PodJ.

Introduction

Cell differentiation relies to a great extent on the asymmetrical localization of polar organizing and signaling proteins (1-2). A fundamental challenge in developmental biology is to understand how this unequal distribution of regulatory proteins is acquired in a $\sim 1\text{-}\mu\text{m}^3$ bacterial cell (1), in which proteins can diffuse to several locations in milliseconds (3-4). Here, we have identified regulators for the subcellular distribution of an asymmetrically localized polar organizing and self-assembling protein from *Caulobacter crescentus*.

The α -proteobacterium *Caulobacter* is a valuable system to study cell differentiation due to its asymmetric cell division that produces two morphologically distinct sibling cells, a sessile stalked cell and a motile smaller swarmer cell, each with the same genetic information, but different developmental programs (5-6). The stalked cell can immediately replicate its DNA (S-phase), whereas the swarmer cell must first differentiate into a stalked cell before initiating DNA replication (5-6). During swarmer-to-stalked cell transition, a flagellum and pili are lost from the swarmer cell pole and replaced by a stalk with holdfast material at its distal tip (5-6). After DNA replication, a new flagellum appears at the pole opposite the stalk creating a cell with two morphologically distinct poles (Fig. 1a) (5-6).

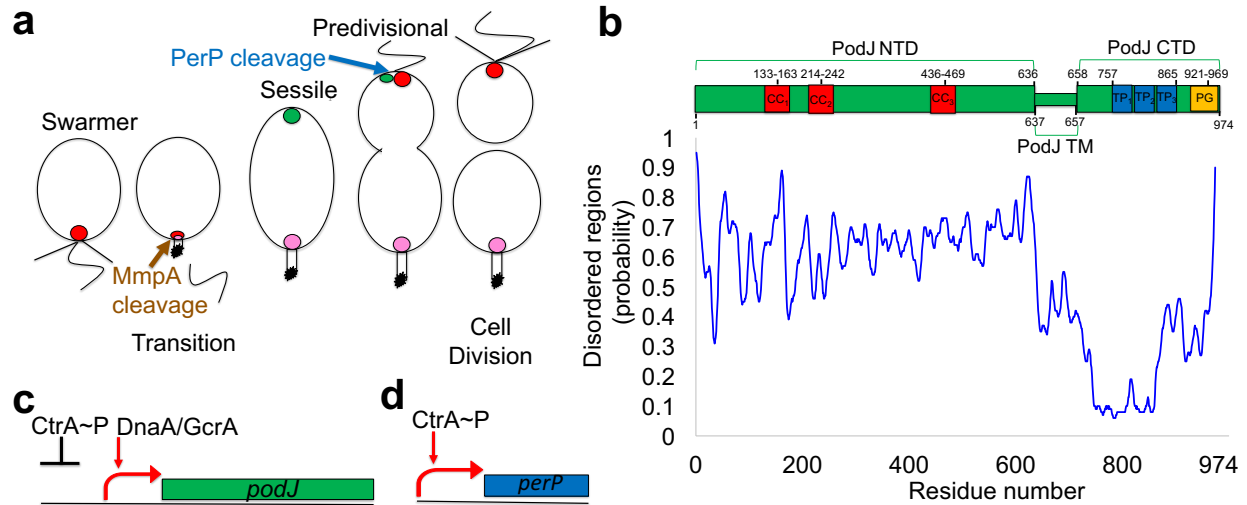


Fig. 1. Spatiotemporal control and domain organization of PodJ. (a) A schematic showing the dynamic localization of the two PodJ isoforms and SpmX. A swarmer pole exhibiting a flagellum (wavy line) and pili (straight lines) is visible. PodJ_s (red circle) is at the swarmer pole. During swarmer-to-stalked cell transition, the flagellum and pili are replaced by an emerging stalk with a holdfast at its tip (white rectangle and black star) and PodJ_s is liberated by MmpA (brown arrow) from the incipient stalked pole, where SpmX (magenta circle) accumulates. In the stalked cell, PodJ_l (green circle) localizes to the new pole. Just before asymmetrical cell division, PodJ_l is converted to PodJ_s by PerP (blue arrow). After cell division, PodJ_s is at the swarmer pole of the swarmer daughter cell and SpmX is at the stalked pole of the sessile daughter cell. (b) Domain organization of PodJ according to Lawler ML et al (2006). Amino acids 1-636, 637-657, and 658-974 correspond to PodJ NTD, PodJ TM and PodJ CTD, respectively (green rectangles). Amino acids 133-163, 214-242 and 436-468 correspond to three coiled-coil regions (CC₁, CC₂, CC₃) (red squares). Amino acids 757-865 and 921-969 correspond to three consecutive tetratricopeptide repeats (TP₁, TP₂ and TP₃) (blue squares) and PG-binding sub-domain (orange square), respectively. The bottom of the schematic shows the prediction (blue wavy line) of disordered regions on PodJ. The Y-axis shows the probability to find a disordered region on the scale from 0 to 1. The X-axis shows the number of residues (1-974) on PodJ. Disordered regions were predicted using PrDOS. The image was adapted from Zhao et al (2018) (7). (c) Schematic of *podJ* regulation. Expression of *podJ* (green box) is down-regulated (black line) by CtrA~P and up-regulated (red arrows) by DnaA and GcrA. (d) Schematic of *perP* regulation. Expression of *perP* (blue box) is up-regulated (red arrows) by CtrA~P (5, 7-21). Note: different studies (7, 22-23) include six coiled-coil areas on PodJ NTD.

A key factor regulating *Caulobacter* cell asymmetry comprises the spatiotemporal activation and degradation of the global response regulator, CtrA, which inhibits DNA replication and controls the expression of least 95 cell cycle-regulated genes, including

those involved in polar morphogenesis, DNA replication initiation, DNA methylation, cell division and cell wall metabolism (24-27). CtrA is present as its active form in the swarmer cell (24, 27). During swarmer-to-stalked cell transition, CtrA is degraded at the incipient stalked pole allowing DNA replication (24). At the mid S-phase, CtrA is resynthesized and then activated by a phosphorylation event (24). Following cell compartmentalization and just before cell division, CtrA is cleared from the stalked compartment, while active CtrA remains in the swarmer compartment (24).

The CtrA activation pathway localizes to the stalk-distal pole, associated with the swarmer compartment, of the predivisional cell through interactions with the polar organizing protein, PodJ (Fig. 1b), which is required for multiple aspects of polar development, including, activation of flagellum rotation, ejection of the flagellum, holdfast formation and pili biogenesis (8-11, 13, 28). PodJ is the primary focus of this report and exists as two dynamically localized isoforms, full length (PodJ_L) and truncated (PodJ_S) (7-9). In the swarmer cell, PodJ_S sits at the flagellated pole, then, during swarmer-to-stalked cell transition, the metalloprotease MmpA releases PodJ_S to the cytoplasm and the master regulators DnaA and GcrA activate the transcription of *podJ* (Fig 1a, c) (8-9, 14, 16-18). Newly synthesized PodJ localizes to the new pole of the stalked cell (Fig. 1a), where it provides positional cues to the PleC phosphatase and the DivL tyrosine kinase proteins (7-9, 22, 29). PleC dephosphorylates the response regulator DivK (DivK~P), allowing DivL to activate the bifunctional histidine kinase/phosphatase CckA signaling protein, which in turn phosphorylates CtrA via the phosphotransferase ChpT protein (30-38). Phosphorylated CtrA (CtrA~P) inhibits and activates the expression of *podJ* and *perP*, respectively (Fig 1c-d) (14-15). Upon cell compartmentalization, the newly synthesized

Chapter 2

PerP protease converts PodJ_L to PodJ_S and, following cell division, PodJ_S remains localized at the flagellated pole of the daughter swarmer cell (Fig. 1a) (8-9, 15).

Notably, PodJ interacts with PleC and DivL, and yet its physical associations extend to other cell fate factors such as the bifunctional PopA protein and self-assembling SpmX and PopZ proteins (7, 22-23, 29, 39). PopA symmetrically localizes in the predivisional cell directing the degradation of CtrA and regulating the flagellar filament length at the staked and new poles, respectively (39-43). During the swarmer-to-staked cell transition, SpmX and PopZ co-oligomerize at the incipient staked pole, allowing the localization and activation of the histidine kinase DivJ, that in turn phosphorylates DivK leading to the dephosphorylation of CtrA via the ChpT-CckA pathway (19, 32-34, 45-48).

Here, we confirmed the interactions of PodJ by systematically studying a putative interactome of PodJ that was obtained by coimmunoprecipitation of crosslinked proteins followed by mass spectrometry. Further, consistent with other studies (7,22), we found that the cytosolic N-terminal domain of PodJ (PodJ NTD) (Fig. 1b) formed high-molecular-weight complexes *in vitro*, and that PodJ self-associated when expressed heterologously in *Escherichia coli*, suggesting that PodJ exists as a polymeric protein in *Caulobacter*. We also monitored the localization of PodJ. Like in other studies (7, 9, 22), we have determined that PodJ retained its polar localization in the absence of PleC, PopA, SpmX, PopZ, and DivJ, and that these cell fate determinants were required for the unipolar localization of PodJ. Notably, in the absence of SpmX, PodJ localized to both poles and the constriction site of the cell. Therefore, we propose that SpmX acts as a major determinant for the subcellular distribution of PodJ.

Results

Cytoplasmic domain of PodJ assembles into high molecular weight complexes.

PodJ is a bitopic protein, with a cytoplasmic PodJ NTD and a periplasmic C-terminal (PodJ CTD) domains that exhibit regions often involved in protein-protein interactions (7-10, 49-51). Indeed, PodJ NTD contains coiled-coil motifs (CC) and disordered regions, and PodJ CTD contains tetratricopeptide repeats (TP, Fig. 1b) (7, 10). To search for interactants of PodJ, we performed coimmunoprecipitation experiments, using merodiploid strains in which the endogenous *podJ* coding sequence was replaced with epitope tagged *podJ-m2* or *podJ NTD-m2* sequences (Fig. S1). In addition, an epitope-tagged CtrA-m2 was used as control (52). A crosslinking agent was added before membrane solubilization with detergents; then epitope-tagged and associated proteins were immunoprecipitated with an anti-m2 antibody and subsequently eluted in the presence of m2-peptides, sodium dodecyl sulfate (SDS), or SDS along with dithiothreitol (SDS-DTT).

The elutions from coimmunoprecipitation were analyzed by Western blot using an anti-m2 antibody. PodJ NTD-m2 was detected in all elutions (Fig. 2a-c), while PodJ-m2 was only detected in the elution obtained with SDS/DTT (Fig. 2c). Notably, PodJ NTD-m2 formed high molecular weight complexes (Figs. 2a-c), suggesting that PodJ NTD-m2 is a self-assembling protein. These high molecular weight complexes of PodJ NTD-m2 were also recognized by a anti-PodJ NTD antibody (Fig S2). At the monomeric level, PodJ NTD-m2 ran as a ~95-KDa size band (Fig. 2a-b) or as a smaller band of ~66-KDa in size (Figs. 2b-c). Likely, PodJ NTD-m2 did not run exclusively as its predicted molecular size (66-KDa), because PodJ NTD-m2 contains many negatively charged residues (pI=4.92)

that give an unusual mass-to-charge to this protein. In contrast, PodJ-m2 formed no high-molecular-weight complexes (Fig. 2c), suggesting that *in vitro*, PodJ CTD, or the transmembrane α -helix (PodJ TM, Fig. 1b), or both inhibit the oligomerization of PodJ NTD. Further, PodJ-m2 ran as a ~105-KDa size band accompanied by a smaller band located just below the 55-KDa marker (Fig. 2c), indicating that PodJ-m2 was cleaved likely by PerP.

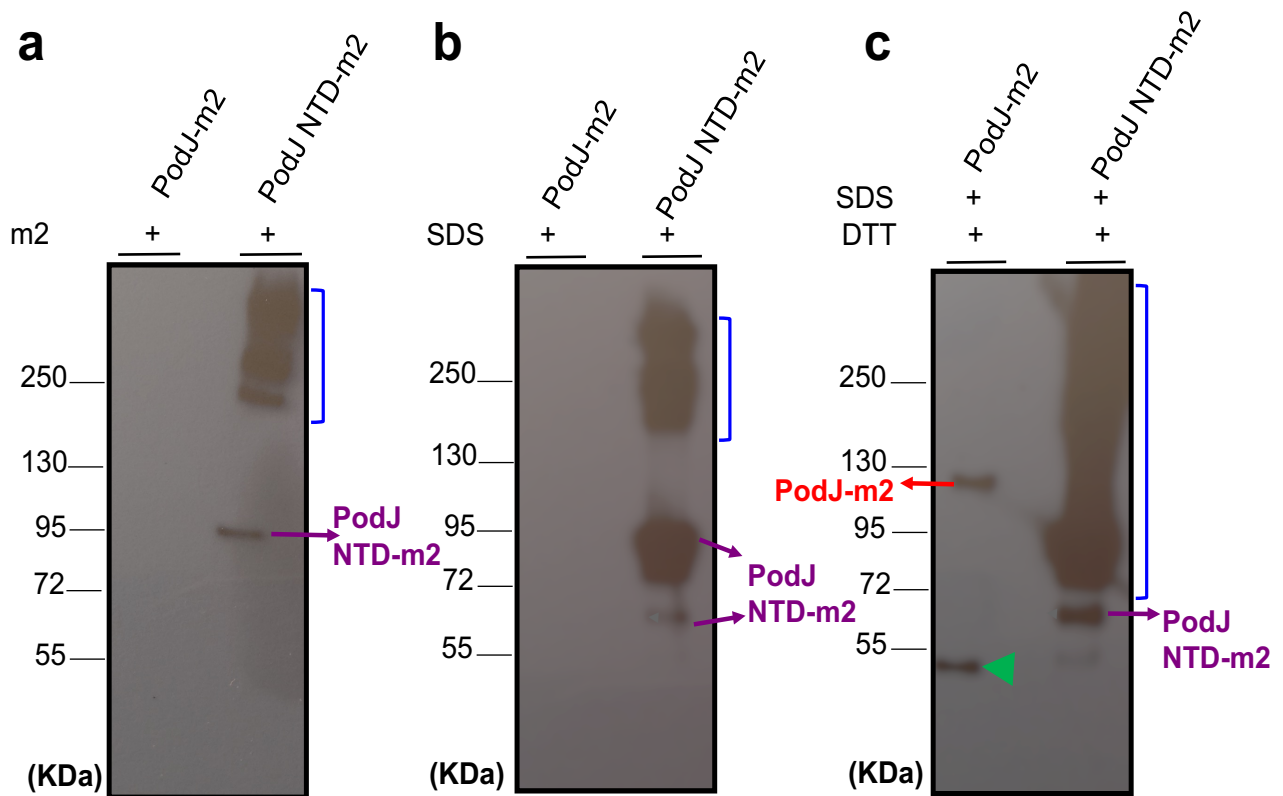


Fig. 2. The Cytosolic domain of PodJ forms high-molecular-weight complexes. (a-c) Immunoprecipitated PodJ-m2 and PodJ NTD-m2 were eluted using m2-peptides, SDS, or SDS/DTT. PodJ-m2 (indicated with a red arrow) and PodJ NTD-m2 (indicated with purple arrows) were detected using an anti-m2 antibody. High-molecular-weight complexes of PodJ NTD-m2 are indicated with blue brackets. The C-terminal domain of PodJ-m2 is indicated with a green arrow head. Molecular size markers in KDa are shown to the left of each blot.

PodJ is in close molecular proximity to more than 200 different proteins. The obtained elutions from coimmunoprecipitation were also analyzed by mass spectrometry. Different peptides corresponding to 204 and 246 proteins were found to coimmunoprecipitate with PodJ-m2 and PodJ NTD-m2, respectively (Tables S1-S2). These interactomes are distinctly different from the putative interactome of CtrA-m2, which was composed of 327 interactants (Table S1-S3). Indeed, PodJ-m2 and PodJ NTD-m2 interactomes exhibit 39.22% and 18.29% of identity by number of interactants to the CtrA-m2 interactome, respectively. Notably, the interactomes of PodJ-m2 and PodJ NTD-m2 contained several cell fate determinants that are required to modulate the CtrA activity (Tables 1, S1-S2). Unexpectedly, PodJ NTD-m2 coimmunoprecipitated with PodJ as evidenced by the presence of peptides corresponding to PodJ CTD (Table 1). Cumulative data argue two trends: 1) PodJ is in close molecular proximity to proteins that regulate the activity of CtrA; and 2) PodJ NTD associates with PodJ.

PodJ self-associates *in Escherichia coli*. PodJ NTD-m2 forms high-molecular-weight complexes (Figs. 2a-c) and likely transiently associates with PodJ (Table 1). To determine whether PodJ self-associates *in vivo*, we utilized an *E. coli* heterologous system, whereby PodJ fused at its C terminus to super folder green fluorescent protein (PodJ-sfGFP) was expressed under the control of the *araBp* promoter (53) (Fig. 3a). The γ -proteobacterium *E. coli* does not encode for PodJ (21). PodJ-sfGFP localized in each cell as a single focus or multiple foci exhibiting different fluorescence intensities (Fig. 3a). A fluorescent profile of hundreds of cells showed that the PodJ-sfGFP foci primarily localized near the mid cell (Fig. 3b). In contrast, PodJ fused at its N terminus to yellow fluorescent protein (YFP-

PodJ) localizes to both poles of the cell (7,22). Therefore, sfGFP fused to the C terminus of PodJ blocks the polar localization of this protein, likely because PodJ exhibits a PG binding subdomain at its C terminus (residues 921-969) (Fig. 1b) (10). Further, formation of fluorescent foci suggests that PodJ-sfGFP self-associates in *E. coli*, potentially through its oligomerization domain, PodJ NTD (Figs. 2a-c).

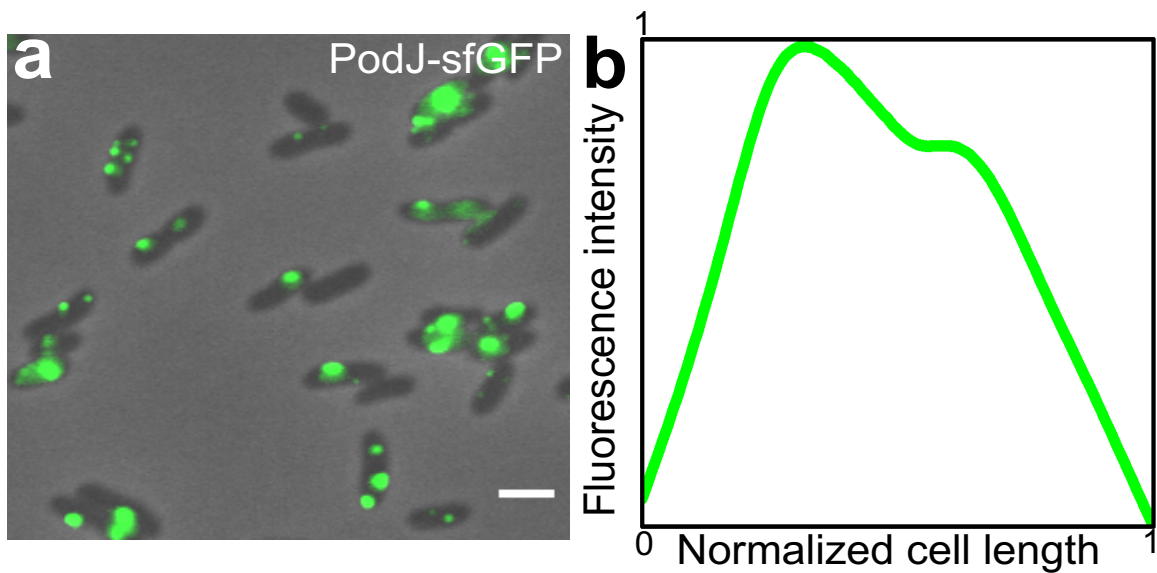


Fig. 3. PodJ-sfGFP self-associates in a heterologous *E. coli* test system. **(a)** *Caulobacter* fluorescent fusion protein PodJ-sfGFP was assayed for its ability to self-associate when expressed in *E. coli*. PodJ-sfGFP exhibits single or more foci exhibiting different fluorescence intensities. PodJ-sfGFP was expressed from a *araBp* promoter using 0.2 % L-arabinose for 2 hours before imaging. **(b)** Cumulative fluorescent profile of PodJ-sfGFP along the normalized *E. coli* cell length. PodJ-sfGFP mainly accumulates near the mid cell. The fluorescent plot was obtained from 200 cells using Object-J. Scale bar on a, 2 μ m (53,54).

Table 1: Key interacting partners of PodJ, as revealed by mass spectrometry analysis of peptides isolated via co-immunoprecipitation

Epitope tagged protein	Identified proteins	Peptides
PodJ-m2	PodJ	TAASPWSVK,RSGMTLGEWLNRMIIEGDGQTADPRLAGDDVPNR,DDA PPRIEIAEHPADEVGR,NAAAITGIDHSVRDALTR,FEGAVDELK,RIESEA AGPRSAEALR,AGHLYEGEARTREAIATLEAKLNQQSSGDPSALVEAVV AR,ELGASFQALDQRLGAVETANPATGVQEGLDLSLAATLTQK,KLGEMA AHVQAAEQR,EIVGVADAFNR,NASAIEQVGGEVAR,ADSVQAQALEK,N ALAIDDVGEQVAR,SSQELVDR,SFEVAEFPAAEPEEPFAFHDDYAIADG FEPESPRYEVEPEVSDFAPAEPSPRMSTRDIIIEQAR,ASGSLFSGFGGF STKK,VAQAIAGRKADVEVNGPEADTTTPGAPRAAVALTTGKVVPAEVEA PAAPPTNEAKALFEDAVRK,WSERAANGGDPRAMHNLALYYFK,NSTTA ASWFRK,WYVIAGR,SQLTAEAQQTADRSALAFRPQTQVQTASLSSAAP AAANANLGVQQRVLSQLGYYQGPRDGVSSPALRMAIAAYQRDQGLPP TGSVDAETLNR
	SpmX	IVIDALVR,TLFLTPANGEWVPAPSPVLRPK,VIAQREEGLPLNVVVPEED APTATEQSAAAVAARLEAILPETPSAPASMAK
	PopA	SQSFDLTLSPPLHPSQAALR
PodJ NTD-m2	PodJ	SGMTLGEWLNRMIIEGDGQTADPRLAGDDVPNRAYLEIVKDDAPPRIE AEHPADEVGR,NAAAITGIDHSVRDALTRLGASEREQIAVAARFEGAVD ELKTEQAR,RIESEAAAGPR,VAGHLYEGEARTREAIATLEAKLNQQSSGD PSALVEAVVARLGERLEAAETRSDALRELGASFQALDQRLGAVETAN PATGVQEGLDLSLAATLTQK,ESADGRFDR,KLGEMAAHVQAAEQR,EIV GVADAFNRR,NASAIEQVGGEVARIAASVEHKLNRADSVQAQALEK,RN ALAIDDVGEQVAR,SSQELVDR, YEVEPEVSDFAPAEPSPRMSTRDIIEQ AR,VVPAEVEEAPAPPTNEAK^a
	SpmX	AAVDLIKRFEGYR,AAQLPDGRWTVGYGHTLTAR,KADFEGERIVIDALV R,TLFLTPANGEWVPAPSPVLRPKVDYDASCAVPK,TEGDRVIAQREEG LPLNVVVPEEDAPTATEQSAAAVAARLEAILPETPSAPASMAK
	CckA	GVAGSSLFAALVQAR,LAPIVVAEPVVEDASPAPVAER,AGVLFGLLIDA ASR,LLAFSR,SQLETAVMNLAVNAR,IFLPVYEAPAGAVAVQAVAEPK R,ILFVEDEDAVR
	DivJ	EGSASLTFNPALGVER,APNQLVGVL
	DivL	TPLTTIIGYSELLER
	PopZ	EWLDQNLPRIVETKVEEEVQR

^a Green highlighted regions belong to PodJ CTD.

PodJ interacts with proteins that regulate the CtrA activity. Given that PodJ-m2 and PodJ NTD-m2 co-immunoprecipitated with cell fate factors required to modulate the CtrA activity (Table 1), and that PodJ provides positional information to PleC, DivL, and PopA proteins (7-9, 22, 29, 39-40), we asked if PodJ interacts with proteins involved in CtrA activation or degradation. We constructed a library into an *E. coli* two-hybrid system (LibETH) by tagging PodJ with the T25 domain of adenylate cyclase and tagging PleC, SpmX, PopZ, DivL, PopA, DivJ and CckA with the T18 domain of the same enzyme. We confirmed that PleC, SpmX, PopZ, DivL and PopA interact with PodJ (Fig. 4, Table 2), while DivJ and CckA do not interact with PodJ (Table 2). Therefore, as previously reported (7,22,29,39), PodJ directly recruits the PleC, DivL and PopA proteins to the cell pole.

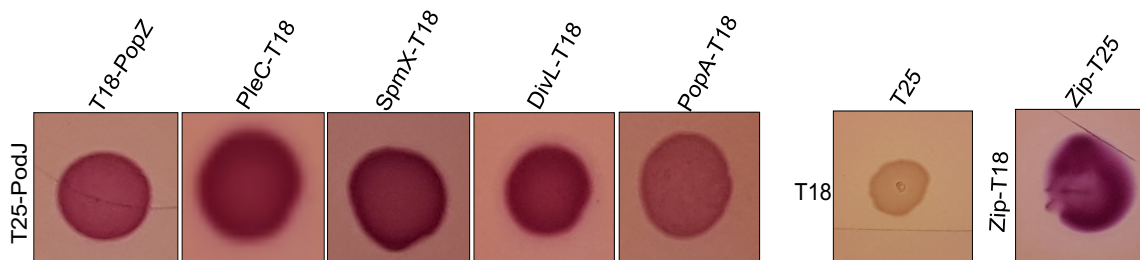


Fig. 4. Screening of PodJ interactions using **LibETH**. The left five panels show *E. coli* BTH101 cells co-expressing the T25 domain of adenylate cyclase fused to PodJ (T25-PodJ) with the T18 domain of the same enzyme fused to PopZ (T18-PopZ), PleC (PleC-T18), SpmX (SpmX-T18), DivL (DivL-T18) and PopA (PopA-T18). The right two panels show negative and positive controls. The negative control shows *E. coli* BTH101 cells co-expressing T25 and T18 domains. The positive control shows T25 and T18 domains fused to leucine zipper (Zip-T25 and Zip-T18) derived from the transcriptional activator GCN4. Cells were grown to mid exponential phase (OD_{600} of 0.5) and 3 μ l from each culture was spotted onto MacConkey agar plates containing 1 % maltose and 0.5 mM isopropyl- β -D-thiogalactopyranoside (IPTG). Plates were imaged after 48 hours of incubation at 30 $^{\circ}$ C.

Table 2. Bacterial two-hybrid assays indicating positive (+) or no (-) interaction with PodJ

18-tagged proteins	Interactions with 25-tagged PodJ
18-PleC	-
PleC-18	+
18-DivJ	-
DivJ-18	-
18-DivL	-
DivL-18	+
18-CckA	-
CckA-18	-
SpmX-18	+
18-PopZ	+
PopZ-18	-
18-PopA	-
PopA-18	+

Asymmetrical localization of PodJ requires PleC. PodJ exhibits an asymmetrical polar distribution in *Caulobacter* cells (Fig. 1a) (7-8, 15-16). We reproduced this localization pattern (76%) using a merodiploid strain in which the *podJ* locus was replaced with *podJ* fused to malachite green-activating peptide *dL5* (*dL5-MG-podJ*) (Figs. S1, 5a). To a lesser extent, dL5-MG-PodJ exhibited two polar foci (14%) of different fluorescent intensities, or three foci (1%) with two polar foci and one focus located at the division site of the cell. In addition, 9% of the cells showed no dL5-MG-PodJ signal (Fig 5a). Consequently, dL5-MG-PodJ serves to demonstrate the subcellular localization pattern of PodJ.

The PleC-DivK-DivJ signaling pathway modulates the levels of PodJ by regulating the proteolysis of PodJ_L to PodJ_S (15). Further, PodJ interacted with cell fate determinants required for the spatiotemporal regulation of the CtrA activity (Fig. 4, Table 2). We compared the localization of dL5-MG-PodJ in mutants lacking PleC (Δ PleC) (55), DivJ (Δ DivJ) (44), SpmX (Δ SpmX) (19), PopA (Δ PopA) (40), and PopZ (Δ PopZ) to that in wild type (WT) cells (Figs. 5a-f). PleC is a member of the CtrA activation pathway and, in its

absence, DivK~P remains phosphorylated, inhibiting the expression of *perP* (1,15,31,34-35). The Δ PleC cells were stalkless and displayed polar foci of dL5-MG-PodJ. However, this localization pattern was preferentially symmetrical (57%) (Fig. 5b), showing that downregulation of *perP* leads to bipolar localization of dL5-MG-PodJ.

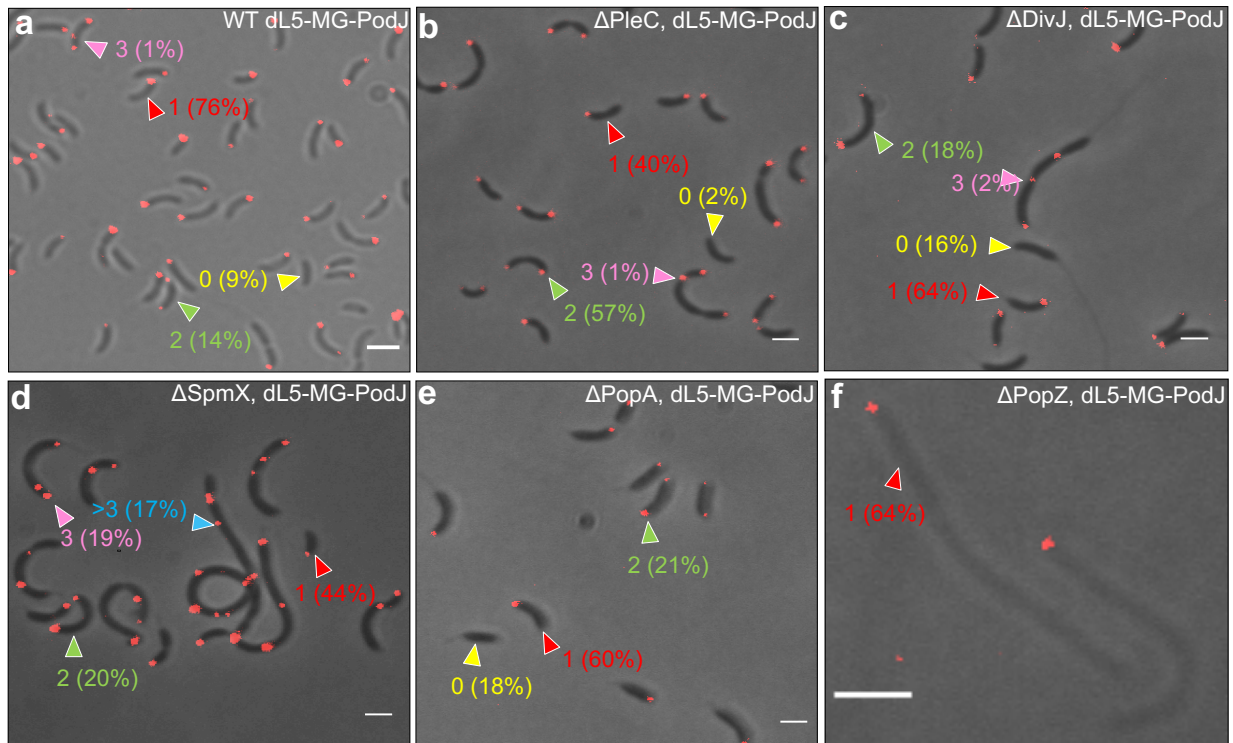


Fig. 5. Regulation of CtrA activity is required for the asymmetrical localization of dL5-MG-PodJ. dL5-MG-PodJ was expressed in WT (a), Δ PleC (b), Δ DivJ (c), Δ SpmX (d), Δ PopA (e), and Δ PopZ (f) strains. (a-f) Cells with one, two, three or more dL5-MG-PodJ foci are shown with red, green, magenta, and blue arrow heads, respectively. Yellow arrow heads indicate cells exhibiting no dL5-MG-PodJ signal. The number of foci per cell were quantified in 100 cells of each strain. Cells were incubated with 0.1 μ M of MG for 15 minutes before imaging. Scale bars: 2 μ m.

Asymmetrical localization of PodJ requires DivJ, SpmX and PopA. DivJ, SpmX and PopA are members of the CtrA degradation pathway (1). In Δ DivJ dephosphorylated DivK predominates throughout the cytoplasm (15, 30-31, 34-35). As shown in figure 5c, Δ DivJ cells were elongated exhibiting polar dL5-MG-PodJ foci and long stalks often at either both poles or in the middle of the cell. Further, more Δ DivJ cells (16%) exhibited no foci

relative to WT (9%) (Figs. 5a, c). This suggests that dL5-MG-PodJ exists in low levels in Δ DivJ. Indeed, proteolysis of PodJ_L to PodJ_S is enhanced in the absence of DivJ, leading to a decrease in the levels of PodJ (15).

In Δ SpmX, dephosphorylated DivK predominates throughout the cytoplasm (19,44). By analogy to Δ DivJ, dL5-MG-PodJ should exist in low levels in the absence of SpmX. However, Δ SpmX cells were elongated often with bipolar stalks and multiple constrictions sites, where dL5-MG-PodJ unexpectedly accumulated (Fig 5d). Indeed, dL5-MG-PodJ exhibited two (20%), three (19%), or more (17%) foci that localized to the constriction sites and both poles of the cell (Fig. 5d). Further, fewer Δ SpmX cells exhibited one polar focus (44%) when compared to that observed in WT (76%) (Figs. 5a, d). These data indicate that SpmX inhibits the subcellular accumulation of dL5-MG-PodJ.

CtrA integrates signals from the PleC-DivK-DivJ signaling pathway (15). In the absence of PopA, CtrA~P is not cleared from the cell (40). DL5-MG-PodJ retained its polar localization in Δ PopA (Fig 5e). Further, more Δ PopA (18%) cells exhibited no foci relative to WT cells (9%) (Figs 5a, e). This suggests that dL5-MG-PodJ exists in low levels in Δ PopA.

PopZ is required for the asymmetrical localization of PodJ. Cells lacking PopZ exhibit low levels of CtrA (56). In the absence of PopZ, cells were elongated, stalkless, and dL5-MG-PodJ retained its polar localization (Figs. 5f, S3a-c). However, as reported for PodJ fused to sfGFP (sfGFP-PodJ) (23), dL5-MG-PodJ in Δ PopZ localized as two polar foci (20%) at a higher frequency compared to that observed in WT (14%) (Figs. 5a, S3a). This suggests that PopZ is required for the unipolar localization of dL5-MG-PodJ.

PodJ and its proteolysis are required for the asymmetrical localization of SpmX.

During the swarmer-to-stalked cell transition, SpmX accumulates to the incipient stalked pole, and remains in there for the subsequent stages of the cell cycle (Fig. 1a) (19, 44). We reproduced this asymmetrical distribution (63%) using a merodiploid strain in which the *spmX* locus was replaced with *spmX* fused to enhanced yellow fluorescent protein (*spmX-eYFP*) (Fig. 6a) (44). These cells also displayed two polar foci (15%) of different fluorescent intensities or three (2%) foci with two polar foci and one focus located at the constriction site of the cell. Further, 20% of the cells exhibited no eYFP signal. Therefore, as previously concluded (44), SpmX-eYFP displays an asymmetrical localization pattern.

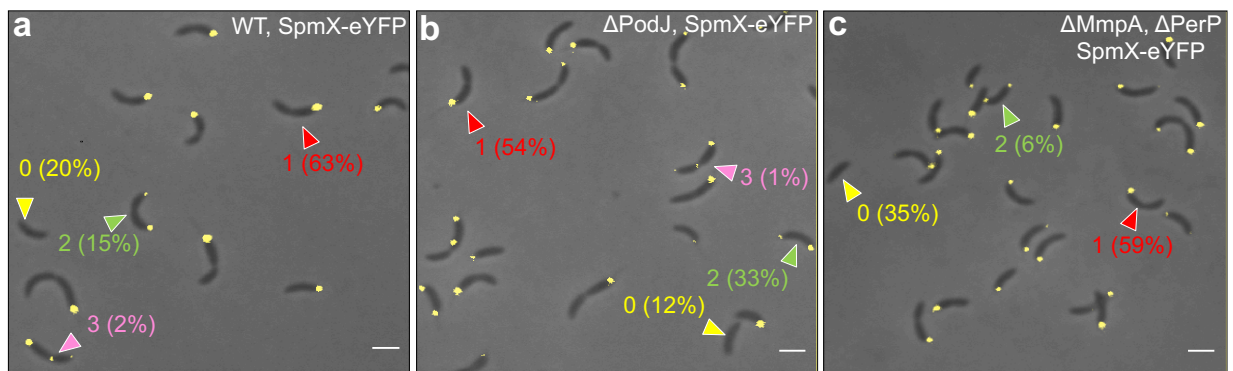


Fig. 6. PodJ is required for the asymmetrical localization of SpmX-eYFP. SpmX-eYFP was expressed in WT (a), Δ PodJ (b) and Δ MmpA, Δ PerP (c) strains. (a-c) Cells displaying one, two, three SpmX-eYFP foci are shown with red, green, and magenta arrowheads respectively. Cells exhibiting no SpmX-eYFP signal are shown with yellow arrowheads. The number of foci per cell were quantified in 100 cells of each strain. Scale bars 2 μ m.

The SpmX levels are likely low in cells lacking PodJ (Δ PodJ) as: 1) The CtrA~P dependent transcription factor, TacA, activates the expression of *spmX* (19); and 2) the CtrA activation pathway is likely downregulated in Δ PodJ, as in this mutant the expression of *perP* is reduced (15-29). SpmX-eYFP retained its polar localization in Δ PodJ (Fig. 6b). Surprisingly, fewer Δ PodJ cells (12%) exhibited no SpmX-eYFP foci compared to WT

Chapter 2

(20%). Further, in Δ PodJ, SpmX-eYFP localized as single polar foci (54%) at a lower frequency compared to that observed in WT (63%) (Figs. 6a-b). Therefore, PodJ contributes to the asymmetrical localization of SpmX-eYFP, but in its absence *spmX* is likely not downregulated.

We also examined the localization of SpmX-eYFP in cells lacking both MmpA and PerP proteases (Δ MmpA Δ PerP). In this double mutant, the levels of PodJ are elevated (15). In Δ MmpA Δ PerP, SpmX-eYFP retained its polar localization (Fig. 6c). However, SpmX-eYFP localized as single polar foci (59%) at a lower frequency compared to that in WT (63%). Further, more Δ MmpA Δ PerP cells exhibited no SpmX-eYFP foci (35%) compared to WT (20%). Thus, proteolysis of PodJ, mediated by PerP or MmpA or both, contributes to the asymmetrical distribution of SpmX-eYFP.

Discussion

Here, we studied the biochemical properties, interactions and localization of the polar organizing PodJ protein (Fig. 1b). PodJ NTD formed high molecular weight complexes *in vitro*, whereas full length PodJ self-associated only when expressed heterologously in *E. coli*, indicating that PodJ CTD or PodJ TM or both inhibit the oligomerization of PodJ *in vitro*, and suggesting that in *Caulobacter*, PodJ exists as polymeric protein, likely formed by PodJ NTD-to-PodJ NTD interactions. Although the interactions of PodJ observed in this study need to be further tested in a purified system; PodJ appeared in close molecular proximity to more than 200 different proteins, physically associating with the PleC, SpmX, PopZ, DivL, and PopA cell fate factors and exhibiting an asymmetrical localization pattern. Below we discuss how the PleC-DivK-DivJ signaling pathway integrated by CtrA and SpmX drive the subcellular distribution of PodJ.

Caulobacter cell differentiation relies on the asymmetrical distribution of CtrA~P (24-25,27). Notably, in the predivisional cell, CtrA~P is present in the swarmer compartment, while absent in the stalked compartment (24). Such asymmetry determines the unipolar localization of PodJ, as PodJ_L is converted to PodJ_S by the CtrA~P dependent PerP protease, thereby proceeding to proteolysis of PodJ_S by the MmpA protease (Figs. 1a, d) (15, 16). At the swarmer pole, PodJ provides positional cues to PleC and DivL, allowing the dephosphorization of DivK~P and activation of CtrA via the CckA-ChpT pathway (30-38). At the stalked pole, PopA is required for the degradation of CtrA (39-43), and SpmX cooligomerize with PopZ to localize and activate DivJ, which in turn phosphorylates DivK leading to the deactivation of CtrA via the ChpT-CckA pathway (19, 32-34, 44-48).

Chapter 2

The CtrA activation pathway or CtrA degradation pathway is essential to maintain PodJ asymmetrically localized. Our work presents evidence for cell fate factors on preserving the unipolar localization of PodJ. Indeed, PodJ shows reduced levels of unipolar localization in the absence of PleC, DivJ, SpmX, PopA, and PopZ. Notably, SpmX inhibited the accumulation the subcellular accumulation of PodJ. Therefore, PodJ_S and SpmX may physically associate to contribute to the removal of PodJ_S from the swarmer pole during the swarmer-to-stalked cell transition and PodJ_L and SpmX may physically associate to prevent the localization of PodJ_L at the stalked pole.

In the absence of SpmX, the sibling cells remain associated (Fig. 5d) with unseparated functional poles (19) that may require PodJ as an organizing center. If PodJ acts as an organizing center at the division plane of Δ SpmX cells, what factors are recruited to this cell site? Obvious candidates are PleC, DivL, PopA and PopZ. But, can PodJ provide positional cues to structural determinants at the multiple constriction sites of Δ SpmX cells? In WT, PodJ localizes the pili secretin CpaE, holdfast attachment Hfa, and holdfast secretin HsfD proteins to the cell pole (8, 11, 13). Further, the PerP levels and the dominant PodJ isoform in Δ SpmX, Δ PopZ, Δ PopA mutants need to be determined. In summary, modulation of the activity of CtrA is critical to asymmetrically localize PodJ. Future research will provide novel insights into how the polymeric PodJ protein acts as an organizing center and how SpmX acts as inhibitor of the subcellular distribution of PodJ.

Materials and Methods

Plasmid construction. A list of plasmids and oligonucleotides used in this study are shown in tables S4 and S5 respectively. pREJSc-001 was constructed by amplifying the 3' end of *podJ* using primers 1c and 2c, which introduced EcoRI and AgeI sites. The *m2* coding region was introduced in the same reaction using primer 2c. The resulting PCR product was ligated into a pFLAG-C2 vector digested with EcoRI and AgeI. To create pREJSc-002, the 5' end of *podJ* was engineered with NdeI and KpnI sites using primers 3c and 4c. The *m2* coding region was introduced using primer 4c. This PCR product was inserted into a NdeI- and KpnI-digested pFLAG-C2 vector. To construct pREJSc-003, three PCR products were generated. First, *podJ* was amplified using primers 5c and 6c; the open reading frame (ORF) of malachite green-activating peptide *dL5* was amplified from AP454 (Table S6) (57-60) using primers 7c and 8c; and then, the 500-bp region upstream of the ORF of *podJ* was amplified using primers 9c and 10c. These PCR products were assembled via Gibson (61) into an EcoRI-digested pMCS-C2 vector. To create pREJSc-004, *podJ* was amplified using primers 11c and 12c; the resulting PCR product containing XbaI and KpnI sites was ligated into a pKT25 vector digested with the corresponding enzymes. The *pleC*, *divL*, *cckA*, and *divJ* genes were amplified with engineered XbaI and KpnI sites using primer pairs 13c-14c, 15c-16c, 17c-18c, and 19c-20c. The resulting PCR products were ligated into a pUT18-C vector digested with XbaI and KpnI to create pREJSc-005, pREJSc-006, pREJSc-007, and pREJSc-011. The *cckA*, and *divJ* genes were amplified with engineered XbaI and KpnI sites using primer pairs 21c-22c, and 25c-26c. These PCR products were ligated into a XbaI- and KpnI-digested pUT18 plasmid, resulting into pREJSc-008, and pREJSc-010. To create pREJSc-009, the

ORF of *spmX* was amplified with engineered XbaI and EcoRI sites using primer pair 23c-24c. The resulting PCR product was ligated into a XbaI- and EcoRI-digested pUT18 vector.

***Caulobacter* strains and cell growth.** A description of the *Caulobacter* strains used in this study is shown in Table S6. Transduction was performed with phage ϕ Cr30 as described by Ely, B (1991) (62). For transformation, cells were grown at 28 °C in agar and liquid peptone-yeast extract (PYE). For co-immunoprecipitation and cell imaging cells were grown at 28 °C in M2G medium (62). When appropriate, the growth medium was supplemented with the following antibiotics: 5 μ g/mL kanamycin, 0.5 μ g/mL gentamicin, or 25 μ g/mL spectinomycin. For microscopy and co-immunoprecipitation, cells were collected at mid exponential phase. Cells expressing dL5-PodJ were incubated with 0.1 μ M Malachite Green (MG) for 15 minutes before cell imaging.

Co-immunoprecipitation. *Caulobacter* cells expressing m2-tagged proteins from a 500 ml culture were washed for three times in 25 ml of IP buffer containing 20 mM HEPES (pH 7.5), 110 mM NaCl and 10% glycerol. The obtained cell pellet was re-suspended in 5 ml of IP buffer containing protease inhibitors (Santa Cruz) and then sonicated. The cell extract was incubated with 20 mM of dithiobis-succinimidyl-propionate (DSP) for 2 hours at 4 °C to crosslink the m2-tagged proteins to their interactants. This reaction was stopped using 20 mM of Tris-HCl (pH 7.5) for 15 minutes at 4 °C. The cell extract containing DSP was centrifuged at 15000 rpm for 15 minutes at 4 °C. The pellet was incubated in 5 ml of RIPA buffer (Thermo Fisher Scientific) for 30 minutes at 4 °C. The protein suspension was centrifuged at 15000 rpm for 15 minutes at 4 °C. The supernatant was diluted ten

times using IP buffer and then dialyzed in a buffer containing 0.5 M Tris, 0.15 M NaCl, 1mM EDTA, and 10% glycerol. To immunoprecipitate m2-tagged proteins with their interactants, the dialyzed solutions were incubated with anti-m2 magnetic beads (Sigma Aldrich) for 3 hours at 4 °C and then washed three times in dialysis buffer. Elutions were performed using 0.1 mg/ml of the m2 peptide, SDS buffer (Bio-Rad) or SDS buffer (Bio-Rad) with 50 mM of DTT. CtrA-m2, PodJ NTD-m2 and PodJ-m2 elutions obtained with SDS, and SDS with DTT, respectively, were sent to Stanford University Mass Spectrometry laboratory.

Immunoblots. Protein elutions were subjected to denaturing gel electrophoresis using Mini-PROTEAN precast SDS-PAGE gels (4-15 % Bio-Rad). Proteins were transferred to PVDF or nitrocellulose membranes and blotted with anti-m2 antibodies (Cell Signaling Technology) (1:5000) followed by a goat-anti-rabbit secondary antibody conjugated to horseradish peroxidase. Blots were imaged with an Odyssey infrared imaging system (Li-Cor).

Bacterial two-hybrid system. A description of the *E. coli* BTH101 derivate strains used in this study is shown in Table S6. Cells were growth in Luria-Bertani (LB) liquid medium at 37 °C until an OD600 of 0.5 was reached (mid-exponential phase). Cell suspensions in LB (3 µl) were plated on MacConkey agar plates supplemented with 1% maltose, 0.5 mM isopropyl-β-D-thiogalactopyranoside (IPTG), ampicillin at 100 µg/mL and kanamycin at 50 µg/mL. MacConkey agar plates were incubated at 30 °C for 48 hours before imaging.

Heterologous expression. *E. coli* BL21(DE3) encoding PodJ-sfGFP (Table S6) was grown at 37 °C in LB. Temperature was switched to 28 °C when cells reached an OD600 of 0.2. Induction was performed with 0,2 % D-arabinose for 2-3 hours before imaging. Medium was supplemented with 100 µg/mL of ampicillin.

Cell imaging. *Caulobacter* or *E. coli* cells expressing fluorescent fusion proteins were immobilized on M2G and LB containing 1 % agarose, respectively. Except for WT and Δ PopZ expressing dL5-MG-PodJ, all *Caulobacter* and *E. coli* strains were imaged using a Leica DM6000 B microscope with a HCX PL APO 100×/1.40 Oil PH3 CS objective. This microscope was operated with the Metamorph software. Images were obtained using a EMCCD, Hammamatsu, camera. First, cells were photograph in the phase contrast field, then through the Cy5 or GFP filter. Images of WT *Caulobacter* cells expressing dL5-MG-PodJ were obtained using a Delta-Vision Elite deconvolution microscope through a PlanApo 100x 1.4NA oil objective. The Delta-Vision microscope was operated using a Soft Worx 5.5 software, and images were captured with a Photometrics CoolSnap HQ CCD camera. First the WT *Caulobacter* cells were imaged in the bright field, and then through a Cy5 filter. *Caulobacter* Δ PopZ cells expressing dL5-PodJ were imaged using a Leica DMI8 S microscope equipped with a Hamamatsu C9100 EM- CCD camera, a 100x oil-immersion objective (1.63 NA), and a SPECTRA X light engine (Lumencor). Micrographs were combined using Image-J (63). The cumulative fluorescent profile of PodJ-sfGFP profiles was obtained with object-J (54). For this, each image was scaled to 12.5 px/um.

Acknowledgments.

We thank Prof. Patricia Zambryski and John Zupan at the Department of Plant and Microbial Biology at University of California, Berkeley, and Steven Ruzin and Denise Schichnes at the College of Natural Resources Biological Imaging Facility at University of California, Berkeley, for assistance with the Delta-Vision microscope. We thank Conrad Woldringh at Swammerdam Institute for Life Sciences (SILS) at University of Amsterdam for the insightful and critical reading of the manuscript. We thank Xiaofeng Zhou and Jiarui Wang from the Shapiro laboratory and Grant Bowman at the Department of Molecular Biology at University of Wyoming for strains and plasmids. J.S.R-E. received fellowship support from the Shapiro laboratory and Secretaría Nacional de Educación Superior, Ciencia, Tecnología, e Innovación, Ecuador.

References

1. K. Lasker, T. H. Mann, L. Shapiro, An intracellular compass spatially coordinates cell cycle modules in *Caulobacter crescentus*. *Curr. Opin. Microbiol.* **33**, 131–139 (2016).
2. J. A. Knoblich, Mechanisms of Asymmetric Stem Cell Division. *Cell* **132**, 583–597 (2008).
3. M. B. Elowitz, M. G. Surette, P. Wolf, J. B. Stock, S. Leibler, Protein Mobility in the Cytoplasm of *Escherichia coli*. *J. Bacteriol.* **181**, 197–203 (1999).
4. D. Lucena, M. Mauri, F. Schmidt, B. Eckhardt, P. L. Graumann, Microdomain formation is a general property of bacterial membrane proteins and induces heterogeneity of diffusion patterns. *BMC Biol* **16** (2018).
5. P. D. Curtis, Y. V. Brun, Getting in the loop: regulation of development in *Caulobacter crescentus*. *Microbiol. Mol. Biol. Rev.* **74**, 13–41 (2010).
6. S. K. Govers, C. Jacobs-Wagner, *Caulobacter crescentus*: model system extraordinaire. *Curr. Biol.* **30** (2020).
7. W. Zhao, *et al.*, A circuit of protein-protein regulatory interactions enables polarity establishment in a bacterium. *BioRxiv.* (2018).
8. P. H. Viollier, N. Sternheim, L. Shapiro, Identification of a localization factor for the polar positioning of bacterial structural and regulatory proteins. *PNAS* **99**, 13831–13836 (2002).
9. A. J. Hinz, D. E. Larson, C. S. Smith, Y. V. Brun, The *Caulobacter crescentus* polar organelle development protein PodJ is differentially localized and is required for polar targeting of the PleC development regulator. *Mol. Microbiol.* **47**, 929–941 (2003).
10. M. L. Lawler, D. E. Larson, A. J. Hinz, D. Klein, Y. V. Brun, Dissection of functional domains of the polar localization factor PodJ in *Caulobacter crescentus*. *Mol. Microbiol.* **59**, 301–316 (2006).
11. J. Javens, Z. Wan, G. G. Hardy, Y. V. Brun, Bypassing the need for subcellular localization of a polysaccharide export-anchor complex by overexpressing its protein subunits. *Mol. Microbiol.* **89**, 350–371 (2013).
12. C. S. Smith, A. Hinz, D. Bodenmiller, D. E. Larson, Y. V. Brun, Identification of genes required for synthesis of the adhesive holdfast in *Caulobacter crescentus*. *J. Bacteriol.* **185**, 1432–1442 (2003).
13. G. G. Hardy, *et al.*, A localized multimeric anchor attaches the *Caulobacter* holdfast to the cell pole. *Mol. Microbiol.* **76**, 409–427 (2010).
14. W. B. Crymes, D. Zhang, B. Ely, Regulation of podJ expression during the *Caulobacter crescentus* cell cycle. *J. Bacteriol.* **181**, 3967–3973 (1999).
15. J. C. Chen, *et al.*, Cytokinesis signals truncation of the PodJ polarity factor by a cell cycle-regulated protease. *EMBO J.* **25**, 377–386 (2006).
16. J. C. Chen, P. H. Viollier, L. Shapiro, A membrane metalloprotease participates in the sequential degradation of a *Caulobacter* polarity determinant. *Mol. Microbiol.* **55**, 1085–1103 (2005).
17. J. Holtzendorff, *et al.*, Oscillating global regulators control the genetic circuit driving a bacterium cell cycle. *Science (80-)*. **304**, 983–987 (2004).
18. A. K. Hottes, L. Shapiro, H. H. McAdams, DnaA coordinates replication initiation and cell cycle transcription in *Caulobacter crescentus*. *Mol. Microbiol.* **58**, 1340–1353 (2005).
19. S. K. Radhakrishnan, M. Thanbichler, P. H. Viollier, The dynamic interplay between a cell fate determinant and a lysozyme homolog drives the asymmetric division cycle of *Caulobacter crescentus*. *Genes Dev.* **22**, 212–225 (2008).
20. T. Ishida, K. Kinoshita, PrDOS: prediction of disordered protein regions from amino acid sequence. **35**, 460–464 (2007).
21. A. T. Fields, *et al.*, The conserved polarity factor PodJ1 impacts multiple cell envelope-associated functions in *Sinorhizobium meliloti*. *Mol. Microbiol.* **84**, 892–920 (2012).
22. C. Zhang, W. Zhao, S. W. Duvall, K. A. Kowallis, W. S. Childers, Regulation of a bacterial

- histidine kinase by a phase separating scaffolding protein. *BioRxiv* (2021).
23. W. Zhao, *et al.*, Scaffold-scaffold interactions regulate cell polarity in a bacterium. *BioRxiv*. (2020).
 24. I. J. Domian, K. C. Quon, L. Shapiro, Cell type-specific phosphorylation and proteolysis of a transcriptional regulator controls the G1-to-S Transition in a bacterial cell cycle. *Cell* **90**, 415–424 (1997).
 25. M. T. Laub, S. L. Chen, L. Shapiro, H. H. McAdams, Genes directly controlled by CtrA, a master regulator of the *Caulobacter* cell cycle. *PNAS*. **99**, 4632–4637 (2002).
 26. K. C. Quon, B. Yang, I. J. Domian, L. Shapiro, G. T. Marczyński, Negative control of bacterial DNA replication by a cell cycle regulatory protein that binds at the chromosome origin. *PNAS* **95**, 120–125 (1998).
 27. K. C. Quon, G. T. Marczyński, L. Shapiro, Cell cycle control by an essential bacterial two-component signal transduction protein. *Cell* **84**, 83–93 (1996).
 28. S. P. Wang, P. L. Sharma, P. V. Schoenleint, B. Ely, A histidine protein kinase is involved in polar organelle development in *Caulobacter crescentus*. *PNAS*. **90**, 630–634 (1993).
 29. P. D. Curtis, *et al.*, The scaffolding and signalling functions of a localization factor impact polar development. *Mol. Microbiol.* **84**, 712–735 (2012).
 30. H. Lam, J.-Y. Matroule, C. Jacobs-Wagner, The asymmetric spatial distribution of bacterial signal transduction proteins coordinates cell cycle events. *Dev. Cell* **5**, 149–159 (2003).
 31. C. Jacobs-Wagner, D. Hung, L. Shapiro, Dynamic localization of a cytoplasmic signal transduction response regulator controls morphogenesis during the *Caulobacter* cell cycle. *PNAS* **98**, 4095–4100 (2000).
 32. T. H. Mann, W. S. Childers, J. A. Blair, M. R. Eckart, L. Shapiro, A cell cycle kinase with tandem sensory PAS domains integrates cell fate cues. *Nat. Commun.* **7** (2016).
 33. C. G. Tsokos, B. S. Perchuk, M. T. Laub, A dynamic complex of signaling proteins uses polar localization to regulate cell-fate asymmetry in *Caulobacter crescentus*. *Dev. Cell* **20**, 329–341 (2011).
 34. R. T. Wheeler, L. Shapiro, Differential localization of two histidine kinases controlling bacterial cell differentiation. *Mol. Cell* **4**, 683–694 (1999).
 35. J.-Y. Matroule, H. Lam, D. T. Burnette, C. Jacobs-Wagner, Cytokinesis monitoring during development; rapid pole-to-pole shuttling of a signaling protein by localized kinase and phosphatase in *Caulobacter*. *Cell* **118**, 579–90 (2004).
 36. A. A. Iniesta, N. J. Hillson, L. Shapiro, Cell pole-specific activation of a critical bacterial cell cycle kinase. *PNAS* **107**, 7012–7017 (2010).
 37. J. Wu, N. Ohta, J. L. Zhao, A. Newton, A novel bacterial tyrosine kinase essential for cell division and differentiation. *PNAS*. **96**, 13068–13073 (1999).
 38. T. H. Mann, L. Shapiro, Integration of cell cycle signals by multi-PAS domain kinases. *PNAS* **115**, 7166–7173 (2018).
 39. J. Wang, W. E. Moerner, L. Shapiro, A localized adaptor protein performs distinct functions at the *Caulobacter* cell poles. *PNAS* **118** (2021).
 40. A. Duerig, *et al.*, Second messenger-mediated spatiotemporal control of protein degradation regulates bacterial cell cycle progression. *Genes Dev.* **23**, 93–104 (2009).
 41. S. Ozaki, *et al.*, Activation and polar sequestration of PopA, a c-di-GMP effector protein involved in *Caulobacter crescentus* cell cycle control. *Mol. Microbiol.* **94**, 580–594 (2014).
 42. S. C. Smith, *et al.*, Cell cycle-dependent adaptor complex for ClpXP-mediated proteolysis directly integrates phosphorylation and second messenger signals. *PNAS*. **111**, 14229–14234 (2014).
 43. K. K. Joshi, M. Bergé, S. K. Radhakrishnan, P. H. Viollier, P. Chien, An adaptor hierarchy regulates proteolysis during a bacterial cell cycle. *Cell* **163**, 419–431 (2015).
 44. A. M. Perez, *et al.*, A localized complex of two protein oligomers controls the orientation of cell polarity. *MBio* **8**, 1–16 (2017).

45. G. R. Bowman, *et al.*, A Polymeric protein anchors the chromosomal origin/ParB complex at a bacterial cell pole. *Cell* **134**, 945–955 (2008).
46. P. D. Dahlberg, *et al.*, Cryogenic single-molecule fluorescence annotations for electron tomography reveal in situ organization of key proteins in *Caulobacter*. *PNAS* **117**, 13937–13944 (2020).
47. Y. E. Chen, *et al.*, Dynamics of two phosphorelays controlling cell cycle progression in *Caulobacter crescentus*. *J. Bacteriol.* **191**, 7417–7429 (2009).
48. C. Lori, *et al.*, Cyclic di-GMP acts as a cell cycle oscillator to drive chromosome replication. *Nature* **523**, 236–239 (2015).
49. A. N. Lupas, M. Gruber, The structure of α -helical coiled coils. *Adv. Protein Chem.* **70**, 37–78 (2005).
50. N. Zeytuni, R. Zarivach, Structural and functional discussion of the tetra-trico-peptide repeat, a protein interaction module. *Structure* **20**, 397–405 (2012).
51. A. K. Dunker, M. S. Cortese, P. Romero, L. M. Iakoucheva, V. N. Uversky, Flexible nets The roles of intrinsic disorder in protein interaction networks. **272**, 5129–5148 (2005).
52. P. T. McGrath, A. A. Iniesta, K. R. Ryan, L. Shapiro, H. H. McAdams, A dynamically localized protease complex and a polar specificity factor control a cell cycle master regulator. *Cell* **124**, 535–547 (2006).
53. J. A. Holmes, *et al.*, *Caulobacter* PopZ forms an intrinsically disordered hub in organizing bacterial cell poles. *PNAS* **113**, 12490–12495 (2016).
54. N. O. E. Vischer, *et al.*, Cell age dependent concentration of *Escherichia coli* divisome proteins analyzed with ImageJ and ObjectJ. *Front. Microbiol.* **6** (2015).
55. P. Aldridge, R. Paul, P. Goymer, P. Rainey, U. Jenal, Role of the GGDEF regulator PleD in polar development of *Caulobacter crescentus*. *Mol. Microbiol.* **47**, 1695–1708 (2003).
56. K. K. Joshi, C. M. Battle, P. Chien, Polar Localization Hub Protein PopZ Restrains AdaptorDependent ClpXP Proteolysis in *Caulobacter crescentus*. *J. Bacteriol.* **200** (2018).
57. S. Saurabh, A. M. Perez, C. J. Comerci, L. Shapiro, W. E. Moerner, Super-resolution microscopy and single-protein tracking in live bacteria using a genetically encoded , photostable fluoromodule. *Curr Protoc Cell Biol* **75**, 43210–43222 (2017).
58. C. Szent-gyorgyi, *et al.*, Fluorogen-activating single-chain antibodies for imaging cell surface proteins. *Nat. Biotechnol.* **26**, 235–240 (2008).
59. S. Saurabh, M. Zhang, V. R. Mann, A. M. Costello, Kinetically tunable photostability of fluorogen-activating peptide – fluorogen complexes. *Chemphyschem* **16**, 2974–2980 (2015).
60. S. Saurabh, A. M. Perez, C. J. Comerci, L. Shapiro, W. E. Moerner, Super-resolution imaging of live bacteria cells using a genetically directed, highly photostable fluoromodule. *J. Am. Chem. Soc.* **138**, 10398–10401 (2016).
61. D. Gibson, *et al.*, Enzymatic assembly of DNA molecules up to several hundred kilobases. *Nat. Methods* **6**, 343–345 (2009).
62. B. Ely, Genetics of *Caulobacter crescentus*. *Methods Enzymol.* **204**, 372–384 (1991).
63. C. A. Schneider, W. S. Rasband, K. W. Eliceiri, NIH Image to ImageJ: 25 years of Image Analysis HHS Public Access. *Nat. Methods* **9**, 671–675 (2012).

Supplemental figures

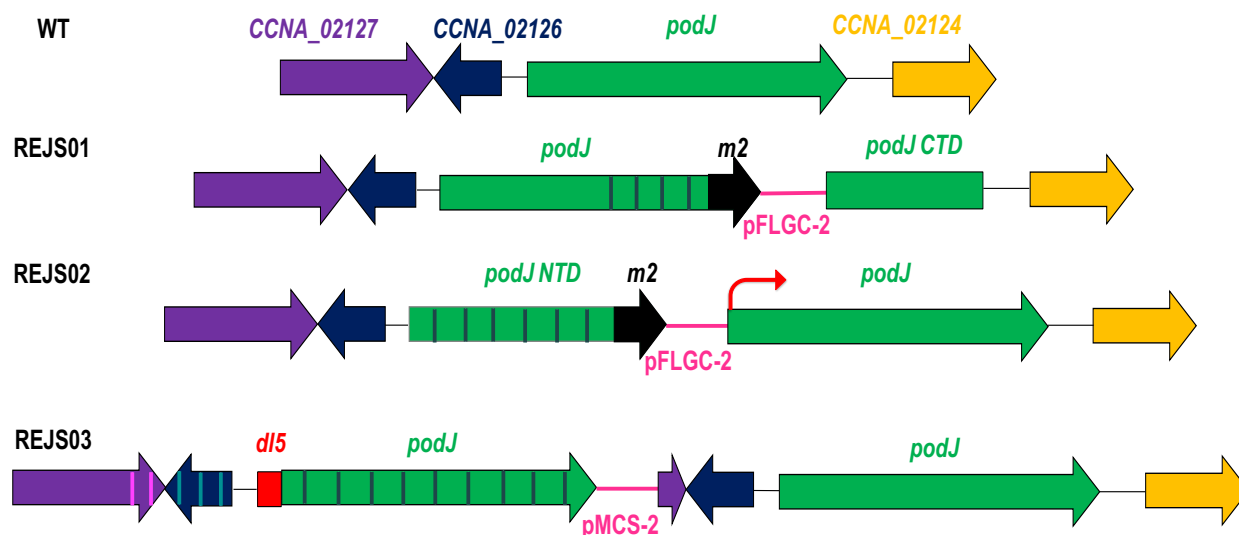


Figure S1. *PodJ* locus in wild type and merodiploid *Caulobacter* strains. REJS01, REJS02, and REJS03 strains (Table S6) were constructed by single cross over in WT cells using pREJSc-001, pREJSc-002, and pREJSc-003 integrating plasmids (Table S4). CCNA_02124 (yellow arrows) and CCNA_02126 (blue arrows) are annotated as hypothetical proteins. CCNA_02127 (purple arrows) encodes for an oxacillin resistance protein. Backbones (pFLGC-2 and pMCS-2) of the three integrating vectors are indicated with horizontal lines in magenta. *PodJ* NTD, *podJ* CTD, and *podJ* are illustrated with green color. The red square and black arrows represent *dL5* and *m2*, respectively. Recombinant regions are indicated with vertical lines. The red arrow indicates active transcription as determined by mass spectrometry analysis (Table 1) (1, 2).

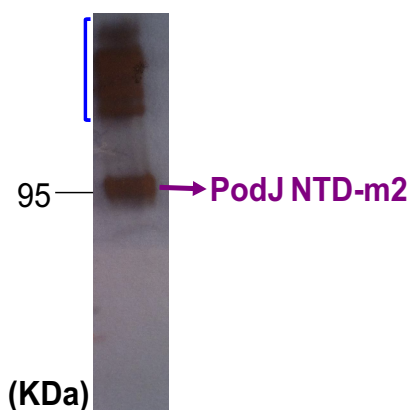


Figure S2. *PodJ* NTD-m2 forms high-molecular-weight complexes. Immunoprecipitated *PodJ* NTD-m2 was detected using an anti *PodJ*-NTD antibody. *PodJ* NTD-m2 and high molecular weight complexes are indicated with purple arrow and blue bracket, respectively. 95 KDa marker is shown at the left of the immunoblot.

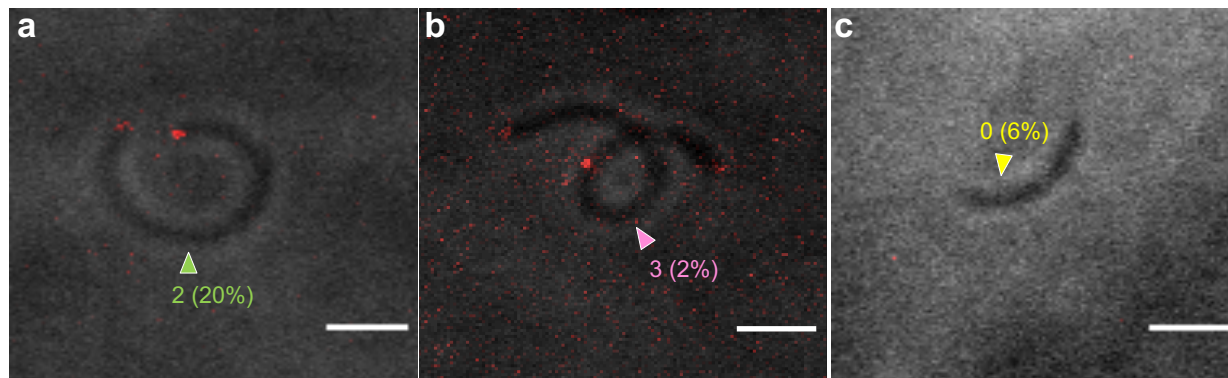


Figure. S3. PopZ is required for the asymmetrical localization of PodJ. (a-c) dL5-MG-PodJ was expressed in Δ PopZ. Cells with two, three or no foci are shown with green, magenta, and yellow arrow heads, respectively. The number of foci per cell were quantified in 100 cells of the Δ PopZ mutant. Cells were incubated with 0.1 μ M of MG for 15 minutes before imaging. (Scale bars: 2 μ m).

Supplemental tables

Table S1: Proteins that co-immunoprecipitated with PodJ-m2

Proteins	Number of peptides	Coverage (%)
Localization factor, PodJ	57	59.45
ATP synthase subunit beta, AtpD	34	71.43
OAR protein, CCNA-00974	28	40.95
Elongation factor Tu, TuF	26	58.08
Type I restrictionmodification system methylation subunit, CCNA-00656	26	51.72
Vitamin B12 receptor, CCNA-01826	23	53.54
TonB dependent receptor, CCNA-01585	23	47.04
ATP synthase subunit alpha, AtpA	22	45.88
5-methyl tetra hydropteroyl triglutamate homocysteine methyltransferase, MetE	17	26.25
TonB dependent receptor, CCNA-00214	17	38.47
NADH quinone oxidoreductase subunit D, NuoD	17	46.39
Exopolysaccharide transport family protein, CCNA-00163	16	32.75
TonB dependent outer membrane receptor, CCNA-01738	15	22.25
TonB dependent receptor, CCNA-03248	14	25.33
Adenosyl homocysteinase, AhcY	14	34.13
Protein translocase subunit, SecA	14	20.69
50S ribosomal protein L2, RplB	13	53.05
TonB dependent outer membrane receptor, CCNA-03108	13	21.04
TonB dependent receptor, CCNA-00210	13	27.15
Pyruvate dehydrogenase E1 component beta subunit, CCNA-01800	11	39.56
DNA directed RNA polymerase subunit beta R, PoB	11	12.98
Translation initiation factor IF2, InfB	10	18.53
Betabarrel assembly machine (BAM) protein, BamB	10	31.09
Succinate dehydrogenase flavoprotein subunit, CCNA-03642	10	26.22
Uncharacterized protein, CCNA-00162	9	29.86
30S ribosomal protein S3, RpsC	9	44.80
TonB accessory protein, ExbB	8	23.84
30S ribosomal protein, RpsH	8	51.51
A Ribonuclease E, RnE	8	14.03
NADH quinone oxidoreductase subunit C, NuoC	7	47.72
DEAD box RNA helicase like protein, CCNA-01546	7	18.76
Chaperone protein, DnaK	7	16.01
TonB dependent receptor, CCNA-02910	7	13.89

Chapter 2

TonB dependent receptor, CCNA-02048	7	14.88
NADH quinone oxidoreductase subunit B, NuoB	6	22.50
Esterase lipase family protein, FzeB	6	16.21
30S ribosomal protein S4, RpsD	6	33.66
Rod shapedetermining protein, MreB	6	25.36
Ribosomal protein L6, RplF	6	46.33
Sadenosylmethionine synthetase, MetK	6	25.06
NADH quinone oxidoreductase, NuoG	6	10.79
ATP dependent RNA helicase, CCNA-00878	6	17.86
ATP dependent zinc metalloprotease, FtsH	6	21.25
Outer membrane protein assembly factor, BamA	6	7.62
TonB dependent outer membrane channel, CCNA-02277	6	11.87
Elongation factor G, FusA	6	13.29
Lysozyme, SpmX	5	18.79
Outer membrane protein, CCNA-03609	5	20.20
Slayer protein, RsaA	5	9.94
Uncharacterized protein, CCNA-02205	5	24.84
Glycosyltransferase, CCNA-00466	5	11.59
30S ribosomal protein S2, RpsB	5	23.51
50S ribosomal protein L15, RplO	5	33.54
Acetylcoenzyme A carboxylase carboxyl transferase subunit alpha, AccA	5	34.37
50S ribosomal protein L22, RplV	5	51.59
30S ribosomal protein S9, RpsI	5	49.68
50S ribosomal protein L5, RplE	5	29.73
TonB dependent receptor, CCNA-00338	5	11.39
DNA directed RNA polymerase subunit alpha, RpoA	5	15.98
Uncharacterized protein, CCNA-01676	5	7.87
Threonine tRNA ligase, ThrS	5	13.13
Two component sensor histidine kinase, PhyK	5	14.46
50S ribosomal protein L4, RplD	4	32.08
30S ribosomal protein S11, RpsK	4	31.78
Protein translocase subunit, SecD	4	10.15
ATP synthase gamma chain, AtpG	4	17.53
50S ribosomal protein L28, RpmB	4	43.43
Phospho ribosyl amino imidazole succino carboxamide synthase, PurC	4	21.03
GTPase, DeR	4	8.67
ATP synthase subunit b, AtpF	4	36.69
YjgP/YjgQ family membrane permease, CCNA-01762	4	17.68
30S ribosomal protein S7, RpsG	4	24.20
30S ribosomal protein S17 R, PsQ	4	27.85

Chapter 2

Elongation factor 4, LepA	4	10.47
Aspartokinase, CCNA-00886	4	10.84
50S ribosomal protein L24, RplX	4	40.38
Sulfate/thiosulfate import ATP binding protein, CysA	4	21.53
50S ribosomal protein L19, RplS	4	27.82
30S ribosomal protein S5, RpsE	4	24.88
Acetylcoenzyme A carboxylase carboxyl transferase subunit beta, AccD	4	24.10
Membrane protease family, stomatin/prohibitinlike protein, CCNA-03485	4	27.47
30S ribosomal protein S10, RpsJ	4	46.08
TonB dependent outer membrane receptor, CCNA-01155	4	5.63
Type I restrictionmodification system specificity subunit, CCNA-00657	4	15.78
Enolase, EnO	4	18.54
30S ribosomal protein S13, RpsM	4	42.62
Probable potassium transport system protein, KuP	4	9.02
3,4 dihydroxy 2 butanone 4 phosphate synthase, RibA	4	19.50
ATP dependent RNA helicase, CCNA-01923	4	17.79
Uncharacterized protein, CCNA-02741	4	39.13
AIM24 family protein, CCNA-01172	4	26.07
Endoglucanase, CCNA-02310	4	4.64
Tryptophan halogenase, CCNA-02898	4	9.63
Ribonucleosidediphosphate reductase, CCNA-03607	4	10.37
Phosphodiesterase I/nucleotide pyrophosphatase, CCNA-01336	4	15.40
Tetratricopeptide repeat family protein, CCNA-01396	4	10.59
Cytochrome c oxidase subunit, CoxB	3	12.30
50S ribosomal protein L21, RplU	3	24.56
50S ribosomal protein L20, RplT	3	31.36
ABC transporter ATP binding protein, CCNA-03714	3	9.92
HD family metaldependent phosphohydrolase, CCNA-03892	3	23.36
30S ribosomal protein S21, RpsU	3	22.08
Isocitrate dehydrogenase [NADP], CCNA-02607	3	10.92
NADH quinone oxidoreductase chain L, NuoL	3	4.23
50S ribosomal protein L14, RplN	3	20.49
Uncharacterized protein, CCNA-00124	3	24.10
ATP dependent Clp protease ATP binding subunit, ClpX	3	8.81
50S ribosomal protein L17, RplQ	3	22.63
50S ribosomal protein L10, RplJ	3	19.77
Glyceraldehyde 3 phosphate dehydrogenase, CCNA-03358	3	16.12
Signal peptidase I, CCNA-01629	3	14.59
ExbD family protein, CCNA-00324	3	30.92
TonB dependent receptor CCNA-00028	3	7.12

Chapter 2

Protein, RecA	3	7.02
Methylaccepting chemotaxis protein, CCNA-00439	3	9.36
Type I secretion outer membrane protein, RsaFb	3	13.04
Acetyltransferase component of pyruvate dehydrogenase complex, CCNA-01803	3	13.08
Methylmalonyl CoA epimerase, CCNA-02011	3	10.07
Acetolactate synthase, CCNA-00397	3	8.40
ABC transporter ATP binding protein, CCNA-02173	3	19.68
HemY domain membrane protein, CCNA-00073	3	8.02
Short chain dehydrogenase, CCNA-01728	3	17.53
50S ribosomal protein L16, RplP	2	18.88
ATP synthase subunit delta, AtpH	2	19.57
ABC transporter, ATP binding protein, CCNA-01586	2	16.60
NADH ubiquinone oxidoreductase subunit, CCNA-03718	2	13.79
Polyprenylphosphate betaDglucosyltransferase, CCNA-02983	2	9.09
Leucyl aminopeptidase, CCNA-03032	2	7.51
NADH quinone oxidoreductase subunit I, Nuol	2	14.11
Nucleoside di-phosphate sugar epimerase, CCNA-02942	2	11.05
Cell cycle transcriptional regulator, CtrA	2	12.12
50S ribosomal protein L27, RpmA	2	22.47
Chaperonin, GroL	2	6.22
Pseudouridine synthase, CCNA-00230	2	6.07
Cytochrome b, CCNA-00506	2	8.69
Uncharacterized protein, CCNA-00582	2	14.59
MoxR like ATPase, CCNA-00601	2	7.74
Type I protein secretion ATP binding protein, RsaD	2	6.23
30S ribosomal protein S18, RpsR	2	18.48
TonB dependent receptor, CCNA-01042	2	3.85
30S ribosomal protein S6, RpsF	2	30.16
PAS family motility and cell cycle regulatory protein, MopJ	2	25.45
Protease 4, SppA	2	5.22
NAD(P) transhydrogenase subunit beta, CCNA-03412	2	5.93
C4 dicarboxylate transport protein, CCNA-00264	2	11.27
30S ribosomal protein S19, RpsS	2	20.65
Probable protein kinase, UbiB	2	5.58
Type II secretion pathway protein F, PulF	2	5.71
Aminopeptidase, CCNA-02933	2	4.55
Cbb3 type cytochrome c oxidase subunit, CcoP	2	10.76
DNA mismatch repair protein, MutL	2	3.77
LipidA disaccharide synthase, LpxB	2	8.29
Bata related transmembrane protein, CCNA-02919	2	5.21

Chapter 2

DNA recombination mediator protein A, SMF family, DprA	2	8.22
DNA directed RNA polymerase subunit beta, RpoC	2	3.08
YicC family protein, CCNA-01752	2	6.83
OAR protein, CCNA-00776	2	2.02
GT1 family glycosyl-transferase, CCNA-00469	2	13.76
Methyltransferase, CCNA-02339	2	20.47
1-acyl glycerol 3-phosphate acyltransferase, CCNA-02302	2	11.44
2-hydroxy-6-oxo-6-phenylhexa 2,4 dienoate hydrolase, CCNA-03749	2	11.00
Ribonuclease BN, CCNA-01916	2	7.62
Protein export membrane protein, SecF	1	5.30
ROS/MUCR transcriptional regulator, CCNA-01418	1	14.19
30S ribosomal protein S14, RpsN	1	12.87
ABC transporter ATPbinding protein, CCNA-03681	1	5.44
Oligopeptide transporter, CCNA-02729	1	4.65
50S ribosomal protein L23, RplW	1	12.24
Transporter, major facilitator superfamily, CCNA-01159	1	3.10
30S ribosomal protein S20, RpsT	1	13.19
Uncharacterized protein, CCNA-00375	1	9.30
GT1/WbuBlike N-acetyl-L-fucosamine transferase, CCNA-03998	1	4.03
50S ribosomal protein L3, RplC	1	4.87
Type I secretion outer membrane protein, RsaFa	1	2.66
50S ribosomal protein L11, RplK	1	8.39
Major facilitator superfamily transporter, CCNA-00025	1	4.36
30S ribosomal protein S12, RpsL	1	6.50
NADH quinone oxidoreductase chain J, NuoJ	1	7.80
MFS sugar transporter, CCNA-03894	1	5.35
Bactofilin B, BacB	1	5.56
50S ribosomal protein L13, RplM	1	7.64
TonB accessory protein, ExbD	1	15.97
Poly(3hydroxyalkanoate) depolymerase, CCNA-00890	1	4.25
TonB1 protein, TonB1	1	9.05
Autotransporter protein, CCNA-00290	1	1.66
GTP 3',8 cyclase, MoeA	1	2.87
Membrane protein insertase, YidC	1	1.14
PHB granule associated protein, phasin 2, CCNA-02242	1	8.33
Uncharacterized protein, CCNA-01784	1	13.85
YjgP/YjgQ family membrane permease, CCNA-01761	1	7.34
2-deoxyDgluconate 3-dehydrogenase, CCNA-01559	1	3.53
Uncharacterized protein, CCNA-02831	1	10.27
PAS family sensor histidine kinase, CCNA-03333	1	1.00

Chapter 2

N-succinyl arginine dihydrolase, AstB	1	6.95
YjgP/YjgQ family membrane permease, CCNA-01761	1	3.53
Porin, CCNA-02982	1	7.18
Ribonuclease D, Rnd	1	2.83
Cyclic diGMP effector protein, PopA	1	4.54
Glutathione Stransferase, CCNA-02730	1	6.51
Release factor glutamine methyltransferase, PrmC	1	2.77
Finger like domain protein, CCNA-02298	1	5.96
Myoinositol 2 dehydrogenase, IdhA	1	8.23
Putative 8-amino-7-oxononanoate synthase, BioF	1	2.34
Inositol monophosphatase family protein, CCNA-02335	1	3.96

Table S2: Proteins that co-immunoprecipitated with PodJ NTD-m2

Proteins	Number of unique peptides	Coverage (%)
Localization factor, PodJ	40	39.22
OAR protein, CCNA_00974	32	41.14
Vitamin B12 receptor, CCNA_01826	31	64.46
TonB-dependent outer membrane receptor, CCNA_01738	29	50.68
TonB-dependent receptor, CCNA_02910	29	38.00
Type I restriction-modification system methylation subunit, CCNA_00656	29	59.25
ATP synthase subunit beta, AtpD	26	60.67
TonB-dependent receptor, CCNA_01585	24	47.76
ATP synthase subunit alpha, AtpA	23	42.55
TonB-dependent receptor, CCNA_03248	18	34.05
TonB-dependent receptor, CCNA_00214	18	39.35
TonB-dependent outer membrane receptor, CCNA_03108	17	21.59
5-methyltetrahydropteroyltriglutamate--homocysteine methyltransferase, MetE	15	23.17
NADH-quinone oxidoreductase subunit D, NuoD	15	45.91
Uncharacterized protein, CCNA_00162	14	42.89
Lysozyme, SpmX	14	32.02
Elongation factor Tu, TuF	13	36.62
50S ribosomal protein L15, RpLO	12	54.04
RNA helicase-like protein, CCNA_01546	12	21.86
50S ribosomal protein L2, RpIB	12	43.01
Chaperonin, GroL	11	31.44
Exopolysaccharide transport family protein, CCNA_00163	11	20.70
GTPase, DeR	11	19.05
TonB-dependent receptor, CCNA_00210	10	16.44
Beta-barrel assembly machine (BAM) protein, BamB	10	28.99
Pseudouridine synthase, CCNA_00230	10	33.25
TonB-dependent receptor, CCNA_02048	10	18.04
50S ribosomal protein L4, RpID	9	51.89
30S ribosomal protein S4, RpsD	9	40.49
NADH-quinone oxidoreductase subunit C, NuoC	9	63.45
TonB-dependent receptor, CCNA_00028	9	16.43
Succinate dehydrogenase flavoprotein subunit, CCNA_03642	9	14.96
TonB accessory protein, ExbB	8	25.17
ATP-dependent RNA helicase, CCNA_00878	8	22.06
30S ribosomal protein S9, RpsI	8	50.32

Chapter 2

TonB-dependent outer membrane channel, CCNA_02277	8	17.46
Autotransporter protein, CCNA_00290	8	11.71
Outer membrane protein, CCNA_03609	8	29.43
Protein translocase subunit, SecA	8	11.48
30S ribosomal protein S5, RpsE	8	40.30
TonB-dependent receptor, CCNA_03023	8	14.42
Sensory transduction histidine kinase/receiver protein, CckA	7	15.63
Esterase lipase family protein, FzeB	7	23.97
Alkaline phosphatase, CCNA_01636	7	20.64
ABC transporter, ATP-binding protein, CCNA_01586	7	47.72
Acetyl-coenzyme A carboxylase carboxyl transferase subunit beta, AccD	7	24.43
Acetyl-coenzyme A carboxylase carboxyl transferase subunit alpha, AccA	6	24.06
30S ribosomal protein S7, RpsG	6	45.86
Phosphoribosylaminoimidazole-succinocarboxamide synthase, PurC	6	26.19
50S ribosomal protein L6, RplF	6	44.07
NADH-quinone oxidoreductase subunit B, NuoB	6	30.50
DNA-directed RNA polymerase subunit beta, RpoB	6	6.86
Ribosomal protein S11, RpsK	5	32.56
ATP synthase gamma chain, AtpG	5	25.09
Translation initiation factor IF-2, InfB	5	6.94
30S ribosomal protein S3, RpsC	5	26.40
Ribonuclease E, RnE	5	7.80
Aspartokinase, CCNA_00886	5	18.80
Rod shape-determining protein, MreB	5	21.04
50S ribosomal protein L16, RplP	5	30.07
30S ribosomal protein, RpsB	5	19.78
S-adenosylmethionine synthetase, MetK	5	13.51
Outer membrane protein assembly factor, BamA	5	7.88
S-layer protein, RsaA	4	6.73
50S ribosomal protein L10, RplJ	4	36.63
50S ribosomal protein L24, RplX	4	46.15
Type I secretion outer membrane protein, RsaFb	4	15.11
30S ribosomal protein S10, RpsJ	4	33.33
3-hydroxybutyryl-CoA dehydrogenase, CCNA_00752	4	17.12
50S ribosomal protein L21, RplU	4	28.65
30S ribosomal protein, RpsU	4	22.08
Outer membrane efflux protein, CCNA_00849	4	14.35
Type I restriction-modification system specificity subunit, CCNA_00657	4	10.00
Peptidyl-prolyl cis-trans isomerase, CCNA_01971	4	8.56

Chapter 2

50S ribosomal protein L17, RplQ	4	24.82
ATP-dependent Clp protease ATP-binding subunit, ClpX	4	12.38
30S ribosomal protein S20, RpsT	4	29.67
30S ribosomal protein, RpsF	4	41.27
TonB1 protein, TonB1	4	27.98
Acetolactate synthase, CCNA_02185	4	7.32
HD family metal-dependent phosphohydrolase, CCNA_03892	4	25.70
Elongation factor G, FusA	4	9.68
Type I secretion adaptor protein, RsaE	4	14.68
30S ribosomal protein S17, RpsQ	4	35.44
50S ribosomal protein L5, RplE	3	20.00
50S ribosomal protein L20, RplT	3	31.36
Cytochrome c oxidase subunit 2, CoxB	3	15.86
NAD(P) transhydrogenase subunit beta, CCNA_03412	3	8.26
ATP synthase subunit delta, AtpH	3	23.37
30S ribosomal protein, RpsN	3	29.70
ATP synthase subunit b, AtpF	3	18.64
Cell cycle transcriptional regulator, CtrA	3	16.88
Ribosomal protein L11, RplK	3	21.68
30S ribosomal protein S13, RpsM	3	22.95
TonB-dependent outer membrane receptor, CCNA_01155	3	3.58
DNA-directed RNA polymerase subunit alpha, RpoA	3	15.38
50S ribosomal protein L22, RplV	3	41.27
NADH-quinone oxidoreductase, NuoG	3	6.41
50S ribosomal protein L19, RplS	3	27.82
Sulfate/thiosulfate import ATP-binding protein, CysA	3	13.57
Nucleoside-diphosphate-sugar epimerase, CCNA_02942	3	11.05
RND family efflux transporter, MFP subunit, CCNA_03300	3	12.74
Membrane protease family, stomatin/prohibitin-like protein, CCNA_03485	3	16.98
FAD/FMN-containing dehydrogenase, CCNA_03500	3	9.59
Cytochrome b, CCNA_00506	3	10.33
Pyruvate dehydrogenase E1 component beta subunit, CCNA_01800	3	10.22
30S ribosomal protein S1, CCNA_03702	3	5.98
RecA Protein, RecA	3	11.52
YjgP/YjgQ family membrane permease, CCNA_01762	3	8.71
Protein translocase subunit, SecD	3	7.52
50S ribosomal protein L3, RplC	3	24.34
Metal-dependent hydrolase, CCNA_01406	3	11.93
Uncharacterized protein, CCNA_01676	3	2.48
30S ribosomal protein S12, RpsL	3	21.95

Chapter 2

Phosphodiesterase I/nucleotide pyrophosphatase, CCNA_01336	3	14.18
ABC transporter ATP-binding protein, CCNA_00188	3	15.00
Cation/multidrug efflux pump, AcrB	3	3.75
3-dehydroquinate synthase, AroB	3	8.65
NADH-ubiquinone oxidoreductase subunit, CCNA_03718	2	10.66
50S ribosomal protein L28, RpmB	2	31.31
50S ribosomal protein L33, RpmG	2	27.27
NADH-quinone oxidoreductase subunit I, Nuol	2	15.34
Stomatin/prohibitin-related protein, CCNA_02619	2	8.31
Protein-export membrane protein, SecF	2	10.90
30S ribosomal protein S8, RpsH	2	18.94
MoxR-like ATPase, CCNA_00601	2	9.60
TolQ protein, TolQ	2	12.07
Protease, SppA	2	6.06
Uncharacterized protein, CCNA_02741	2	14.78
Amino acid permease, CCNA_01242	2	5.84
ATP-dependent zinc metalloprotease, FtsH	2	6.55
50S ribosomal protein L27, RpmA	2	22.47
Ribosomal protein L23, RplW	2	32.65
30S ribosomal protein S19, RpsS	2	11.96
50S ribosomal protein L36, RpmJ	2	21.95
UDP-N-acetylglucosamine 4,6-dehydratase, CCNA_00233	2	6.96
Membrane protein insertase, YidC	2	3.90
Enolase, EnO	2	8.69
Histidine protein kinase, DivJ	2	4.62
2-polyprenyl-6-methoxyphenol hydroxylase, CCNA_00106	2	6.89
Phosphatidylglycerophosphate synthase, CCNA_01217	2	5.87
Outer membrane pilus secretion, CpaC	2	3.75
ABC transporter ATP-binding protein, CCNA_03681	2	8.84
CarD-family transcriptional regulator, CCNA_00690	2	17.96
Methyltransferase, CCNA_01415	2	9.06
Cobyric acid synthase, CobQ	2	6.40
Phospho-2-dehydro-3-deoxyheptonate aldolase, CCNA_02385	2	5.66
Probable potassium transport system protein, KuP	2	3.16
Uncharacterized protein, CCNA_00375	2	13.95
Metallophosphatase related protein, CCNA_03671	2	11.83
Uncharacterized protein, CCNA_00124	2	15.38
Aminopeptidase, CCNA_02933	2	4.03
GTPase, ErA	2	6.65
Pole-organizing protein, PopZ	2	11.86

Chapter 2

Uncharacterized protein, CCNA_02527	2	7.95
Conserved hypothetical membrane protein, CCNA_00605	2	9.92
Peptidyl-tRNA hydrolase family protein, CCNA_01272	2	14.69
Ferritin superfamily protein, CCNA_00592	2	7.61
PAS-containing EAL phosphodiesterase, CCNA_01140	2	4.49
LPS-assembly protein, LptD	2	4.57
Uncharacterized protein, CCNA_02160	2	17.16
Uncharacterized protein, CCNA_02219	2	12.60
Cys-tRNA(Pro)/Cys-tRNA(Cys) deacylase, CCNA_01014	2	15.19
Uncharacterized protein, CCNA_00729	2	8.29
Methylmalonyl-CoA mutase alpha subunit, CCNA_02459	2	3.36
MarR-family transcriptional regulator, CCNA_00682	2	15.79
PurR-family transcriptional regulator, CCNA_00609	2	8.62
Proton/sodium-glutamate symport protein, CCNA_01161	1	3.79
Uncharacterized protein, CCNA_02831	1	10.27
Uncharacterized protein, CCNA_01026	1	7.11
AIM24 family protein, CCNA_01172	1	4.64
50S ribosomal protein L14, RplN	1	10.66
Protein-export protein, SecB	1	8.59
C4-dicarboxylate transport protein, CCNA_00264	1	4.08
TonB-dependent receptor, CCNA_01042	1	1.56
NADH-quinone oxidoreductase chain J, NuoJ	1	7.80
Adenosylhomocysteinase, AhcY	1	3.46
Methylmalonic acid semialdehyde dehydrogenase, CCNA_02357	1	2.81
50S ribosomal protein L13, RplM	1	8.28
Oxygen sensory histidine kinase, FixL	1	3.03
50S ribosomal protein L1, RplA	1	5.68
Uncharacterized protein, CCNA_03674	1	17.54
ABC transporter ATP-binding protein, CCNA_03714	1	4.37
ExbD-family protein, CCNA_00324	1	5.92
Electron transfer flavoprotein-ubiquinone oxidoreductase, FzeA	1	3.05
Imidazolonepropionase related amidohydrolase, CCNA_02051	1	2.89
Polyprenyl-phosphate beta-D-glucosyltransferase, CCNA_02983	1	4.85
Bactofilin A, BacA	1	10.56
Glyceraldehyde 3-phosphate dehydrogenase, CCNA_03358	1	3.58
Two-component sensor histidine kinase, DivL	1	1.95
GTP-binding protein TypA/BipA, CCNA_00778	1	2.46
Putative pyruvate, phosphate dikinase regulatory protein, CCNA_00001	1	5.65
Uncharacterized protein, CCNA_00478	1	7.76
PAS-family motility and cell cycle regulatory protein, MopJ	1	9.70

Chapter 2

TonB accessory protein, ExbD	1	15.97
Cell wall hydrolase family protein, CCNA_02965	1	6.05
Trigger factor, TiG	1	3.10
UDP-galactopyranose mutase, CCNA_00465	1	4.59
NADH-quinone oxidoreductase chain L, NuoL	1	2.92
Transporter, major facilitator superfamily, CCNA_01159	1	3.10
RNA polymerase sigma factor, RpoD	1	2.61
Transcription termination factor, Rho	1	3.14
Peptidoglycan-associated lipoprotein, PaL	1	5.85
Adenylyl-sulfate kinase, CysC	1	2.20
Uncharacterized protein, CCNA_01081	1	3.47
Thiol:disulfide interchange protein DsbA, CCNA_00379	1	11.27
Phosphoenolpyruvate carboxylase, PpC	1	2.09
D-3-phosphoglycerate dehydrogenase, CCNA_03322	1	3.04
Outer membrane protein oprM, CCNA_03299	1	2.98
Uncharacterized protein, CCNA_00698	1	8.48
Imidazolonepropionase related amidohydrolase, CCNA_02050	1	4.09
Type I secretion outer membrane protein, RsaFa	1	2.66
Glycosyltransferase, CCNA_01065	1	5.51
Sodium export permease protein, CCNA_03407	1	3.57
Lipoprotein, CCNA_02747	1	7.04
ABC membrane transporter, periplasmic component, CCNA_02405	1	5.13
Uncharacterized protein, CCNA_00822	1	7.02
Uncharacterized protein, CCNA_02343	1	3.10
ABC transporter ATP-binding protein, CCNA_02231	1	1.62
Trypsin-like peptidase, CCNA_00135	1	3.97
N-succinylglutamate 5-semialdehyde dehydrogenase, AstD	1	4.54
YjgP/YjgQ family membrane permease, CCNA_01761	1	3.53
Probable cytosol aminopeptidase, PepA	1	3.25
Phosphate regulon response regulator, PhoB	1	4.35
Tyrosine--tRNA ligase, TyrS	1	4.06
ABC transporter ATP-binding protein, CCNA_03483	1	4.78
Pirin, CCNA_00514	1	4.71
Short chain dehydrogenase, CCNA_01345	1	2.69
Cbb3-type cytochrome C oxidase, subunit III, CCNA_02882	1	12.03
Xylonolactonase, XylC	1	3.46
Uncharacterized protein, CCNA_02433	1	31.25
Uncharacterized protein, CCNA_03308	1	5.79
Translation initiation factor IF-3, InfC	1	7.51
Cation/multidrug efflux pump, AcrB5	1	0.98

Chapter 2

Uncharacterized protein, CCNA_00909	1	3.27
Chorismate mutase-family protein, CCNA_02305	1	7.89
ABC transporter ATP-binding protein, CCNA_02173	1	6.83
Acetyl-CoA acetyltransferase, CCNA_00544	1	5.88
Phosphoenolpyruvate-protein phosphotransferase/phosphocarrier protein HPr/PTS system, glucose-specific IIA subunit, CCNA_00571	1	1.37
BK6BK6 Sulfite reductase (NADPH) flavoprotein alpha-component, CCNA_03159	1	2.38
Acyl-acyl carrier protein synthetase, CCNA_01807	1	2.32
Ketol-acid reductoisomerase (NADP(+)), IlvC	1	3.24
Cation/multidrug efflux pump, AcrB2	1	1.43
Zinc metalloprotease, CCNA_03619	1	1.56
Two component sensor histidine kinase, CCNA_01352	1	3.13
Type II secretion pathway protein L, CCNA_00180	1	2.99

Table S3: Proteins that co-immunoprecipitated with CtrA-m2

Proteins	Number of unique peptides	Coverage (%)
OAR protein, CCNA-00974	36	46.73
Cell cycle transcriptional regulator, CtrA	33	79.65
Vitamin B12 receptor, CCNA-01826	31	68.92
ATP synthase subunit beta, AtpD	28	64.56
Elongation factor Tu, TuF	28	60.10
Protein translocase subunit, SecA	26	39.65
5-methyltetrahydropteroyltriglutamate--homocysteine methyltransferase, MetE	24	40.93
ATP synthase subunit alpha, AtpA	22	45.49
30S ribosomal protein S1, CCNA-03702	22	42.53
TonB-dependent receptor, CCNA-01585	21	45.45
Translation initiation factor IF-2, InfB	21	31.52
Elongation factor G, FusA	20	45.81
TonB-dependent receptor, CCNA-00214	20	41.26
Type I restriction-modification system methylation subunit, CCNA-00656	18	47.46
30S ribosomal protein S4, RpsD	16	55.61
TonB-dependent outer membrane receptor, CCNA-01738	15	26.95
Ribosomal protein L2, RplB	14	55.56
30S ribosomal protein S2, RpsB	13	54.48
Beta-barrel assembly machine (BAM) protein, BamB	13	44.33
TonB-dependent receptor, CCNA-00210	13	23.04
NADH-quinone oxidoreductase subunit D, NuoD	13	41.35
ATP-dependent RNA helicase, CCNA-01923	13	40.43
60 kDa chaperonin, GroL	12	32.54
Exopolysaccharide transport family protein, CCNA-00163	12	25.58
50S ribosomal protein L4, RplD	11	56.13
Uncharacterized protein, CCNA-00162	11	36.26
Ribosomal protein S3, RpsC	11	46.40
ATP-dependent RNA helicase, CCNA-00878	11	29.83
50S ribosomal protein L17, RplQ	11	56.20
TonB-dependent receptor, CCNA-02048	11	21.90
DEAD-box RNA helicase-like protein, CCNA-01546	11	22.27
Protein translocase subunit, SecD	11	28.01
Adenosyl homocysteinase, AhcY	10	25.05
50S ribosomal protein L15, RplO	10	44.72
30S ribosomal protein S7, RpsG	10	61.15
DNA-directed RNA polymerase subunit beta, RpoB	10	14.38

Chapter 2

TonB-dependent receptor, CCNA-02910	9	15.02
Acetyl-coenzyme A carboxylase carboxyl transferase subunit alpha, AccA	9	38.12
TonB-dependent outer membrane receptor, CCNA-01155	9	15.15
TonB-dependent outer membrane receptor, CCNA-03108	9	13.27
Ribonuclease E, RnE	9	14.37
50S ribosomal protein L5, RplE	9	39.46
Nitrogen assimilation regulatory protein, NtrC	9	21.56
NADH-quinone oxidoreductase, NuoG	9	20.55
TonB-dependent outer membrane channel, CCNA-02277	9	19.24
NAD-specific glutamate dehydrogenase, GdhZ	9	7.16
ATP-dependent Clp protease ATP-binding subunit, ClpX	8	23.57
NADH-quinone oxidoreductase subunit C, NuoC	8	57.36
D-3-phosphoglycerate dehydrogenase, CCNA-03322	8	22.24
TonB-dependent receptor, CCNA-03248	8	15.89
30S ribosomal protein S9, RpsI	8	50.96
Outer membrane protein assembly factor, BamA	8	12.83
TonB-dependent receptor, CCNA-00028	8	13.07
Multimodular transpeptidase-transglycosylase, PbpX	8	15.77
Peptidase, M16 family, CCNA-02721	8	13.52
DNA-directed RNA polymerase subunit beta', RpoC	8	7.59
Methylenetetrahydrofolate--tRNA-(uracil-5-)-methyltransferase, TrmFO	8	31.65
Esterase lipase family protein, FzeB	7	18.95
Signal recognition particle protein, SrP	7	15.94
NADH-ubiquinone oxidoreductase subunit, CCNA-03718	7	38.24
Rod shape-determining protein, MreB	7	21.04
50S ribosomal protein L1, RplA	7	30.13
30S ribosomal protein S5, RpsE	7	38.81
Glycosyltransferase, CCNA-00466	7	15.70
ABC transporter ATP-binding protein, CCNA-02231	7	12.43
Autotransporter protein, CCNA-00290	7	10.14
50S ribosomal protein L6, RplF	7	50.28
30S ribosomal protein S13, RpsM	7	50.00
Arginine biosynthesis bifunctional protein, ArgJ	7	18.50
Chromosomal replication initiator protein, DnaA	7	21.63
C8I6A0A0H3C8I6 Uncharacterized protein, CCNA-01676	7	8.16
Phosphoribosylaminoimidazole-succinocarboxamide synthase, PurC	6	26.59
ABC transporter, ATP-binding protein, CCNA-01586	6	38.17
Elongation factor Ts, TsF	6	25.32
2-isopropylmalate synthase, LeuA	6	19.85
50S ribosomal protein L10, RplJ	6	40.70

Chapter 2

Outer membrane protein, CCNA-03609	6	23.44
AIM24 family protein, CCNA-01172	6	33.57
MoxR-like ATPase, CCNA-00601	6	28.17
3,4-dihydroxy-2-butanone 4-phosphate synthase, RibA	6	28.25
NADH-quinone oxidoreductase subunit B, NuoB	6	46.50
GTP-binding protein TypA/BipA, CCNA-00778	6	14.43
RecA Protein, RecA	6	26.12
50S ribosomal protein L3, RplC	6	27.34
Adenylyl-sulfate kinase, CysC	6	13.54
Localization factor, PodJ	6	9.86
Transcription termination/antitermination protein, NusA	6	17.15
DNA topoisomerase 1, TopA	6	11.57
Acetyl esterase, CCNA-00810	6	25.79
Urea carboxylase, CCNA-01905	6	7.62
Threonine--tRNA ligase, ThrS	6	10.23
S-layer protein, RsaA	5	9.94
Elongation factor 4, LepA	5	12.96
Trigger factor, TiG	5	18.81
S-adenosylmethionine synthetase, MetK	5	16.71
Ribosomal protein S8, RpsH	5	51.51
50S ribosomal protein L22, RplV	5	49.21
GT1-family glycosyltransferase, CCNA-00469	5	14.99
Ribosomal protein L9, RplI	5	36.60
50S ribosomal protein L16, RplP	5	32.17
Electron transfer flavoprotein beta subunit, CCNA-00764	5	33.87
Acetyl-coenzyme A carboxylase carboxyl transferase subunit beta, AccD	5	19.87
Aspartokinase, CCNA-00886	5	17.59
TonB accessory protein, ExbB	5	20.20
Methylenetetrahydrofolate reductase, CCNA-02224	5	21.02
Aminotransferase, CCNA-01446	5	17.98
Protease 4, SppA	5	12.12
Succinate dehydrogenase flavoprotein subunit, CCNA-03642	5	10.59
50S ribosomal protein L24, RplX	5	34.62
DNA gyrase subunit B, GyrB	5	8.32
GDP-mannose 4,6-dehydratase, GmD	5	24.86
Iron-sulfur cluster carrier protein, CCNA-02180	5	21.04
ATP-dependent zinc metalloprotease, FtsH	5	7.35
Cyclic di-GMP effector protein, PopA	5	18.37
Dihydrolipoyllysine-residue succinyltransferase component of 2-oxoglutarate dehydrogenase complex, OdhB	5	13.93
DNA-directed RNA polymerase subunit alpha, RpoA	5	21.89

Chapter 2

Two-component response regulator, ChvI	5	33.19
Sensory transduction protein kinase, CenK	5	11.38
DNA modification methyltransferase-related protein, CCNA-00869	5	8.63
Flagellin, CCNA-03071	5	19.81
30S ribosomal protein S11 RpsK	4	31.78
Ribosomal protein L20, RplT	4	31.36
30S ribosomal protein S6, RpsF	4	41.27
50S ribosomal protein L21, RplU	4	28.65
GTPase, DeR	4	7.99
50S ribosomal protein L13, RplM	4	21.02
Chemotaxis response regulator protein-glutamate methyltransferase, CheB	4	18.90
Cytochrome b, CCNA-00506	4	14.08
50S ribosomal protein L19, RplS	4	27.82
Pseudouridine synthase, CCNA-00230	4	19.17
Ribosome-binding ATPase, YchF	4	13.93
50S ribosomal protein L14, RplN	4	39.34
Cytochrome c oxidase subunit 2, CoxB	4	17.80
30S ribosomal protein S21, RpsU	4	22.08
Uncharacterized protein, CCNA-02205	4	23.90
ABC transporter ATP-binding protein, CCNA-03714	4	21.03
AsnC-family transcriptional regulator, CCNA-03281	4	32.73
Protein-export membrane protein, SecF	4	13.08
ATP synthase gamma chain, AtpG	4	16.84
ABC-type sulfate transport system, periplasmic component, CCNA-00288	4	17.48
Anti-anti sigma factor/receiver protein, PhyR	4	18.42
Succinate--CoA ligase [ADP-forming] subunit beta, SucC	4	18.80
Cell division protein, FtsZ	4	12.99
Cobyric acid synthase, CobQ	4	16.74
Ribonucleoside-diphosphate reductase, CCNA-03607	4	9.25
UDP-N-acetylglucosamine 1-carboxyvinyltransferase, MurA	4	19.58
Acetoacetyl-CoA reductase, CCNA-00545	4	20.00
Pyruvate dehydrogenase E1 component beta subunit, CCNA-01800	4	13.78
Gamma-glutamyl phosphate reductase, ProA	4	9.67
Phospho-2-dehydro-3-deoxyheptonate aldolase, CCNA-02385	4	12.64
TonB1 protein, TonB1	4	26.75
Peptidyl-prolyl cis-trans isomerase, CCNA-01971	4	13.76
DNA recombination-mediator protein A, SMF family, DprA	4	12.05
ATP-dependent clp protease ATP-binding subunit, ClpA	4	8.89
ADP-heptose-LPS heptosyltransferase, CCNA-01103	4	23.22
Acylamino-acid-releasing enzyme, CCNA-03355	4	10.89

Chapter 2

Alanine dehydrogenase, CCNA-03689	4	20.54
DegP/HtrA-family serine protease, CCNA-02846	4	13.96
Ubiquinone/menaquinone biosynthesis C-methyltransferase, UbiE	4	28.97
TonB-dependent maltose outer membrane transporter, MalA	4	7.82
1-deoxy-D-xylulose-5-phosphate synthase, DxS	4	6.41
Glycine--tRNA ligase beta subunit, GlyS	4	9.83
3-oxoadipate enol-lactonase/4-carboxymuconolactone decarboxylase, CCNA-02494	4	19.59
Aldo/keto reductase family protein, CCNA-03097	4	16.82
Aminopeptidase, CCNA-02933	4	7.01
ABC transporter ATP-binding cassette domain protein, CCNA-03389	4	18.01
Aconitate hydratase, AcnA	4	6.15
DNA ligase, LigA	4	5.36
30S ribosomal protein S10, RpsJ	3	27.45
50S ribosomal protein L11 RplK	3	24.48
ArsR family/SAM-dependent transcriptional regulator, CCNA-02225	3	15.08
Ribosomal protein S18, RpsR	3	43.48
Rubrum transdehydrogenase NAD-binding, CCNA-03414	3	11.05
30S ribosomal protein S16, RpsP	3	21.82
50S ribosomal protein L33, RpmG	3	30.91
Chaperone protein, DnaK	3	6.97
Transcription termination/antitermination protein, NusG	3	19.46
30S ribosomal protein S12, RpsL	3	15.45
Multidrug resistance efflux pump, CCNA-02174	3	21.86
Metal-dependent hydrolase, CCNA-01406	3	12.28
Uncharacterized protein, CCNA-01026	3	22.59
Biotin carboxylase, CCNA-01961	3	10.49
Glucose-6-phosphate 1-dehydrogenase, ZwF	3	14.78
50S ribosomal protein L27, RpmA	3	35.95
YjgP/YjgQ family membrane permease, CCNA-01762	3	14.51
Short chain dehydrogenase, CCNA-01728	3	14.34
RNA polymerase sigma factor, RpoD	3	6.44
UDP-N-acetylglucosamine--N-acetylmuramyl-(pentapeptide) pyrophosphoryl-undecaprenol N-acetylglucosamine transferase, MurG	3	12.74
Type I secretion outer membrane protein, RsaFa	3	9.49
Amino acid permease, CCNA-01242	3	12.43
UDP-glucose 6-dehydrogenase, CCNA-02465	3	9.43
Signal peptidase, CCNA-01629	3	16.37
Uridylate kinase, PyrH	3	17.89
GntR-family transcriptional regulator, CCNA-02744	3	21.85
Probable GTP-binding protein, EngB	3	18.34

Chapter 2

Putrescine-binding periplasmic protein CCNA-03239	3	12.77
3-hydroxybutyryl-CoA dehydrogenase, CCNA-00752	3	20.55
Acylamino-acid-releasing enzyme, CCNA-03839	3	9.60
DNA mismatch repair protein, MutL	3	5.65
Thiol:disulfide interchange protein DsbA, CCNA-00378	3	12.87
Isoprenyl transferase, CCNA-01996	3	12.36
TonB-dependent receptor, CCNA-01194	3	5.14
TonB-dependent receptor protein, CCNA-00224	3	8.08
Ketol-acid reductoisomerase (NADP(+)), IlvC	3	15.63
Glucokinase, GIK	3	18.73
Uncharacterized protein, CCNA-00519	3	27.65
C9H0A0A0H3C9H0 FeS assembly SUF system protein, CCNA-01935	3	33.90
C3L7A0A0H3C3L7 Major facilitator superfamily transporter, CCNA-00025	3	12.18
Type I secretion outer membrane protein, RsaFb	3	13.87
Single-stranded-DNA-specific exonuclease, RecJ	3	6.27
UvrABC system protein C, UvrC	3	5.62
Ferredoxin-NADP reductase, CCNA-03314	3	15.16
Uncharacterized protein, CCNA-02093	3	6.67
Class II aldolase and Adducin protein, CCNA-01259	3	7.39
ATP synthase subunit b, AtpF	2	23.08
50S ribosomal protein L23, RplW	2	25.51
ABC transporter ATP-binding protein, CCNA-03681	2	9.18
Uncharacterized protein, CCNA-02207	2	7.59
Ribosome-associated factor Y, CCNA-03711	2	9.62
Sulfate/thiosulfate import ATP-binding protein, CysA	2	13.27
ATPase, CCNA-03646	2	7.80
Type I secretion adaptor protein, RsaE	2	4.82
Chemotaxis receiver domain protein cheYII, CCNA-00446	2	14.73
50S ribosomal protein L30, RpmD	2	32.79
NADH-quinone oxidoreductase chain L, NuoL	2	3.94
ATP-dependent protease ATPase subunit, HslU	2	5.35
Transcription termination factor, Rho	2	5.87
4D8RS19 30S ribosomal protein S19, RpsS	2	23.91
ATP synthase subunit delta, AtpH	2	19.57
30S ribosomal protein S17, RpsQ	2	26.58
ABC transporter ATP-binding protein, CCNA-00188	2	14.69
AAA-family response regulator, FibD	2	8.35
GTPase Obg/CgtA, CgtA	2	12.71
30S ribosomal protein S20, RpsT	2	21.98
Peptidoglycan binding endopeptidase, DipM	2	4.76

Chapter 2

Acyl-CoA dehydrogenase, CCNA-02413	2	6.46
Two-component receiver protein, SpdR	2	12.97
NAD(P) transhydrogenase subunit beta, CCNA-03412	2	7.63
Photosensory histidine protein kinase, LovK	2	4.62
Enolase, EnO	2	8.22
Gluconate 2-dehydrogenase/glyoxylate reductase/hydroxypyruvate reductase, CCNA-03838	2	9.76
Dihydrolipoyl dehydrogenase, CCNA-01805	2	7.08
CsgG-related curli protein, CCNA-01766	2	15.71
Aminotransferase, CCNA-01603	2	7.75
Aspartate-semialdehyde dehydrogenase, AsD	2	7.02
Uncharacterized protein, CCNA-01303	2	17.56
Riboflavin-specific deaminase family protein, CCNA-00929	2	5.74
Uncharacterized protein, CCNA-00582	2	9.19
Stomatin/prohibitin-related protein, CCNA-02619	2	7.31
Ribose-phosphate pyrophosphokinase, PrS	2	11.54
Trans-isoprenyl diphosphate synthase, CCNA-02198	2	8.93
Dihydrolipoyl dehydrogenase, CCNA-00346	2	6.44
3-isopropylmalate dehydratase large subunit, LeuC	2	5.01
Phosphatidylglycerophosphate synthase, CCNA-01217	2	5.87
Phosphoenolpyruvate carboxylase, PpC	2	3.85
Electron transfer flavoprotein alpha subunit, CCNA-00763	2	14.38
GT1/WbuB-like N-acetyl-L-fucosamine transferase, CCNA-03998	2	12.80
Acetyltransferase component of pyruvate dehydrogenase complex, CCNA-01803	2	9.81
Type II secretion pathway protein F, PulF	2	8.68
Membrane protein insertase, YidC	2	2.11
Uncharacterized protein, CCNA-03557	2	6.22
Membrane lipoprotein, CCNA-02406	2	16.67
Peptide deformylase, DeF	2	30.64
Thiol:disulfide interchange protein DsbA, CCNA-00379	2	25.00
AAA-family ATPase, CCNA-02917	2	8.36
AsnC-family transcriptional regulator, CCNA-03688	2	7.01
Peptide methionine sulfoxide reductase, MsrA	2	17.05
Cell wall hydrolase family protein, CCNA-02965	2	11.14
NAD/NADH-dependent eicosanoid dehydrogenase, CCNA-02095	2	9.38
GTP 3',8-cyclase, MoaA	2	8.60
Uncharacterized protein, CCNA-03937	2	13.11
Uncharacterized protein, CCNA-02939	2	15.25
Pole-organizing protein, PopZ	2	21.47
Two-component sensor histidine kinase, PhyK	2	4.59

Chapter 2

Outer membrane efflux protein, CCNA-00849	2	10.06
50S ribosomal protein L7/L12, RplL	1	12.60
C4-dicarboxylate transport protein, CCNA-00264	1	4.08
30S ribosomal protein S14, RpsN	1	12.87
Tyrosine--tRNA ligase, TyrS	1	3.10
Phosphate import ATP-binding protein, PstB	1	5.47
LptE superfamily protein, CCNA-03866	1	10.84
50S ribosomal protein L28, RpmB	1	11.11
NADH-quinone oxidoreductase subunit I, Nuol	1	9.82
Proton/sodium-glutamate symport protein, CCNA-01161	1	3.12
Peptidoglycan-associated lipoprotein, PaL	1	5.85
PAS-family motility and cell cycle regulatory protein, MopJ	1	9.70
Probable chemoreceptor glutamine deamidase, CheD	1	6.42
SH3 domain-containing cell surface protein, CCNA-00359	1	6.42
dATP pyrophosphohydrolase, CCNA-01212	1	4.17
Cytochrome C1, CCNA-00507	1	2.85
Acyl carrier protein, AcpP	1	15.38
Translation initiation factor IF-3, InfC	1	5.20
Peroxiredoxin, CCNA-03505	1	6.87
Glyceraldehyde 3-phosphate dehydrogenase, CCNA-03358	1	2.99
Phosphate-specific transport system accessory protein, PhoU	1	6.52
S-adenosylmethionine-dependent methyltransferase, CCNA-00065	1	3.50
Esterase lipase Family protein, CCNA-00388	1	5.46
Uncharacterized protein, CCNA-03773	1	3.58
Quinone oxidoreductase, CCNA-00809	1	4.53
Mitochondrial-type Fe-S cluster assembly protein NFU, CCNA-00060	1	6.32
50S ribosomal protein L36, RpmJ	1	19.51
Probable potassium transport system protein, KuP	1	1.95
ExbD-family protein, CCNA-00324	1	5.92
50S ribosomal protein L32, RpmF	1	23.33
2-dehydropantoate 2-reductase, CCNA-00262	1	6.55
Chemotaxis protein CheW, CCNA-00803	1	7.28
Phosphate regulon response regulator, PhoB	1	4.35
CarD-family transcriptional regulator, CCNA-00690	1	12.57
Transporter, major facilitator superfamily, CCNA-01159	1	3.10
Lipoprotein, CCNA-02747	1	7.04
Protein CicA, CicA	1	5.41
30S ribosomal protein S15, RpsO	1	7.87
Glutathione S-transferase, CCNA-01376	1	5.13
Abi superfamily/CAAX amino terminal protease, CCNA-03885	1	4.63

Chapter 2

50S ribosomal protein L35, RpmI	1	10.61
50S ribosomal protein L34, RpmH	1	15.91
Uncharacterized protein, CCNA-00124	1	8.21
Uncharacterized protein, CCNA-01784	1	13.85
Bifunctional protein HldE, RfaE	1	2.90
CBV1A0A0H3CBV1 Acetyl ornithine aminotransferase, CCNA-03233	1	1.71
Conserved hypothetical membrane protein, CCNA-01724	1	4.00
C8H3A0A0H3C8H3 Putative hexuronate transporter, major facilitator superfamily, CCNA-01039	1	2.97
Uncharacterized protein, CCNA-01632	1	5.88
N-succinylarginine dihydrolase, AstB	1	6.95
Uncharacterized protein, CCNA-02722	1	8.41
Uncharacterized protein, CCNA-03769	1	5.95
SpsG-related polysaccharide biosynthesis protein, FlmD	1	5.78

Table S4: Plasmids

Plasmid	Description	Backbone	Source
pMCS-C2	Integrating plasmid	pMCS-C2	(1)
pFLAG-C2	Integrating plasmid	pFLAG-C2	(1)
pREJSc-001	<i>podJ::podJ-m2</i>	pFLAG-C2	This study
pREJSc-002	<i>podJ::podJ NTD-m2</i>	pFLAG-C2	This study
pREJSc-003	<i>podJ::dL5-podJ</i>	pMCS-C2	This study
pKT25	Replicating plasmid	pKT25	(3)
pUT18	Replicating plasmid	pUT18	(3)
pUT18-C	Replicating plasmid	pUT18-C	(3)
pKT25-Zip	Replicating plasmid	pKT25-Zip	(3)
pUT18-Zip	Replicating plasmid	pUT18-Zip	(3)
pREJSc-004	<i>Plac::T25-podJ</i>	pKT25	This study
pREJSc-005	<i>Plac::T18-pleC</i>	pUT18-C	This study
pREJSc-006	<i>Plac::T18-divL</i>	pUT18-C	This study
pREJSc-007	<i>Plac::T18-cckA</i>	pUT18-C	This study
pJW211	<i>Plac::T18-popZ</i>	pUT18-C	(4)
pJW199	<i>Plac::T18-popA</i>	pUT18-C	(4)
pREJSc-008	<i>Plac::cckA-T18</i>	pUT18	This study
pREJSc-009	<i>Plac::spmX-T18</i>	pUT18	This study
pXF-001	<i>Plac::pleC-T18</i>	pUT18	pXF-001
pXF-002	<i>Plac::divL-T18</i>	pUT18	pXF-002
pJW212	<i>Plac::popZ-T18</i>	pUT18	pW212
pJW200	<i>Plac::popA-T18</i>	pUT18	pJW200
pREJSc-010	<i>Plac::divJ-T18</i>	pUT18	This study
pREJSc-011	<i>Plac::T18-divJ</i>	pUT18-C	This study
pAP411	<i>PspmX::SpmX-eYFP</i>	pAP411	(5)

Table S5: Primers

Name	Sequence	Propose
1c	atagaattcatgcccagccgctgccc	5' primer for cloning into pFLAG-C2 the 3' end of <i>podJ</i> with an engineered EcoRI site.
2c	tataccggttactgtcatcgtcatcctttagtagcgcgcgtagaccgacagg	3' primer for cloning into pFLAG-C2 the 3' end of <i>podJ</i> , introducing an AgeI site and a <i>m2</i> coding sequence.
3c	tatcatatgacggcggttcgat	5' primer for cloning into pFLAG-C2 the 5' end of <i>podJ</i> with an engineered NdeI site.
4c	tatggtaccttactgtcatcgtcatcctttagtagcgcctccgaggcggc	3' primer for cloning into pFLAG-C2 the 5' end of <i>podJ</i> , introducing a KpnI site and a <i>m2</i> coding sequence.
5c	taagatctcgagctccggagatgacggcggcttcgcat	5' primer for cloning <i>podJ</i> into pMCS-C2
6c	accggtacgcgtaacgttcgtagcgcgcgtagaccgac	3' primer for cloning <i>podJ</i> into pMCS-C2
7c	gtgcggggagatcgattcgcgcagggcgtgctacc	5' primer for cloning <i>dL5</i> into pMCS-C2
8c	catggcgaagccgccgtcatggagaggacggtcagctggg	3' primer for cloning <i>dL5</i> into pMCS-C2
9c	taagatctcgagctccggagacatcgggctgctgctgc	5' primer for cloning the first 500bp upstream of <i>podJ</i> into pMCS-C2
10c	gggtaacgacggcctgcatgcgaatcgatctccccgcac	3' primer for cloning the first 500bp upstream of <i>podJ</i> into pMCS-C2
11c	atatctagaaatgacggcggcttcgcatggagcggttaag	5' primer for cloning <i>podJ</i> into pKT25 with an engineered XbaI site
12c	tatggtaccttagcgcgcgtagaccgacaggcgttgagggt	3' primer for cloning <i>podJ</i> into pKT25 with an engineered KpnI site
13c	aaatctagaaatggcagacacggggg	5' primer for cloning <i>pleC</i> into pUT18-C with an engineered XbaI site
14c	aaaggtacctcaggccgccgaagtc	3' primer for cloning <i>pleC</i> into pUT18-C with an engineered KpnI site
15c	aaatctagaaatgacttcgtacgacctgatcctcg	5' primer for cloning <i>divL</i> into pUT18-C with an engineered XbaI site
16c	aaaggtaccctagaagccgagttcgggctg	3' primer for cloning <i>divL</i> into pUT18-C with an engineered KpnI site
17c	aaatctagaaatggccgacttcagctcc	5' primer for cloning <i>cckA</i> into pUT18-C with an engineered XbaI site

Chapter 2

18c	ttaggtaccctacgccgctgcagctg	3' primer for cloning <i>cckA</i> into pUT18-C with an engineered KpnI site
19c	aaatctagaaatggaattcgaaacgctccagaccggt	5' primer for cloning <i>divJ</i> into pUT18-C with an engineered XbaI site
20c	ataggtacctcagcgcgcgcaaaggc	3' primer for cloning <i>divJ</i> into pUT18-C with an engineered KpnI site.
21c	aaatctagaaatggccgactgcagctccag	5' primer for cloning <i>cckA</i> into pUT18 with an engineered XbaI site
22c	ttaggtacctcagccgctgcagctgctg	3' primer for cloning <i>cckA</i> into pUT18 with an engineered KpnI site
23c	atatctagacatgaaaccgctcatcaggtc	5' primer for cloning <i>spmX</i> into pUT18 with an engineered XbaI site
24c	tatgaattctcttcgctcaccatcgg	3' primer for cloning <i>spmX</i> into pUT18 with an engineered EcoRI site.
25c	aaatctagaaatggaattcgaaacgctccagaccggt	5' primer for cloning <i>divJ</i> into pUT18 with an engineered XbaI site
26c	ttaggtaccatgcgcgcgcaaaggc	3' primer for cloning <i>divJ</i> into pUT18 with an engineered KpnI site.

Table S6: Bacterial Strains

<i>Caulobacter</i> strains	Relevant genotype	Construction or reference
CB15N	Synchronizable derivative of WT CB15N	(6)
REJSc001	<i>podJ::podJ-m2</i>	pREJSc001 electroporated into CB15N
REJSc002	<i>podJ::podJ NTD-m2</i>	pREJSc002 electroporated into CB15N
REJSc003	<i>podJ::dl5-podJ</i>	pREJSc003 electroporated into CB15N
AP454	<i>xyl::cres-dL5</i>	(7)
LS4326	<i>ctrA::ctrA-m2</i>	(8)
Δ SpmX	<i>spmX::\Delta</i>	(9)
AP496	<i>divJ::\Delta</i>	(5)
UJ506	<i>pleC::\Delta</i>	(10)
JP315	<i>popZ::\Delta</i>	(11)
UJ2827	<i>popA::\Delta</i>	(12)
REJSc004	<i>spmX::\Delta; podJ::dl5-podJ</i>	pREJSc003 electroporated into Δ SpmX.
REJSc005	<i>divJ::\Delta; podJ::dl5-podJ</i>	pREJSc003 electroporated into AP496.
REJSc006	<i>pleC::\Delta; podJ::dl5-podJ</i>	pREJSc003 electroporated into UJ506.
REJSc007	<i>popZ::\Delta; podJ::dl5-podJ</i>	Transduction performed with ϕ Cr30 from JP315 into REJSc003
pV17	<i>podJ::\Delta</i>	(13)
JOE1998	<i>perP::\Delta; mmpA::\Delta</i>	(14)
AP414	<i>spmX::spmX-eYFP</i>	(5)
REJSc008	<i>podJ::\Delta; spmX::spmX-eYFP</i>	pAP411 electroporated into pV7.
REJSc009	<i>perP::\Delta; mmpA::\Delta; spmX::spmX-eYFP</i>	pAP411 electroporated into JOE1998
REJSc010	<i>popA::\Delta; podJ::dl5-podJ</i>	pREJSc003 Electroporated into UJ2827

<i>E. coli</i> stains	Relevant genotype/description	Construction, source or reference
BTH101	F ⁻ , <i>cya-99</i> , <i>araD139</i> , <i>galE15</i> , <i>galK16</i> , <i>rpsL1</i> (Str ^r), <i>hsdR2</i> , <i>mcrA1</i> , <i>mcrB1</i>	Euromedex
REJSc011	<i>Plac::T25-podJ</i> ; <i>Plac::T18-pleC</i>	pREJSc-004 and pREJSc-005 co-electroporated into BTH101
REJSc012	<i>Plac::T25-podJ</i> ; <i>Plac::pleC-T18</i>	pREJSc-004 and pXF-001 co- electroporated into BTH101
REJSc013	<i>Plac::T25-podJ</i> ; <i>Plac::T18-divL</i>	pREJSc-004 and pREJSc-006 co-electroporated into BTH101
REJSc014	<i>Plac::T25-podJ</i> ; <i>Plac::divL-T18</i>	pREJSc-004 and pXF002 co- electroporated into BTH101
REJSc015	<i>Plac::T25-podJ</i> ; <i>Plac::T18-cckA</i>	pREJSc-004 and pREJSc-007 co-electroporated into BTH101
REJSc016	<i>Plac::T25-podJ</i> ; <i>Plac::cckA-T18</i>	pREJSc-004 and pREJSc-008 co-electroporated into BTH101
REJSc017	<i>Plac::T25-podJ</i> ; <i>Plac::T18-popZ</i>	pREJSc-004 and pJW211 co- electroporated into BTH101
REJSc018	<i>Plac::T25-podJ</i> ; <i>Plac::popZ-T18</i>	pREJSc-004 and pJW212 co- electroporated into BTH101
REJSc019	<i>Plac::T25-podJ</i> ; <i>Plac::spmX-T18</i>	pREJSc-004 and pREJSc-009 co-electroporated into BTH101
REJSc020	<i>Plac::T25-podJ</i> ; <i>Plac::T18-divJ</i>	pREJSc-004 and pREJSc-011 co-electroporated into BTH101
REJSc021	<i>Plac::T25-podJ</i> ; <i>Plac::divJ-T18</i>	pREJSc-004 and pREJSc-010 co-electroporated into BTH101
REJSc022	<i>Plac::T25-podJ</i> ; <i>Plac::T18-popA</i>	pREJSc-004 and pJW199 co- electroporated into BTH101
REJSc023	<i>Plac::T25-podJ</i> ; <i>Plac::popA-T18</i>	pREJSc-004 and pJW200 co- electroporated into BTH101
PodJ-sfGFP	<i>araBp::podJ-sfgfp</i>	(15)

Supplemental references

1. M. Thanbichler, A. A. Iniesta, L. Shapiro, A comprehensive set of plasmids for vanillate and xylose-inducible gene expression in *Caulobacter crescentus*. *Nucleic Acids Res.* **35** (2007).
2. K. Lasker, *et al.*, CauloBrowser: A systems biology resource for *Caulobacter crescentus*. *Nucleic Acids Res.* **44** (2016).
3. G. Karimova, J. Pidoux, A. Ullmann, D. Ladant, A bacterial two-hybrid system based on a reconstituted signal transduction pathway. *Proc. Natl. Acad. Sci.* **95**, 5752–5756 (1998).
4. J. Wang, W. E. Moerner, L. Shapiro, A localized adaptor protein performs distinct functions at the *Caulobacter* cell poles. *PNAS* **118** (2021).
5. A. M. Perez, *et al.*, A localized complex of two protein oligomers controls the orientation of cell polarity. *MBio* **8**, 1–16 (2017).
6. M. Evinger, N. Agabian, Envelope associated nucleoid from *Caulobacter crescentus* stalked and swarmer cells. *J. Bacteriol.* **132**, 294–301 (1977).
7. S. Saurabh, A. M. Perez, C. J. Comerci, L. Shapiro, W. E. Moerner, Super-resolution imaging of live bacteria cells using a genetically directed, highly photostable fluoromodule. *J. Am. Chem. Soc.* **138**, 10398–10401 (2016).
8. P. T. McGrath, A. A. Iniesta, K. R. Ryan, L. Shapiro, H. H. McAdams, A dynamically localized protease complex and a polar specificity factor control a cell cycle master regulator. *Cell* **124**, 535–547 (2006).
9. S. K. Radhakrishnan, M. Thanbichler, P. H. Viollier, The dynamic interplay between a cell fate determinant and a lysozyme homolog drives the asymmetric division cycle of *Caulobacter crescentus*. *Genes Dev.* **22**, 212–225 (2008).
10. P. Aldridge, R. Paul, P. Goymer, P. Rainey, U. Jenal, Role of the GGDEF regulator PleD in polar development of *Caulobacter crescentus*. *Mol. Microbiol.* **47**, 1695–1708 (2003).
11. G. R. Bowman, *et al.*, A Polymeric protein anchors the chromosomal origin/ParB complex at a bacterial cell pole. *Cell* **134**, 945–955 (2008).
12. A. Duerig, *et al.*, Second messenger-mediated spatiotemporal control of protein degradation regulates bacterial cell cycle progression. *Genes Dev.* **23**, 93–104 (2009).
13. P. H. Viollier, N. Sternheim, L. Shapiro, Identification of a localization factor for the polar positioning of bacterial structural and regulatory proteins. *PNAS* **99**, 13831–13836 (2002).
14. J. C. Chen, *et al.*, Cytokinesis signals truncation of the PodJ polarity factor by a cell cycle-regulated protease. *EMBO J.* **25**, 377–386 (2006).
15. J. A. Holmes, *et al.*, *Caulobacter* PopZ forms an intrinsically disordered hub in organizing bacterial cell poles. *PNAS* **113**, 12490–12495 (2016).

Chapter 3

GROWTH POLE RING protein forms a 200-nm-diameter ring structure essential for polar growth and rod shape in *Agrobacterium tumefaciens*

J. R. Zupan^a, R. Grangeon^a, J. S. Robalino-Espinosa^{a,b}, N. Garnica^a, and P. Zambryski^{a,1}

^aDepartment of Plant and Microbial Biology, University of California, Berkeley, CA 94720; and ^bDepartment of Molecular Cell Biology, Vrije Universiteit Amsterdam, 1081 HV Amsterdam, The Netherlands

¹To whom correspondence should be addressed. Email: zambrysk@berkeley.edu.

3

Format adjusted from: Proc Natl Acad Sci U S A 2019 May 28;116(22):10962-10967.

Abstract

Polar growth in *Agrobacterium* pirates and repurposes well-known bacterial cell cycle proteins, such as FtsZ, FtsA, PopZ, and PodJ. Here we identify a heretofore unknown protein that we name GROWTH POLE RING (GPR) due to its striking localization as a hexameric ring at the growth pole during polar growth. GPR also localizes at the midcell late in the cell cycle just before division, where it is then poised to be precisely localized at new growth poles in sibling cells. GPR is 2,115 aa long, with two N-terminal transmembrane domains placing the bulk of the protein in the cytoplasm, N- and C-terminal proline-rich disordered regions, and a large 1,700-aa central region of continuous α -helical domains. This latter region contains 12 predicted adjacent or overlapping apolipoprotein domains that may function to sequester lipids during polar growth. Stable genetic deletion or riboswitch-controlled depletion results in spherical cells that grow poorly; thus, GPR is essential for wild-type growth and morphology. As GPR has no predicted enzymatic domains and it forms a distinct 200-nm-diameter ring, we propose that GPR is a structural component of an organizing center for peptidoglycan and membrane syntheses critical for cell envelope formation during polar growth. GPR homologs are found in numerous Rhizobiales; thus, our results and proposed model are fundamental to understanding polar growth strategy in a variety of bacterial species.

Agrobacterium | bacterial polar growth | apolipoprotein | rod-shape morphology |
GROWTH POLE RING protein

Significance

The extensively studied rod-shaped bacteria *Escherichia coli*, *Bacillus subtilis*, and *Caulobacter crescentus* grow by dispersed insertion of new cell wall material along the entire length of the cell. An alternative prokaryotic growth mode—polar growth—is used by some Actinomycetales and Proteobacteria. The latter phylum includes the family Rhizobiaceae, of which *Agrobacterium tumefaciens* is a prominent member. The factors responsible for polar growth are largely unknown. Here we describe GROWTH POLE RING (GPR) protein from *Agrobacterium* with a striking localization as a ring of six foci at the growth pole. GPR is potentially the polar growth organizer in *Agrobacterium*, as its absence leads to severe morphological defects, including loss of cylindrical cell shape, while its overproduction leads to ectopic growth poles.

Introduction

How bacteria grow and divide is intensely investigated, given the importance of bacteria across all of biology, from microbes to man. Several model systems, including *Escherichia coli*, *Bacillus subtilis*, and *Caulobacter crescentus*, have provided a wealth of fundamental insights into lateral dispersed cell elongation (1). However, as more bacteria enter the ring of scrutiny, another mode of cell elongation, limited to one or both poles, has emerged (2–5). In gram-negative bacteria, a single growth pole is used by the Rhizobiales order of Alphaproteobacteria, which includes the plant pathogen/genetic engineer *Agrobacterium* and plant nitrogen-fixing symbiont *Rhizobium*, as well as the animal pathogens *Brucella* and *Bartonella* (2–14).

Little is known about the enzymes involved, their spatiotemporal expression, or what mechanisms regulate bacterial polar growth. To date, several molecular players for polar growth have been identified in *Agrobacterium tumefaciens*. First, *Agrobacterium* specific homologs of the classic cell division factors FtsA and FtsZ localize to the growth pole during cell elongation and then migrate to the midcell during initiation and completion of septation (6, 9, 12, 13). At the division site, FtsA and FtsZ are then precisely located at the new growth poles in resulting sibling cells. Second, homologs of *Caulobacter* old and new pole-specific markers, PopZ_{Cc} (15, 16) and PodJ_{Cc} (17, 18), respectively, have opposite localizations in *Agrobacterium*. PopZ_{At} exclusively marks the growing pole (13). PodJ_{At} initially marks the old pole but then also accumulates at the growth pole later in the cell cycle; this re- location is correlated with the transition of the growth pole to an old pole, and PodJ_{At} is proposed to facilitate this transition (13). It is likely that FtsZ also plays

a role in the transition to an old pole, as cells depleted of FtsZ fail to divide but continue to grow (12). Genetic deletion or depletion of PodJ_{At} or PopZ_{At} causes severe growth defects (14, 19–21), attesting to their essential roles.

Notably, the amino acid sequences of PopZ_{At} and PodJ_{At} are distinct from their *Caulobacter* counterparts, each with only 23% identity (13). Nevertheless, as the search for *Caulobacter* homologs successfully identified critical pole-specific factors in *Agrobacterium*, we used this approach again to search for potential homologs of *Caulobacter* TipN, dubbed a landmark protein for establishing and perpetuating new pole polarity throughout most of its cell cycle (22, 23). We found an uncharacterized *Agrobacterium* protein with little amino acid identity to TipN but an overall similarity in secondary structural domains. Most remarkably, the *Agrobacterium* protein localizes into six subpolar foci arranged in a hexameric ring at the growth pole.

The lack of significant amino acid sequence similarity to TipN and its distinctive localization pattern led us to name the newly identified *Agrobacterium* protein GROWTH POLE RING (GPR). Here we describe the domain architecture of GPR, its localization during the *Agrobacterium* cell cycle, and genetic analyses revealing that GPR is essential for polar growth and rod shape morphology.

Results

Identification of GPR Protein. As polar growth in *Agrobacterium* is not well understood, it is critical to identify factors that localize to the growth pole that may function to facilitate such growth. We used the *C. crescentus* new pole-localizing protein, TipN, as a query and identified an uncharacterized *Agrobacterium* protein, A9CJ72 (24), Atu1348 in the *A. tumefaciens* proteome, with low (~20%) amino acid sequence identity to TipN. For reasons described below, we named *Agrobacterium* A9CJ72 the GPR protein.

Fig. 1 diagrams the predicted structural domains of GPR (25); SI Appendix, Fig. S1A provides more detailed predictions of secondary structure according to PHYRE2 (26). Two predicted N-terminal transmembrane domains suggest that the bulk of the protein resides in the cytoplasm (Fig. 1 and SI Appendix, Fig. S1A). The N (80 aa) and C (110 aa) termini are enriched in proline residues and are predicted to be disordered. Strikingly, 82% of GPR, encompassing 1,720 residues (160–1,890), is predicted to be comprised of contiguous α -helices (SI Appendix, Fig. S1A). This large central α -helical region (blue area in Fig. 1) contains numerous nonoverlapping and overlapping subdomains homologous to eukaryotic apolipoproteins (ApoLPs; Pfam P01442) (25) with solved structures (27–30). SI Appendix, Table S1 lists the locations of 12 predicted ApoLP domains in GPR, 8 of which have significant e-values and an average size of 204 aa. *Caulobacter* TipN and *Agrobacterium* GPR differ dramatically in length (882 aa vs. 2,115 aa), but have an overall similar placement of related structural domains, N-terminal membrane-spanning domains, N- and C-terminal disordered regions, and central regions of continuous alpha helices (26) (SI Appendix, Fig. S1 A and B). TipN is distinct from

GPR, however, with a much shorter central α -helical region (520 aa) and no predicted ApoLP domains.

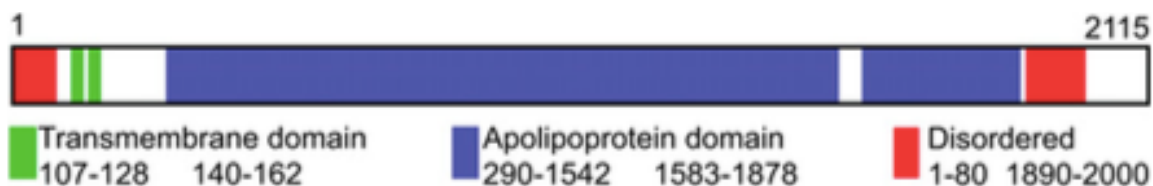


Fig. 1. GPR domain structure. Predicted transmembrane regions are shown in green, disordered regions are in red, and overlapping and/or adjacent ApoLP domains (SI Appendix, Table S1 lists exact locations and lengths) are in blue. Other areas (white) are predominantly α -helical according to Pfam (25). SI Appendix, Fig. S1 provides more details.

ApoLPs have been extensively studied in eukaryotes, as they are essential for the formation of cardioprotective high-density lipoproteins (reviewed in ref. 31), where α -helical domains of ApoLPs sequester lipid droplets (reviewed in ref. 32). ApoLPs also have been identified in prokaryotes, primarily as structural components of lipid droplets (33–35). Due to data mining of bacterial genomes, their numbers are increasing; in 2015, prokaryotic ApoLPs represented approximately 16% of the total PF01442 family members, while as of October 2018, this proportion had more than doubled, to 41% (SI Appendix, Fig. S2). Interestingly, 272 of 326 (83%) bacterial sequences reported to date that contain predicted ApoLPs (Pfam P01442) (25) are from the Rhizobiales order, which includes *Rhizobium* and *Agrobacterium* species. Most ApoLPs in the Rhizobiales are large proteins and have an overall architecture similar to GPR, including two transmembrane domains near the N terminus.

To date, no ApoLPs have been identified in the Caulobacterales order, consistent with the absence of ApoLP domains in TipN. Furthermore, TipN and GPR likely have distinct functions, as they participate in distinctly different means of growth, dispersed in *Caulobacter* compared with polar in *Agrobacterium*. Potentially, the large central region of GPR carrying ApoLP domain in *Agrobacterium* represents an evolutionary diversification in the Rhizobiales order compared with the Caulobacterales order, which creates a new function (36–38).

GPR Localization. We created GFP fusions to the N and C termini of *Agrobacterium* GPR and visualized their localization. GFP fused to the N terminus reveals a broad, almost flat region of fluorescence near the growing pole (Fig. 2A; arrowheads) that differs from the tight focus of fluorescence observed with fusions to other growth pole-specific factors, such as FtsZ, FtsA, and PopZ (6, 13). On image enlargement, this broad band appears as paired foci very near, but not at, the tip of the growth pole (Figs. 2A, Insets and 3A).

As paired foci in single optical sections are indicative of a potential ring structure, we used high-resolution structured illumination microscopy (SIM) to better resolve these polar foci. Indeed, GPR resolves into a ring of four to six foci subpolar to the growth pole (Fig. 2B). Some foci are round and likely represent single foci, while other foci likely represent overlapping fluorescence from two adjacent round foci, as exemplified by the cell shown in Fig. 2B, i. Movies S1–S4 show different rotations of the four cells shown in Fig. 2B. These multiple foci with a unique ring-like localization at the growth pole are the basis for naming *Agrobacterium* protein A9CJ72 the GPR protein.

GFP-GPR occasionally exhibits bipolar localization (Fig. 2A, arrow), and we performed time-lapse studies to further analyze this observation (see below). C-terminal GFP fusions to GPR resulted in abnormal growth patterns with multiple ectopic growth poles (SI Appendix, Fig. S3) suggesting that GFP blocks an essential function at the C terminus of GPR.

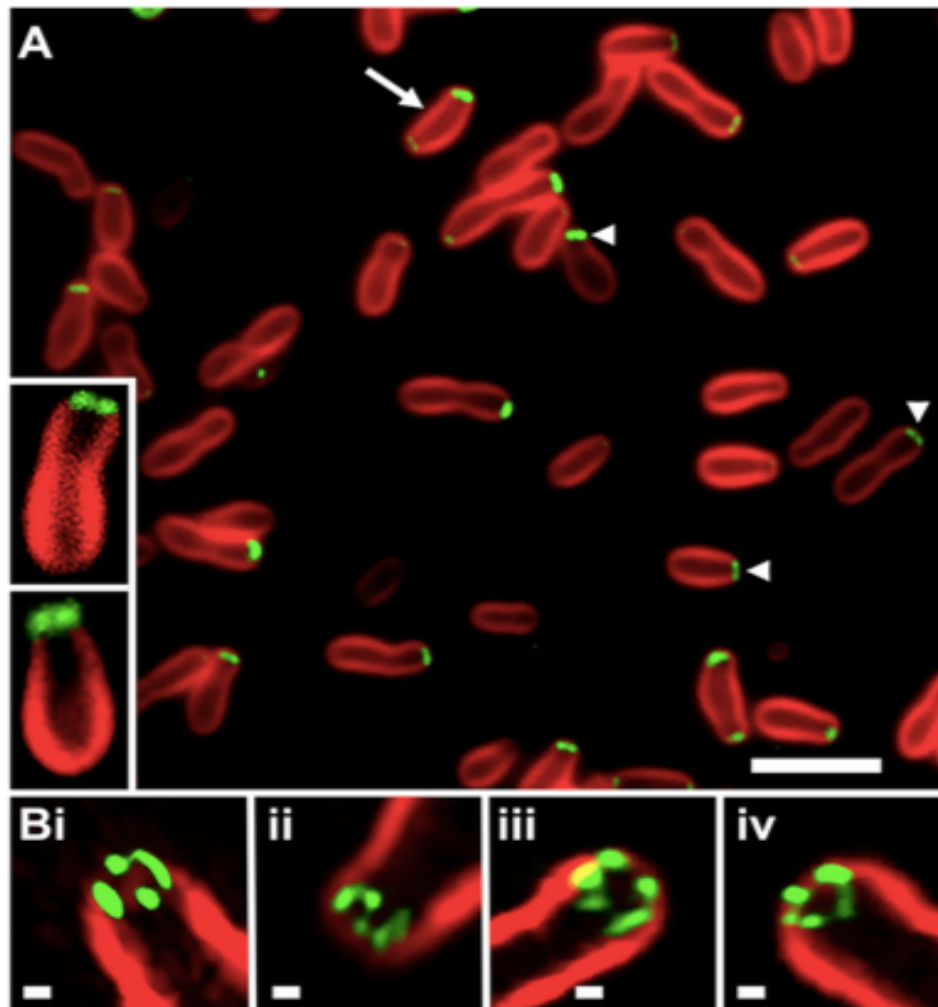


Fig. 2. Localization of GFP-GPR at the growth pole. (A) On WFM, most cells show a single broad polar focus of GFP (arrowheads), and a few cells (arrow) show additional weak localization at the opposite pole. (Insets) Cells with paired polar foci. (Scale bar: 3 μm .) (B) SIM 3D reconstructions show subpolar localization and multiple foci. Movies S1–S4 correspond to Fig. 2B, i–iv, respectively. FM4-64 stains the older nongrowing pole; weak or no FM4-64 staining occurs at the growth pole. (Scale bar: 100 nm.)

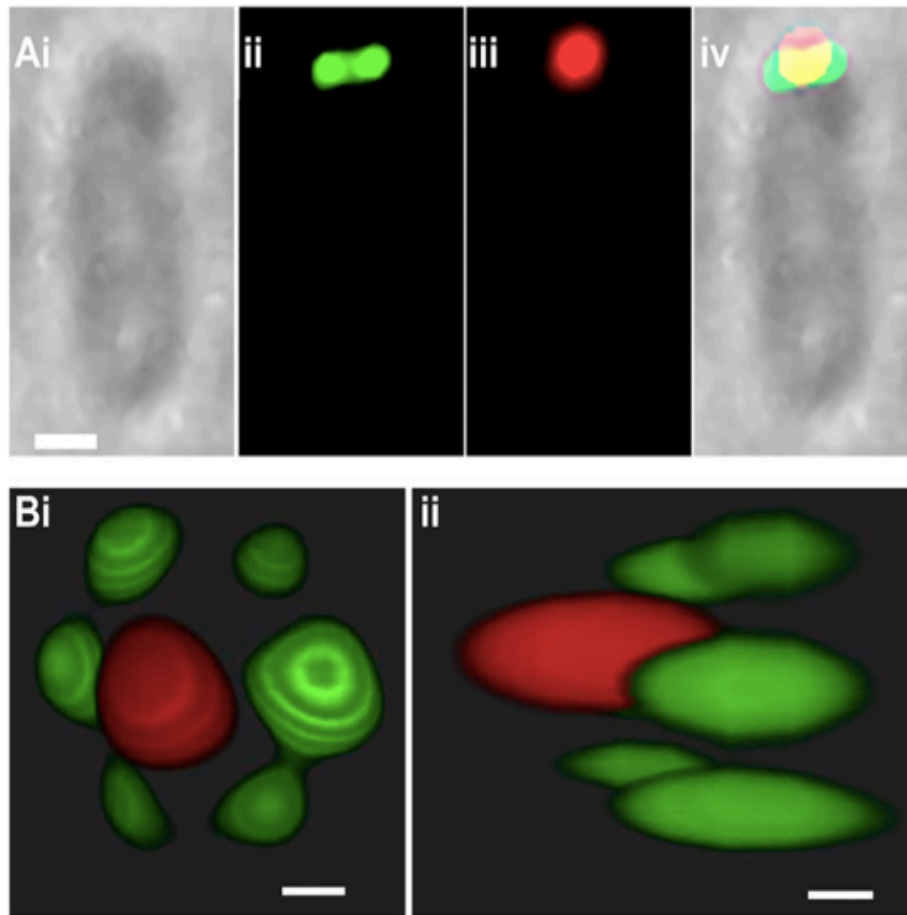


Fig. 3. Localization of PopZ-GFP and GFP-GPR. (A) PopZ-RFP fluorescence overlaps with GFP-GPR. Some PopZ-RFP extends beyond GFP-GPR toward the tip of the growth pole, while the bulk of PopZ overlaps with GPR. Compare bright field (i), green (ii), and red (iii) fluorescence with both green and red fluorescence in the merged image (iv). (Scale bar: 500 nm.) (B) SIM confirms that PopZ localizes at the tip of growth pole, while GFP-GPR is subpolar and peripheral. (i) growth-pole view; (ii) lateral view. Movie S5 shows an animation of the 3D reconstruction of PopZ and GPR localization from SIM images. BF, bright field. (Scale bar: 50 nm.)

GPR Function Is Sensitive to Levels of Ectopic GFP-GPR. For the images presented in Fig. 2 and throughout, we used very low levels of induction of GFP-GPR expression. Here, as in previous work, we cloned genes of interest (as fusions to GFP) into a low-copy number plasmid carrying a tightly regulated lac promoter (39), and induced protein expression by adding 2.5–10 mM isopropyl β -D-1-thiogalactopyranoside (IPTG) (6, 9, 13,

14, 19). For example, 10 mM and 5 mM IPTG resulted in expression of FtsZ-GFP or FtsA-GFP at approximately 10% of the levels of endogenous FtsZ or FtsA, respectively; these levels of ectopic induction did not alter cell morphology or cell cycle timing (6, 9, 13, 14, 19). However, for cells to remain viable during ectopic expression of GFP-GPR, it was essential to reduce the IPTG concentration to only 0.25 mM. SI Appendix, Fig. S4 shows cells carrying GFP-GPR induced for expression with 0.25 mM, 0.5 mM, 1.0 mM, and 2 mM IPTG. As the concentration of IPTG increased, the fluorescence of GFP-GPR increased, as expected; however, with more GFP-GPR expression, cells produced more ectopic growth poles. Ectopic growth poles were first observed with 0.5 mM IPTG induction, but not with 0.25 mM IPTG induction, and 0.25 mM induction was sufficient to allow observation of GFP-GPR by fluorescence microscopy.

The foregoing data suggest that WT GPR function is very sensitive to ectopic expression of GFP-GPR, potentially because GFP-GPR was induced to higher levels than expected. We tested the relative protein levels of GFP-GPR compared with WT GPR under different IPTG induction conditions. SI Appendix, Fig. S5 shows that 0.1 mM IPTG was not sufficient to induce GFP-GPR expression, 0.25 mM IPTG resulted in GFP-GPR expression at approximately 20% of WT levels, and 0.5 mM or 1.0 mM IPTG resulted in GFP-GPR expression at 50% or higher compared with WT. Thus, higher levels of IPTG significantly increased the ratio of the ectopic GFP fusion protein compared with endogenous WT GPR, and this may account for the altered cell shape and ectopic poles observed.

GPR Forms a Large Hexameric Ring at the Growth Pole. Wide-field fluorescence microscopy (WFM) revealed GFP-GPR as paired foci near the growth pole tip (Fig. 2). Similar WFM during coexpression of GFP-GPR with PopZ-RFP showed PopZ-RFP closer to the tip of one end of the cell and GFP-GPR just below and overlapping PopZ-RFP (Fig. 3A). SIM imaging confirmed this localization and further revealed that GFP-GPR forms six distinct foci (Fig. 3B), as suggested by images in Fig. 2B; this notable localization is further evidenced in Movie S5. Each GFP-GPR focus is approximately 50 nm in diameter, similar in size to the PopZ-RFP focus. As the space between each focus is also ~50 nm, the ring has a circumference of ~600 nm with a diameter of ~200 nm.

Localization of GPR During the *Agrobacterium* Cell Cycle. Fig. 4A presents images of a single cell expressing GFP-GPR following time-lapse observation. GFP-GPR is at the growing pole until cell division (at 90 min) and then is located at the new growth poles, resulting from midcell constriction in sibling cells (at 120 min). The previous new pole has become an old pole (4), yet GFP-GPR remains at this site, reflecting that GPR is membrane-anchored. That GPR remains at this old growth pole even until the next cell division (at 180 min) may suggest the time it takes for its removal and/or degradation. These results imply that GFP-GPR observed in the sibling new cell poles is likely to be newly synthesized; that is, it is unlikely that a membrane-anchored protein would easily migrate to the new poles. Movie S6 shows the same cell shown in Fig. 4.

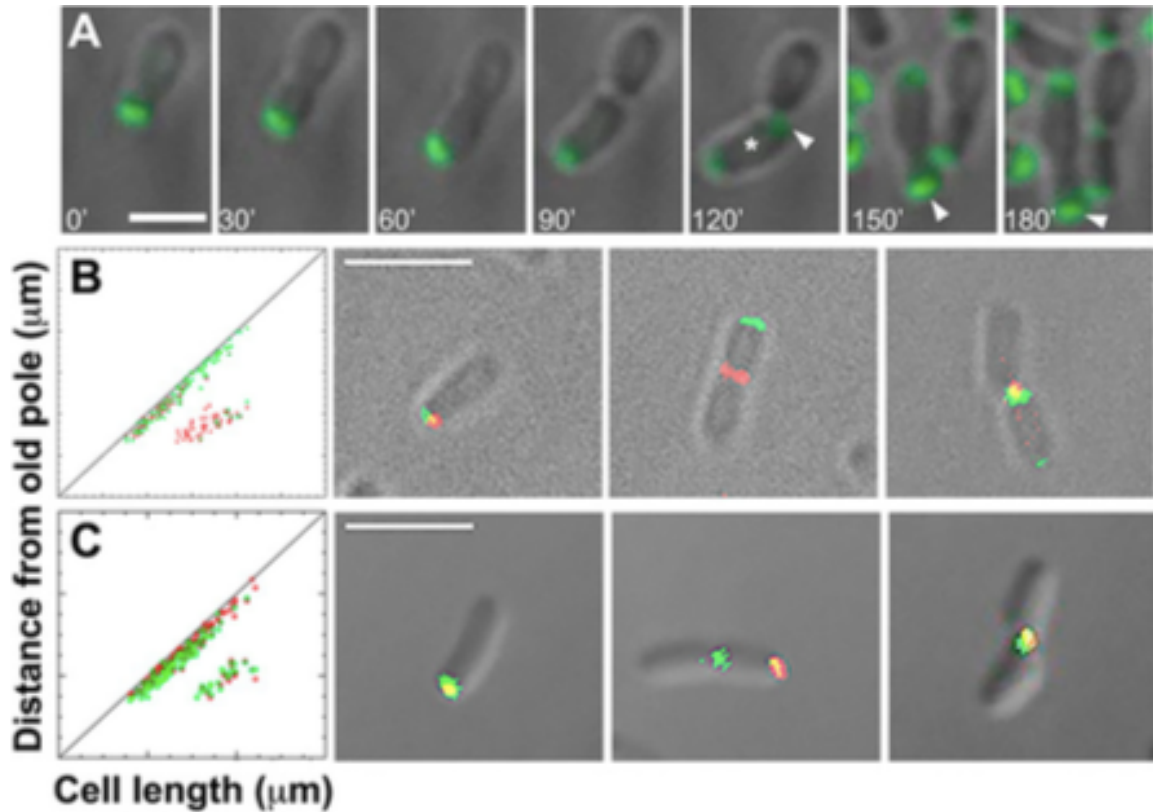


Fig. 4. GPR localization during the cell cycle and quantification of GPR, FtsZ, and PopZ localization to the growth pole or the midcell. (A) Time-lapse localization of GFP-GPR. Note that between 120 and 150 min, the lower cell (white asterisk) rotates (Movie S7) approximately 120° (clockwise), so that its growth pole faces downward at 150 min. The old pole is indicated by an arrowhead. (B and C) Coexpression of GFP-GPR and FtsZ-RFP (B) and GFP-GPR and PopZ-RFP (C). Red and green foci at the growth pole and the midcell were plotted along the diagonal or in the region between the diagonal and the x-axis, respectively, in 127 cells (B) and 100 cells (C). The tick marks on the x- and y-axes correspond to 0.5 μm . Representative cell images are shown to the right of each graph. While red and green foci occur together at the growth pole, FtsZ-RFP can occur at the midcell without GFP-GPR (but not vice versa), and GFP-GPR can occur at the midcell without PopZ-RFP (but not vice versa). (Scale bar: A, 2 μm ; B and C, 3 μm .)

Notably, how long GFP-GPR remains at the new old pole varies. Movie S7 shows two different cells, one cell in which GFP-GPR remains at the new old pole and another cell in which it disappears relatively soon after the first cell division. The daughter that contains the original old pole does not contain GFP-GPR at its (very) old pole; in contrast, the daughter that originates from polar growth at the new pole contains GFP-GPR at its (new)

old pole. These results also underscore that daughter cells are not equivalent.

To independently assess GPR localization during the cell cycle, we performed a quantitative assessment of the localization of GFP-GPR in cells coexpressing FtsZ-RFP or PopZ-RFP that each exhibit distinct time frames for their relocation from the growth pole to the midcell. FtsZ marks the new growth pole in *Agrobacterium* and then relocates to the midcell region approximately 60–70 min before septation (13), while PopZ remains at the growth pole until septation (13). Instead of elapsed time, we used cell length as a measure of progression through the cell cycle, and more than 100 green or red fluorescent foci were plotted relative to cell length (Fig. 4 B and C); foci that localize at the growth pole are plotted on the diagonal, and foci that occur at the midcell are plotted between the diagonal and the x-axis. GPR and FtsZ colocalize at the growth pole in shorter cells, corresponding to early stages of the cell cycle, and GPR remains at the growth pole as cells elongate up to 4 μm . In contrast, in cells ranging from 2.6 to 4 μm , FtsZ is rarely found at the growth pole and instead occurs at the midcell.

Coexpression of GFP-GPR and PopZ-RFP confirms that PopZ remains at the growth pole throughout the cell cycle (13) and in the longest cells, as expected. However, GPR relocates to the midcell just slightly before PopZ, as (i) there are a few more green foci in cells 2–3.5 μm long, (ii) we detect green foci at the midcell without red foci, and (iii) we rarely detect red PopZ foci at the midcell without green GPR foci.

Deletion or Depletion of GPR Causes Severe Growth Defects. To test whether GPR is essential for polar growth, we created a genetic deletion of *gpr* (SI Appendix, Fig. S6 shows deletion strategy). Δgpr cells grow slowly, with a doubling time of 4–5 h in liquid

cultures (vs. 90 min for WT); however, cell cycle length varies between cells (see below). Strikingly, Δgpr cells are coccoid and vary in diameter and overall shape (Fig. 5A). Few cells are elongated but misshapen (Fig. 5A, arrows). There is little evidence of normal polar growth, except some cells produce round projections (Fig. 5A, encircled). A few cells produce two small “buds” (Fig. 5A, arrowheads) that may lead to mini cells.

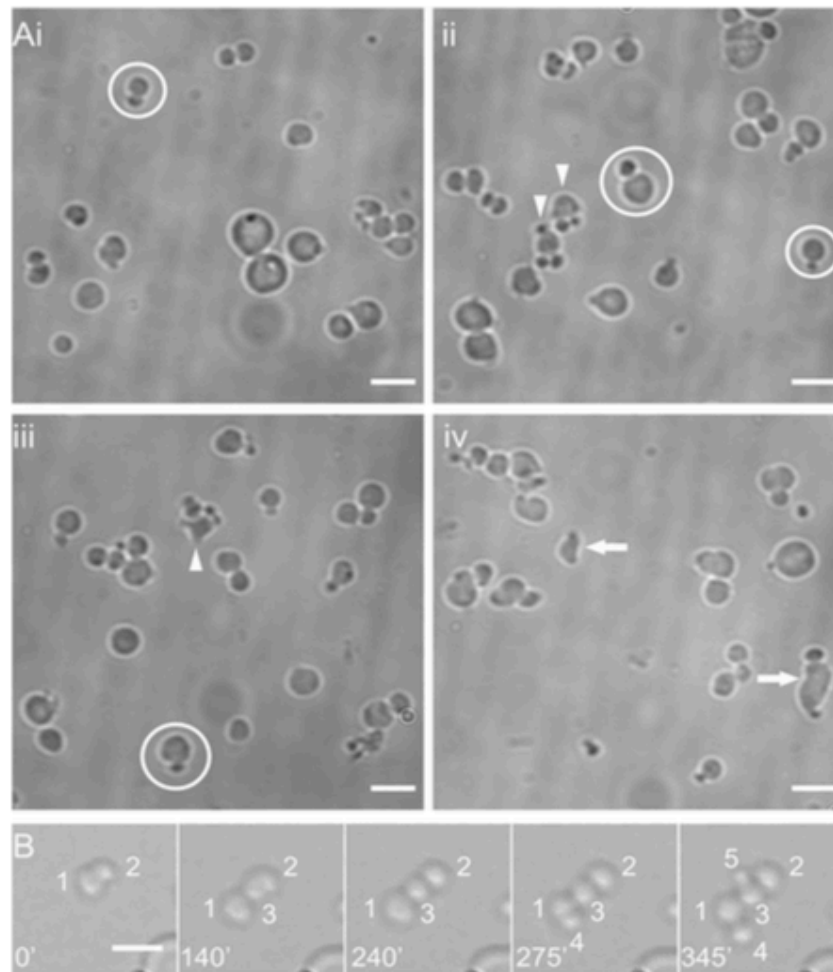


Fig. 5. Deletion of GPR results in spherical cells. (A) Δgpr cells are mostly coccoid. Some cells appear to be making new round cells (encircled), a few cells produce two buds (arrowheads), and a few cells are elongated but misshapen (arrows). (B) Time-lapse imaging of two dividing cells, labeled 1 and 2 (0 min), giving rise to cells numbered 3, 4, and 5 (images derived from Movie S8). The times shown were chosen to illustrate newly arising or dividing cells and do not represent a constant time difference between each panel. (Scale bar: 3 μm .)

Nevertheless, at least some Δgpr cells grow in liquid culture and form small colonies on agar plates. Time-lapse imaging (Fig. 5B and Movie S8) shows that round cell 1 produces cell 2, which produces cell 3; after a delay cell 2 produces cell 4, and then cell 5 forms. Thus, Δgpr daughter cells are not synchronous in their cell cycle progression. Normally, two cells should produce four cells and then eight cells; instead, we observe cell number 3 before cell number 4, and cell number 5 before cell number 6.

Δgpr daughter cells have an additional phenotype, failure to separate following division, so one can easily distinguish the order of formation of cells 3, 4, and 5 (Fig. 5B); such images are representative of 20% of Δgpr cells with round protrusions (Fig. 5A). In addition, at least 40% of the cells are unusually large and spherical; such cells grow in all directions over a long period (14 h) and produce a quartet of daughter cells that remain attached (Movie S9).

The coccoid phenotype of Δgpr disappeared following ectopic expression of WT GPR under control of the lac promoter (SI Appendix, Fig. S7). Surprisingly, rescue occurred following extremely low levels (0.025 mM) of IPTG (10-fold less IPTG than used previously to induce GFP-GPR expression), suggesting that cells do not require high amounts of GPR to survive. In support, higher levels of IPTG resulted in abnormal branched cells with ectopic poles. Thus, GPR levels must be tightly controlled in WT cells.

Since stable genetic deletion of *gpr* caused such a strong phenotype, we next used a riboswitch strategy (SI Appendix, Fig. S8) to make $RS::gpr$. Without theophylline, $RS::gpr$ exhibits a coccoid phenotype identical to Δgpr , and WT cell shape is re-stored on addition

of theophylline (Fig. 6 A and B). Notably, inducible expression of GFP-GPR with low levels of IPTG (0.025 mM) also rescues *RS::gpr* grown in the absence of theophylline (Fig. 6C).

Loss of GPR Impacts Localization of PopZ. PopZ localizes very close to GPR (Fig. 3), and GPR relocates to the midcell just before PopZ. To test whether PopZ position is dependent on GPR, we monitored PopZ localization following depletion of GPR in *RS::GPR* (Fig. 6 D and E). In GPR-depleted cells, PopZ-GFP appears mostly diffuse, with a few random foci in the misshapen cells (Fig. 6D). WT PopZ-GFP localization is rescued when this strain is grown in the presence of theophylline (Fig. 6E). Thus, PopZ can still form foci on its own, but that proper localization to the cell pole requires rod shape morphology, dependent on GPR. These data demonstrate the utility of *RS::gpr* to assay phenotypic effects following depletion of GPR.

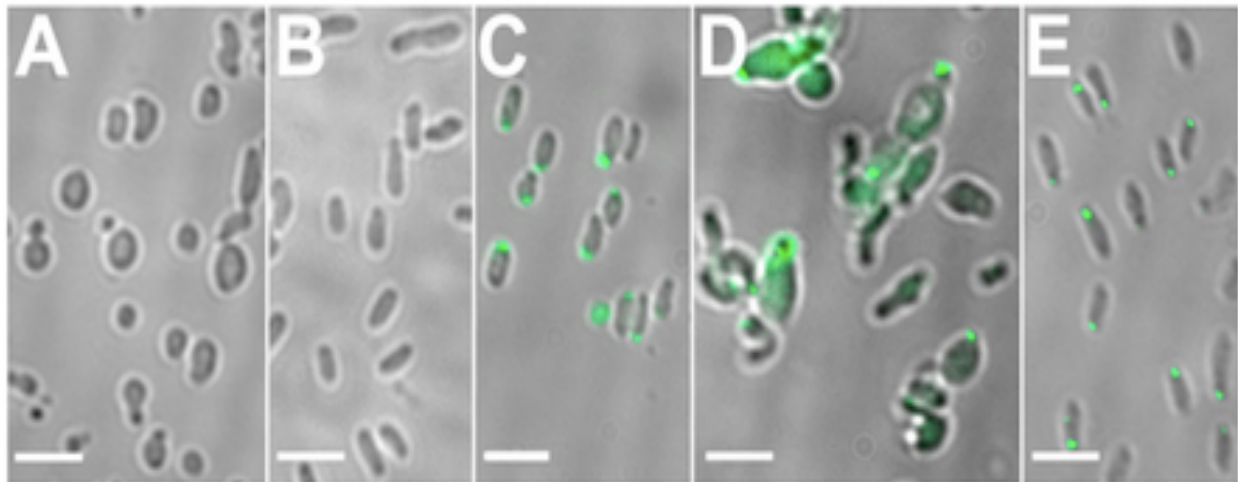


Fig 6. Riboswitch-controlled depletion of GPR mimics stable genetic deletion of GPR and alters PopZ-RFP localization. *RS::gpr* cells were imaged at 24 h after growth without theophylline (A) or at 24 h after growth in 0.5 mM theophylline (B). Expression of GFP-GPR was induced with 0.025 mM IPTG for 24 h in the *RS::gpr* strain grown in the absence of theophylline (C). PopZ-RFP was introduced into *RS::gpr* and grown in the presence of 0.25 mM IPTG without theophylline (D) or 0.25 mM IPTG plus 0.5 mM theophylline (E).

Discussion

We have identified a previously unknown protein, which we named GROWTH POLE RING (GPR), with a striking localization as a ring of six foci at the growth pole in *A. tumefaciens*. GPR plays a major role in polar growth, as its absence leads to severe morphological defects, including loss of cylindrical cell shape. In corollary, its overproduction leads to ectopic growth poles; the finding that overproduction only slightly above WT levels leads to multiple growth poles implies that GPR expression must be tightly regulated. While prokaryotic proteins with single ApoLP domains (associated with lipid droplets) have been reported (33), to date, GPR is the first prokaryotic protein identified with an extended multiple ApoLP domain structure anchored in the inner membrane. GPR potentially represents a new class of proteins with a critical role in polar growth and cell morphogenesis in the Rhizobiales.

We propose that GPR functions as a scaffold for assembly of polar growth machinery essential for peptidoglycan (PG) and/or phospholipid (PL)-dependent membrane biogenesis (Fig. 7A). Polar growth necessitates a mechanism to ensure that the growing pole is not amorphous or unstructured. This need is compounded by the fact that *A. tumefaciens* lacks an underlying cytoskeleton, such as provided by the actin homolog MreB in model systems like *E. coli* and *B. subtilis*, where MreB serves as a scaffold for circumferential PG synthesis during cell elongation by interspersed growth (40–42). Indeed, the numerous ApoLP domains in GPR support the hypothesis that GPR provides a scaffold for membrane assembly, as ApoLPs are well known to sequester lipids in eukaryotes (32). The dramatically abundant α -helical regions of GPR, including a continuous stretch of more than 1,700 amino acids, may provide a hydrophobic

environment for lipid assembly.

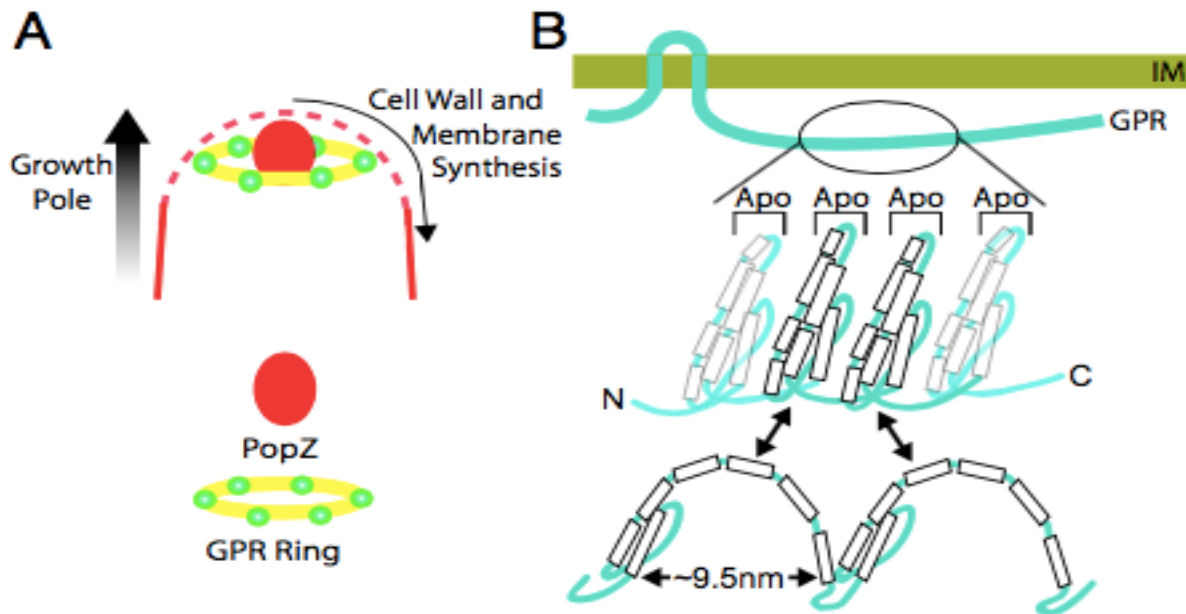


Fig. 7. Models of the GPR hexamer ring (A) and monomer secondary structure (B). (A) Six GPR complexes (green spheres) form a (yellow) ring- shaped scaffold ~100 nm from the tip of the growth pole to organize membrane and PG synthesis. The solid red line indicates outer membrane (OM) staining with red lipophilic dye FM4-64; the dashed red line indicates OM stains less intensively at the growth pole (6). (B) Flexible/reversible structure (based on a model for ApoLP A1; figure 5B in ref. 44) of GPR ApoLP domains (extended vs. compact) may facilitate a variety of configurations between adjacent GPR monomers that maintain the diameter of the GPR scaffold. C, C terminus; IM, inner membrane; N, N terminus.

Mycobacterium also grows by polar growth and produces a polar complex that contains at least three PG synthetic enzymes (MurG, GlfT2, and Pks13) (43). This complex resides in a band called the subpolar space, 0.5 μm from the tip of the growth pole, and the diameter of the complex corresponds to the diameter of the mature cylindrical cell. In striking contrast, the GPR ring complex localizes approximately 100 μm below the tip of the new pole, and the diameter of the GPR ring is only approximately 200 nm. These latter data reveal that *Agrobacterium* polar growth initially occurs in a much narrower ring

of activity. Indeed, independent measurements of new pole cell diameter in different-sized new cells demonstrated that approximately one-third of the upper part of the new cell is of significantly narrower diameter during the early stages of polar growth, and later, PG synthesis increases the new cell diameter until it corresponds to the diameter of the old cell compartment just before division (9). *Mycobacterium* and *Agrobacterium* present surprisingly different examples of what might comprise the geometry of cell wall synthesis complexes during polar growth. Nevertheless, they both suggest a general mechanism for polar growth via a ring structure near the growth pole(s).

How might GPR foci be organized to be ~50 nm apart in a GPR hexamer of ~200 nm diameter? An extended linear string of 1,700 helically arranged amino acids would be ~600 nm long. More likely, GPR ApoLP domains fold into specific 3D shapes. The ApoLP structure is very dynamic, and monomers fold as bundles of helices or extended curved structures in the presence of lipids (44, 45). ApoLPs form two types of complexes of ~9–10 nm diameter when associated with lipids: (i) three ApoLPs arranged in a trefoil with their alpha helical regions on the surface of lipid spheres or (ii) two stacked ApoLPs around a lipid disk (reviewed in ref. 32).

Our data suggest that the 1,700-aa central region of GPR contains approximately eight ApoLPs, each ~200 aa long. These eight ApoLPs may provide an extremely flexible region that may undergo significant rearrangements from bundled to extended configurations during the assembly of membranes and PG. Based on the structure of ApoLP A4 (44), Fig. 7B graphically depicts two ApoLP domains in GPR, alternating between helix bundles and extended conformations. It is highly likely that additional, as-

Chapter 3

yet unidentified proteins may be structural and functional components of the GPR hexamer. Future investigations using a variety of approaches likely will lead to abundant and informative discoveries regarding GPR function during polar growth in the Rhizobiales.

Materials and Methods

Strains and Cell Growth Conditions. The strains and plasmids used in this study are listed in SI Appendix, Table S2. WT *A. tumefaciens* C58 was transformed with the relevant plasmids and grown at 28 °C in Luria Broth (LB) medium containing appropriate antibiotics.

Bioinformatics. We used TipN protein from *C. crescentus* (CC_1485 from strain CB15) as the query in a BLAST search of the Uniprot database Microbial Proteomes with default search parameters (24). GPR (Atu1348) was identified from a manual inspection of the list of hits generated by this search. GPR domains were identified using Pfam (25) and Phyre2 (26).

Molecular Cloning and Strain Construction. Standard molecular cloning techniques were used (46). To construct pJZ251 ($P_{lac}::gpr-gfp$), *gpr* was amplified by PCR from *A. tumefaciens* genomic DNA with NdeI sites at each end and subcloned into pCR2.1-Topo (Thermo Fisher Scientific), and then *gpr* was isolated from NdeI digestion and ligated to similarly digested pJZ210. A similar strategy was used to construct pJZ253 ($P_{lac}::gfp-gpr$), except that *gpr* was PCR-amplified with 5' AvrII and 3' KpnI sites.

Δgpr and $RS::gprAt$ were created as described previously (14, 19). In brief, C58 was transformed with pJZ298 (Δgpr) or pJZ274 ($RS::gpr$) (SI Appendix, Table S2), followed by selecting for a single cross-over into the genome by growth on carbenicillin and then selecting for a second recombination by growth on sucrose. Δgpr and $RS::gprAt$ were verified by PCR amplification of the relevant genomic region and sequencing.

Time-Lapse and Fluorescence Microscopy. Unless noted otherwise, lactose- inducible expression was achieved by diluting overnight cultures to 10^8 cells/mL and adding 0.25 mM IPTG for 4–5 h before single-time or time-lapse imaging by deconvolution fluorescence microscopy as described previously (13). Long-term time-lapse imaging of *Δgpr* was done using the CellASIC ONIX system (EMD Millipore) on a Zeiss Axio Observer Z1 microscope. For quantitative analyses, C58 cells were cotransformed with pJZ253 (GFP-GPR) and pJZ269 (PopZ-RFP) or with pJZ253 and pTC077 (FtsZ-RFP); cell length and position of the fluorescent foci were determined using ObjectJ (47). All images were processed using Fiji software (48).

Superresolution Microscopy. Superresolution images were captured using a Zeiss Elyra PS.1 structured illumination microscope (SIM) equipped with a Zeiss Plan-Apochromat 100×/1.46 oil immersion objective lens and a pco.edge scientific complementary metal-oxide semiconductor camera with a 1.6× tube lens. GFP-GPR fluorescence was detected with 488-nm laser excitation. FM4-64 or RFP fluorescence was detected with 561-nm laser excitation. The lateral pixel size was 41 nm × 41 nm in the recorded images. Z-stacks were acquired by capturing 20 slices with a 0.1-μm step size. The 3D SIM images were reconstructed using ZEN 2012 (black edition) (Zeiss) and processed with Imaris 8.1 (Bitplane).

Protein Analysis. Preparation of *Agrobacterium* cell lysates, gel electrophoresis, and Western blot analysis were performed as described previously (49). The primary antibody was commercially prepared rabbit polyclonal anti-GPR antibody (Genscript) generated against the peptide FEEKPETRKTAKPK (amino acids 27–41) and used at a dilution of 1:1,000.

Acknowledgments. We thank our colleagues John-Marc Chandonia and Steven Brenner for discussions on ApoLP. We also thank Steven Ruzin and Denise Schichnes (College of Natural Resources Biological Imaging Facility at University of California, Berkeley) for assistance with fluorescent imaging and SIM. The Biological Imaging Facility is supported in part by National Institutes of Health Program S10 (Award 1S1OD018136-01). Research in the P.Z. laboratory is supported by National Science Foundation Grant MCB- 0923840. J.S.R.-E. received fellowship support from the Secretaria Nacional de Educacion Superior, Ciencia y Tecnologia, Ecuador. N.G. received support from the College of Natural Resources Sponsored Projects for Undergraduate Research program.

Author contributions: J.R.Z., R.G., J.S.R.-E., and P.Z. designed research; J.R.Z., R.G., J.S.R.-E., and N.G. performed research; J.R.Z., R.G., J.S.R.-E., and P.Z. analyzed data; and P.Z. wrote the paper.

This article contains supporting information online at www.pnas.org/lookup/suppl/doi:10.1073/pnas.1905900116/-/DCSupplemental.

References

1. den Blaauwen T, de Pedro MA, Nguyen-Distèche M, Ayala JA (2008) Morphogenesis of rod-shaped sacculi. *FEMS Microbiol Rev* 32:321–344.
2. Howell M, Brown PJ (2016) Building the bacterial cell wall at the pole. *Curr Opin Microbiol* 34:53–59.
3. Brown PJB, Kysela DT, Brun YV (2011) Polarity and the diversity of growth mechanisms in bacteria. *Semin Cell Dev Biol* 22:790–798.
4. Cameron TA, Zupan JR, Zambryski PC (2015) The essential features and modes of bacterial polar growth. *Trends Microbiol* 23:347–353.
5. Kysela DT, Brown PJB, Huang KC, Brun YV (2013) Biological consequences and advantages of asymmetric bacterial growth. *Annu Rev Microbiol* 67:417–435.
6. Zupan JR, Cameron TA, Anderson-Furgeson J, Zambryski PC (2013) Dynamic FtsA and FtsZ localization and outer membrane alterations during polar growth and cell division in *Agrobacterium tumefaciens*. *Proc Natl Acad Sci USA* 110:9060–9065.
7. Figueroa-Cuilan WM, Brown PJB (2018) Cell wall biogenesis during elongation and division in the plant pathogen *Agrobacterium tumefaciens*. *Curr Top Microbiol Immunol* 418:87–110.
8. Brown PJB, et al. (2012) Polar growth in the alphaproteobacterial order Rhizobiales. *Proc Natl Acad Sci USA* 109:1697–1701.
9. Cameron TA, Anderson-Furgeson J, Zupan JR, Zik JJ, Zambryski PC (2014) Peptidoglycan synthesis machinery in *Agrobacterium tumefaciens* during unipolar growth and cell division. *MBio* 5:e01219-14.
10. Eswara PJ, Ramamurthi KS (2017) Bacterial cell division: Nonmodels poised to take the spotlight. *Annu Rev Microbiol* 71:393–411.
11. Kuru E, et al. (2012) In Situ probing of newly synthesized peptidoglycan in live bacteria with fluorescent D-amino acids. *Angew Chem Int Ed Engl* 51:12519–12523.
12. Howell ML, et al. (2019) *Agrobacterium tumefaciens* divisome proteins regulate the transition from polar growth to cell division. *Mol Microbiol* 111:1074–1092.
13. Grangeon R, Zupan JR, Anderson-Furgeson J, Zambryski PC (2015) PopZ identifies the new pole, and PodJ identifies the old pole during polar growth in *Agrobacterium tumefaciens*. *Proc Natl Acad Sci USA* 112:11666–11671.
14. Anderson-Furgeson JC, Zupan JR, Grangeon R, Zambryski PC (2016) Loss of PodJ in *Agrobacterium tumefaciens* leads to ectopic polar growth, branching, and reduced cell division. *J Bacteriol* 198:1883–1891.
15. Ebersbach G, Briegel A, Jensen GJ, Jacobs-Wagner C (2008) A self-associating protein critical for chromosome attachment, division, and polar organization in *Caulobacter*. *Cell* 134:956–968.
16. Bowman GR, et al. (2008) A polymeric protein anchors the chromosomal origin/ParB complex at a bacterial cell pole. *Cell* 134:945–955.
17. Viollier PH, Sternheim N, Shapiro L (2002) Identification of a localization factor for the polar positioning of bacterial structural and regulatory proteins. *Proc Natl Acad Sci USA* 99:13831–13836.
18. Hinz AJ, Larson DE, Smith CS, Brun YV (2003) The *Caulobacter crescentus* polar organelle development protein PodJ is differentially localized and is required for polar targeting of the PleC development regulator. *Mol Microbiol* 47:929–941.
19. Grangeon R, Zupan J, Jeon Y, Zambryski PC (2017) Loss of PopZA_t activity in *Agrobacterium tumefaciens* by deletion or depletion leads to multiple growth poles, minicells, and growth defects. *MBio* 8:e01881-17.

20. Howell M, et al. (2017) Absence of the polar organizing protein PopZ causes aberrant cell division in *Agrobacterium tumefaciens*. *J Bacteriol* 199:e00101-17.
21. Ehrle HM, et al. (2017) Polar organizing protein PopZ is required for chromosome segregation in *Agrobacterium tumefaciens*. *J Bacteriol* 199:e00111-17.
22. Lam H, Schofield WB, Jacobs-Wagner C (2006) A landmark protein essential for establishing and perpetuating the polarity of a bacterial cell. *Cell* 124:1011–1023.
23. Huitema E, Pritchard S, Matteson D, Radhakrishnan SK, Viollier PH (2006) Bacterial birth scar proteins mark future flagellum assembly site. *Cell* 124:1025–1037.
24. The UniProt Consortium (2017) UniProt: The universal protein knowledge base. *Nucleic Acids Res* 45:D158–D169.
25. El-Gebali S, et al. (2019) The Pfam protein families database in 2019. *Nucleic Acids Res* 47:D427–D432.
26. Kelley LA, Mezulis S, Yates CM, Wass MN, Sternberg MJE (2015) The Phyre2 web portal for protein modeling, prediction and analysis. *Nat Protoc* 10:845–858.
27. Davidson WS, Thompson TB (2007) The structure of apolipoprotein A-I in high-density lipoproteins. *J Biol Chem* 282:22249–22253.
28. Huang R, et al. (2011) Apolipoprotein A-I structural organization in high-density lipoproteins isolated from human plasma. *Nat Struct Mol Biol* 18:416–422.
29. Deng X, et al. (2012) The structure of dimeric apolipoprotein A-IV and its mechanism of self-association. *Structure* 20:767–779.
30. Walker RG, et al. (2014) The structure of human apolipoprotein A-IV as revealed by stable isotope-assisted cross-linking, molecular dynamics, and small-angle X-ray scattering. *J Biol Chem* 289:5596–5608.
31. Rothblat GH, Phillips MC (2010) High-density lipoprotein heterogeneity and function in reverse cholesterol transport. *Curr Opin Lipidol* 21:229–238.
32. Phillips MC (2013) New insights into the determination of HDL structure by apolipoproteins: Thematic review series: High density lipoprotein structure, function, and metabolism. *J Lipid Res* 54:2034–2048.
33. Yang L, et al. (2012) The proteomics of lipid droplets: Structure, dynamics, and functions of the organelle conserved from bacteria to humans. *J Lipid Res* 53:1245–1253.
34. Ding Y, et al. (2012) Identification of the major functional proteins of prokaryotic lipid droplets. *J Lipid Res* 53:399–411.
35. Chen Y, et al. (2014) Integrated omics study delineates the dynamics of lipid droplets in *Rhodococcus opacus* PD630. *Nucleic Acids Res* 42:1052–1064.
36. Vetsigian K, Goldenfeld N (2005) Global divergence of microbial genome sequences mediated by propagating fronts. *Proc Natl Acad Sci USA* 102:7332–7337.
37. Liang P, Riley M (2001) A comparative genomics approach for studying ancestral proteins and evolution. *Adv Appl Microbiol* 50:39–72.
38. Barton HJ, Zeng K (2018) New methods for inferring the distribution of fitness effects for INDELs and SNPs. *Mol Biol Evol* 35:1536–1546.
39. Khan SR, Gaines J, Roop RM, 2nd, Farrand SK (2008) Broad-host-range expression vectors with tightly regulated promoters and their use to examine the influence of TraR and TraM expression on Ti plasmid quorum sensing. *Appl Environ Microbiol* 74: 5053–5062.
40. Bisson-Filho AW, et al. (2017) Treadmilling by FtsZ filaments drives peptidoglycan synthesis and bacterial cell division. *Science* 355:739–743.
41. Yang X, et al. (2017) GTPase activity-coupled treadmilling of the bacterial tubulin FtsZ organizes septal cell wall synthesis. *Science* 355:744–747.
42. van Teeffelen S, et al. (2011) The bacterial actin MreB rotates, and rotation depends on cell wall assembly. *Proc Natl Acad Sci USA* 108:15822–15827.
43. Meniche X, et al. (2014) Subpolar addition of new cell wall is directed by DivIVA in

Chapter 3

- mycobacteria. *Proc Natl Acad Sci USA* 111:E3243–E3251.
44. Mei X, Atkinson D (2011) Crystal structure of C-terminal truncated apolipoprotein A-I reveals the assembly of high-density lipoprotein (HDL) by dimerization. *J Biol Chem* 286:38570–38582.
 45. Mei X, Liu M, Herscovitz H, Atkinson D (2016) Probing the C-terminal domain of lipid-free apoA-I demonstrates the vital role of the H10B sequence repeat in HDL formation. *J Lipid Res* 57:1507–1517.
 46. Green MR, Sambrook J (2012) *Molecular Cloning: A Laboratory Manual* (Cold Spring Harbor Laboratory Press, New York), 4th Ed.
 47. Vischer NOE, et al. (2015) Cell age-dependent concentration of *Escherichia coli* divisome proteins analyzed with ImageJ and ObjectJ. *Front Microbiol* 6:586.
 48. Schindelin J, et al. (2012) Fiji: An open-source platform for biological-image analysis. *Nat Methods* 9:676–682.
 49. Baron C, Llosa M, Zhou S, Zambryski PC (1997) VirB1, a component of the T-complex transfer machinery of *Agrobacterium tumefaciens*, is processed to a C-terminal secreted product, VirB1. *J Bacteriol* 179:1203–1210.

Supporting Informaton Appendix

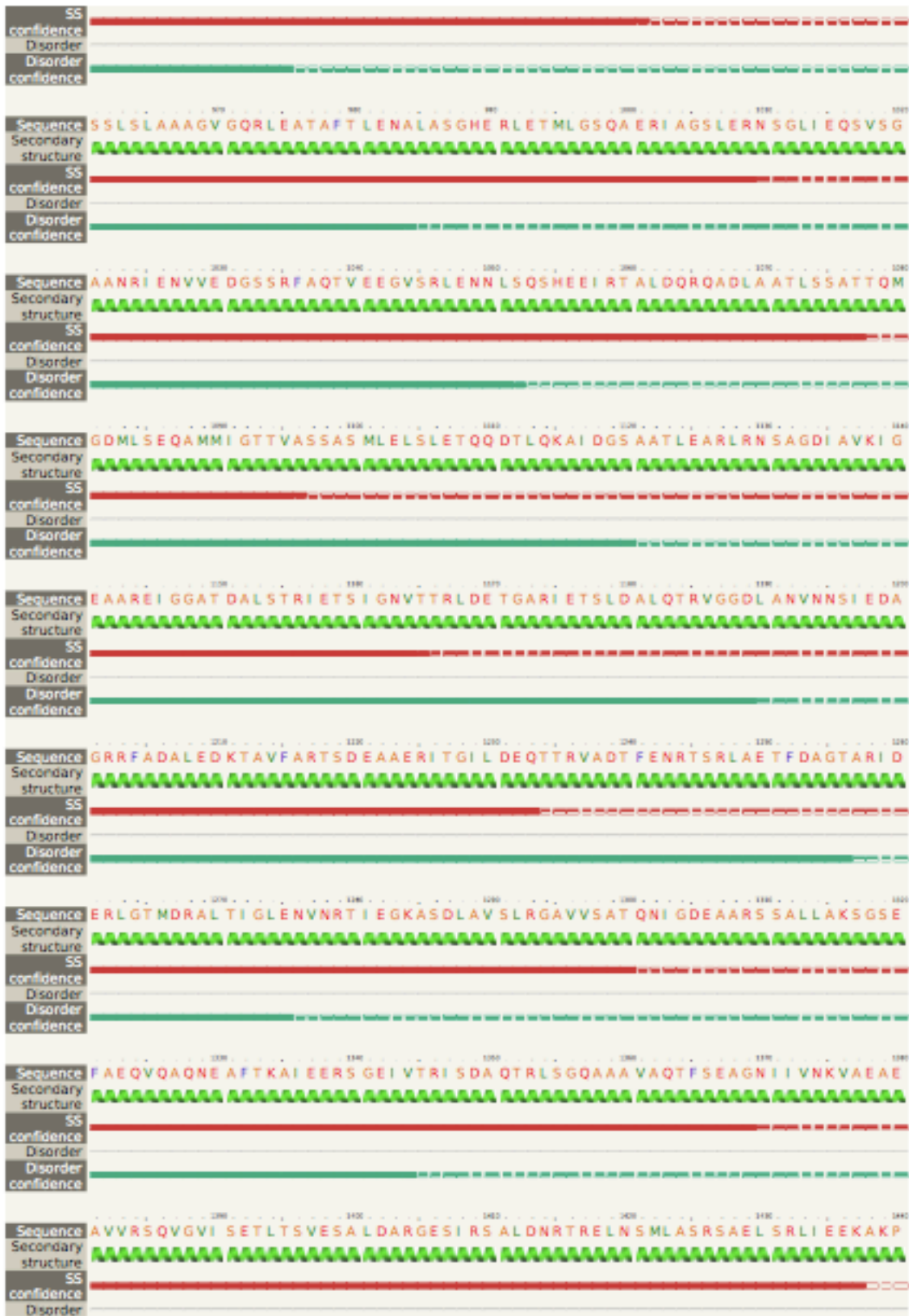
Figure S1. Secondary structure predictions from PHYRE (1). A) *Agrobacterium tumefaciens* protein GPR. B) *Caulobacter crescentus* protein TipN.

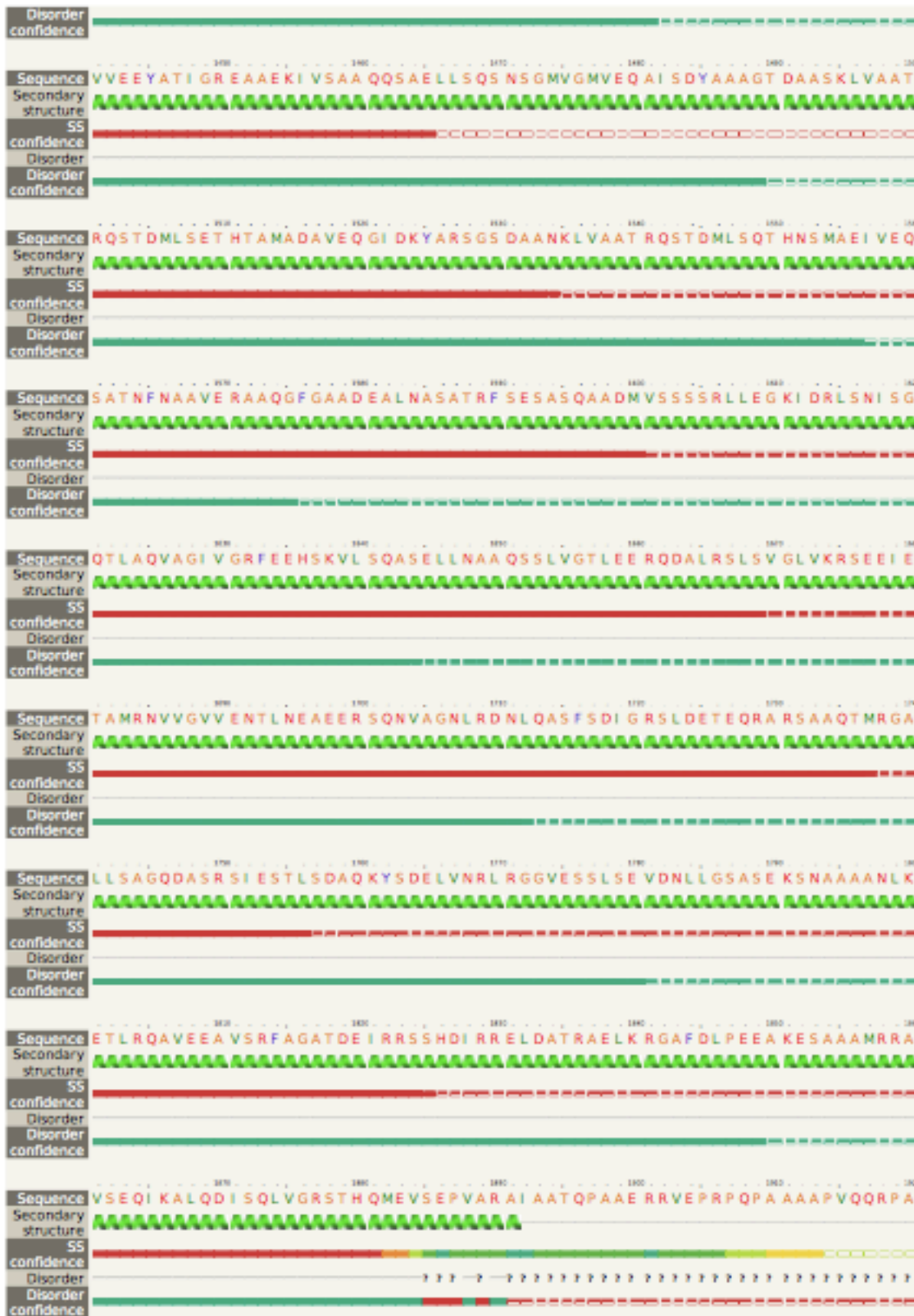
A.



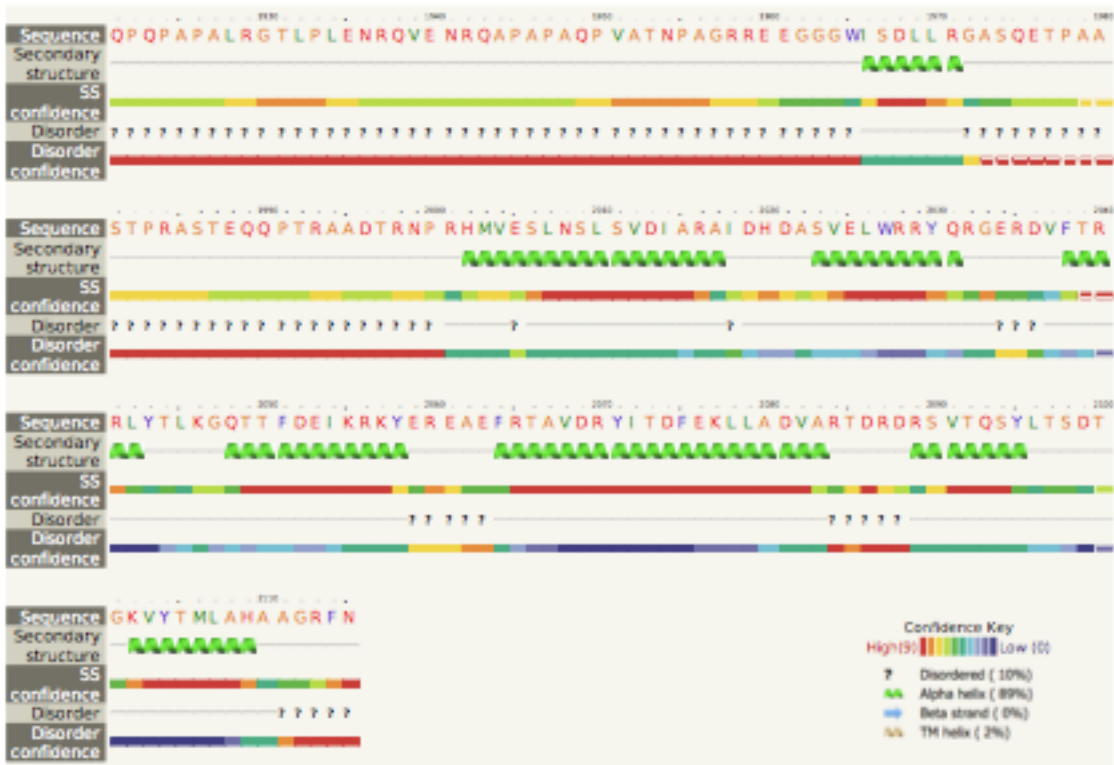
Chapter 3







Chapter 3

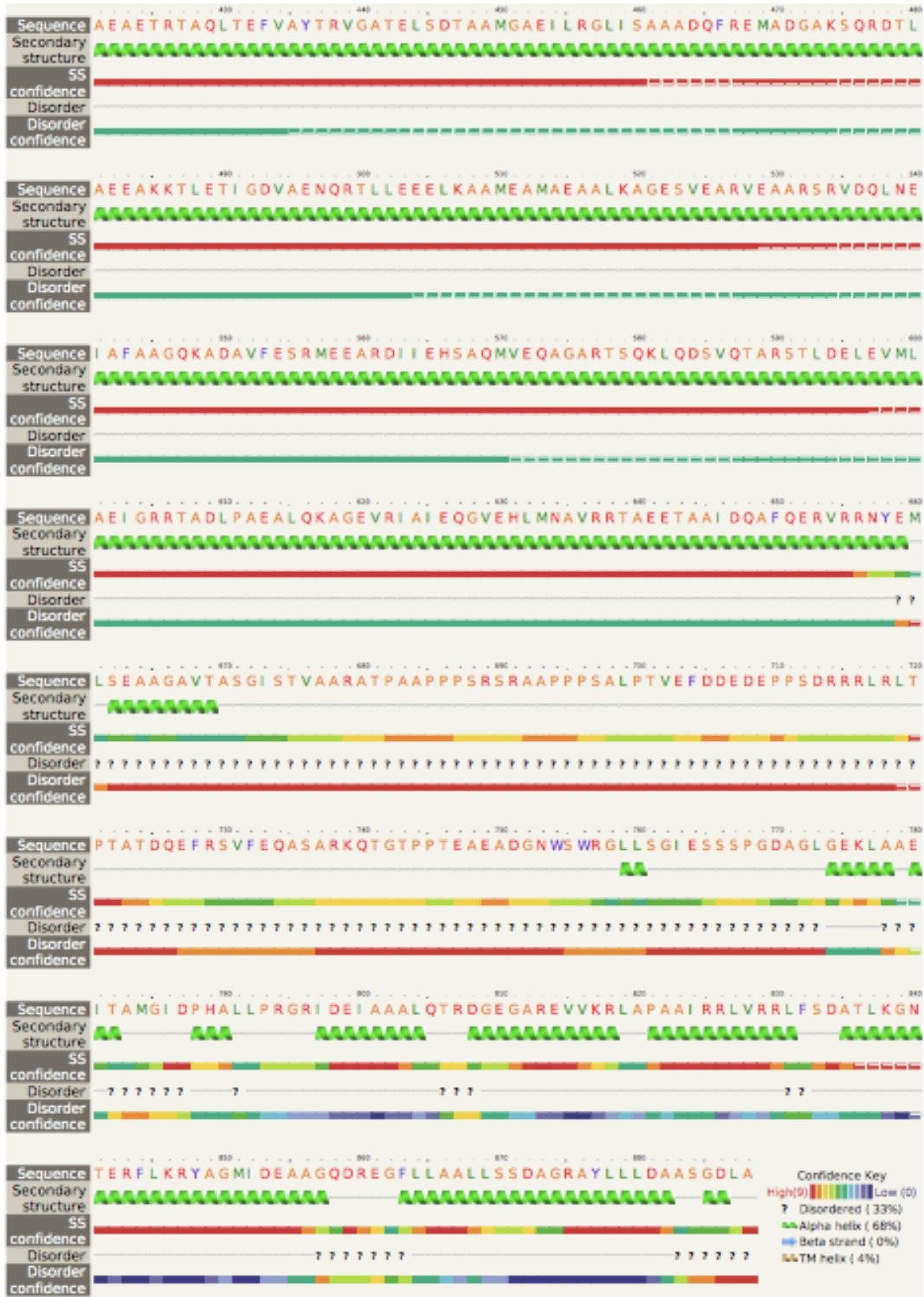


Chapter 3

B.



Chapter 3



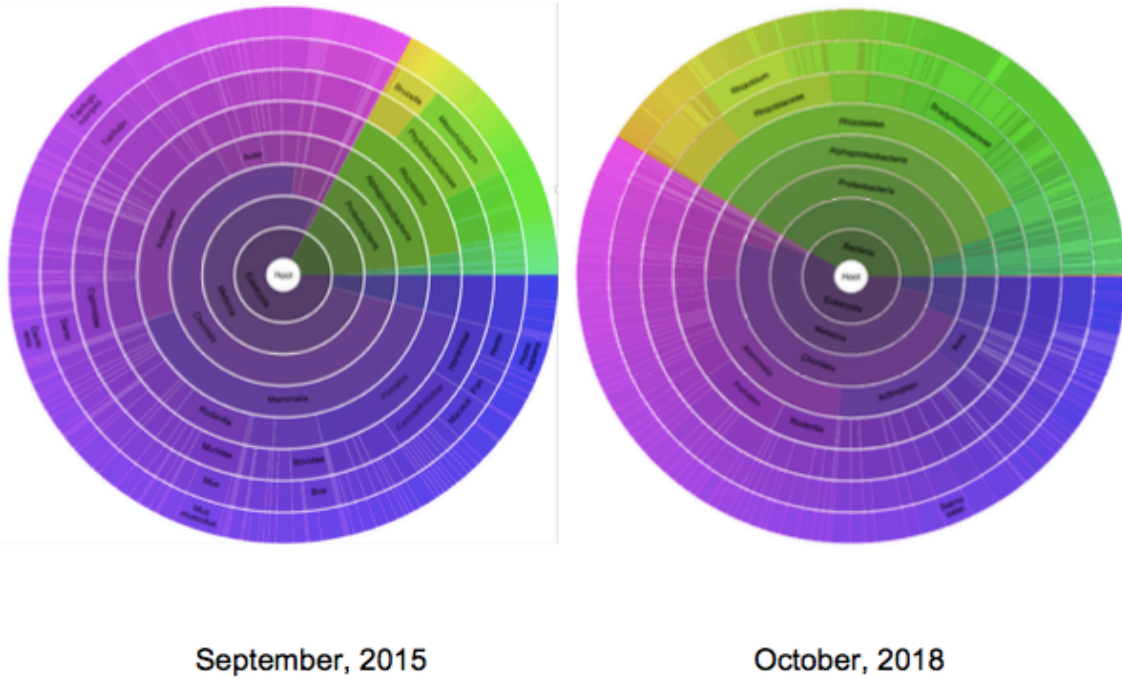


Figure S2. Change in species distribution of apolipoproteins (Pfam, PF01442, (2)) between Sept., 2015, and October, 2018.

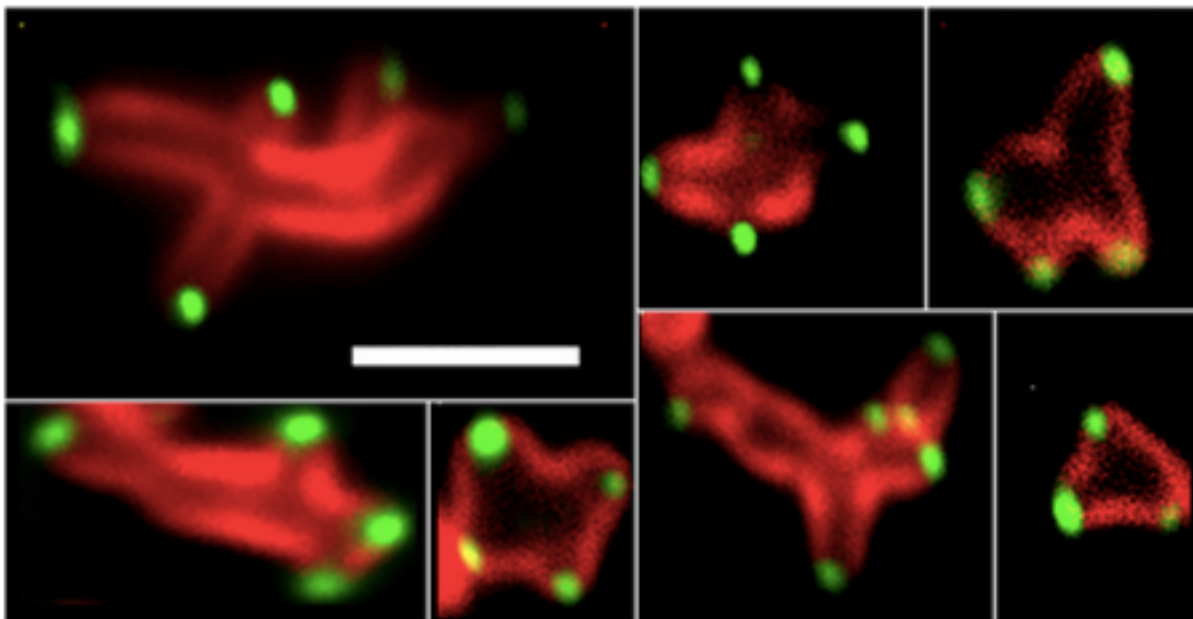


Figure S3. Expression of GPR-GFP *in trans* to WT GPR results in formation of ectopic poles. Cells are counterstained with FM4-64. Scale bar = 3 μ m.

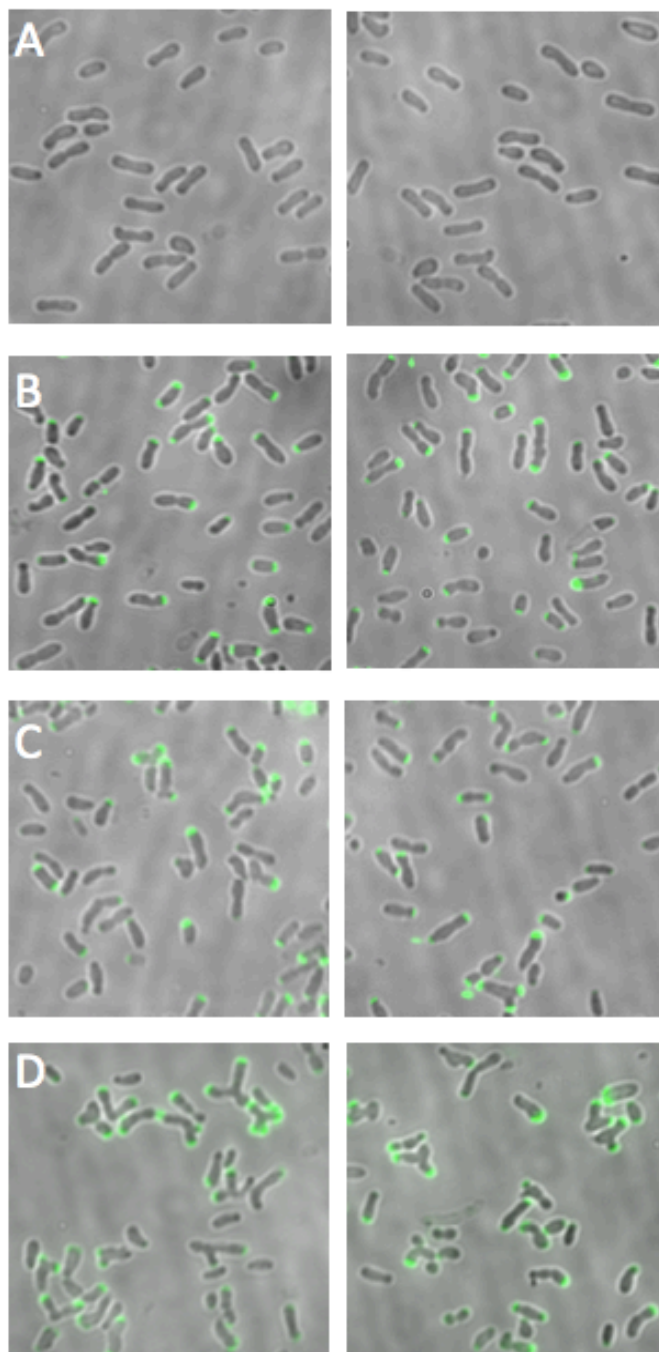


Figure S4. Induction of GFP-GPR in WT *Agrobacterium tumefaciens* with increasing concentrations of IPTG. Ectopic poles are formed at higher concentrations of IPTG. Cells were grown for 24 hours prior to imaging in the IPTG concentration indicated. A) 0mM IPTG, B) 0.25mM IPTG, C) 0.5mM IPTG, D) 1.0mM IPTG.

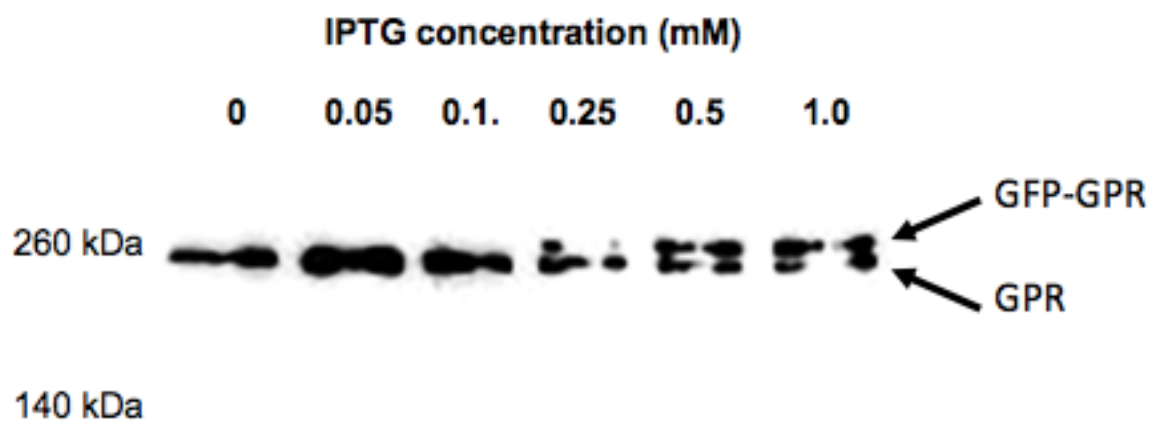


Figure S5. Western blot to detect WT GPR or GFP-GPR. Different concentrations of IPTG were used to induce GPR-GFP expression, cell extracts were separated by SDS-gel electrophoresis, and GPR was detected following Western blotting using antibodies to GPR.

TGCTGACCGCAGGTGCGCCGCGTAATTATCGGGAGCTTCGAAAACAATACTGACCGCTGCCAT
 GGCTGGAATCCTGTCTCGCCGTTTCCTGTTTCATGTCACATATGTGTCTGATTACACGCATGCTG
 GCGGCTGCTATCGGCTTAAATTACGGCGTGACGCAGGCCGAAAATCTTCTGCTATGGTTAATTTA
 TGTTAAACTTATGCGAAACAAGGCGTTCAGCGTGAAACTCAGGTTTAAAAACTGTTAAAAAGCC
 GACACTTCGCTGCCGTGCAAAATCCGCTAAATGTGTCACTACGGTACTGCCGTTCTCGCAGGGC
TTAAGCTCAAGCTTGTATTGCGGCACAGTGATGTAATTTGCCCCGAAAGCTGGACCACCAGC
AATTCGGGATTTGGTAAGTGGCGGAAGTCTCTCTCTTGGAGGAAAGTTTCGTTGGCATGATGG
CGGCAGTCCGCTTGCTGATCGCAAGTGGGTCAACGGCATGAAGCCGGGCGTATGTGTAACGAGG
CGTAACCGCATGGCGAATAACAAGATCAGCGACTCTGTGACGAGACTGCATTTACAGGCATTGG
AAGATGCCCTTGACGCTTGGCGCTTTCGAAGAAAAGCCGGAGACGCGGAAAAGTGCAAAGCCGAA
GCAGCCGGAGGCCAGAGTGAAGGAAGCAAGCAGACAGACCCCTGCTCCCGAGGCCACCCGCGCG
CCTGTGCAACAGACGCCCAGATCGCCCAATCTCGAAGCCGCCAATGACGGCTCCAAGCGCAGCC
CGGCATGATCCTGAAATCGCTGGAAGGCGGCTCCATCGGCGGTGCATTGCGCAACGCCACGAT
CATGTCGGTGATCTGGGCACTCGGCGCCTTGGCATCGCACATCTCCTTTACGGCAATGCGCTG
TGGAGTATCGGCTCGCTCGCCGATCTCACCGCGATCCCCGGCCTGATGGCGATCGTCTGCGCA
TCCTCGTTCCCGTCATGCTGTTCTTCGCCTTCGCGATCATGATGGCGGTGCCCGCGATCTGCG
CAACGCTGCCCGCTCGATGGCCGAAAGTTGCCCTTCGCCTTGCAGAACCGGAAACGGTAGCGTCC
GACCGCATCATGTCCGTGCGCCAAGCGGTTGCGCCGGAAGTTTCGGCCATGAATGACGGTATCG
AGCGCACCATTGCCCGTGCAGCGGAACTCGAAACCTCGTGCATTCCGAAGTCAACGCGCTTGA
GCGCAGCTATGCCGACAACGAATTGCGCGTGCGCAGCCTCGTGCAGGAACTGACCGCCGAGCGC
GACGCCATCGTCAACCATGCCGAGCGCATCCGCTCCTCCATTGTGCGGCGCGCAGGAACAGATCA
AGGAAGAACTGTCCATCGTCGGCGAAGAGCTTTCGATGCGGATCGCCACGACCGGTGAAGCTTT
CGCCTCGATGATCGATACGCGCTCGGCCGCGCTGCTCGAAAAATCGCGGGCCTCGACCGAAGCG
ATGGGTAGCCTGATCGCCGCCAAGACAGAAAACCTGCTGCAGGCGCTGAACTCCTCCGGCTCGA
CGATATCAAACGAATTTGACATGCGCCTGCATAACCTCACGTGACGCTGGACGAGCGCGGTGA
AGTGCTGCTGGAGCGTTTCGCGATCCATGCATCGACGCTGGATAGCGGTGTGGAAAGTCTCAAC
AGCGCGCTTGAGGAGCGCACCCGCCAGCTCAACGAGACGCTGTCCGCGCGCTCCCTGGAAC TCA
ACCGCAATATCGAACCGCGCCAGCAGGTCATCGGCGGTTTCGCTGGATACGGTTCTCGACAAGCT
GTCCACGACGCTTGAAGAAAAGGGCCTCTCCTTCCGCCAGAGCCTGCAGAGCACGGCCGACGAT
GCGATCATGGATCTCGATCTTCGCTCCGGCCTTTACGAAGAGCGCATGCAAGCGACGGTTCGGCC
AGGTCAATTCGGCCTTCGACGAGCATGTGGCGCAATTTGCCAGCGCCTTCGACCAGCGCGCCGG
CAGCCTCGACAGCAAGCTGATGGAAAGCCTCGCACGGATCAACGAAACCGTTGCCGGCGGCTCC
GAAGCCCTCGACACCATTCTGACAAGCGGTCTTGAGCGCATCGGCAGCACCATGACCGACCAGT
CTCTGGCGCTCGCTACCGCGCTGGGCACGGGTGAGGAAATGCTGGAAAACGCACTCGAAAGCCG
GACCCAGGCCTTCAGCGACGCCATCGGCCAGCGCACCCGCCGAAATTACAGATGCCTTACCAAT
TCGCACGCGAAGATCGATACCGTTCTGGCGGAACGCAGCAACGCCCTGTTCCGGCGCGCTTTCGG
CCAGCCAGGACCGTTTCGACGAAGCACTCGCCAGCCGTTCTCTCGCCATTACCGGCTCGGTTTC
CGGCACGGCCGAACACCTTGCCGCGATGCTCGATGAACGCGCCCGCGATCAACAGCGTCGTT
GCCGACGTCGAACGTCGCCTGACGGAGACGCTCGAAACCCGCGCCGACGCCATCACCGGCGCTG
TCTCCGGCATCGAGGACCGCATCTCCGACACGCTGGAAAGCCGCACGGCTGCCCTGCATGATGT
CGTTTCCGGCGCGGAGAGCCGCATCGCCGATACGCTTGACGGCCGACCCGCCGCTCTTTCAGC
GCGATTTCCGGTGTGAGGAACGTATTGCCGACACGATGGACAGCCGCACGCTGTCACTCGACA
TGACCTTCGCCAATGTTGAGGAACGGCTTTCGAGACGCTCGACAACCGCACCTCCGCTCTGAC
AGGCATTGTTGCAAGCGCCGAAGAAAAGATCGCCGGGGCGCTCGATAGCCGCACGGCCACCTTC
GGTGACGTGGTTGCCGGTGTGAAACCCGTATCGCCGAAACGCTTGATGGCCGCACCCGACGCGC
TCAATGCCGTGGTTCCGGTGCCGAGGAGCGCATCGCGGATGCTCTCGACAGCCGTACCATGGC

GCTCGACATGACCTTCTCCGGCGCCGAGGAAAAGATCGCCGAAGCGCTCGACACGCGCACCGCA
 GCCCTTGGTGAGCTGGTGGCAAGCGCCGAGACCCGTATTGCCGGCGCGCTCGACAGCCGCACGG
 ATTGCTGAAAACCGTCGTTTCCGGCGCGGAAGAGCGGATCACCGATGTGCTCGACAGCCGCAC
 CATGGCGCTCGACATGAGCTTCTCCGGCGTTCGAGGAAAAGATCACCGATATTCTCGATGGCCGC
 ACCGCCGCGCTGAAGAGCGCCGTGTCGGTGTGAGGACCGCATTGCCGGTGCCTCGACAGCC
 GTACTGCTGCCCTTCCGGCATCGTGTGAGGCGCGGAAGAAGCATCGCCGAGGCGCTCGATAG
 CCGCACCTGGCACTCGACATGACAATTTCCGGTGTGAAAGAGCGGATCGCCGAGGCGATGGAT
 GCGAGAGCCTCGTCGCTTTCGCTTGCCGCTGCCGGCGTCCGGCCAGCGTCTCGAAGCCACGGCCT
 TCACGCTTGAGAATGCCCTTGCCAGCGGTACAGAGCGGTGGAAACCATGCTTGGCTCGCAGGC
 GGAGCGCATTGCCGGTTCGCTGGAGCGCAATAGCGGCCGTGATCGAACAGAGCGTTTCCGGTGCC
 GCCAACCGCATCGAAAACGTTGTGGAAGATGGCAGCAGCCGTTTTGCGCAGACGGTGGAAAG
 GCGTCTCGCGCCTCGAAAACAATCTGTGCAATCGCACGAAGAAATCCGCACCGCGCTTGACCA
 GCGCCAGGCGGACCTTGCCGCGACGCTCAGCTCCGCCACCACCCAGATGGGCGACATGCTCTCC
 GAGCAGGCGATGATGATCGGCACCACTGTGCGCTCCAGCGCCAGCATGCTCGAATTGTCGCTCG
 AAACCCAGCAGGACACGTTGCAGAAGGCAATCGATGGCAGTGTGCAACGCTGGAGGCCCGTCT
 TCGCAACAGCGCCGGCGACATTGCCGTCAAGATCGGTGAAGCCGCCCGCAAATCGGCGGTGCG
 ACCGACGCCCTCTCCACTCGTATTGAAACCTCAATCGGCAATGTCACCACCCGTCTCGACGAGA
 CCGGCGCCCGCATCGAGACCTCTCTCGACGCCCTCCAGACCCGCGTCGGCGGTGATCTGGCCAA
 CGTCAACAATTCGATCGAAGATGCCGGCCGCGCTTCGCGGACGCGCTGGAAGACAAGACGGCC
 GTGTTGCCCGCACCAGCGACGAGGCCGCCGAACGCATCACCGCATCTGGACGAGCAGACGA
 CCCGCGTCGCAGACACGTTGAAAACCGCACCGCGTCTGGCTGAAACCTTTGATGCCGGCAC
 GGCCCGTATCGACGAACGCCTCGGCACCATGGACCGGGCCCTGACCATCGGTCTCGAAAATGTC
 AACCGCACCATCGAAGGCAAGGCGAGCGATCTCGCCGTCAGCCTGCGCGGCGCCGTTGTCTCCG
 CCACCCAGAACATCGGCGACGAAGCGGCTCGCTCCTGCCCCTGCTCGAAAAGTCCGGCTCGGA
 ATTTGCCGAACAGGTGCAGGCGCAGAACGAGGCCTTACCAAGGCCATCGAGGAACGTTCCGGC
 GAGATCGTCACTCGCATCTCCGATGCCAGACCCGTCTTCCGGCCAGGCTGCTGCCGTGCGCG
 AGACCTTCTCCGAAGCGGGCAACATCATCGTCAACAAGGTGGCCGAAGCTGAAGCCGTCGTTCCG
 CTCCAGGTCCGGCGTCATCTCGGAGACACTGACGAGTGTGCAATCCGCCCTCGATGCACGCGGC
 GAATCGATCCGCTCGGCGCTTGATAAACCGCACCCGCGAACTCAACTCGATGCTGGCCAGCCGTT
 CTGCCGAAGTGTGCGCCTGATCGAGGAGAAGGCGAAACCGGTGTCGAGGAATATGCCACCAT
 CGGCCGGGAAGCCGCCGAAAAGATCGTTTCCGCCGCCAGCAGAGCGCAGAGCTTCTGTGCGAG
 AGCAACAGCGGCATGGTGGAAATGGTGGAAACAGGCGATCAGCGATTACGCCGCCCGGAAACGG
 ATGCAGCAAGCAAACCTCGTCCGCCACCCGCCAGAGCACCGACATGCTGTGCGAAACCCATAC
 GGCCATGGCGGACGCCGTCGAACAGGGTATCGACAAATATGCCCGCTCGGGCAGCGATGCCGCC
 AACAACTCGTGCAGCCACACGCCAGAGCACGGATATGCTGTGCGAGACCCATAACAGCATGG
 CCGAGATCGTTGAGCAGTCCGGCGACCAACTTCAACGCCCGCGTTCGAGCGCGCCGCACAGGGCTT
 CGGCGCGGCGAGATGAAGCGCTGAACGCCCTCCGCGACCCGCTTCTCGGAATCCGCCCTCGAGGCT
 GCCGACATGGTCTCGAGCTCCAGCCGTGCTCGAAGGAAAGATCGACCGTCTGTCGAATATTT
 CCGGCCAGACGCTGGCTCAGGTCGCCGGCATCGTTGGCCGCTTCGAGGAACATTCGAAGGTGCT
 GAGCCAGGCGTCCGAACTACTCAACGCCGCACAGTTCGAGCCTCGTCGGAACGCTGGAAGAAGCT
 CAGGATGCGCTTCGCAGCCTGTCGGTCCGGCCTCGTCAAGCGTTCGGAAGAAATCGAAACCGCCA
 TCGCAACGTCGTCGGCGTCTGGAAAACACCCCTCAACGAGGCGGAGGAGCGTTCACAGAAGCT
 CGCGGGTAATCTGCGTGACAATCTGCAGGCCTCCTTCTCCGATATCGGCCGCTCGCTCGACGAG
 ACCGAACAGCGTGCCCGTTCGGCGGCACAGACCATGCCGGGCGCCTTGCTGTCTGCCGGTCAGG
 ATGCCAGCCGCTCGATCGAAAGCACGCTTCCGACGCGCAGAAATATTCGATGAGCTGGTCAA
 CCGCCTGCGTGGTGGCGTCGAATCCTCGCTGTGCGAAGTCGACAATCTTCTCGGTAGTGCCTCG
 GAGAAATCCAATGCCGCCGCCGCAACCTCAAGGAAACGCTGCGTCAGGCCGTCGAGGAGGCCG
 TTAGCCGCTTTGCCGGTGCAGACAGACGAAATCCGCCGTTCCAGCCACGATATCCGCCGCGAGCT


```

GGATGCGACCCGCGCCGAACCTGAAGCGTGGCGCATTCGACCTGCCGGAAGAAGCCAAGGAAAGT
GCGGCCGCCATGCGCCGCGCCGTTTCCGAACAGATCAAGGCCCTGCAGGATATTTCCCAACTCG
TCGGTCGCTCGACCCACCAGATGGAAGTGTCCGAACCGGTCGCCCGTGCCATCGCCGCAACCCA
GCCGGCCGCGAGAACGCCGCGTTCGAGCCGCGTCCGCAGCCGGCGGCAGCCGCTCCGGTGCAGCAG
CGCCCGGCACAGCCGAGCCTGCCCCTGCATTGCGTGGCACACTGCCGCTTGAGAACCGTCAGG
TCGAAAACCGTCAGGCACCCGCCCCGGCGCAGCCGGTCGCAACCAACCCGGCCGGACGCCGGGA
AGAAGGCGGCGGCTGGATCAGCGATCTGCTACGCGGCGCGTCCCAGGAGACGCCAGCAGCATCT
ACACCGCGCGCCAGCACTGAGCAGCAGCCCACCCGTGCGGGCCGACACCCGCAATCCCCGGCACA
TGGTGGAAATCGCTGAATTCACCTCTCGGTTCGATATCGCCCGCGCCATCGATCACGATGCCTCCGT
GGAACTGTGGCGCCGCTATCAGCGCGGCGAGCGCGACGTCTTCACACGTGCCTCTACACGCTG
AAGGGCCAGACGACGTTTGACGAGATCAAGCGCAAATACGAACGCGAAGCGGAATTCCGCACCG
CCGTGGACCCTACATCACCATTTCGAGAAGCTGCTCGCCGACGTGGCCCGCACCAGCCGCGA
CCGGAGCGTCAACCAGTCTACCTCACCTCCGATACCGCAAGGTCTATACGATGCTTGCCCAT
GCGGCGGGCCGGTTTAATTGA

```

Figure S6. *gpr* deletion strategy. Atu1349 partial protein coding sequence in blue. Atu1348 (GPR) coding sequence in red. Intergenic region in black **bold**. Deleted sequence (underlined) comprises 238 bp upstream of the *gpr*-ATG and the first 2140 bp of the coding sequence for Atu1348 (total *gpr* protein coding sequence is 6345 bp).

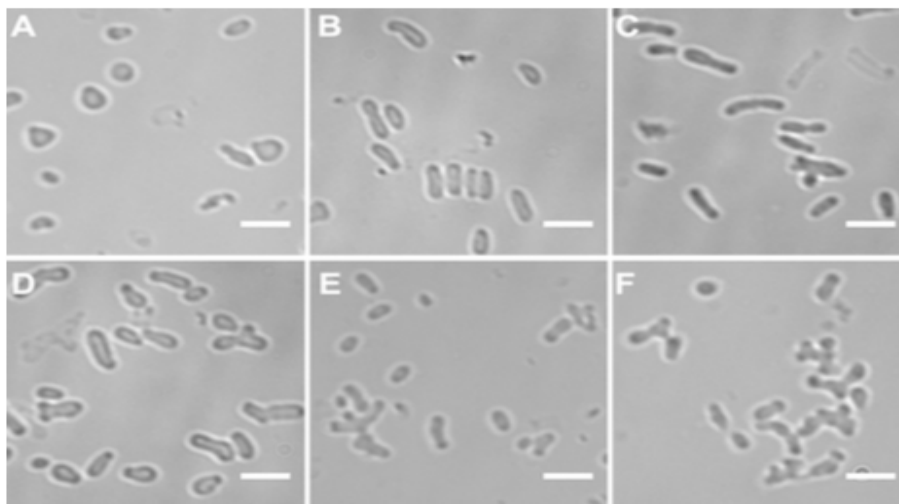


Figure S7. Δgpr complementation. Unipolar growth and cell division were restored in Δgpr following introduction of a plasmid carrying WT *gpr* under the control of the *lac* promoter ($P_{lac}::gpr$ (pSRKGm)). Cells were grown for 24 hours prior to imaging in the IPTG concentration indicated. A) 0 μ M IPTG, B) 25 μ M IPTG, C) 50 μ M IPTG, D) 100 μ M IPTG, E) 250 μ M IPTG, and F) 500 μ M IPTG. Scale bar = 3 μ m.

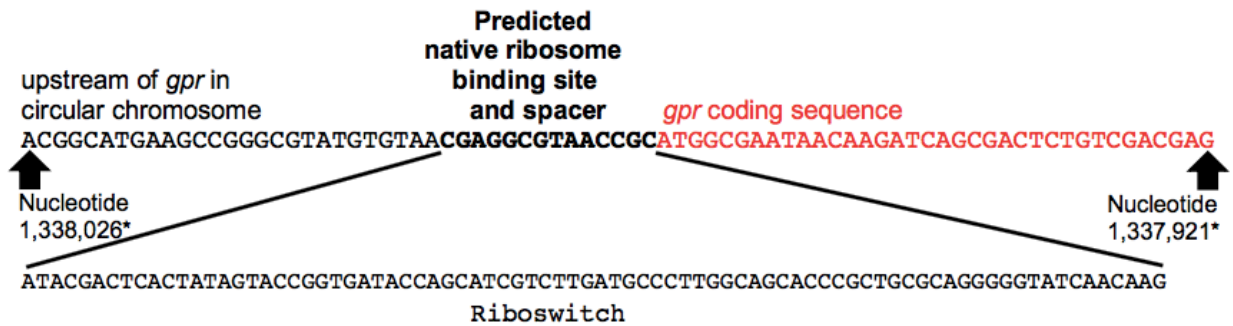


Figure S8. Riboswitch strategy for controlling GPR expression in circular chromosome. The predicted ribosome binding site and spacer (**bold**) were replaced by the riboswitch. *Nucleotide coordinates are for the circular chromosome of *Agrobacterium tumefaciens* (Accession AE007869.2, ncbi.nlm.nih.gov).

Supplementary Table 1. Apolipoprotein domains (Family PF01442) in GPR identified by www.pfam.xfam.org (2). ^aamino acid number

Position in GPR^a	Domain Length (amino acids)	e-value
290-450	161	9.7×10^{-1}
323-523	201	3.6×10^{-1}
416-612	197	1.5×10^{-2}
495-718	224	7.3×10^{-3}
625-824	201	7.2×10^{-5}
821-1008	188	5.5×10^{-2}
937-1126	190	7×10^{-6}
1115-1338	224	1.9×10^{-4}
1291-1439	149	13
1335-1542	208	6.5×10^{-4}
1583-1783	201	5.3×10^{-4}
1784-1878	95	290

Table S2. Strains and plasmids used in this study.

Strains	Relevant genotype and features	Source
XL1 Blue E. coli	cloning strain, endA1 gyrA96(nal ^R) thi-1 recA1 relA1 lac glnV44 F'[::Tn10 proAB+ lacIq Δ(lacZ)M15] hsdR17(rKmK+), Tet ^R	Lab stock
C58	wild-type <i>A. tumefaciens</i> strain C58	Lab stock
A185	C58 carrying pJZ251	This work
A187	C58 carrying pJZ253	This work
A202	C58 carrying pJZ253 and pJZ269	This work
A212	C58 with the native <i>gpr</i> ribosome binding (RBS) site substituted with a riboswitch, referred to as RS:: <i>gpr</i> in text	This work
A248	C58 with a deletion of 2378bp including 238bp upstream of the <i>gpr</i> ATG and the first 2140bp of the <i>gpr</i> coding sequence, referred to as Δ <i>gpr</i> in text	This work
A239	A212 carrying pJZ253	This work
A253	A248 carrying pJZ280	This work
A256	A212 carrying pRG001	This work
RESJ001	C58 carrying pJZ253 and pTC077	This work
Plasmids	Relevant genes and construction information	Source
pSRKGm	Broad host-range, <i>lacI</i> , gentamycin ^R	(3)
pSRKKm	Broad host-range, <i>lacI</i> , kanamycin ^R	(3)
pBluescript II SK	Phagemid, carbenicillin ^R	Stratagene
pJZ156	pBSKII+ with <i>sacB</i> , carbenicillin ^R	(4)
pJZ210	pSRKGm with P _{lac} :: <i>gfp</i>	This work
pJZ251	pSRKGm with P _{lac} :: <i>gpr</i> _{AC} <i>gfp</i>	This work

pJZ253	pSRKGm with $P_{lac}::gfp-gpr$	This work
pJZ269	pSRKKm with $P_{lac}::popZ_{At}-rfp$	This work
pJZ274	pJZ156 carrying 2kb sequence homologous to C58 genomic DNA in which the native <i>gpr</i> RBS is replaced with a riboswitch (Fig. S8)	This work
pJZ280	pSRKGm with $P_{lac}::gpr$	This work
pJZ298	pJZ156 carrying 1kb homologous to C58 genomic DNA on either side of the sequence to be deleted (Fig. S6)	This work
pRG001	pSRKGm with $P_{lac}::popZ_{At}-gfp$	(5)
pTC077	pDW029 with $P_{lac}::ftsZ-rfp$, streptomycin/spectinomycin ^R	(6)

Supplemental references

1. Kelley LA, Mezulis S, Yates CM, Wass MN, Sternberg MJE (2015) The Phyre2 web portal for protein modeling, prediction and analysis. *Nature Protocols* 10(6):845–858.
2. El-Gebali S, et al. (2019) The Pfam protein families database in 2019. *Nucleic Acids Res* 47(D1):D427–D432.
3. Khan SR, Gaines J, Roop RM, Farrand SK (2008) Broad-host-range expression vectors with tightly regulated promoters and their use to examine the influence of TraR and TraM expression on Ti plasmid quorum sensing. *Appl Env Microbiol* 74(16):5053–5062.
4. Anderson-Furgeson JC, Zupan JR, Grangeon R, Zambryski PC (2016) Loss of PodJ in *Agrobacterium tumefaciens* leads to ectopic polar growth, branching, and reduced cell division. *J Bacteriol* 198(13):1883–1891.
5. Grangeon R, Zupan JR, Anderson-Furgeson J, Zambryski PC (2015) PopZ identifies the new pole, and PodJ identifies the old pole during polar growth in *Agrobacterium tumefaciens*. *Proc Natl Acad Sci USA* 112(37):11666–11671.
6. Cameron TA, Anderson-Furgeson J, Zupan JR, Zik JJ, Zambryski PC (2014) Peptidoglycan synthesis machinery in *Agrobacterium tumefaciens* during unipolar growth and cell division. *MBio* 5(3):e01219–14.

Supplemental Movies

Movie S1, S2, S3, S4. *Agrobacterium* cells expressing GFP-GPR display a ring of foci just below the growth pole. GFP-GPR localization in 4 cells shown by rotational animation of 3-dimensional renderings from images obtained with structured illumination superresolution microscopy.

Movie S5. *Agrobacterium* cells expressing GFP-GPR and PopZ-RFP display a ring of green foci just below the growth pole and a single red focus. Localization shown in rotational animation of 3-dimensional rendering from images obtained with structured illumination superresolution microscopy.

Movie S6. Time lapse of *Agrobacterium* cell expressing GFP-GPR shown in Fig. 4.

Movie S7. Time lapse of 2 *Agrobacterium* cells expressing GFP-GPR show variability in persistence of GPR at old pole.

Movie S8. Time lapse of Δgpr cell in Fig. 5.

Movie S9. Δgpr cell division produces quartet of cells.

Chapter 4

Segregation of four *Agrobacterium tumefaciens* replicons during polar growth: PopZ and PodJ control segregation of essential replicons

J. S. Robalino-Espinosa^{a,b}, J. R. Zupan^a, A. Chavez-Arroyo^a, and P. Zambryski^a

^aDepartment of Plant and Microbial Biology, University of California, Berkeley, CA 94720; ^bDepartment of Molecular and Cell Biology, Vrije Universiteit Amsterdam, 1081 HV Amsterdam, The Netherlands.

¹To whom correspondence should be addressed. Email: zambrysk@berkeley.edu.

4

Format adjusted from: Proc Natl Acad Sci U S A. 2020 Oct 20;117(42):26366-26373.

Abstract

Agrobacterium tumefaciens C58 contains four replicons, circular chromosome (CC), linear chromosome (LC), cryptic plasmid (pAt), and tumor-inducing plasmid (pTi), and grows by polar growth from a single growth pole (GP), while the old cell compartment and its old pole (OP) do not elongate. We monitored the replication and segregation of these four genetic elements during polar growth. The three largest replicons (CC, LC, pAt) reside in the OP compartment prior to replication; post replication one copy migrates to the GP prior to division. CC resides at a fixed location at the OP and replicates first. LC does not stay fixed at the OP once the cell cycle begins and replicates from varied locations 20 min later than CC. pAt localizes similarly to LC prior to replication, but replicates before the LC and after the CC. pTi does not have a fixed location, and post replication it segregates randomly throughout old and new cell compartments, while undergoing one to three rounds of replication during a single cell cycle. Segregation of the CC and LC is dependent on the GP and OP identity factors PopZ and PodJ, respectively. Without PopZ, replicated CC and LC do not efficiently partition, resulting in sibling cells without CC or LC. Without PodJ, the CC and LC exhibit abnormal localization to the GP at the beginning of the cell cycle and replicate from this position. These data reveal PodJ plays an essential role in CC and LC tethering to the OP during early stages of polar growth.

Agrobacterium tumefaciens | polar growth | replication and segregation | multipartite genomes | PopZ and PodJ

Significance

Bacteria are ubiquitous, essential, and remarkably diverse. Many infectious species do not follow rules established in model bacteria where growth occurs by insertion of new material along the cell length; instead, many pathogens grow from their poles. Pathogenic bacteria also carry multipartite genomes for adaptation to different ecological niches. How multiple chromosomes replicate and segregate in the context of polar growth is largely unknown. Here, four replicons of the plant pathogen *Agrobacterium tumefaciens* exhibit distinct temporal and spatial replication/segregation patterns during the polar growth cycle, and specific proteins, targeted to the nongrowing and new growth poles, regulate replicon transmission. Uncovering the mechanisms underlying polar growth and chromosome segregation will present new opportunities to design strategies to limit bacterial diseases.

Introduction

Alphaproteobacteria (especially the order Rhizobiales) have complex genomes with multiple elements classified as primary or secondary chromosomes, as well as very large plasmids (1, 2). The 5.67-Mb sequenced genome of the well-known Rhizobiales pathogen, *Agrobacterium tumefaciens* C58, is organized into four replicons, circular chromosome (CC) (2.8 Mbp), secondary linear chromosome (LC) (2.0 Mbp), cryptic plasmid (pAt) (0.5 Mbp), and tumor-inducing plasmid (pTi) (0.2 Mbp) (3, 4). Essential genes are present only on CC and LC (3, 4). Multipartite genomes have arisen independently in nearly 10% of bacterial species from diverse phyla (5). The prevalence of multipartite organization in plant symbionts (*Sinorhizobium meliloti*) (6), plant pathogens (*A. tumefaciens*) (3, 4), animal symbionts (*Vibrio fischeri*) (7), and animal (*Brucella abortus*) (8) and human (*Vibrio cholerae*) (9) pathogens suggests that a divided genome may be important for viability in diverse niches by enabling coordinated expression of sets of genes in response to specific conditions (5). For example, pAt encodes proteins for diverse metabolic and detoxification functions likely advantageous in the species-rich, competitive soil environment (3, 4, 10), and pTi encodes essential functions specific to virulence that create the unique plant tumor environment exploited by *Agrobacterium* (10, 11).

Multipartite genomes, however, likely require mechanisms that coordinate replication and segregation of replicons to ensure sibling cells inherit complete genomes. Each of the four genetic elements in *Agrobacterium* encodes its own segregation system that includes a specific binding site and factors that bind to this site to facilitate separation and partitioning of newly replicated chromosomal elements. The CC encodes a *parABS*

partitioning system (2), whereas LC, pTi, and pAt each encode their own *repABC* cassette (2–4).

An early report described two patterns of localization for the four replicons of *Agrobacterium*: CC, LC, and pAt localization was either unipolar in short cells or bipolar in longer cells, while pTi exhibited a subpolar localization pattern in short and long cells (12). These studies were performed before it was known that *Agrobacterium* undergoes polar growth from a single pole (13–15). Polar growth produces two distinct poles, an actively growing new growth pole (GP), and a nongrowing old pole (OP) (Fig. 1). A more recent study focused on the *Agrobacterium* CC (16); CC first localized to the OP, and after replication, one CC remained at the OP, while the other migrated to the GP. After division, each sibling had a CC localized at their OP.

Here we characterize and compare the replication and segregation of all four *Agrobacterium* replicons (CC, LC, pAt, pTi) during polar growth. There are several obvious questions: 1) do all replicons localize to the OP prior to replication, or do some replicons replicate at other locations; 2) where do replicons migrate during their segregation; and 3) what is the timing of replication and segregation of the different elements? Our studies were facilitated by the ability to distinguish the GP and OP: the GP has a distinct morphology as a bud with a narrow diameter, while the nongrowing OP has dimensions of a fully grown cell (Fig. 1). Furthermore, GP and OP specific marker proteins have been identified: PopZ marks the GP, and PodJ marks the OP (Fig. 1) (17–19). We demonstrate that each of the four genetic elements exhibits a distinct pattern of localization and timing for their replication and segregation during polar growth. We monitor the replication/segregation of the essential CC and LC in detail and demonstrate

that their segregation is critically dependent on PopZ and PodJ.

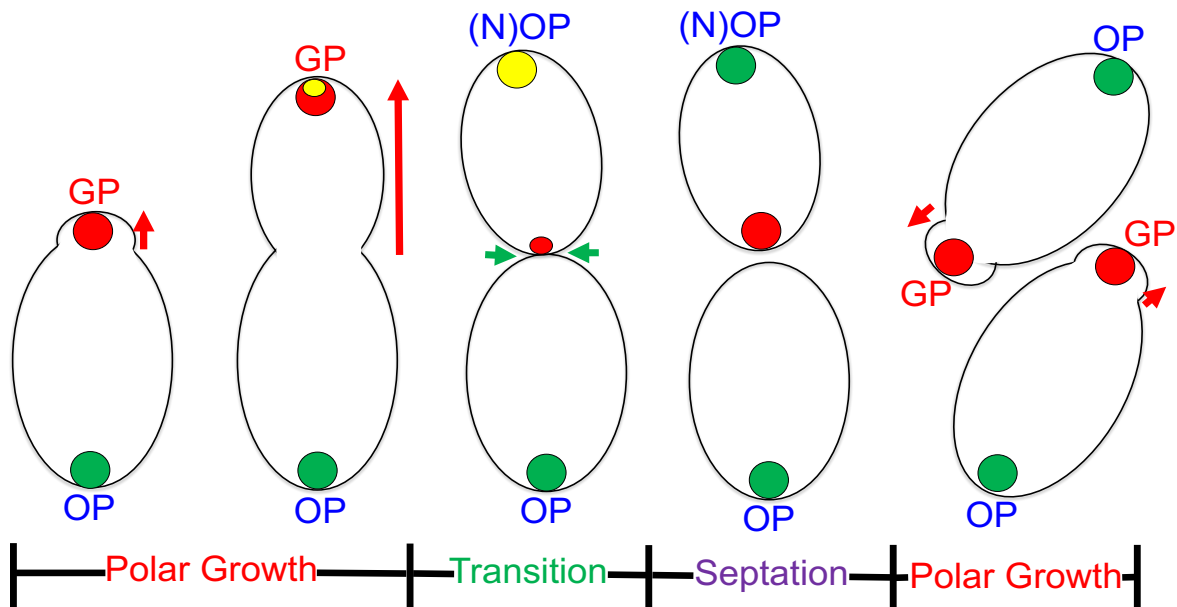


Fig. 1. Polar growth in *Agrobacterium*. First, a GP bud is visible in early stages of the cell cycle. PopZ (red circles) is at the GP, and PodJ (green circles) is at the OP. The GP increases in width and length (red arrows), while the OP does not grow. During elongation, PodJ begins to accumulate at the GP (yellow circles, due to colocalization of PopZ and PodJ). When the new cell compartment reaches its final size, the GP transitions into a “new” OP ([N]OP), and the cell divides at the midcell (green arrows) to produce two sibling cells which will restart polar growth. During transition and septation, PopZ is mobilized from the (N)OP to the nascent GP of the upper cell at the septation site. PopZ is synthesized and localized to the new GP in the lower cell as polar growth begins. For details, see refs. 13–18.

Results

We monitored the replication and segregation of the four genetic elements in *A. tumefaciens* strain C58 by fluorescence microscopy of enhanced green fluorescent protein (eGFP) or red fluorescent protein (RFP) fused to the cognate partitioning protein of each genetic element: ParB, CC; RepB, LC; RepB-At, pAt; RepB-Ti, pTi.

Replication and Segregation of the Agrobacterium Circular Chromosome. The CC displays a very specific pattern of dynamic localization and movement during polar growth (monitored by eGFP fused to ParB). Immediately after cell division, a sibling cell has already replicated its CC, so that one CC is at the OP, and the other CC has migrated almost halfway through the old cell compartment (Fig. 2A, 0', Movie S1). In just 10 min, the newly replicated CC arrives at the GP in the new cell compartment. As polar growth continues, the CC remains associated with the GP and ensures one CC copy is segregated to the GP before elongation is complete. The tight association of replicated CC with the GP and OP suggests a mechanism(s) that targets the CC to these specific cellular locations.

While the overall pattern of replication and segregation is similar in sibling cells, the timing of these events is different during late stages of cell elongation when CCs are localized to both the GP and OP (Fig. 2B and Movie S2); the shorter, narrower GP compartment (Fig. 2B, 0') is distinguished from the longer nongrowing OP compartment. Just before cell division, the CC in the OP compartment (cell 2) replicates at 40 min. CC replication in the GP compartment sibling (cell 1) occurs at 60 min. Thus, siblings do not replicate their CCs synchronously, as also previously reported (16).

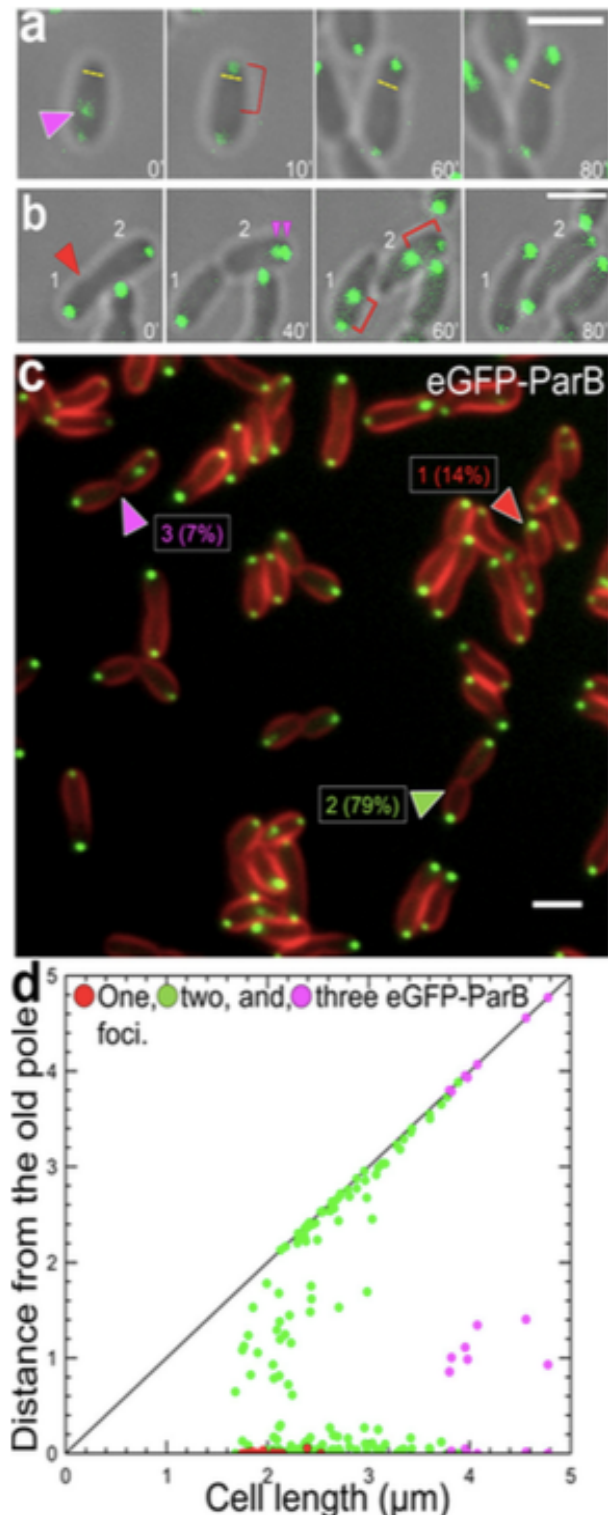


Fig. 2. Replication and segregation of the CC during polar growth. (A) Time-lapse imaging of CC localization (monitored as eGFP-ParB fluorescence). Yellow dashed line indicates the boundary between the older sibling and the emerging newer sibling. The CC is already replicated at 0' (magenta arrowhead). CC migration to GP (red bracket) is complete by 10' where it remains during polar growth (up to 80' shown). (B) Time lapse of asynchronous CC replication in sibling cells 1 and 2. CCs are at the GP (nascent sibling 1, red arrowhead), and at the OP in nascent sibling 2 (0'). The CC replicates in nascent sibling 2 (40', double magenta arrowheads) but not in the still elongating nascent sibling 1. The CC in sibling 1 replicates between 40' and 60'. Migration of both newly replicated CC (60', red brackets) to new GPs is complete by 80'. (C) Localization of eGFP-ParB in 100 FM4-64 stained cells. Percentages of cells displaying one, two, or three foci, are shown with, red, green, and magenta arrowheads. (D) Distances of eGFP-ParB foci from the OP in 100 cells containing one (red), two (green), or three (magenta) foci are plotted versus cell length. Foci on the x axis are at the OP, and foci on the diagonal are at the GP. Foci between the x axis and the diagonal represent foci in transit to the GP; 27 such foci can be easily seen, representing 34% of cells with two foci (i.e., 27 out of 79 cells with two foci); by corollary, 66% of cells have their newly replicated CC at the GP. (Scale bars in A–C, 2 μm).

At the population level, the CC mainly localizes as two foci (79%), while 14% of cells contained one focus at the OP, and 7% of cells displayed three foci (Fig. 2C). To estimate the timing of CC movement post replication, we plotted the distance of CC (eGFP-ParB foci) from the nongrowing OP versus cell length (Fig. 2D). Cell length is an estimate of cell cycle stage during polar growth (20). Foci on the x axis or along the diagonal are at OPs or GPs, respectively; foci between these two lines represent foci in transit from the OP to the GP (SI Appendix, Fig. S1). The data reveal three trends. First, the shortest cells (1.8–2 μm) have one unreplicated CC at the OP as expected. Many short cells also contain two foci, indicating that CC replication occurs immediately after cell division. Second, in cells with two foci, 66% show newly replicated CCs at the GP, underscoring that CC transit to the GP is rapid; fewer cells (34%) show foci in transit between the x axis and the diagonal. Extremely long cells (3.8–4.8 μm) have three foci with CCs localized at the OP, GP, and a third focus just distal to the OP. Cells with three foci support that replication can occur prior to cell division as seen in Fig. 2B. Finally, CCs localize to GP in all cells 3 μm and longer; thus, replication and segregation of CC are complete before most new cells are halfway to their final length ($\sim 4 \mu\text{m}$). As the *A. tumefaciens* cell cycle is ~ 90 min (in Luria broth [LB] at 28 °C), the CC is replicated and segregated within the first 45 min of the cell cycle. The precision of CC replication/segregation is distinct from that observed for other *Agrobacterium* replicons.

Replication and Segregation of the Linear Chromosome. Replication and segregation of the LC (monitored by eGFP-RepB fluorescence) is strikingly complex. In two sibling cells just undergoing cell division, LC foci are at or close to the OP (Fig. 3A, 0' and Movie S3). By 30', the single LC focus in sibling cell 2 migrates through the old cell compartment

and localizes just below the junction between the new and old cell compartments; by 40 min, this LC has replicated, and one copy localizes at the GP, while the other copy moves back to the OP (Fig. 3A, 60', 80'). Like the CC, LC replication is not synchronous in the two siblings, but occurs 20 min later in the younger sibling 1 (Fig. 3A, 60'). By 80 min, both siblings have a similar localization of LC at their GPs and OPs. In summary, the LC initially localizes at or near the OP, but, unlike the CC, the LC migrates away from the OP before it replicates. After replication, one LC returns to the OP, while the other copy migrates to the GP.

The frequency of cells with one, two, or more LC foci (Fig. 3B) is unlike that observed for the CC (Fig. 2C). The LC localizes as two foci at a lower frequency (29.6%) compared to the CC (79%), while more cells contained one focus (50.4%) compared to the CC (14%). The LC also localizes as three (4.8%) or four (1.6%) foci. Unexpectedly, no foci were observed in 13.6% of cells that show a diffuse signal (Fig. 3B). Time-lapse imaging shows distinct LC foci can change to a diffuse signal and then return to a distinct focus during the course of a cell cycle (SI Appendix, Fig. S2).

To estimate the timing of LC segregation post replication, we plotted the distance of LC foci from the OP (Fig. 3C). The distribution of LC foci is clearly different from the CC (Fig. 2D). Notably, single LC foci (prior to replication) are widely distributed throughout the entire old cell compartment ranging from the OP in the shortest cells (1.73 μm) to close to the midcell in long cells (3.4 μm). This distribution likely reflects the variable movement of LC foci away from the OP prior to replication as seen by time-lapse microscopy (Fig. 3A). Most replicated foci (85%) reside between the poles. Interestingly, some LC foci (15%) localize just below, but not "on" the diagonal as seen for CC; thus, the LC is slightly

distal to the GP post segregation. Cells with three LC foci occur in cells as short as 2.5 μm suggesting that occasionally (4.8%) there may be a second round of LC replication during the elongation phase of the cell cycle. Four LC foci occur in elongating cells with an average length of 3.75 μm , less than the 4 μm achieved just prior to cell division. Thus, the LC displays variable localization and replication patterns.

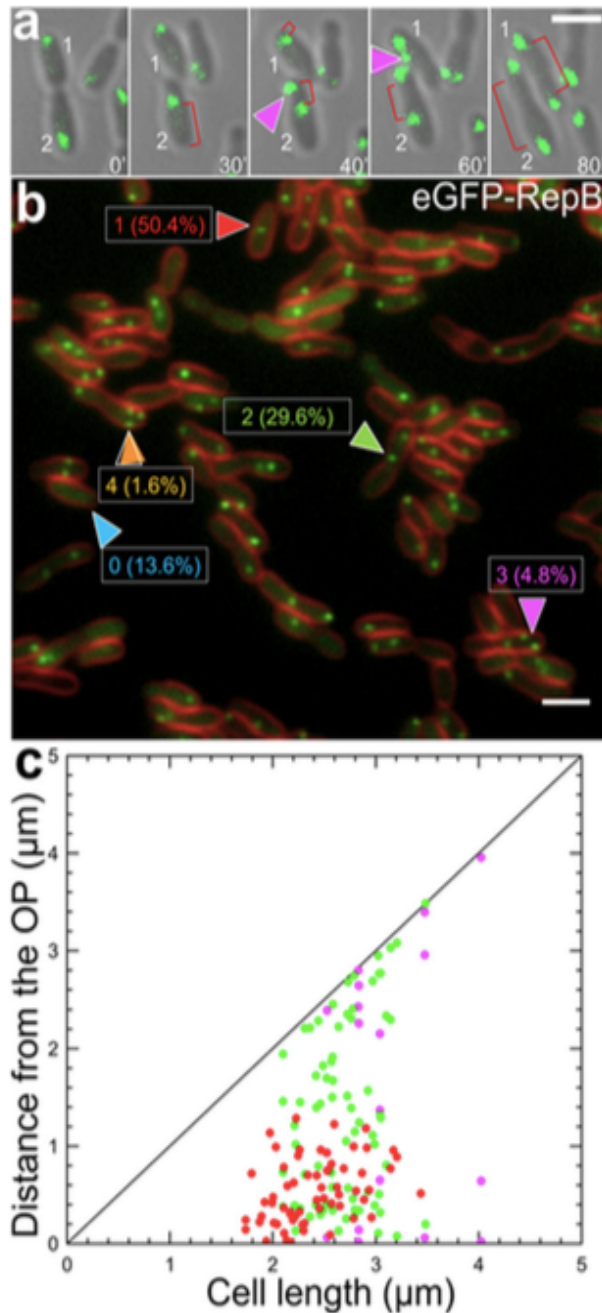


Fig. 3. Replication and segregation of the LC during polar growth. (A) Time lapse of LC localization (monitored as eGFP-RepB fluorescence). At 0', two siblings (1, 2) have an LC very near their OP. By 30', the LC in the lower older (slightly longer) cell (cell 2) has migrated (red bracket) to the junction between the new and old cell compartments, while LC in the upper cell (cell 1) remains at its OP. At 40' a newly replicated LC (cell 2, magenta arrowhead) has moved (red bracket) close to the GP, while its other copy remains in the old cell compartment. At 40' the LC in cell 1 has moved away from the old pole (red bracket). Replication of the LC in cell 1 does not initiate until 60' (cell 1, magenta arrowhead), while one LC copy in cell 2 is migrating (red bracket) back toward the OP. By 80', one LC is at the GP, and the other LC has migrated back to the OP in both cells 1 and 2 (red brackets). (B) Localization of eGFP-RepB in 125 FM4-64 stained cells. Percentages of cell displaying one, two, three, or four foci are shown with red, green, magenta, or orange arrowheads; cell with diffuse signal indicated by cyan arrowhead. (C) Distance of eGFP-RepB foci from the OP in 100 cells containing one (red), two (green), or three (magenta) foci. (Scale bars in A and B, 2 μm .)

The Circular Chromosome Replicates First and Arrives at the Growth Pole before the Linear Chromosome. To determine the timing of CC versus LC replication/segregation we coexpressed eGFP- ParB (binds to CC) and RFP-RepB (binds to LC) and monitored their dynamics (Fig. 4 and Movie S4). At 0 min, the CC has replicated, revealing one CC at the OP and one CC in the middle of the old cell compartment; at this time, the LC localizes just above the OP. At 10 min, the newly replicated CC arrives in the new cell compartment, while the LC has not moved. By 20 min, the newly replicated CC arrives at the GP, and the LC has just replicated. At 30 min, CC localization has not changed, while the newly replicated LC arrives in the new cell compartment. The LC arrives at the GP at 40 min. In summary, the LC replicates 20 min later than the CC and arrives at the GP 20 min later than the CC.

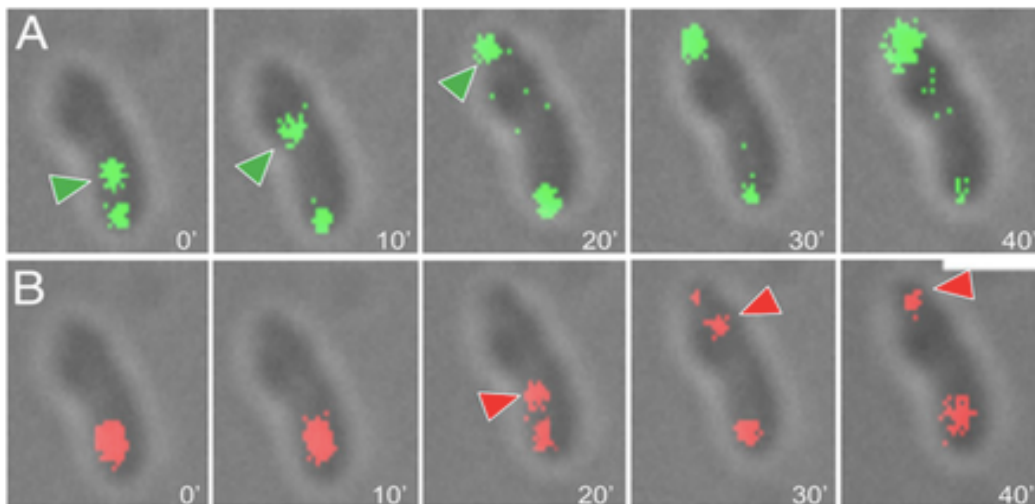


Fig. 4. The circular chromosome replicates and arrives at the growth pole before the linear chromosome. Time lapse of the CC and LC chromosomes (monitored by eGFP-ParB [CC] and RFP-RepB [LC] fluorescence, respectively); (A) CC and (B) LC. Green and red arrowheads indicate newly replicated CC and LC chromosomes, respectively, and show their movement to the GP. (Scale bar, 2 μm .)

Replication and Segregation of the Cryptic Plasmid. Replication and segregation of the cryptic At plasmid was monitored by eGFP-RepB-At (Fig. 5 and Movie S5). Just after cell division, sibling cells inherit a single pAt at their OPs (Fig. 5A, 0'). Similar to the LC, pAt first migrates away from the OP. The distance migrated prior to replication varies between siblings; in sibling 1, pAt migrates to more than midway through the old cell compartment, while in sibling 2, pAt migrates a short distance from the OP (Fig. 5A, 40'). Sibling 2 replicates pAt at 40', while sibling 1 replicates pAt at 70'. The newly replicated pAt arrives at the GP at 70' in sibling 2 and at 90' in sibling 1. By 90', both siblings have pAt at their GP and OP.

pAt mainly localizes as single foci (64%), 31% showed two foci, 3% showed diffuse signal, and a few cells showed three (1%) or four (1%) foci (not visible in the field of view in Fig. 5B). As above, cells with three or four foci suggest a second round of replication occurs before the cell cycle ends (see also SI Appendix, Fig. S3). There is a wide distribution of single pAt foci prior to replication, ranging from foci at the OP in the shortest cells to foci near the middle of the old cell compartment (ranging in size from 1.49~2.64 μm in length) (Fig. 5C), but not as great a range as displayed by the LC (Fig. 3C). Cells with two foci resemble the CC in their distribution with most foci at (or very close to) the GP (81%) and few cells in transit to the GP (19%). However, upon arrival in the new cell compartment, pAt requires 30 min to arrive at the GP (Fig. 5D), while the CC is at the GP immediately upon arrival in the new cell compartment and stays at the GP during polar growth (Fig. 2A).

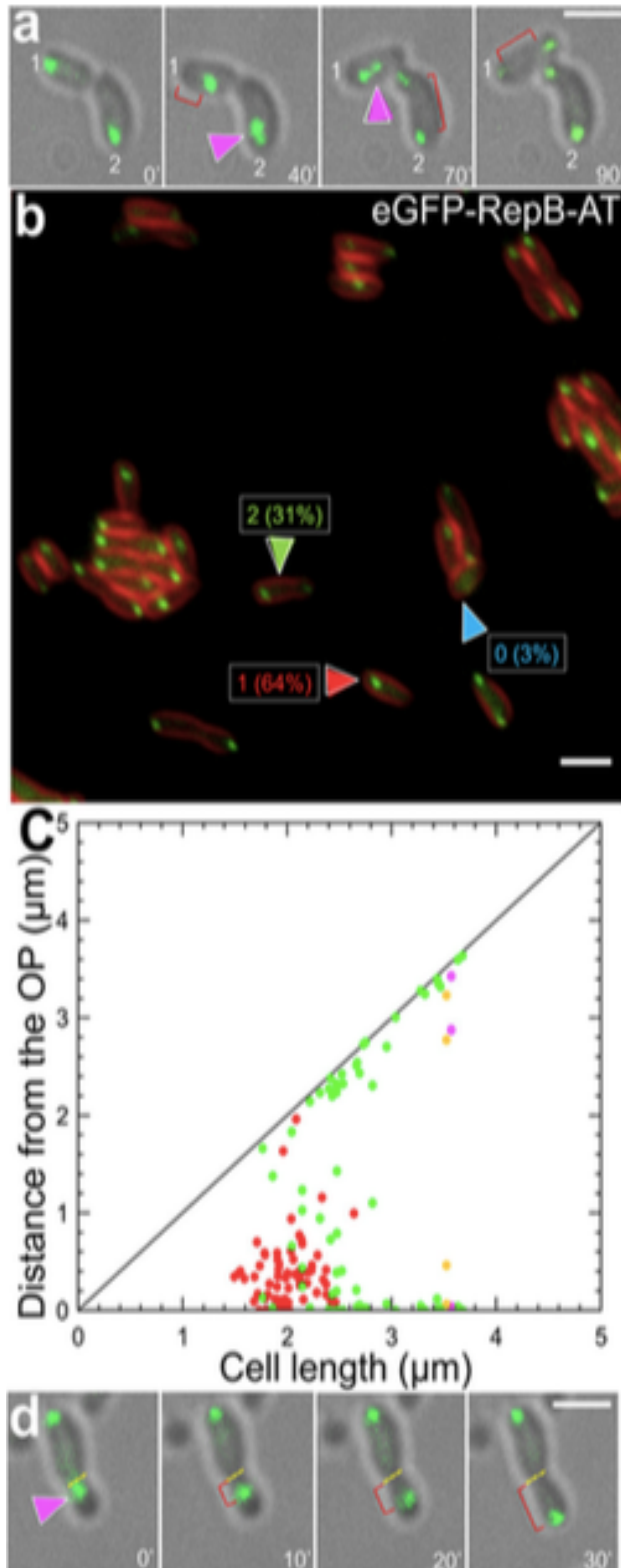


Fig. 5. Replication and segregation of the pAt during polar growth. (A) Time-lapse imaging of eGFP-RepB-At. At 0', two sibling cells inherit a single focus of eGFP-RepB-At at each OP. At 40', pAt has replicated (magenta arrowhead) in cell 2, and pAt in cell 1 migrates toward the midcell (red bracket). At 70', newly replicated pAt in cell 2 moves (red bracket) toward the GP, and pAt in cell 1 replicates (magenta arrowhead). By 90', newly replicated pAt in cell 1 moves (red bracket) to the GP. (B) Localization of eGFP-RepB-At in 100 FM4-64 stained cells. Percentages of cell displaying one or two foci are shown in red or green, and cells with a diffuse signal are indicated in cyan. (C) Distance of eGFP-RepB-At foci from the OP in 100 cells containing one (red), two (green), three (magenta), or four (orange) foci. (D) Timing of pAt arrival at the GP. At 0' a cell displays two pAt foci, one at the OP and the second copy just inside the new cell compartment (magenta arrowhead; yellow dashed line indicates the boundary between old and new cells). By 10', this second focus has migrated to the middle of the new cell compartment. At 20' this focus still has not arrived at the GP. The replicated pAt arrives at the GP at 30'. Red brackets indicate the migration of the replicated pAt. (Scale bars in A, B, and D, 2 μm .)

Due to their variable localization prior to replication, it is difficult to deduce the order of LC versus pAt replication from plots of cell lengths during the entire cell cycle (Figs. 3C and 5C). To precisely determine the order of LC versus pAT replication, we measured the lengths of only the very shortest cells with two foci for each replicon. SI Appendix, Table S1 shows the mean cell length for the first observable replication of CC, LC, and pAt is 2.06, 2.61, and 2.4 μm , respectively. Thus, pAt replicates in shorter cells before LC.

Replication and Segregation of the Ti Plasmid. Overall, the Ti plasmid (monitored by eGFP- RepB-Ti) does not occupy specific regions of the cell during its replication and segregation (Fig. 6). Cells showed single (33%), two (21%), three (16%), four (8%), five (7%), six (1%), or no (13%) foci. Unexpectedly, the foci are spread throughout the entire distance between the OP and GP with no apparent clustering close to either pole. That single foci localize throughout the old and new cell compartments illustrates that Ti plasmid replication and segregation is independent of cell length and cycle progression during vegetative growth.

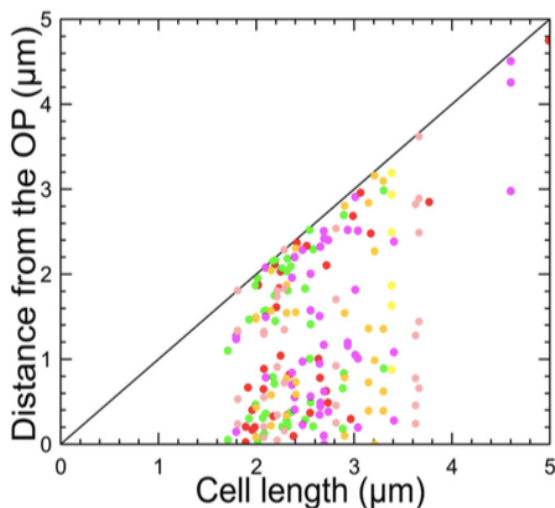


Fig. 6. Replication and segregation of the Ti plasmid. Distance of eGFP-RepB-Ti foci from the old pole in 100 cells containing one (red), two (green), three (magenta), four (orange), five (pink), or six (yellow) foci.

PopZ Is Required for Segregation of Circular and Linear Chromosomes. Of the four genetic elements in *Agrobacterium*, only CC and LC are required for viability. We were curious whether pole-specific essential factors such as PopZ and PodJ (17–19) are required to ensure partitioning of the essential CC or LC. Loss of PopZ or PodJ strongly impacts polar growth, resulting in ectopic poles, and interrupted cell division (16–18, 21). To remove PopZ, we used a strain carrying a theophylline- binding riboswitch sequence (RS) upstream of the *popZ* open reading frame (ORF) (17). In the presence of theophylline to induce PopZ expression, localization of ParB foci resembled the wild type (WT) (SI Appendix, Fig. S4A versus Fig. 2B). Without theophylline, most cells (74%) exhibit diffuse eGFP-ParB fluorescence (Fig. 7A); likely, eGFP-ParB cannot bind to the CC (to produce a focus) because the CC is lost. Indeed, DAPI staining is weak/absent in $\Delta popZ$ (16, 21). Other PopZ-depleted cells (26%) displayed abnormal morphology, ectopic growth poles, and/or multiple foci at abnormal locations (Fig. 7A).

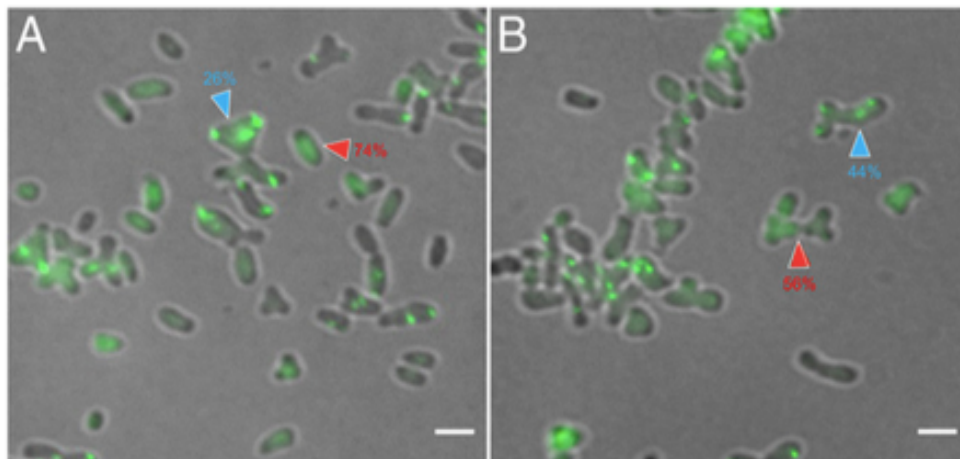


Fig. 7. Segregation of CC and LC is inefficient in PopZ-depleted cells. (A) Localization of eGFP-ParB in PopZ-depleted cells. Percentage of cells expressing eGFP-ParB showing diffuse fluorescence (red arrowhead) or multiple foci (blue arrowhead). (B) Localization of eGFP-RepB (LC) in PopZ- depleted cells. Percentage of cells expressing eGFP-RepB (LC) showing diffuse fluorescence (red arrowhead) or multiple foci (blue arrowhead). (Scale bars, 2 μ m.)

Cells without a ParB focus previously were observed in only 28% of cells carrying a genetic deletion of *popZ* (16). Our strategy to induce PopZ depletion may constitute a more severe and acute loss of PopZ. This difference is underscored by the discovery that genetic deletion of *popZ* frequently produced revertants that grew like WT when purified from single colonies and cultured (17). Thus, *popZ* deletion strains likely exist as a mixed population of mutant and WT cells. PopZ is also essential for LC partitioning. We expressed eGFP-RepB in the RS-*popZ* strain. With theophylline, cells resembled WT (SI Appendix, Fig. S4B versus Fig. 3B). In contrast, most cells (57%) grown without theophylline show diffuse or no RepB foci (Fig. 7B). Other PopZ-depleted cells (44%) exhibited many foci and abnormal morphology (Fig. 7B).

PodJ Is Required for Old Pole Localization of Circular and Linear Chromosomes.

PodJ identifies the old pole (19), and PodJ is required for the transition of the GP into an OP (18). To determine whether PodJ has a role in CC partitioning, we monitored eGFP-ParB localization in cells carrying a deletion of the ORF of *podJ* ($\Delta podJ$) (18). To differentiate between WT and $\Delta podJ$ strains, we refer to the OP in WT, and the cognate pole lacking PodJ protein in $\Delta podJ$ as the nongrowth pole (NGP). The CC exhibits remarkably abnormal behavior in $\Delta podJ$ cells, where the CC no longer localizes to the NGP but instead localizes to the GP at the beginning of the cell cycle (Fig. 8 A and B, 0'). We monitored 40 movies of individual cells for at least 2 h and observed two main patterns at approximately equal frequency. 1) Following cell division, CC replication continues from the GP used in the previous cell cycle (Fig. 8A, 0', 10', and Fig. 8B, 0', 10' 20', and 120'–170'). 2) Or, following division, a CC moves away from the former GP (Fig. 8A, 40' red bracket) and takes up a position in the middle of the resulting sibling cell post cell division

(similar to the location in the other sibling); in both siblings, CC then replicates from this middle location, and one copy migrates to the new GPs resulting from septation (Fig. 8A, 50'–70'). The cell in Fig. 8A transitions from growing and replicating the CC at the GP in the first cell cycle (0'–30'; only the later stages of this cell cycle are captured) to produce siblings where growth occurs normally from new GPs created at the septum. Nevertheless, these latter cells are abnormal as the CC does not localize to the NGP, but instead localizes to the middle of what was the old cell NGP compartment in the previous division. In contrast, the cell in Fig. 8B continues to produce two distinct siblings post cell division (Fig. 8B, 120'–170'); one sibling continues to use the previous GP for new growth and CC replication, and the other sibling replicates its CC from the middle of the NGP compartment like the siblings in Fig. 8A.

PodJ is also essential for the correct localization and segregation of the LC. In WT, the LC does not have dominant localization patterns prior to and post replication (Fig. 3C), making it potentially difficult to assign LC localization in Δ PodJ. To facilitate these studies, we used the localization of CC foci to the GP in Δ podJ to mark the GP in cells coexpressing CC-eGFP-ParB and LC-RFP-RepB. Surprisingly, in Δ podJ, the LC consistently colocalizes with the CC. SI Appendix, Fig. S5 presents a gallery of 60 Δ podJ cells coexpressing eGFP-ParB and RFP-RepB; 90% of the cells showed yellow fluorescent foci, representing colocalization of CC and LC. Only five cells (SI Appendix, Fig. S5, cells numbered 7, 25, 37, 51, and 60) show green and red foci next to each other.

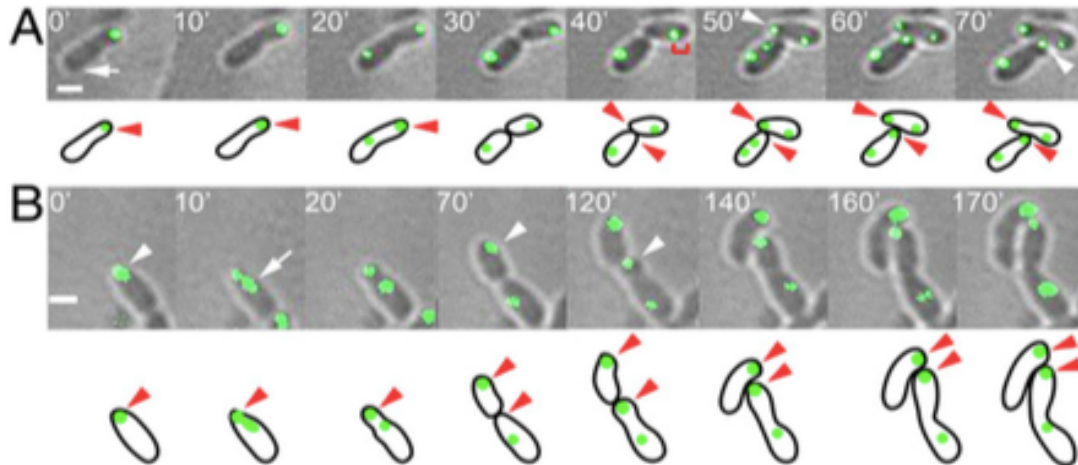


Fig. 8. CC localization is altered in $\Delta podJ$ cells. CCs were monitored by eGFP-ParB in time-lapse imaging. (A) Cell where GP transitions to an NGP. CC (in cell that did not transition in previous cycle) localizes to the GP and not the NGP (0', white arrow). After replication (20'), one copy remains at GP, and one copy moves to the NGP compartment. As the GP transitions to an NGP, CC moves to the middle of the cell (40', red bracket). Post division, CC replication occurs near the middle of both sibling cells (50'); one copy localizes to the GP (50' and 70', white arrowheads), while one copy remains in the NGP compartment in each sibling. (B) Cell where GP fails to transition to an NGP. Initially, the CC is at the GP (0', white arrowhead). After CC replication at the GP (10', white arrow); one copy remains at the GP (20'–170'), and one copy moves into the NGP compartment (20'). At septation, the GP in the upper cell does not become an NGP (70', upper cell, white arrowhead), and growth continues from this pole (70'–170'). In the lower cell after replication, one copy of the CC localizes at the GP created at the septation site (120', lower cell, white arrowhead), and one copy is in the NGP compartment cell. CC position is indicated by green circles, and GPs are indicated by red arrowheads in the accompanying diagrams. (Scale bar, 1 μ m.)

As foci are dynamic it is not surprising that they sometimes do not exactly coincide, Fig. 9 shows representative higher-resolution images of three $\Delta podJ$ cells showing colocalization, or one cell showing both no colocalization and overlapping red and green foci of eGFP-ParB and RFP-RepB. Overall, CC and LC are clearly colocalized or in close proximity. Thus, the LC follows the abnormal pattern of localization of CC in $\Delta podJ$ cells.

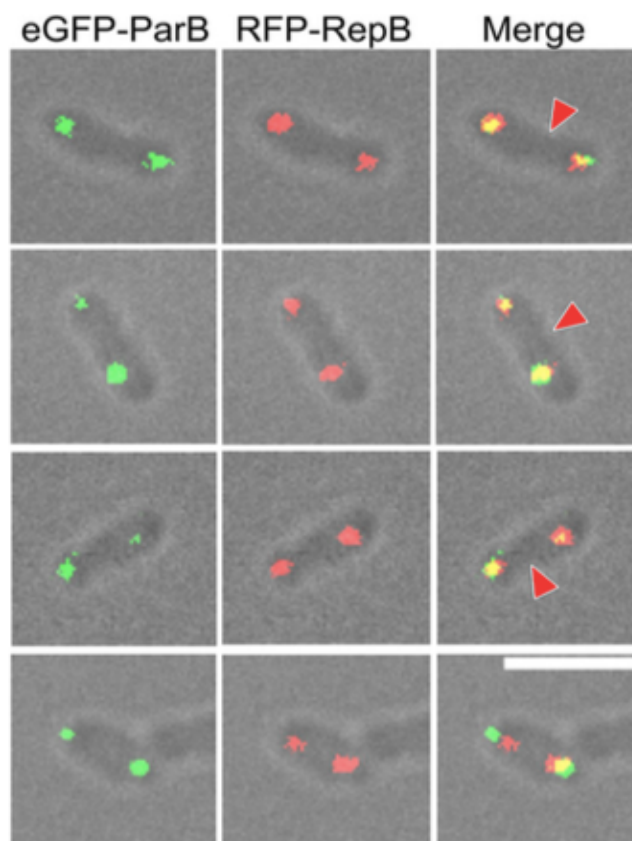


Fig. 9. LC mislocalization is similar to CC in Δ podJ cells. CC monitored by eGFP-ParB (Left) and LC monitored by eGFP-RepB-LC (Middle) in four cells. (Right) Merged images with yellow fluorescence indicating colocalization. Red triangles indicate (slight) constriction at base of the shorter GP compartment cell. The GP could not be identified in the bottom cell. CCs and LCs are colocalized (yellow fluorescence) or in close proximity in all cases (Right). From top to bottom, cells shown are numbers 30, 45, 54, and 25, respectively, seen in SI Appendix, Fig. S5. (Scale bar, 2 μ m.)

Discussion

We investigate the patterns of replication and segregation of the four replicons of *Agrobacterium* during its polar growth cell cycle. Larger replicons replicate in a distinct temporal order: first, CC; second, pAt; and third, LC. Their replication is also spatially distinct: CC always replicates at the OP suggesting a factor(s) must mediate its localization. In contrast, while LC and pAt localize initially close to the OP, they migrate anywhere between the OP and the other end of the OP compartment prior to replication. That pTi can be everywhere in the old or new cell compartments prior to replication, and pTi undergoes one or two rounds of replication per cell cycle, suggests there is no active segregation mechanism. Below we discuss notable features of the replication/segregation of the essential CC and LC during polar growth to provide insight into mechanisms underlying their faithful propagation.

Polar growth is intrinsically asymmetric. Once new GPs are formed at the septum, cell elongation begins as buds to generate the new cell compartments in sibling cells. The old cell compartment does not change in dimension during polar growth, while the new cell compartment undergoes major increases in diameter and length until it reaches the size of the old cell compartment (20). Such asymmetries may underlie asynchronous timing of CC and LC replication in sibling cells; both CC and LC replicate in the older sibling before they replicate in the younger sibling. The GP and OP identity factors PopZ and PodJ also exhibit asymmetries in the timing of their localization (16, 19). PopZ is removed from the GP during its transition to an OP and reappears at the “new” GP created by septation in the new cell compartment sibling (16). In contrast, in the old cell compartment sibling, PopZ must be synthesized de novo and localized to the “new” GP resulting from

septation (16). PodJ is at the OP during the early stages of the cell cycle, and then PodJ appears at the GP when PopZ leaves and is essential for the transition of the GP to an OP (18, 19).

In fact, pole identity is critical to both the temporal and spatial regulation of *Agrobacterium* chromosome dynamics during replication/segregation. OP identity is already established in the older sibling, and this may promote earlier replication of CC and LC; by contrast, the younger sibling must change the identity of its GP to an OP prior to division (Fig. 1); potentially, there is a maturation phase of this “new” OP to allow chromosome anchoring and subsequent replication. Here we present strong evidence for the role(s) of pole identity in chromosome replication/ segregation: deletion of GP and OP identity factors, PopZ and PodJ, results in dramatically altered patterns of CC and LC replication/segregation. Without PopZ, cells lose their CC and LC, implicating PopZ in segregating and/or anchoring chromosomes to GPs post replication. Ehrle et al. (16) also observed loss of the CC in the absence of PopZ. Early in the cell cycle prior to replication, we demonstrate that correct localization of the CC and LC to the OP is mediated by PodJ.

The critical importance of PodJ in *Agrobacterium* chromosome dynamics is underscored by the following numerous abnormal phenotypes produced in the absence of PodJ. 1) The fate of the GP is not fixed; either it continues as a GP in the next cell cycle, or it does not, and this choice occurs with approximately equal frequency. When the GP is not used for continued growth in the next cell cycle, the CC migrates to the middle of the GP compartment prior to cell division and subsequent replication. 2) Replicated CCs do not localize to the OP at the end of the cell cycle, but instead either remain at the GP in the GP compartment, or localize in the middle of the NGP compartment. 3) As the CC can

replicate at the GP or in the middle of the NGP compartment, it does not require factors at the OP for replication to occur. 4) The LC colocalizes with the CC and exhibits the above three abnormal phenotypes.

An understudied feature of polar growth is the generation of a presumptive division site, observed as a “constriction” between old and new cell compartments that develops soon after polar growth initiates. This constriction may restrict movement of replicons from the old to the new cell compartment. In contrast, during cell elongation by circumferential longitudinal growth, the growing cell has the same diameter along its length (22). In longitudinal growth in *Caulobacter*, a gradient of ParA ATPase drives movement of the replicated chromosome to one end of the cell, and the gradient shrinks in late stages of the cell cycle when segregation is complete (23, 24). By analogy, segregation of CC and LC may be facilitated by ParA and RepA gradients, respectively, that act sequentially. To date, all we know is that replication/segregation cassettes confer specificity (25); when the *repABC* system of *Sinorhizobium* megaplasmid pSymA was transferred to a small plasmid it exhibited the replication/segregation pattern of pSymA (26).

Besides PopZ, what factors might mediate GP localization of the CC and LC in Δ PodJ cells? At first glance, growth-pole-ring protein (GPR) might be an obvious candidate based on its precise three-dimensional structure at the GP (27) compared to the intrinsically disordered structure of PopZ (28). However, GPR is present in cells lacking PopZ; yet, multiple growth poles and abnormal chromosome segregation still occur. Instead, GPR is more likely an organizing center for peptidoglycan and lipid biogenesis at the GP during polar growth (27).

In summary, PodJ is required, directly or indirectly, to localize the CC and LC at/near the OP prior to replication in new sibling cells, and post replication, PopZ is essential for GP localization of CC and LC. A fascinating unanswered question is what happens when the GP transitions into an OP? Are PopZ and PodJ sufficient, or are additional factors required to anchor chromosomes during the switch in pole identity? How does PodJ anchor the CC strongly to the tip of the OP and allow replication of the CC before it is released to migrate to the GP compartment? Are additional OP factors required? Whatever factors mediate OP localization, OP localization per se is not essential for CC or LC replication, as CC and LC can replicate when positioned at the GP or the middle of the NGP compartment in $\Delta podJ$. What determines that LC and pAt are less tightly anchored to the OP tip as they migrate away from the tip prior to replication? Finally, what determines the order of replication/segregation of CC, pAt, and LC? Notably, in *Sinorhizobium*, primary chromosome partitioning genes are expressed 20'–30' before pSym megaplasmid partitioning genes (29). Thus, timing of replicon segregation may be partly regulated by transcriptional regulation of partitioning proteins.

Future studies will provide novel insights into the evolution and function of *Agrobacterium*-specific PopZ/PodJ mediated replicon dynamics, especially given that what occurs in *Agrobacterium* (16–19, 21) is remarkably different from what is known in the best studied PopZ/PodJ system in *Caulobacter crescentus* (30–34). Segregation of the chromosome in *Caulobacter* is all about PopZ. PopZ anchors the chromosome at the old pole, and then PopZ accumulates at the new pole as replication starts. Finally, PopZ at the new pole tethers one copy of the chromosome so that each sibling inherits a chromosome. In further contrast, in *Caulobacter*, PodJ tethers the histidine kinase PleC at the new pole to

Chapter 4

regulate morphogenesis of the swarmer pole (34). The *Agrobacterium* PodJ is longer than *Caulobacter* PodJ (by 273 amino acids [aa]) and only shares 23% aa identity (19), so it may have evolved different function(s). Finally, the multi-partite genome of *Agrobacterium* offers additional complexities to the list of unsolved mechanisms that coordinate their spatiotemporal replication and segregation during polar growth.

Materials and Methods

Plasmid Construction. Standard molecular cloning techniques were used (35). We used GenBank AE007869.2, AE007870.2, AE007872.2, and AE007871.2 for nucleotide sequences of the CC, LC, pAt, and pTi, respectively. Genomic DNA was prepared from an exponential growth-phase culture of *A. tumefaciens* C58 using the Qiagen DNeasy Blood and Tissue kit according to the instructions for Gram-negative bacteria. Polymerase chain reaction (PCR) was performed with the proofreading enzyme Phusion HF DNA Polymerase and the High GC buffer (New England Biolabs). PCR conditions were determined empirically for each gene of interest. For pJZ254, the coding sequence for *parB* (Atu2828, GenBank AAK88539.2) was amplified by PCR from *Agrobacterium* genomic DNA with *AvrII* and *HindIII* sites at the 5' and 3' ends, respectively, and ligated into pJZ210 (27) using these restriction sites. For pACE001, the coding sequence for *repB* (Atu3923, GenBank AAK89497.1) was amplified by PCR from *Agrobacterium* genomic DNA with *AvrII* and *HindIII* sites at the 5' and 3' ends, respectively, and ligated into pRG019 (19) using these restriction sites. For pREJS001, *egfp* was cloned from pJZ253 (27) into pSRKKm (36) using *NdeI* and *XbaI* restriction sites. *repB* (Atu2828, GenBank AAK88539.2), *repB-At* (Atu5001, GenBank AAK9038.1), and *repB-Ti* (Atu6044, GenBank AAK91002.1) were amplified by PCR from *A. tumefaciens* strain C58 genomic DNA with *XbaI* and *KpnI* restriction sites at their 5' and 3' ends, respectively, and introduced into the single copy number plasmid pREJS001 (SI Appendix, Table S2) using these restriction sites to create pREJS002, pREJS003, and pREJS004, respectively. All constructs were verified by sequencing. SI Appendix, Table S2 contains additional information on plasmids and strains. Resulting plasmids, based on pSRK vectors (36),

placed cloned genes under control of a tightly regulated lactose inducible promoter resulting in expression between 10 and 20% of WT levels (15).

Bacterial Strains and Growth Conditions. Cloning of above plasmids was performed using *Escherichia coli* XL Blue. All *Agrobacterium* strains were grown in LB at 28 °C. When appropriate, growth media were supplemented with 50 µg/mL gentamicin and/or 40 µg/mL kanamycin to select for plasmids carrying GFP fusion constructs. The riboswitch-popZ strain (17) was grown with 0.5 mM theophylline to induce PopZ expression; for depletion experiments, cells were grown overnight in the absence of theophylline.

Fluorescence and Time-Lapse Microscopy. Lactose-inducible expression of cloned partitioning genes was achieved by diluting overnight cultures to 10^8 cells/mL and adding 0.25 mM isopropyl β-D-1-thiogalactopyranoside for 3–4 h before single-time or time-lapse imaging as described (17). For widefield fluorescence, cells were imaged on LB 1% agarose pads. All images were processed using Fiji/ImageJ software (37). Cell length and position of the fluorescent foci were determined using ObjectJ (38). Each image was scaled to 15.5 px/µm. Time-lapse imaging was performed using the CellASIC ONIX system (EMD Millipore) as described (17).

Acknowledgments.

We thank Steven Ruzin, Ph.D., and Denise Schichnes, Ph.D., at the College of Natural Resources Biological Imaging Facility at University of California, Berkeley, for assistance with fluorescent imaging. The Biological Imaging Facility is supported in part by National Institutes of Health Program S10 (Award 1S1OD018136-01). Research in the P.Z. laboratory is supported by National Science Foundation Grant MCB-0923840. J.S.R.- E. received fellowship support from the Secretaría Nacional de Educación Superior, Ciencia, Tecnología, e Innovación, Ecuador.

Author contributions: J.S.R.-E., J.R.Z., A.C.-A., and P.Z. designed research; J.S.R.-E., J.R.Z., and A.C.-A. performed research; J.S.R.-E., J.R.Z., and P.Z. analyzed data; and J.S.R.-E., J.R.Z., and P.Z. wrote the paper.

This article contains supporting information online at <https://www.pnas.org/lookup/suppl/doi:10.1073/pnas.2014371117/-/DCSupplemental>.

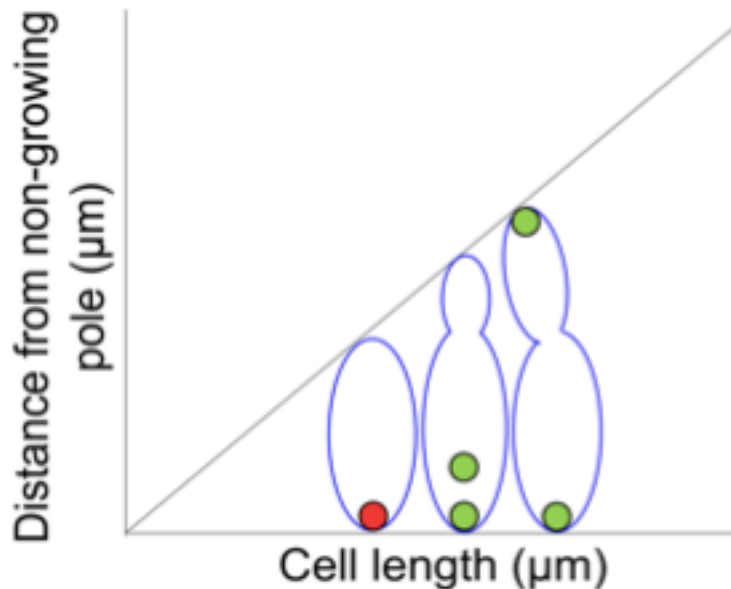
References

1. M. A. Cevallos, R. Cervantes-Rivera, R. M. Gutiérrez-Ríos, The repABC plasmid family. *Plasmid* 60, 19–37 (2008).
2. U. M. Pinto, K. M. Pappas, S. C. Winans, The ABCs of plasmid replication and segregation. *Nat. Rev. Microbiol.* 10, 755–765 (2012).
3. B. Goodner et al., Genome sequence of the plant pathogen and biotechnology agent *Agrobacterium tumefaciens* C58. *Science* 294, 2323–2328 (2001).
4. D. W. Wood et al., The genome of the natural genetic engineer *Agrobacterium tumefaciens* C58. *Science* 294, 2317–2323 (2001).
5. G. C. diCenzo, T. M. Finan, The divided bacterial genome: Structure, function, and evolution. *Microbiol. Mol. Biol. Rev.* 81, 208 (2017).
6. F. Galibert et al., The composite genome of the legume symbiont *Sinorhizobium meliloti*. *Science* 293, 668–672 (2001).
7. E. G. Ruby et al., Complete genome sequence of *Vibrio fischeri*: A symbiotic bacterium with pathogenic congeners. *Proc. Natl. Acad. Sci. U.S.A.* 102, 3004–3009 (2005).
8. S. M. Halling et al., Completion of the genome sequence of *Brucella abortus* and comparison to the highly similar genomes of *Brucella melitensis* and *Brucella suis*. *J. Bacteriol.* 187, 2715–2726 (2005).
9. J. F. Heidelberg et al., DNA sequence of both chromosomes of the cholera pathogen *Vibrio cholerae*. *Nature* 406, 477–483 (2000).
10. T. G. Platt, E. R. Morton, I. S. Barton, J. D. Bever, C. Fuqua, Ecological dynamics and complex interactions of *Agrobacterium* megaplasmids. *Front. Plant Sci.* 5, 635 (2014).
11. E. W. Nester, *Agrobacterium*: Nature’s genetic engineer. *Front. Plant Sci.* 5, 730 (2015).
12. L. S. Kahng, L. Shapiro, Polar localization of replicon origins in the multipartite genomes of *Agrobacterium tumefaciens* and *Sinorhizobium meliloti*. *J. Bacteriol.* 185, 3384–3391 (2003).
13. P. J. B. Brown et al., Polar growth in the Alphaproteobacterial order Rhizobiales. *Proc. Natl. Acad. Sci. U.S.A.* 109, 1697–1701 (2012).
14. E. Kuru et al., In situ probing of newly synthesized peptidoglycan in live bacteria with fluorescent D-amino acids. *Angew. Chem. Int. Ed. Engl.* 51, 12519–12523 (2012).
15. J. R. Zupan, T. A. Cameron, J. Anderson-Furgeson, P. C. Zambryski, Dynamic FtsA and FtsZ localization and outer membrane alterations during polar growth and cell division in *Agrobacterium tumefaciens*. *Proc. Natl. Acad. Sci. U.S.A.* 110, 9060–9065 (2013).
16. H. M. Ehrle et al., Polar organizing protein PopZ is required for chromosome segregation in *Agrobacterium tumefaciens*. *J. Bacteriol.* 199, 752 (2017).
17. R. Grangeon, J. Zupan, Y. Jeon, P. C. Zambryski, Loss of PopZ_{At} activity in *Agrobacterium tumefaciens* by deletion or depletion leads to multiple growth poles, minicells, and growth defects. *MBio* 8, e01881-17 (2017).
18. J. C. Anderson-Furgeson, J. R. Zupan, R. Grangeon, P. C. Zambryski, Loss of PodJ in *Agrobacterium tumefaciens* leads to ectopic polar growth, branching, and reduced cell division. *J. Bacteriol.* 198, 1883–1891 (2016).
19. R. Grangeon, J. R. Zupan, J. Anderson-Furgeson, P. C. Zambryski, PopZ identifies the new pole, and PodJ identifies the old pole during polar growth in *Agrobacterium tumefaciens*. *Proc. Natl. Acad. Sci. U.S.A.* 112, 11666–11671 (2015).
20. T. A. Cameron, J. Anderson-Furgeson, J. R. Zupan, J. J. Zik, P. C. Zambryski, Peptidoglycan synthesis machinery in *Agrobacterium tumefaciens* during unipolar growth and cell division. *MBio* 5, e01219-14 (2014).
21. M. Howell et al., Absence of the polar organizing protein PopZ causes aberrant cell division

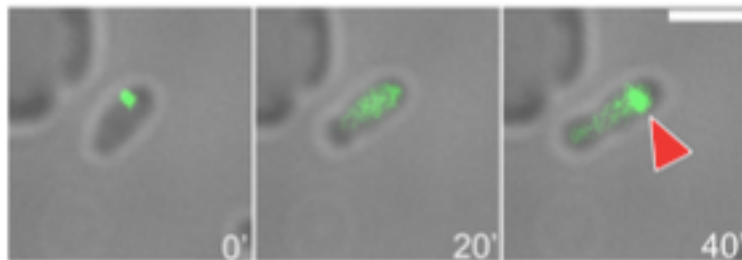
- in *Agrobacterium tumefaciens*. *J. Bacteriol.* 199, e00101-17 (2017).
22. N. Ouzounov et al., MreB orientation correlates with cell diameter in *Escherichia coli*. *Biophys. J.* 111, 1035–1043 (2016).
 23. W. B. Schofield, H. C. Lim, C. Jacobs-Wagner, Cell cycle coordination and regulation of bacterial chromosome segregation dynamics by polarly localized proteins. *EMBO J.* 29, 3068–3081 (2010).
 24. H. C. Lim et al., Evidence for a DNA-relay mechanism in ParABS-mediated chromosome segregation. *eLife* 3, e02758 (2014).
 25. P. Koper, K. Zębracki, M. Marczak, A. Skorupska, A. Mazur, RepB proteins of the multipartite *Rhizobium leguminosarum* bv. *trifolii* genome discriminate between centromere-like parS sequences for plasmid segregational stability. *Mol. Microbiol.* 102, 446–466 (2016).
 26. B. Frage et al., Spatiotemporal choreography of chromosome and megaplasmids in the *Sinorhizobium meliloti* cell cycle. *Mol. Microbiol.* 100, 808–823 (2016).
 27. J. R. Zupan, R. Grangeon, J. S. Robalino-Espinosa, N. Garnica, P. Zambryski, GROWTH POLE RING protein forms a 200-nm-diameter ring structure essential for polar growth and rod shape in *Agrobacterium tumefaciens*. *Proc. Natl. Acad. Sci. U.S.A.* 116, 10962–10967 (2019).
 28. J. A. Holmes et al., *Caulobacter* PopZ forms an intrinsically disordered hub in organizing bacterial cell poles. *Proc. Natl. Acad. Sci. U.S.A.* 113, 12490–12495 (2016).
 29. N. J. De Nisco, R. P. Abo, C. M. Wu, J. Penterman, G. C. Walker, Global analysis of cell cycle gene expression of the legume symbiont *Sinorhizobium meliloti*. *Proc. Natl. Acad. Sci. U.S.A.* 111, 3217–3224 (2014).
 30. G. R. Bowman et al., A polymeric protein anchors the chromosomal origin/ParB complex at a bacterial cell pole. *Cell* 134, 945–955 (2008).
 31. G. Ebersbach, A. Briegel, G. J. Jensen, C. Jacobs-Wagner, A self-associating protein critical for chromosome attachment, division, and polar organization in *Caulobacter*. *Cell* 134, 956–968 (2008).
 32. J. L. Ptacin et al., Bacterial scaffold directs pole-specific centromere segregation. *Proc. Natl. Acad. Sci. U.S.A.* 111, E2046–E2055 (2014).
 33. P. H. Viollier, N. Sternheim, L. Shapiro, Identification of a localization factor for the polar positioning of bacterial structural and regulatory proteins. *Proc. Natl. Acad. Sci. U.S.A.* 99, 13831–13836 (2002).
 34. A. J. Hinz, D. E. Larson, C. S. Smith, Y. V. Brun, The *Caulobacter crescentus* polar organelle development protein PodJ is differentially localized and is required for polar targeting of the PleC development regulator. *Mol. Microbiol.* 47, 929–941 (2003).
 35. MR Green, J Sambrook, *Molecular Cloning: A Laboratory Manual*, (Cold Spring Harbor Laboratory Press, ed. 4, 2012).
 36. S. R. Khan, J. Gaines, R. M. Roop 2nd, S. K. Farrand, Broad-host-range expression vectors with tightly regulated promoters and their use to examine the influence of TraR and TraM expression on Ti plasmid quorum sensing. *Appl. Environ. Microbiol.* 74, 5053–5062 (2008).
 37. J. Schindelin et al., Fiji: An open-source platform for biological-image analysis. *Nat. Methods* 9, 676–682 (2012).
 38. N. O. E. Vischer et al., Cell age dependent concentration of *Escherichia coli* divisome proteins analyzed with ImageJ and ObjectJ. *Front Microbiol.* 6, 586 (2015).

Supporting information appendix

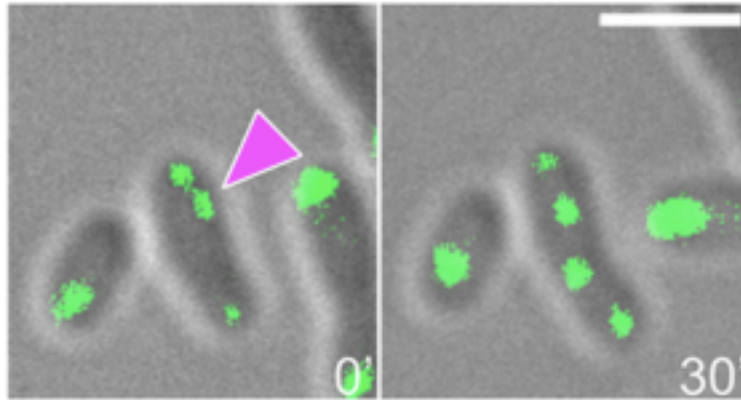
SI Figures.



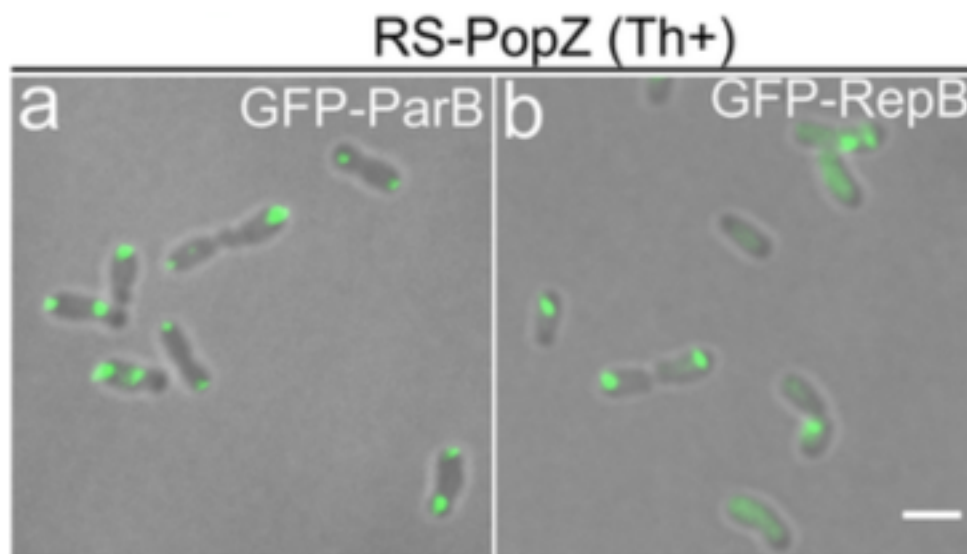
SI Figure S1. Positions of CC foci versus cell length are diagrammed at three times during polar growth. Cell length is an indicator of cell cycle progression (1). First, there is one red (unreplicated) CC focus at the OP in the shortest cells. Then the CC replicates to form two green foci: one focus remains at the OP and the other focus transits through the old cell compartment and then arrives at the GP. x-axis: cell length. Y-axis: distance of foci away from the OP. Once a focus reaches the GP it no longer moves and falls on the diagonal line. Foci in transit between the OP and GP locate between the x-axis and the diagonal. The shortest cells have one unreplicated focus. Two longer cells with 2 replicated foci are drawn: both have one focus at the OP and the other focus either in transit (just post replication) or arrived at the GP (later in cell cycle in the longest cell shown).



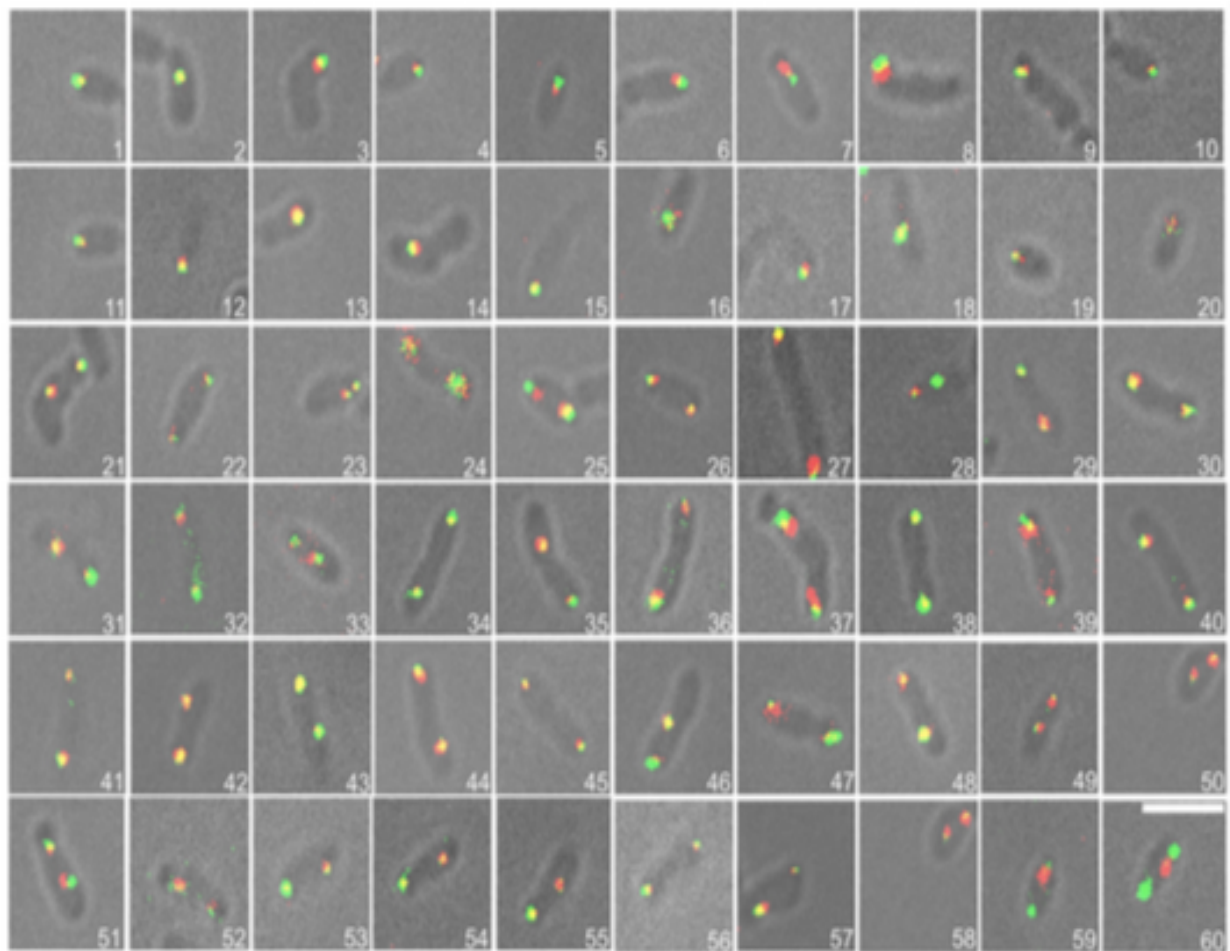
SI Figure S2. eGFP-RepB shows diffuse signal. Time-lapse imaging of eGFP-RepB after 4hr of IPTG induced expression. At 0', a single eGFP-RepB focus localizes close to the OP. By 20', the cell exhibits diffuse eGFP-RepB signal. At 40', eGFP-RepB begins to appear as a focus just above the OP (red arrowhead). Scale bar: 2 μ m.



S/ Figure S3. The cryptic plasmid replicates more than once per cell cycle. Time-lapse of eGFP-RepB- At after 4 hr of IPTG induced expression. In the middle cell at 0', a third focus appears near the OP (magenta arrowhead). By 30', the pAt focus that is near the GP (at 0') has replicated creating a cell with four pAt foci. Scale bar is 2 μ m.



S/ Figure S4. CC and LC localization in *RS::popZ* cells grown in 0.5 mM theophylline to induce PopZ expression are similar to WT. (a) CC localization (GFP-ParB). (b) LC localization (GFP-RepB). Scale bar is 2 μ m.



S/ Figure S5. Coexpression of eGFP-ParB and RFP-RepB shows that CC and LC both localize at GP in $\Delta podJ$ cells. Colocalization of eGFP-ParB and RFP-RepB indicated by yellow fluorescence in gallery of $\Delta podJ$ cells. The extent of colocalization indicates deletion of *podJ* has similar effects on the replication and segregation of both CC and LC. Cells numbered 1-20 have one unreplicated focus, and cells numbered 21-60 have two foci post-replication. Scale bar is 2 μ m.

S/ Table S1. Cell length at time of replication indicates the order of replication for CC, Lc, and pAT. Cell lengths were measured for each replicon in the shortest cells with two foci (n= 20 cells for each replicon).

Replicon	Mean cell length (μm) (standard deviation, μm)
CC	2.1 ^{a,b} (0.19)
Lc	2.61 ^{a, c} (0.29)
pAt	2.4 ^{b, c} (0.29)

^aMean cell length at time of CC replication is shorter than mean cell length at time of Lc replication ($p < 0.05$, two-tailed T-test)

^bMean cell length at time of CC replication is shorter than mean cell length at time of pAt replication ($p < 0.05$, two-tailed T-test)

^cMean cell length at time of Lc replication is longer than mean cell length at time of pAt replication ($p < 0.05$, two-tailed T-test)

Table S2: Bacterial strains and plasmids used in this study

Plasmid	Description	Source
pSRKKm	Broad host-range, <i>lacI</i> , kanamycin ^R	(2)
pJZ210	<i>Plac::eGFP</i> , gentamycin ^R	(3)
pJZ253	<i>Plac::eGFP-gpr</i> , gentamycin ^R	(3)
pJZ254	<i>Plac::eGFP-parB</i> , gentamycin ^R <i>parB</i> = Atu2828, GenBank AAK88539.2	This work
pRG019	<i>Plac::RFP</i> , kanamycin ^R	(3)
pACE001	<i>Plac::RFP-repB</i> , kanamycin ^R <i>repB</i> = Atu3923, GenBank AAK89497.1	This work
pREJS001	<i>Plac::eGFP</i> , kanamycin ^R	This work
pREJS002	<i>Plac::eGFP-repB</i> , kanamycin ^R	This work
pREJS003	<i>Plac::eGFP-repB-At</i> , kanamycin ^R <i>repB-At</i> = Atu5001, GenBank AAK9038.1	This work
pREJS004	<i>Plac::eGFP-repB-Ti</i> , kanamycin ^R <i>repB-Ti</i> = Atu6044, GenBank AAK91002.1	This work
Strains	Relevant genotype	Source
XL Blue (<i>E. coli</i>)	cloning strain, <i>endA1 gyrA96(nalR) thi-1 recA1 relA1 lac glnV44 F[::Tn10 proAB+ lacIq Δ(lacZ)M15] hsdR17(rKmK+)</i> , Tet ^R	Lab stock
C58	wild-type <i>A. tumefaciens</i> strain C58	Lab Stock
ARG074	<i>RS::popZ</i>	(4)
A164	<i>ΔpodJ</i>	(5)
A188	C58 carrying pJZ254	This work
pACA009	C58 carrying pJZ254 and pACE001	This work
REJS002	C58 carrying pREJS002	This work
REJS003	C58 carrying pREJS003	This work
REJS004	C58 carrying pREJS004	This work
REJS005	ARG074 carrying pREJS002	This work
REJS006	ARG074 carrying pJZ254	This work
REJS007	A164 carrying pJZ254 and pACE001	This work

SI References

1. Cameron TA, Anderson-Furgeson J, Zupan JR, Zik JJ, Zambryski PC (2014) Peptidoglycan synthesis machinery in *Agrobacterium tumefaciens* during unipolar growth and cell division. *MBio* 5(3):e01219–14.
2. Khan SR, Gaines J, Roop RM, Farrand SK (2008) Broad-host-range expression vectors with tightly regulated promoters and their use to examine the influence of TraR and TraM expression on Ti plasmid quorum sensing. *Applied and Environmental Microbiology* 74(16):5053–5062.
3. Zupan JR, Grangeon R, Robalino-Espinosa JS, Garnica N, Zambryski P (2019) GROWTH POLE RING protein forms a 200-nm-diameter ring structure essential for polar growth and rod shape in *Agrobacterium tumefaciens*. *Proc Natl Acad Sci USA* 116(22):10962–10967.
4. Grangeon R, Zupan J, Jeon Y, Zambryski PC (2017) Loss of PopZ At activity in *Agrobacterium tumefaciens* by Deletion or Depletion Leads to Multiple Growth Poles, Minicells, and Growth Defects. *MBio* 8(6):e01881–17.
5. Anderson-Furgeson JC, Zupan JR, Grangeon R, Zambryski PC (2016) Loss of PodJ in *Agrobacterium tumefaciens* Leads to Ectopic Polar Growth, Branching, and Reduced Cell Division. *J Bacteriol* 198(13):1883–1891.

SI Movie Legends **SI Movie S1.** Time lapse for Cc from Fig. 2a.

SI Movie S2. Time lapse of Cc from Fig. 2b.

SI Movie S3. Time lapse of Lc from Fig. 3.

SI Movie S4. Time lapse of Cc and Lc from Fig. 4.

SI Movie S5. Timelapse of pAt from Fig. 5a.

Chapter 5

Studies to be continued: Cell shape dependent on GPR and PopZ is required for the subcellular distribution of ParA; and PodJ and PopZ are required for the partitioning of the pAt replicon

J. S. Robalino-Espinosa^{a,b}, J. R. Zupan^b, P. Zambryski^{b,1}

^aDepartment of Plant and Microbial Biology, University of California, Berkeley, CA 94720; ^bPresent Address: Department of Molecular Cell Biology, Vrije Universiteit Amsterdam, 1081 HV, Amsterdam, The Netherlands.

5

Abstract

DNA segregation has been primarily studied in bacteria that grow by dispersed insertion of cell wall precursors along the entire length of the cell. *Agrobacterium tumefaciens* C58 grows from a single growth pole (GP) and its four genetic elements the circular chromosome (CC), linear chromosome (LC), cryptic plasmid (pAt) and tumor-inducing plasmid (pTi) display different timing of replication and segregation. The CC encodes for a ParABS partitioning system, while LC, pAt and pTi each encode their own RepABC partitioning system. The segregation of CC and LC is dependent on the GP and non-growing old pole (OP) and identity factors PopZ and PodJ, respectively. Here, we monitored the localization of the Walker A-type ATPase ParA encoded by the *parABS* partitioning system within the context of polar growth. ParA alternated from a large dense patch (LDP) located in a large region of the non-growing old pole (OP) compartment in the shortest cells to a gradient with the strongest accumulation of ParA at or near the GP in the longest cells. Notably, localization of ParA required rod cell shape morphology dependent on PopZ and the growth pole ring protein, GPR, a GP specific factor that forms a 200-nm diameter hexameric ring required to maintain the rod shape morphology. We then monitored the CC and LC localization in the absence of GPR. Rod shape morphology dependent on GPR was required for the partitioning of the CC and LC replicons. Furthermore, we monitored the pAt localization in the absence of PopZ and PodJ. These polarity factors were required for pAt localization to discrete foci to enable partitioning following replication. These data indicate that rod shape morphology dependent on polarity factors is essential for DNA segregation.

Introduction

Approximately ten percent of bacteria have their genomes split between two or more replicons ((1)). For example, the 5.67-Mb genome of the Rhizobiales plant pathogen, *Agrobacterium tumefaciens* C58, is divided into four replicons: circular chromosome (CC) (2.8 Mbp), secondary linear chromosome (LC) (2.0, Mbp), cryptic plasmid (pAt) (0.5 Mbp), and tumor inducing plasmid (pTi) (0.2 Mbp) (2-3). Essential genes are located only on the CC and LC (2-3). The pAt replicon encodes proteins involved in metabolic and detoxification activities (2-4)., whereas pTi encodes for virulence factors required to produce crown gall tumors on host plants (4-5). Additional examples of organisms containing more than one replicon are found in human and animal pathogens, nitrogen-fixing rhizobia, and symbionts including *Vibrio cholerae* (6), *Brucella abortus* (7), *Borrelia burgdorferi* (8), *Sinorhizobium meliloti* (9), and *Vibrio fischeri* (10).

Agrobacterium tumefaciens utilizes a polar growth mechanism with an active growth pole (GP) and an inactive non-growing old pole (OP) (Fig.1) (11-13). Polar growth is dramatically distinct from dispersed growth along the length of the bacterial cell, that occurs in well-known bacterial species such as *E. coli* (14). The GP and OP can be distinguished morphologically: the GP starts as a small bud and then elongates and widens until it reaches the size of the OP compartment, while the OP compartment does not change in size or morphology (11-12). GP and OP specific factors have been identified (15-16). PopZ and PodJ localize as distinct foci at the GP or OP respectively (15). Growth pole ring protein (GPR) forms a striking 200 nm diameter hexameric ring at

the GP (16). Fluorescent tagging of these pole specific factors allows easy identification of the GP and OP during the cell cycle (15-16).

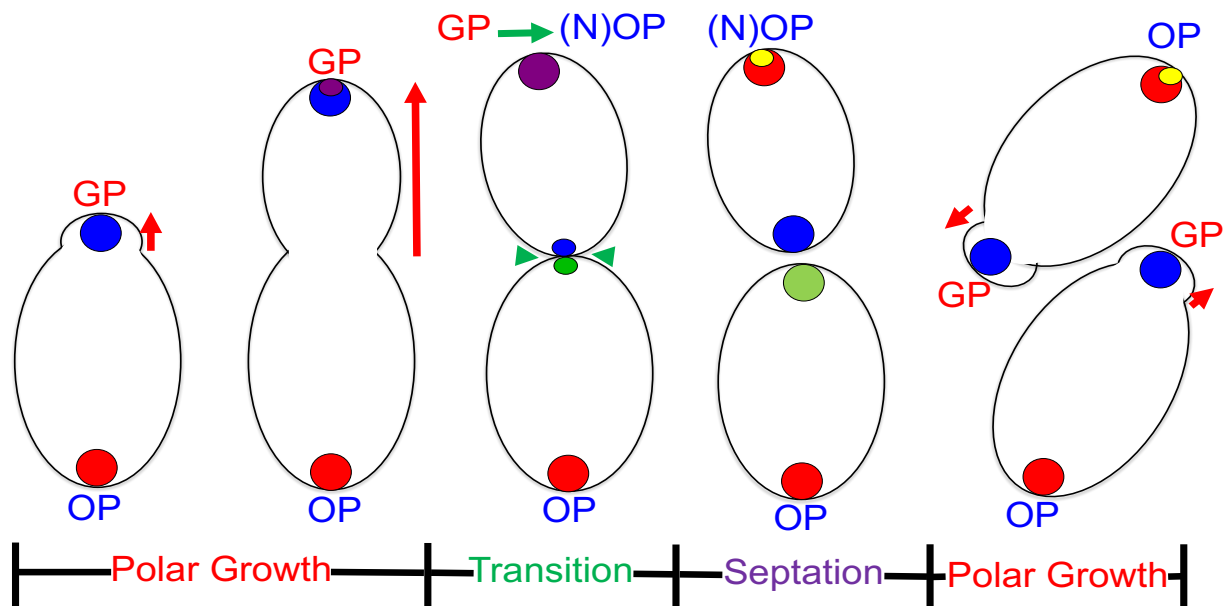


Figure 1. Polar growth in *Agrobacterium* and dynamics of polarity factors. First, a GP bud is visible in early stages of the cell cycle. PopZ and GPR (blue circles) are at the GP, and PodJ (red circles) is at the OP. The GP increases in width and length (red arrows), while the OP does not grow. During elongation, PodJ begins to accumulate at the GP (purple circles, due to colocalization with GPR, and PopZ). When the new cell compartment reached its final size, the GP transitions into a “new” OP ([N]OP) (green arrow), and the cell is divided at the septation site (green arrows heads) to produce two sibling cells which will restart polar growth. During transition and septation, GPR and PodJ are at the N(OP) (yellow circles) and PopZ is removed from the GP. PopZ and GPR accumulate at “new” GPs of the new sibling cell. GPR (green circles) accumulates at the “new” GP of the old sibling cell (11-13,16-21). The image and text were adapted from Robalino-Espinosa et al (2020) (21).

Partitioning systems mediate the faithful segregation of the complete genome from the mother cells into daughter cells (22). Bacteria with multiple genetic elements utilize different partitioning systems (23-24). In *Agrobacterium*, the CC encodes a ParABS partitioning system, consisting of a Walker A-type ATPase ParA protein, a *parS*-binding protein ParB, and a *parS* binding site (23). The LC, pAt, pTi each encode their own RepABC partitioning system (2-3, 23), as occurs with major chromosomes and plasmids

of other α -proteobacteria (23, 25). The RepABC partitioning system consists of a RepA protein that likely functions similarly to ParA, a *par*-binding protein RepB, a *par* binding site and a replication initiator protein RepC (23).

We previously described the replication and segregation of the four *Agrobacterium* genetic elements within the context of polar growth (21). Early in the growth cell cycle, the largest replicons (CC, LC, pAT) reside at the OP. The CC replicates first at the OP (18, 21, 26) while LC and pAT move away from the OP prior to replication (21). Following replication, one copy of the CC, LC, and pAt migrate to the GP (18, 21, 26). In contrast, the pTi replicon does not occupy specific regions during replication and segregation (21). Segregation of the essential replicons (CC and LC) is dependent on the GP and OP identity factors PopZ and PodJ, respectively (Fig. 1) (13, 15, 19-20). PopZ is required for effective post-replication segregation of CC and LC to the GP (13, 21), while PodJ is required for tethering the CC and LC to the OP (21).

Here, we study the localization of ParA in the context of polar growth. ParA formed a large dense patch (LDP) in a large region of the OP compartment in the shortest cells. In contrast, in the longest cells, ParA exhibited a gradient, with the strongest accumulation at or near the GP. In the absence of GP factors PopZ and GPR, ParA failed to accumulate to the GP. Furthermore, without GPR, partitioning of the CC and LC was disrupted, suggesting that localization of the CC and LC replicons to the GP requires rod shape morphology, dependent on GPR. We also monitored the pAt localization in the absence of PopZ or PodJ. Without these specific pole factors, the segregation of the pAt replicon was disrupted, potentially indicating that PopZ and PodJ and/or rod shape morphology is required for the partitioning of pAt.

Results

ParA exhibits a large dense patch and a gradient. The subcellular distribution of the ParA ATPase in *Agrobacterium*, has not been described previously. We monitored the localization of ParA by creating a ParA-mCh fusion protein. To distinguish the GP versus the OP, we performed a long pulse (~90') of PG labeling using nitrobenzofurazanyl-amino-D-alanine (NADA) followed by its removal. Growth of *Agrobacterium* in the presence of NADA for one generation results in an asymmetrical fluorescence, where the GP remains unlabeled (13). Figure 2a shows that ParA-mCh exhibited two major patterns, 1) a gradient of fluorescence, with the strongest fluorescence displayed as a focus at or close to the GP and the weakest fluorescence in the rest of the cytoplasmic space; 2) a large dense patch (LDP) encompassing a large region of the OP compartment. We monitored the different patterns of fluorescence in 100 cells (Fig S1): The highest percentage of cells showed a diffuse signal accompanied by a focus of ParA-mCh (43%) (Fig. S1, cells numbered 1-43) or a LDP of fluorescence (32%) (Fig. S1, cells numbered 44-75). Fewer cells displayed a diffuse signal (18%) (Fig. S1, cells numbered 76-92) or multiple patches (7%) (Fig. S1, cells numbered 94-100). As a control for these experiments, we expressed *Agrobacterium* ParA in *E. coli*, which does not encode a ParABS system (25). Indeed, *Agrobacterium* specific mCh-ParA expressed in *E. coli* BL21(DE3) displayed only non-specific fluorescence localized throughout most of the cytoplasm (Fig. S2a), and did not localize to the cell poles (Fig. S2b).

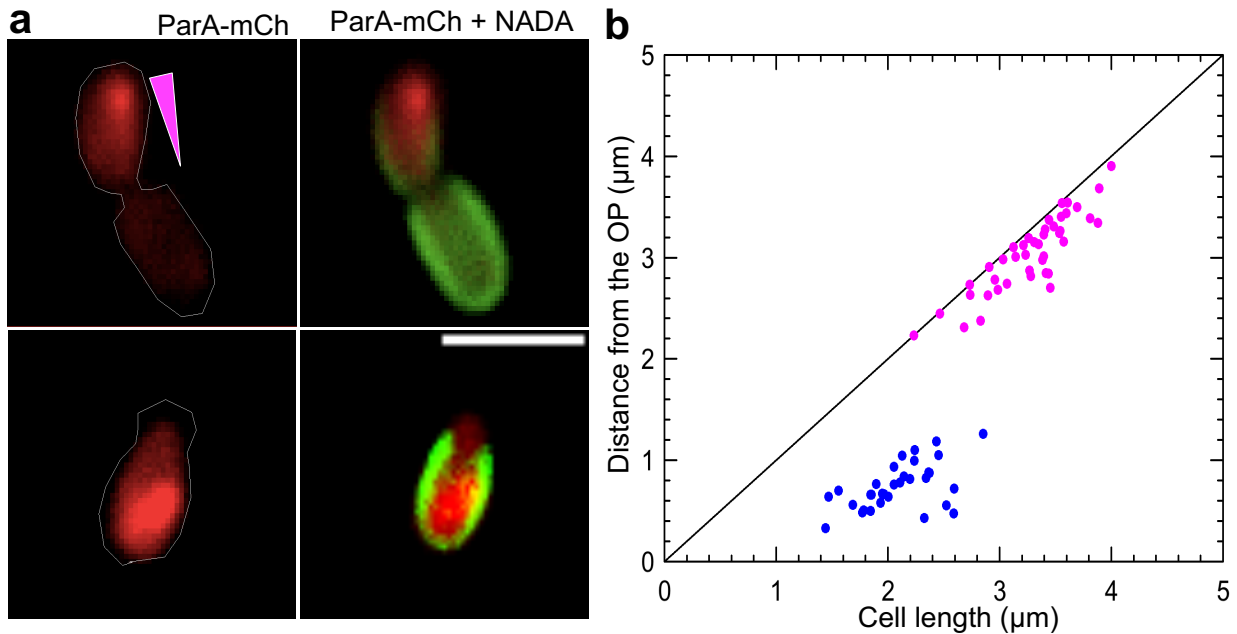


Fig 2. ParA-mCh exhibits two main patterns of localization. (a) ParA-mCh in two NADA labelled cells. Red fluorescence in the non-merged images (left) indicate the subcellular distribution of ParA-mCh. Cell contours are shown with white lines. Green fluorescence on the merged images (right) indicate PG labeling. The GP is not labelled with NADA (since the images are taken following a chase without NADA). The upper cell exhibits a focus and lower cell exhibits a LDP. Magenta triangle indicates differences on ParA-mCh fluorescence intensity from strongest signal to weakest signal in the new cell compartment. From top to bottom, cells shown are number 2 and 52, respectively, seen in Fig. S1. (b) Distances of ParA-mCh versus cell length in 75 cells. Blue dots represent the centers of the large regions encompassed by LDPs and magenta dots represent the single foci. (Scale bar on a, $2\mu\text{m}$).

To estimate the localization of ParA during the *Agrobacterium* cell cycle, we plotted the distance of fluorescent LDPs or discrete foci of ParA-mCh versus cell length (Fig. 2b). Cell length is an estimate of cell cycle stage during polar growth (12, 16, 21). We represented LDPs of fluorescence with blue dots (that represent the centers of the large regions encompassed by LDPs) and tight foci with magenta dots. Fluorescent signals on the x-axis or along the diagonal are at the OPs or GPs respectively, whereas fluorescence between these lines occurs between the cell poles. Notably, the shortest cells ($1.44\text{-}2.85\mu\text{m}$) displayed the LDPs of fluorescence that extended from near the OP to the rest

of the old OP compartment. In contrast, the largest cells (2.23-4 μ m) exhibited single foci at or near the GP (Fig. 2b), suggesting that ParA-mCh relocates from the old cell compartment to the GP as the cell elongates.

Localization of ParA depends on PopZ. As PopZ marks the GP during polar growth of *Agrobacterium* (Fig. 1) (15, 18), we tested whether PopZ might play a role on the recruitment of ParA to the GP. ParA-mCh was expressed in a strain, *RS-PopZ*, containing a theophylline binding riboswitch (*RS*) sequence upstream of the open reading frame (ORF) of *popZ*. In this strain, PopZ is expressed only in the presence of theophylline (19). In the absence of theophylline (Fig. 3a), cells were misshapen and ParA-mCh showed mainly a diffuse signal. Thus, PopZ or rod shape morphology, or both are required for the accumulation of ParA at the GP.

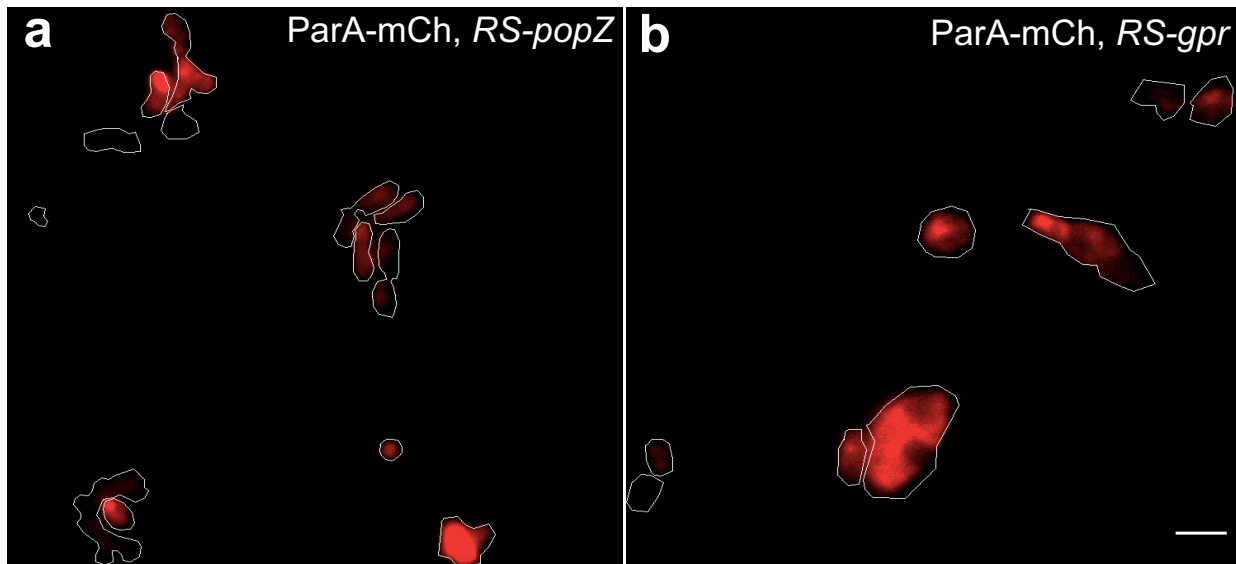


Fig. 3. Subcellular distribution of ParA in PopZ and GPR depleted cells. (a) Fluorescent micrograph of ParA-mCh in PopZ depleted cells. (b) Fluorescent micrograph of ParA-mCh in GPR depleted cells. Cell contours are indicated with white lines. (Scale bar on b, 2 μ m).

GPR is essential for the localization of ParA. GPR is essential for rod cell morphology, as in its absence cells become spherical (16). Without GPR, PopZ no longer localizes to the GP (16). Here, we expressed ParA-mCh in a strain, *RS-gpr*, carrying a theophylline dependent RS upstream of the ORF of *gpr* (16). Without theophylline, GPR depleted cells are wide and abnormally shaped, and ParA-mCh exhibited predominantly multiple patches or a diffuse signal (Figs. 3b). Given that cell shape is so strongly altered in the absence of GPR, it is not surprising that ParA-mCh, like PopZ, is dependent on GPR for its correct localization to distinct polar foci.

Segregation of circular and linear chromosomes is impaired in the absence of GPR.

As localization of PopZ to the cell pole requires rod shape morphology, dependent on GPR ((16)), we tested whether GPR is required for the segregation of CC and LC replicons. We monitored eGFP-ParB or eGFP-RepB (21) to detect the localization of the CC and LC replicons, respectively, in the *RS-gpr* strain. In the presence of theophylline, the *RS-gpr* strain resembled WT (Fig. S3) (21). In contrast, without theophylline, most cells were elongated with multiple constrictions sites or spherical bulges. Such cells predominantly displayed single or multiple foci of eGFP-ParB (Fig. 4a) and eGFP-RepB (Fig. 4b) suggesting that these proteins can still bind respective chromosomes (Fig. 4a-b). However, the abnormal shape of cells likely prevents their segregation in an orderly manner. Future studies should follow such cells by time lapse of chromosome through the entire cell cycle to confirm this hypothesis.

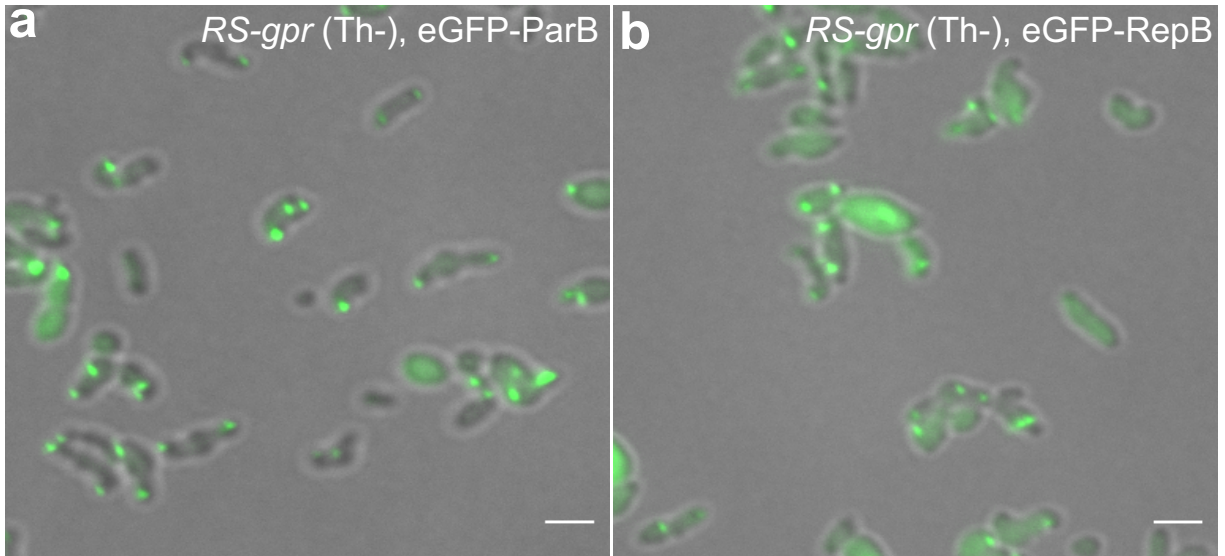


Fig. 4. Segregation of the circular and linear chromosomes is inefficient in GPR-depleted cells. (a) Localization of eGFP-ParB in GPR-depleted cells. (b) Localization of eGFP-RepB in GPR-depleted cells. (Scale bars 2 μ m).

Segregation of the cryptic plasmid is dependent on PopZ and PodJ. PopZ and PodJ are essential for efficient segregation of the two essential replicons (CC and LC) (21). Here, we tested whether PopZ or PodJ are also required to segregate pAt. First, we expressed eGFP-RepB-At in the *RS-popZ* strain (19, 21). Without theophylline, most cells exhibited ectopic poles and a diffuse fluorescence signal, with few cells exhibiting distinct foci (Fig. 5a). In contrast, with theophylline (Fig. S4), eGFP-RepB-At showed WT localization of foci to the GP (21). Next, we expressed eGFP-RepB-At in a strain containing an in-frame deletion of *podJ* ($\Delta podJ$) (20). Cells were elongated with several constriction sites indicating a defect on cell division. Most cells exhibited mislocalized foci between the poles and some cells showed a diffuse signal throughout the cytoplasm. Thus, PodJ and PopZ are required for pAT localization to discrete polar foci to enable partitioning following replication. The diffuse localization patterns observed are likely a consequence of abnormal cell shape resulting from loss of PopZ or PodJ. Future studies

with time-lapse imaging through the cell cycle may help to distinguish the time frames of when defects occur to highlight when PopZ and PodJ activities are most needed.

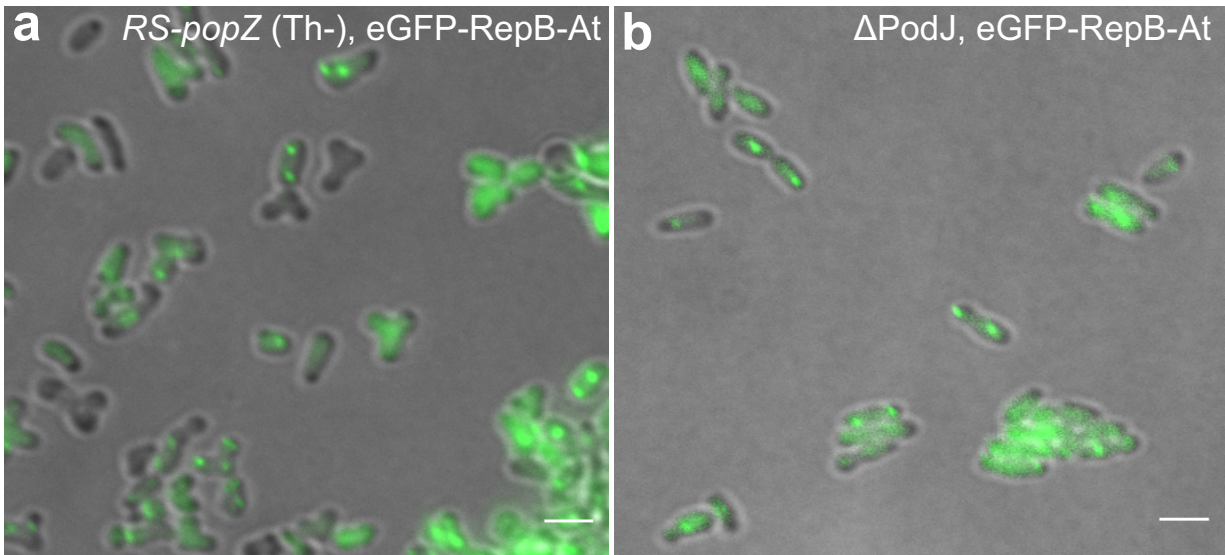


Fig. 5. Segregation of cryptic plasmid is inefficient in PopZ-depleted cells or in the absence of PodJ. (a) Localization of eGFP-RepB-At in PopZ-depleted cells. (b) Localization of eGFP-RepB-At in Δ PodJ cells. (Scale bars 2 μ m).

Discussion

Here, we studied the localization of ParA within the context of polar growth, monitored the localization CC and LC in the absence of GP specific factor, GPR, and observed the localization of pAt without PopZ and PodJ. In the shortest cells, ParA exhibited LDP located in a large region of the non-growing OP compartment. In contrast, in the longest cells, ParA formed a gradient containing a focus at or near the GP, suggesting that ParA relocates from the old cell compartment to the GP as the cell elongates. Partitioning of the CC or LC is impaired in the absence of GPR as a consequence of altered cell morphology which, in turn, prevents PopZ from correctly localizing (16). Furthermore, while PopZ and PodJ appear to be required for pAt localization to discrete polar foci to enable partitioning following replication, this effect may be a consequence of abnormal cell shape resulting from the loss of PopZ and PodJ. Below we discuss how features of the ParA gradient during polar growth may provide insight into the mechanisms underlying chromosome segregation.

Polar growth in *Agrobacterium* is intrinsically asymmetric. Early in the cell cycle, a bud emerges at the cell septum, and as the cell matures, the bud increases its dimensions to produce a new cell compartment, which grows until the GP transitions into a “new” non-growing old pole [(N)OP] (Fig. 1) (11, 12). Such asymmetry may determine the localization of ParA. PopZ and GPR are known to display asymmetries on their dynamic localization in the cell cycle (15-16, 18). During the GP to OP transition, PopZ is removed from the GP and relocates at the “new” GP created by septation in the new cell compartment sibling (15,18). Meanwhile, the “new” GP generated by septation of the old cell compartment sibling is occupied by newly synthesized PopZ (Fig. 1) (15,18). GPR is

at the GP until cell division and then is located at the new GPs, resulting from mid cell constriction in sibling cells (Fig. 1) (16).

Indeed, rod shape morphology dependent on PopZ or GPR is required to accumulate ParA at or near the GP. Here we present evidence for the role of rod shape morphology in determining the ParA gradient in the GP compartment. In the absence of PopZ or GPR, ParA displays a diffuse signal. Early in the cell cycle of WT cells, a presumptive division site is visible as a “constriction” between the old and new cell compartments that develops soon after polar growth initiates (11, 12). This constriction may restrict the movement of ParA from the old cell compartment into the new cell compartment. Indeed, ParA is present as a LDPs located in a large region of the non-growing OP (Fig. S1). In dispersed growth, the width of the growing cell remains identical in both the new and old cell compartments (27). Differences on the subcellular distribution of ParA can be appreciated between *Caulobacter* and *Agrobacterium* in the early stage of the cell cycle. In *Caulobacter*, ParA does not display a LDP and instead it localizes as a gradient that extends from the new pole to the old pole of short cells (28-32). However, in long cells of *Caulobacter*, ParA concentrates to the new pole (28-32). By analogy, this suggests that ParA is required for the segregation of CC in *Agrobacterium*.

Besides PopZ and GPR, which other factors might be required for the subcellular distribution of ParA? One obvious candidate is PodJ. In the absence of PodJ, the CC is abnormally located at the GP and it replicates from this position (21). What is the meaning of the multiple ParA patches in the absence of GPR (Fig. 3b)? In *Caulobacter* in the absence of the landmark protein TipN (a protein with homology to GPR) , ParA also exhibits aberrant localization patterns due to a failure on its localization dynamics (30).

Chapter 5

Therefore, does GPR regulate the dynamics of ParA in *Agrobacterium*? Probably only indirectly as cell shape is clearly important for the subcellular distribution of ParA. Furthermore, it needs to be determined how RepA proteins localize. In summary, cell shape dependent on PopZ and GPR is critical for the subcellular distribution of ParA. Future research will provide novel insights into how ATPases mediate the segregation of essential and nonessential replicons.

Materials and Methods

Plasmid construction. A list of plasmids or oligonucleotides used in this study is shown in tables S1 and S2 respectively. *mCh* was amplified from pCHYC-2 ((33)) with primers 1 and 2, which introduced NdeI and XbaI sites. The resulting product was ligated into NdeI and XbaI pSRKKm digested vector to raise pREJS005. To create pREJS007, *parA* was engineered with XbaI and KpnI sites using the pair of primers 7-8. This PCR product was inserted into a XbaI and KpnI pREJS005 digested vector. To create pREJS006, *mCh* and *parA* were amplified using pair primers 3-4 and 5-6. These PCR products were assembled via Gibson ((34)) into a NdeI pSRKKm digested vector. *mCh-parA* was amplified using pair of primers 1-8 from. This PCR product was assembled into a NdeI and KpnI pACYCDuet-1 digested vector to create pREJS008.

***Agrobacterium* strains and cell growth.** A description of the *Agrobacterium* strains used in this study is shown in Table S1. Cells were grown at 28°C in Luria-Bertani (LB) medium. When appropriate the growth media was supplemented with the following antibiotics: 40 µg/mL kanamycin, 50µg/mL gentamicin, or 300µg/mL spectinomycin. The *rs-popZ* and *rs-gpr* strains were grown in the presence of 0.5mM of Theophylline to induce the expression of PopZ and GPR. For depletion, *RS* strains were grown in the absence of Theophylline. Induction of the fluorescent fusions was performed by using 0.25-0.5mM isopropyl β-D-1-thiogalactopyranoside (IPTG) for 3-4h. Labeling of the PG with NADA was performed according to the protocol of Kuru E *et al* (35). In brief, to label the PG, early exponential cells were growth in the presence of 250 µM NADA for one generation.

This reaction was quenched with formaldehyde and NADA was removed from the cells using a phosphate-buffered saline (PBS) (pH 7.4) solution.

Heterologous expression of fluorescent fusions in *E. coli*. *E. coli* BL-21(DE3) containing the pREJS008 vector (Table S1) was grown at 37°C in LB. The temperature was switched to 28°C when cells reached an OD of 0.2. Cells were induced with 100 µM IPTG for 2-3 hours. Media were supplemented with 34 µg/mL chloramphenicol.

Cell imaging. Mid-exponential phase cells of *Agrobacterium* or *E. coli* expressing fluorescent fusion proteins were immobilized on 1% of agarose in LB. Bright field images were obtained using a DeltaVision Elite deconvolution microscope through PlanApo 100x, 1.4NA Japan oil objective. This microscope was operated with the Soft Worx 5.5 software. Micrographs were obtained using a Photometrics CoolSnap HQ CCD camera. First, cells were photographed in the bright field, then through the GFP, and mCh filters. Phase contrast Images were obtained with a Zeiss Z1 AxioObserver microscope through 100X oil objective. The AxioObserver microscope was operated using IVision software, and images were captured with a Q-Imaging Retiga-SRV Fast 1394 CCD camera. First cells were imaged in phase contrast field, and then through mCh filter. Micrographs were combined using Image-J ((36)). The mCh-ParA cumulative fluorescent profile and ParA-mCh dot-plot were generated using Object-J ((37)). Each image was scaled to 15.5 px/um.

Acknowledgments.

We thank Steven Ruzin and Denise Schichnes at the College of Natural Resources Biological Imaging Facility at University of California, Berkeley, for assistance with fluorescent imaging. The Biological Imaging Facility is supported in part by National Institutes of Health Program S10 (Award 1S1OD018136-01). We thank Prof. Lucy Shapiro at Department of Developmental at Stanford University for plasmids. We thank Dirk Bald at Department of Molecular and Cell Biology at Vrije University Amsterdam and Conrad Woldringh at Swammerdam Institute for Life Sciences (SILS) at University of Amsterdam for the insightful and critical reading of the manuscript. Research in the P.Z. laboratory is supported by National Science Foundation Grant MCB-0923840. J.S.R-E. received fellowship support from the Secretaría Nacional de Educación Superior, Ciencia, Tecnología, e Innovación, Ecuador.

References

1. G. C. DiCenzo, T. M. Finan, The divided bacterial genome: Structure, function, and evolution. *Microbiol Mol Biol Rev* **81** (2017).
2. G. B, *et al.*, Genome sequence of the plant pathogen and biotechnology agent *Agrobacterium tumefaciens* C58. *Science* **294**, 2323–2328 (2001).
3. D. W. Wood, *et al.*, The genome of the natural genetic engineer *Agrobacterium tumefaciens* C58. *Science*. **294**, 2317–2324 (2001).
4. T. G. Platt, E. R. Morton, I. S. Barton, J. D. Bever, C. Fuqua, Ecological dynamics and complex interactions of *Agrobacterium* megaplasmids. *Front Plant Sci* **5** (2014).
5. E. W. Nester, *Agrobacterium*: nature ' s genetic engineer. *Front Plant Sci* **5** (2015).
6. J. F. Heidelberg, *et al.*, DNA sequence of both chromosomes of the cholera pathogen *Vibrio cholerae*. *Nature* **406**, 477–483 (2000).
7. S. M. Halling, *et al.*, Completion of the Genome Sequence of *Brucella abortus* and Comparison to the Highly Similar Genomes of *Brucella melitensis* and *Brucella suis*. *J. Bacteriol.* **187**, 2715–2726 (2005).
8. C. M. Fraser, *et al.*, Genomic sequence of a Lyme disease spirochaete, *Borrelia burgdorferi*. *Nature* **390**, 580–586 (1997).
9. F. Galibert, *et al.*, The Composite Genome of the Legume Symbiont *Sinorhizobium meliloti*. *Science (80-.)*. **5530**, 668–672 (2001).
10. E. G. Ruby, *et al.*, Complete genome sequence of *Vibrio fischeri* : A symbiotic bacterium with pathogenic congeners. *PNAS* **102**, 3004–3009 (2005).
11. P. J. B. Brown, *et al.*, Polar growth in the Alphaproteobacterial order Rhizobiales. *PNAS*. **109**, 1697–1701 (2012).
12. T. A. Cameron, J. Anderson-Furgeson, J. R. Zupan, J. J. Zik, P. C. Zambryski, Peptidoglycan synthesis machinery in *Agrobacterium tumefaciens* during unipolar growth and cell division. *mBio*. **5** (2014).
13. E. Kuru, *et al.*, In situ probing of newly synthesized peptidoglycan in live bacteria with fluorescent D-amino acids. *Angew. Chem. Int. Ed. Engl.* **51**, 12519–12523 (2012).
14. T. A. Cameron, J. R. Zupan, P. C. Zambryski, The essential features and modes of bacterial polar growth. *Trends Microbiol.* **23**, 347–353 (2015).
15. R. Grangeon, J. R. Zupan, J. Anderson-furgeson, P. C. Zambryski, PopZ identifies the new pole, and PodJ identifies the old pole during polar growth in *Agrobacterium tumefaciens*. *PNAS*. **112**, 1166–11671 (2015).
16. J. R. Zupan, R. Grangeon, J. S. Robalino-Espinosa, N. Garnica, P. Zambryski, GROWTH POLE RING protein forms a 200-nm-diameter ring structure essential for polar growth and rod shape in *Agrobacterium tumefaciens*. *PNAS*. **116**, 10962–10967 (2019).
17. J. R. Zupan, T. A. Cameron, J. Anderson-furgeson, P. C. Zambryski, Dynamic FtsA and FtsZ localization and outer membrane alterations during polar growth and cell division in *Agrobacterium tumefaciens*. *PNAS* **110**, 9060–9065 (2013).
18. H. M. Ehrle, *et al.*, Polar Organizing Protein PopZ is required for chromosome segregation in *Agrobacterium tumefaciens*. *J. Bacteriol.* **199** (2017).
19. R. Grangeon, J. Zupan, Y. Jeon, P. C. Zambryski, Loss of PopZ At activity in *Agrobacterium tumefaciens* by deletion or depletion leads to multiple growth poles. *mBio*. **8** (2017).
20. J. C. Anderson-furgeson, J. R. Zupan, R. Grangeon, P. C. Zambryski, Loss of PodJ in *Agrobacterium tumefaciens* leads to ectopic polar growth, branching, and reduced cell division. *J. Bacteriol.* **198**, 1883–1891 (2016).
21. J. S. Robalino-Espinosa, J. R. Zupan, A. Chavez-Arroyo, P. Zambryski, Segregation of four *Agrobacterium tumefaciens* replicons during polar growth : PopZ and PodJ control segregation of essential replicons. *PNAS* **117**, 26366–26373 (2020).

22. C. Gogou, A. Japaridze, C. Dekker, A. Leonard, Mechanisms for Chromosome Segregation in Bacteria. *Front. Microbiol.* **12** (2021).
23. U. M. Pinto, K. M. Pappas, S. C. Winans, The ABCs of plasmid replication and segregation. *Nat. Rev. Microbiol.* **10**, 755–765 (2012).
24. A. S. B. Jalal, T. B. K. Le, Bacterial chromosome segregation by the ParABS system. *Open Biol.* **10** (2020).
25. J. Livny, Y. Yamaichi, M. K. Waldor, Distribution of Centromere-Like parS Sites in Bacteria : Insights from Comparative Genomics. *J. Bacteriol.* **189**, 8693–8703 (2007).
26. L. S. Kahng, L. Shapiro, Polar Localization of Replicon Origins in the Multipartite Genomes of *Agrobacterium tumefaciens* and *Sinorhizobium meliloti*. *J. Bacteriol.* **185**, 3384–3391 (2003).
27. Campos Manuel, *et al.*, A constant size extension drives bacterial cell size homeostasis. *Cell* **159**, 1433–1446 (2014).
28. H. C. Lim, *et al.*, Evidence for a DNA-relay mechanism in ParABS-mediated chromosome segregation. *Elife* **23** (2014).
29. J. L. Ptacin, *et al.*, A spindle-like apparatus guides bacterial chromosome segregation. *Nat. Cell Biol.* **12**, 791–798 (2010).
30. W. B. Schofield, H. C. Lim, C. Jacobs-Wagner, Cell cycle coordination and regulation of bacterial chromosome segregation dynamics by polarly localized proteins. *EMBO J.* **29**, 3068–3081 (2010).
31. C. W. Shebelut, J. M. Guberman, S. Van Teeffelen, A. A. Yakhnina, Z. Gitai, Caulobacter chromosome segregation is an ordered multistep process. *PNAS* **107**, 14194–14198 (2010).
32. I. V Surovtsev, H. C. Lim, C. Jacobs-Wagner, The slow mobility of the ParA partitioning protein underlies its steady-state patterning in Caulobacter. *Biophys J* **110**, 2790–2799 (2016).
33. M. Thanbichler, A. A. Iniesta, L. Shapiro, A comprehensive set of plasmids for vanillate and xylose-inducible gene expression in *Caulobacter crescentus*. *Nucleic Acids Res.* **35** (2007).
34. D. Gibson, *et al.*, Enzymatic assembly of DNA molecules up to several hundred kilobases. *Nat. Methods* **6**, 343–345 (2009).
35. E. Kuru, S. Tekkam, E. Hall, Y. V Brun, M. S. Van Nieuwenhze, Synthesis of fluorescent d-amino acids and their use for probing peptidoglycan synthesis and bacterial growth in situ. *Nat. Protoc.* **10**, 33–52 (2015).
36. C. A. Schneider, W. S. Rasband, K. W. Eliceiri, NIH Image to ImageJ: 25 years of Image Analysis HHS Public Access. *Nat. Methods* **9**, 671–675 (2012).
37. N. O. E. Vischer, *et al.*, Cell age dependent concentration of *Escherichia coli* divisome proteins analyzed with ImageJ and ObjectJ. *Front. Microbiol.* **6** (2015).

Supplemental figures

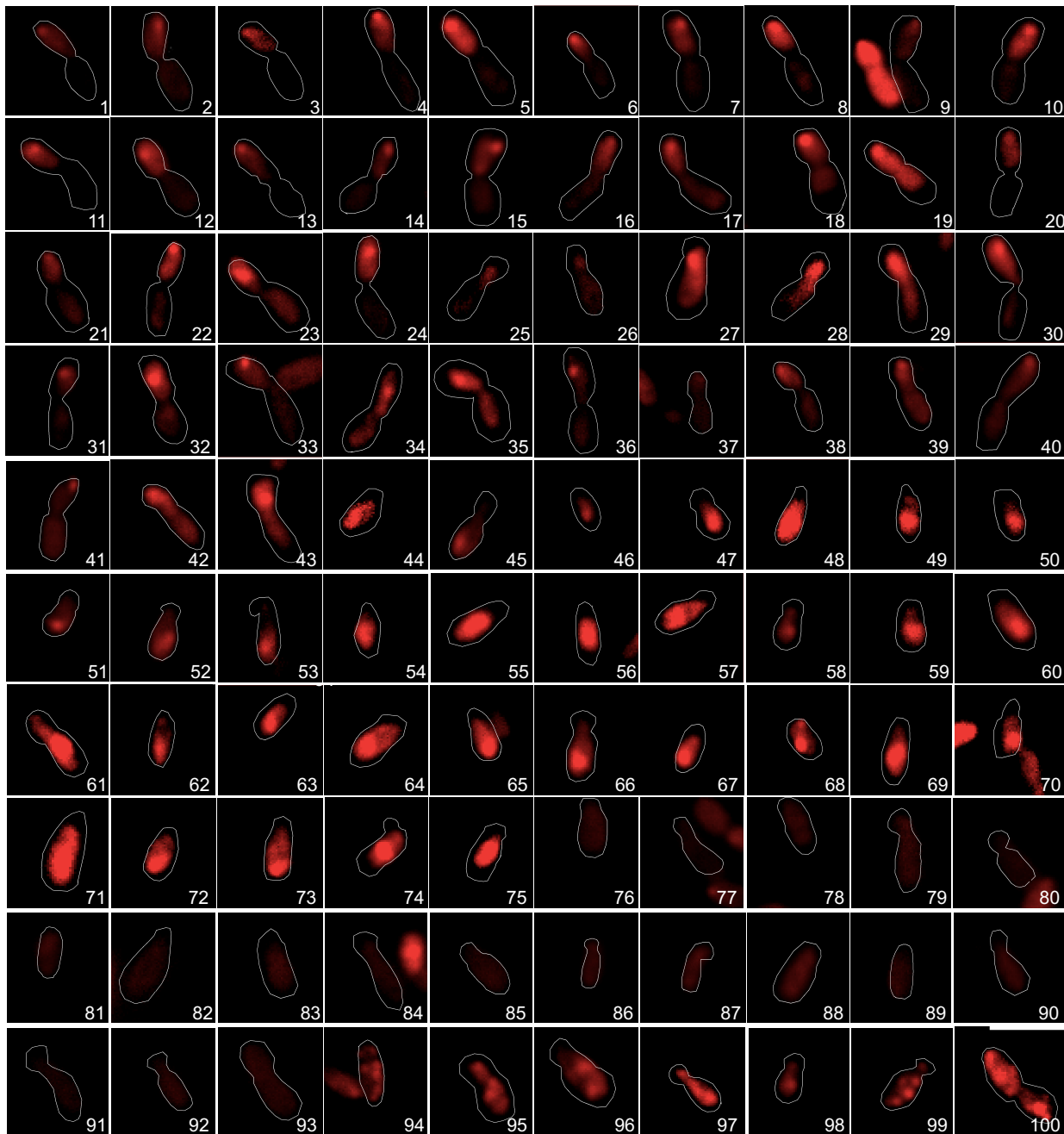


Figure S1. ParA-mCh exhibits different patterns of localization. Subcellular distribution of ParA-mCh in a gallery of 100 cells. Cells numbered 1-43, 44-75, 76-93, 94-100 exhibited foci, LDP, diffuse signal or multiple patches, respectively. Foci locate near or at the GP, whereas the LDPs locate in the OP compartment. (Scale bar is 2 μ m).

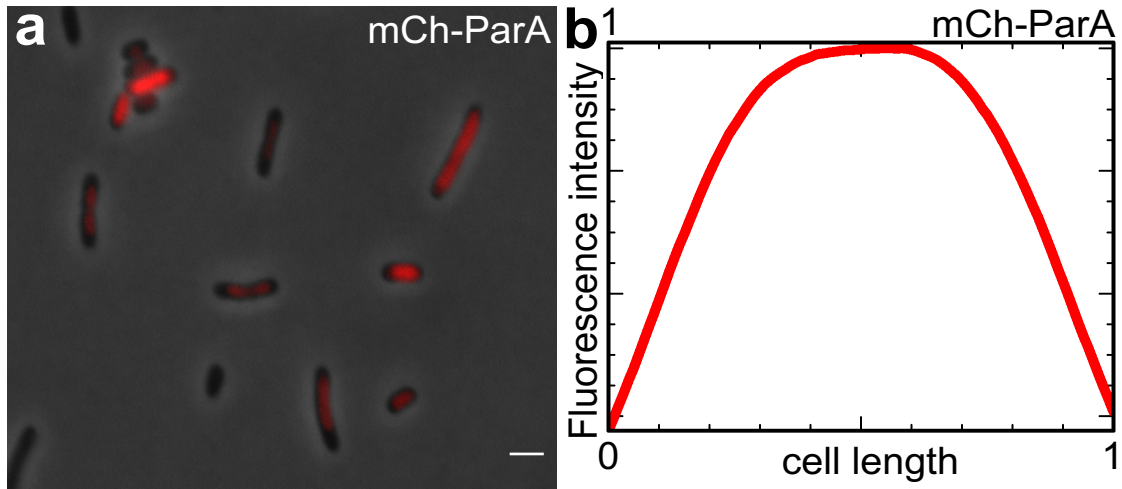


Figure S2. Expression of mCh-ParA in a heterologous *E. coli* test system. (a) Expression of mCh-ParA in *E. coli* BL21(DE3) cells. mCh-ParA shows a diffuse localization. (b) Plot representing quantitatively the subcellular distribution of mCh-ParA as the normalized fluorescence intensity over normalized cell length of 300 cells. (Scale bar on a, 2 μ m).

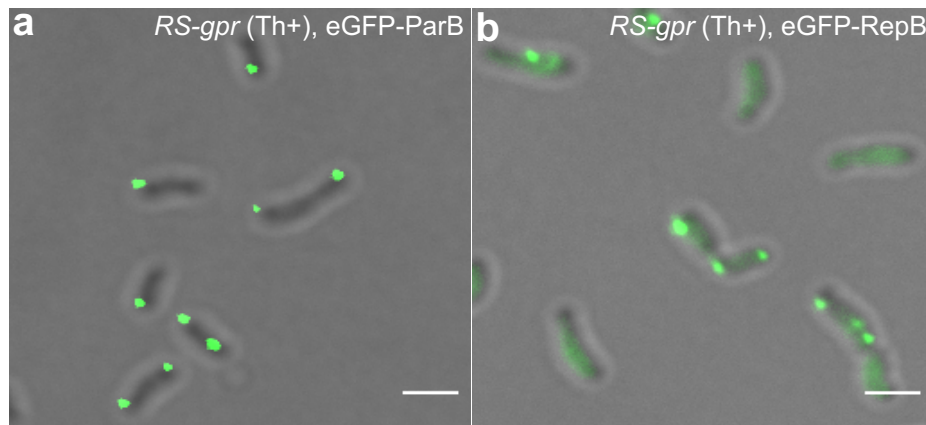


Figure S3. Circular and linear chromosomes localization in the *RS-gpr* strain. (a) CC localization (eGFP-ParB). (b) LC localization (eGFP-RepB). (a-b) Cells grew in 0.5mM theophylline to induce GPR expression are similar to wild type. (Scale bars in a-b, 2 μ m).

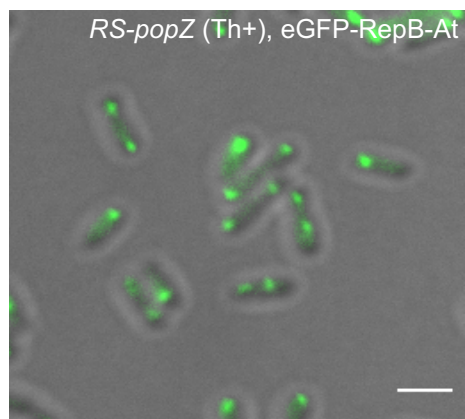


Figure S4. Cryptic plasmid localization in the *RS-popZ* strain. pAt localization (eGFP-RepB-At). Cells grew in 0.5mM theophylline to induce PopZ expression are similar to wild type. (Scale bar, 2 μ m).

Supplemental tables

Table S1: Plasmids

Plasmid	Description	Backbone	Source
pSRKKm	Broad host range vector, <i>lacI</i> , kanamycinR	pSRKKm	(1)
pCHYC-2	Integrating plasmid, kanamycinR	pCHYC-2	(2)
pACYCDuet-1	Replicating plasmid, chloramphenicolR	pACYCDuet-1	Novagen
pREJS005	<i>Plac::mCherry</i> , kanamycinR	pSRKKm	This study
pJZ254	<i>Plac::eGFP-parB</i> , gentamycinR	pSRKGm	(3)
pREJS002	<i>Plac::eGFP-repB</i> , kanamycinR	pSRKKm	(3)
pREJS003	<i>Plac::eGFP-repB-At</i> , kanamycinR	pSRKKm	(3)
pREJS006	<i>Plac::parA-mCherry</i> , kanamycinR	pSRKKm	This study
pREJS007	<i>Plac::mCherry-parA</i> , kanamycinR	pSRKKm	This study
pREJS008	<i>Pt7::mCherry-parA</i> , chloramphenicolR	pACYCDuet-1	This study

Table S2: Primers

Name	Sequence	Propose
1	aaacatatgatggtgagcaagggcgaggaggataacatggc	5' primer for cloning <i>mCherry</i> from pCHYC-2 into pSRKKm with an engineered NdeI site or to amplify <i>mCherry-parA</i>
2	aaatctagactgtacagctcgtccatgccgccggt	3' primer for cloning <i>mCherry</i> from pCHYC-2 into pSRKKm with an engineered XbaI site
3	ggaattgtgagcggataacaatttcacacaggaaacagcaatgtcagtcacacttttgccaataccaagggcgggg	5' primer for cloning <i>parA</i> via Gibson into pSRKKm fused to <i>mCherry</i>
4	tcctcgcccttgctcaccatggcagcttgcgcgtcacgagacgt	3' primer for cloning <i>parA</i> via Gibson into pSRKKm fused to <i>mCherry</i>
5	tcgtgacgcgcaaagctgccatggtgagcaagggcgaggaggataacatggcc	5' primer for cloning <i>mCherry</i> via Gibson into pSRKKm fused to <i>parA</i>
6	ttagtgagggttaatttcgagcttggcgtaatcatggtcattactgtacagctcgtccatgccgccggt	3' primer for cloning <i>mCherry</i> via Gibson into pSRKKm fused to <i>parA</i>
7	aaatctagaatgtcagtcacacttttgccaataccaagggcgggg	5' primer for cloning <i>parA</i> into pREJS005 with an engineered XbaI site
8	aaaggtacctcaggcagcttgcgcgtcacgagacgtgcta	3' primer for cloning <i>parA</i> into pREJS005 with an engineered KpnI site or to amplify <i>mCherry-ParA</i>

Table S3: Bacterial Strains

<i>Agrobacterium</i> strains	Relevant genotype/description	Construction, source or reference
C58	Wild type <i>Agrobacterium</i> , strain C58	(4)
A212	<i>RS::gpr</i>	(5)
REJS009	<i>RS::gpr, Plac::eGFP-parB</i>	pJZ254 electroporated into A212
REJS010	<i>RS::gpr, Plac::eGFP-repB</i>	pREJS002 electroporated into A212
ARG074	<i>RS-popZ</i>	(6)
REJS011	<i>RS-popZ, Plac::eGFP-repB-At</i>	pREJS003 electroporated into ARG074
A164	<i>podJ:: Δ</i>	(7)
REJS012	<i>podJ:: Δ, Plac::eGFP-repB-At</i>	pREJS003 electroporated into A164
REJS013	<i>Plac::parA-mCherry</i>	pREJS006 electroporated into C58
REJS014	<i>RS-popZ, Plac::parA-mCherry</i>	pREJS006 electroporated into ARG074
REJS015	<i>RS-gpr, Plac::parA-mCherry</i>	pREJS006 electroporated into A212
<i>E. coli</i> stains	Relevant genotype/description	Source
BL21(DE3)	<i>E. coli</i> str. B <i>F- ompT gal dcm lon hsdSB(rB-mB-) λ(DE3 [lacI lacUV5-T7p07 ind1 sam7 nin5]) [malB+]K-12(λS)</i>	(8)
REJS016	<i>Pt7::mCherry-parA</i>	pREJS008 electroporated into BL21(DE3)

Supplemental references

1. S. R. Khan, J. Gaines, R. M. R. li, S. K. Farrand, Broad-Host-Range Expression Vectors with Tightly Regulated Promoters and Their Use To Examine the Influence of TraR and TraM Expression on Ti Plasmid Quorum Sensing. *Appl. Environ. Microbiol.* **74**, 5053–5062 (2008).
2. M. Thanbichler, A. A. Iniesta, L. Shapiro, A comprehensive set of plasmids for vanillate and xylose-inducible gene expression in *Caulobacter crescentus*. *Nucleic Acids Res.* **35** (2007).
3. J. S. Robalino-Espinosa, J. R. Zupan, A. Chavez-Arroyo, P. Zambryski, Segregation of four *Agrobacterium tumefaciens* replicons during polar growth: PopZ and PodJ control segregation of essential replicons. *PNAS* **117**, 26366–26373 (2020).
4. R. Hamilton, M. Fall, The loss of tumor-initiating ability in *Agrobacterium tumefaciens* by incubation at high temperature. *Experientia* **27**, 229–230 (1971).
5. J. R. Zupan, R. Grangeon, J. S. Robalino-Espinosa, N. Garnica, P. Zambryski, GROWTH POLE RING protein forms a 200-nm-diameter ring structure essential for polar growth and rod shape in *Agrobacterium tumefaciens*. *PNAS*. **116**, 10962–10967 (2019).
6. R. Grangeon, J. Zupan, Y. Jeon, P. C. Zambryski, Loss of PopZ At activity in *Agrobacterium tumefaciens* by deletion or depletion leads to multiple growth poles. *mBio*. **8** (2017).
7. J. C. Anderson-furgeson, J. R. Zupan, R. Grangeon, P. C. Zambryski, Loss of PodJ in *Agrobacterium tumefaciens* leads to ectopic polar growth, branching, and reduced cell division. *J. Bacteriol.* **198**, 1883–1891 (2016).
8. M. Chambedin, *et al.*, Use of T7 RNA Polymerase to Direct Expression of Cloned Genes. *Methods Enzymol.* **185**, 60–89 (1990).

Chapter 6

**General discussion, suggested additional
experiments and future perspectives**

6

Cell development is a highly polarized process, often involving the dynamic accumulation of cell fate determinants to specific cell areas (e.g. cell poles) (1-4). A fascinating question in developmental biology is how this subcellular accumulation of these cell fate determinants is regulated (2,4). In this thesis, “Studies of cell identity factors reveal their role in cell differentiation, polar growth and DNA segregation”, studies of cell identity factors were performed using *Caulobacter crescentus* and mainly *Agrobacterium tumefaciens* as model systems. **Chapter II** and a different study (5) show that the stalked pole determinant SpmX physically associates with the polar organizing PodJ protein of *Caulobacter* (PodJ_{Cc}) to inhibit the subcellular accumulation of PodJ_{Cc} (5). As suggested by Zhao et al (2018) (5), the SpmX-PodJ_{Cc} interaction may share similarities with the FtsZ-MipZ and FtsZ-MinCD regulatory interactions that are required to prevent accumulation of the cell division FtsZ protein to the cell poles (5-7). **Chapter II** and Zhao et al (2018) (5) report that the cytosolic domain of PodJ_{Cc} (PodJ_{Cc} NTD) acts as an oligomerization domain of PodJ_{Cc}, which forms foci when heterologously expressed in *Escherichia coli*, suggesting that PodJ_{Cc} self-associates to phase separate (5). In corollary, PodJ_{Cc} exhibits a diffuse signal when coexpressed with SpmX in *E. coli* (5). However, the PodJ_{Cc}-SpmX regulatory interaction should also be tested in a purified system. Further, it needs to be determined, whether the inhibitory effect of SpmX extends to other polymeric proteins.

Recent studies have tested the interactions of PodJ_{Cc} by expressing this protein with its binding patterns in the heterologous *E. coli* test system (5,8-9). However, it's unknown whether PodJ_{Cc} remains as full length in *E. coli*, which is a far related bacterium of *Caulobacter* and encodes for YaeL, a homologue of the metalloprotease MmpA (15). In

the group of Dr. Dirk Bald, his tagged *podJ_{Cc}* (*h-podJ_{Cc}*) under the control of an IPTG driven T7 promoter was expressed in *E. coli*. Immunoblot analysis of cell lysates using an anti-his antibody revealed that H-PodJ_{Cc} runs just above the 100 KDa marker accompanied by three smaller bands that likely represent truncated variants of H-PodJ_{Cc}. To further test whether these H-PodJ_{Cc} variants are associated to the cell membrane, I prepared cytosolic and membrane fractions, and conducted an immunoblot analysis. Notably, the different variants of H-PodJ_{Cc} were present in the cell membrane, whereas almost absent from the cytosol (Fig. 1). Therefore, the previously observed polar foci of PodJ_{Cc} (5,8-9), likely represent a physical association of multiple PodJ_{Cc} variants.

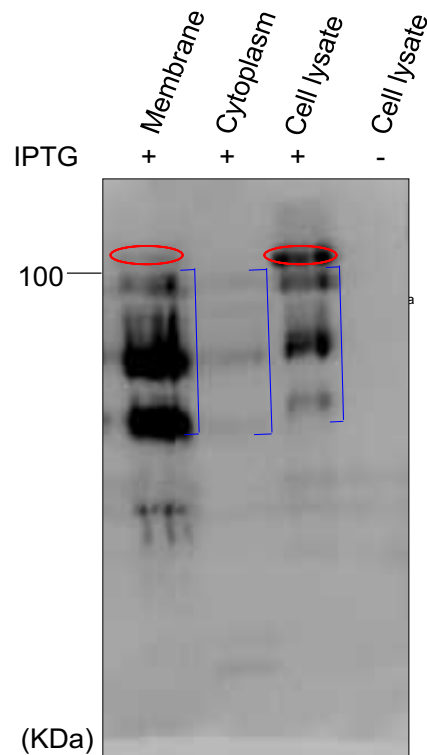


Fig. 1. H-PodJ_{Cc} is cleaved in *E. coli*. Different cell fractions and cell lysates were prepared and tested via Western Blot using an anti-his antibody. Full length H-PodJ_{Cc} and its variants are indicated with red circles and blue brackets, respectively. Induction was performed in cells exhibiting an OD₆₀₀ 2-3 with 1mM IPTG, for 3 hours at 37 °C and cell fractions were prepared using ultracentrifugation. The 100 KDa molecular size marker is indicated at the left of immunoblot.

Chapter II and different studies (5,8) report the interaction of PodJ with PleC when both proteins are heterologously expressed in *E. coli*. However, it is unknown whether the PodJ-PleC interaction occurs with PleC associated to the cell membrane. Strep-tagged *pleC* (*pleC-S*) under the control of an IPTG driven T7 promoter was expressed in *E. coli*. Immunoblot analysis of cell lysates using an anti-strep antibody revealed that PleC-S runs above the 75 KDa marker. Further, I prepared cytosolic and membrane fractions and test them via an immunoblot analysis. This revealed that PleC-S is absent from the cytosol, whereas present in the membrane exhibiting little degradation or aggregation (Fig. 2a). Thus, PleC and PodJ likely interact in the cell membrane of *E. coli*. Notably, PleC-S can be isolated from the cell membrane in the presence of the detergent lauryl maltose neopentyl glycol (LMNG) (Fig. 2b). Future studies should resolve the structure of PleC, either alone or in the presence of PodJ_{Cc} NTD.

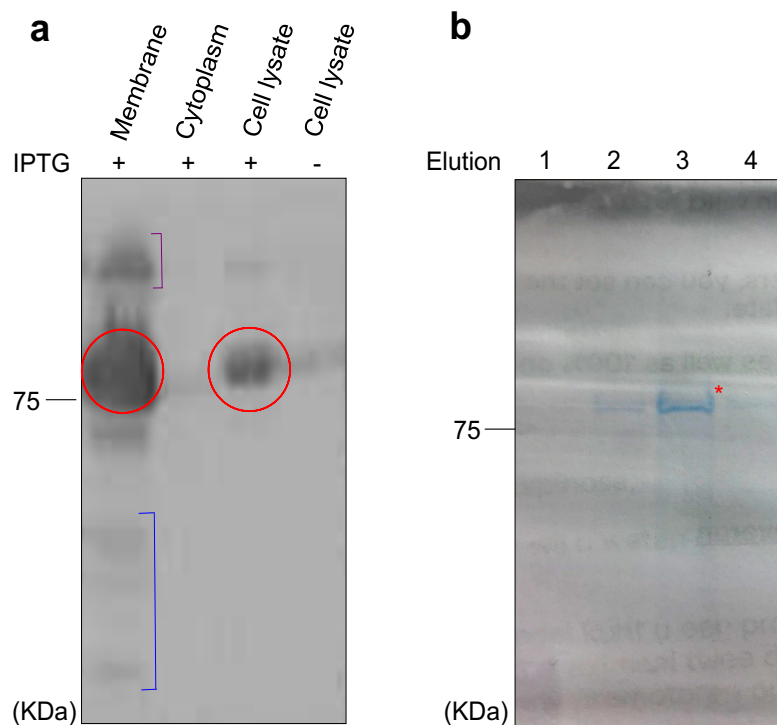


Fig. 2. Expression and purification of PleC-S. (a) PleC-S is in the cell membrane of *E. coli*. Different cell fractions and cell lysates were prepared and tested via Western Blot

using an anti-strep antibody. PleC-S, degradation products and aggregated PleC are shown with red circles, blue and purple brackets, respectively. Induction was performed in cells exhibiting an OD_{600} 2-3 with 1mM IPTG, for 3 hours at 37 °C and cell fractions were prepared using ultracentrifugation. (b) Purification of membrane bound PleC-S. Different elutions were performed using 0.5-2.5 mM of desthiobiotin and analyzed via an SDS-PAGE gel followed by a Coomassie staining. Purified LMNG PleC-S protein is indicated with a red asterisk. (a-b) The 75 KDa molecular size markers are indicated at the left of each panel.

In *Caulobacter*, *spmX* arose as a result of a “domestication” of a prophage peptidoglycan hydrolase gene into a developmental gene (10). *Agrobacterium* lacks a homologue of SpmX (10), why? First, to elongate, *Caulobacter* uses interspersed growth, while *Agrobacterium* elongates from one end of the cell, the growth pole (11). Further, *Agrobacterium* PodJ (PodJ_{At}) shows an opposite dynamic localization pattern compared to PodJ_{Cc}, which exists in full length (PodJ_L) and truncated (PodJ_S) variants (5,12-13). PodJ_L localizes to the new pole of the stalked cell and, upon cell compartmentalization and just before cell division, is converted to PodJ_S by the CtrA cell cycle regulated PerP protease (5,12-14). After cell division, PodJ_S localizes to the flagellated pole of the swarmer cell and, during swarmer-to-stalked cell transition, is released to the cytoplasm by MmpA (5,12-13,15). In contrast, PodJ_{At} localizes to the non-growing old pole and, during the transition from growth pole to a new old pole, relocates to both poles (16). Therefore, the SpmX-PodJ_{Cc} regulatory interaction likely appeared during evolutionary diversification to define the cell polarity axis of *Caulobacter*.

Agrobacterium lacks most of the components needed for dispersed growth, and instead has developed structural proteins required for polar growth (11, 17-19) [For details see the review of Cameron, TA. *et al* (2015)] (11). **Chapter III** (18) describes a previously uncharacterized *Agrobacterium* protein (Atu1348) with low degree of amino acid

sequence identity (~20%) to the land mark TipN protein, which marks the new pole in *C. crescentus* (18, 20-21). Atu1348 forms a striking hexameric ring at the growth pole, and therefore was named as GROWTH POLE RING (GPR) protein (18). Notably, GPR is essential for polar growth (18-19). Indeed, in the absence of GPR, cells lose the rod shape and adopt an essentially spherical morphology (18-19).

Chapter III (18) hypothesized that GPR acts as a scaffold to assemble the polar growth machinery essential for peptidoglycan synthesis and phospholipid dependent membrane biogenesis (18). GPR is a 2,115 amino acids protein containing an extremely large region (75% of the protein) with nonoverlapping and overlapping apolipoprotein (ApoLP) subdomains (18-19). In higher eukaryotes, ApoLPs are the principal protein component of the high-density lipoprotein (HDL), which sequesters lipids from the blood stream (22). In prokaryotes, ApoLPs form part of lipid droplets and are mainly found in the Rhizobiales order (18-19,23). Insights for the organization of lipid domains in the membrane have come predominantly from studies on bacteria that elongate by inserting growth precursors along the cell length (24). However, how lipid domains are distributed during polar growth is still unknown. Membrane alteration in the absence of GPR may be tracked using fluorescent dyes (e.g. Laurdan) that interact or bind to different types of lipids. Interaction studies of purified proteins are needed to determine if GPR interacts with enzymes required for lipid biosynthesis. Further, localization and depletion studies are required to determine whether these enzymes localize at the growth pole or if they are required for polar growth. During polar growth, peptidoglycan synthesis occurs unidirectionally from the growth pole (17,19,25-26). However, in cells lacking GPR, the synthesis of

peptidoglycan is primarily distributed around the cell periphery (19). This suggests that localization of L,D-transpeptidases (e.g. Atu0845) is affected in the absence of GPR.

Chapter III (18) and a more recent study (19) showed that expression of GPR fused at its C terminus to Green Fluorescent Protein (GPR-GFP) leads to the formation of multiple ectopic growth poles (18-19). This indicates that the C terminus of GPR plays a significant role on GPR function. Indeed, several C terminal deletions are unable to restore rod shape morphology of genetically depleted cells (19). A related question is, what are the regions of GPR required to establish its ring-like structure? Notably, A-IV-1, an ApoLP subdomain comprising the amino acids 1037-1382 on GPR, was shown to be essential to establish the ring-like conformation (19). However, this structure is not sufficient to maintain the function of GPR (19).

An overriding question is, what factors are required for the formation of the GPR ring?

Chapter III (18) reported that the six-fold symmetry of GPR surrounds another *Agrobacterium* GP marker, PopZ (PopZ_{At}) (16,18,27). Further, genetic deletion or depletion of PopZ_{At} produces ectopic growth poles (27-29). Therefore, PopZ_{At} might be required for the formation of the GPR ring. In the laboratory of Prof. Patricia Zambryski, GPR fused to GFP (GFP-GPR) was expressed in a strain containing a theophylline sensitive riboswitch (RS) sequence upstream of the open reading frame of *popZ_{At}* (*rs-popZ_{At}*) (Fig. 3a-d) (16,26). In the absence of theophylline in *rs-popZ_{At}*, the expression of PopZ_{At} was blocked, resulting in the formation ectopic growth poles as seen previously (27-29). Most notably, however, GFP-GPR formed its characteristic ring-like structure (Fig 2a-d). Therefore, PopZ_{At} does not appear to be required to form GFP-GPR rings, as previously suggested from the close association of PopZ_{At} in the center of GPR rings (18).

Future studies using high resolution 3D-SIM may reveal if the dimensions of the GPR ring (600nm circumference with a diameter of 200nm at a distance of 100nm from the tip of the growth pole) (18) are modulated/alterd by lack of PopZ_{At} at the growth pole.

RS-popZ_{At} (Th-), eGFP-GPR

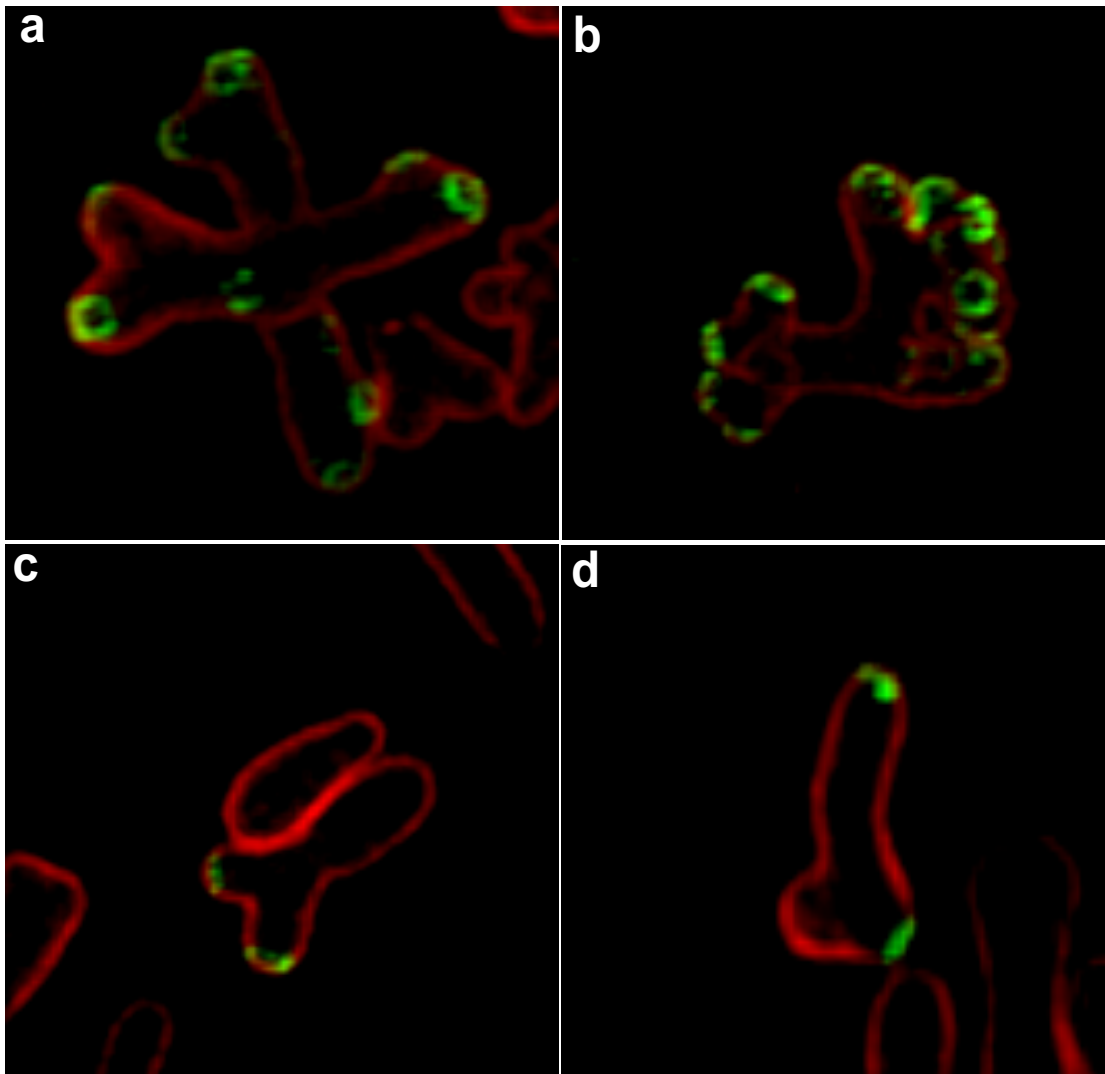


Fig. 3. Localization and subcellular structure of GPR in cells depleted of PopZ_{At}. (a-d) Imaging of eGFP-GPR in FM4-64 stained *rs-popZ_{At}* cell by 3D-SIM. The distinctive ring-like is present at the ectopic GPs. (a-b) Expression of eGFP-GPR was performed in *trans* and cells grew in the absence of theophylline.

Chapter III (18) described the dynamic localization pattern of GPR during the cell cycle.

GPR resides at the GP until cell division and then is located to the new growth poles,

resulting from mid cell constriction (18). Does GPR relocate to the sibling new growth poles? As hypothesized in Chapter III (18), probably not, since GPR is a membrane tethered protein that will not easily migrate to the new growth poles (18). Experiments using photoactivated localization microscopy (PALM) to track the localization of GPR tagged with a photoconvertible fluorescent protein (e.g. Dendra or MEos3.2) may confirm this hypothesis. This approach was previously used to determine the migration of non-membrane associated PopZ_{At} molecules from the new old pole to the sibling new pole resulting from mid cell constriction (27). A related question is, what are the cell cycle events required to disassemble the GPR ring from the growth pole? A critical factor is likely the growth pole to new old pole transition, that requires PodJ_{At} and the *Agrobacterium* cell division FtsZ protein (FtsZ_{At}) (30-31). Indeed, after cell division, cells lacking PodJ_{At} continue to grow from the pole opposite to the septation site (30). Further, in the absence of FtsZ_{At}, growth at the growth pole continues until the cell lyses (31). Thus, either PodJ_{At} and FtsZ_{At} or both may be essential for GPR disassembly?

Chapter III (18) reported that rod shape morphology dependent on GPR is required for the localization of PopZ_{At}, which in turn is needed for segregation of the circular chromosome of *Agrobacterium* (CC, 2 Mbp) (18,27,32). Indeed, in the absence of PopZ_{At}, cells exhibit a diffuse signal for eGFP-ParB or YFP-ParB (26,32). In wild type, fluorescent tagged ParB binds to its cognate *parS* sequence forming foci (27, 32-33). Further, in cells deprived of PopZ_{At}, one copy of the CC replicon remains polarly localized, while the other localizes between the poles (27). This suggests that PopZ_{At} physically interacts with the ParB-*parS* complex to tether the CC at the growth pole. Consistent with this hypothesis,

after CC replication in WT, one CC copy remains at the old pole, while the other migrates to the growth pole, where PopZ_{At} localizes (16,32-34).

A related question is, what tethers the CC at the old pole? The single 4.02-Mbp chromosome of *Caulobacter* is tethered at the old pole through a direct interaction of PopZ_{Cc} with the ParB-*parS* complex (35-36). PopZ_{Cc} exhibits an opposite localization pattern compared to *Agrobacterium* (16, 27-28, 35-36). Indeed, PopZ_{Cc} resides at the old pole of the swarmer cell, and relocates to both poles in the stalked cell (35,36). In contrast, PopZ_{At} marks only the growth pole during the cell cycle and after cell division it relocates to the new growth poles of the sibling cells (16, 27). Therefore, by a spatiotemporal limitation PopZ_{At} is unable to anchor the CC at the old pole. Notably, **Chapter IV** (32) reported that PodJ_{At} is required to tether the CC at the old pole (32). This suggests that PodJ_{At} directly interacts with the ParB-*parS* complex.

Besides CC, *Agrobacterium* contains an additional essential replicon, the linear chromosome (LC, 2.0 Mbp) and two nonessential replicons, the cryptic plasmid (pAT, 0.5 Mbp) and tumor-inducing plasmid (pTi, 0.2 Mbp) (37-38). Like CC, segregation of the LC replicon requires PopZ_{At} and PodJ_{At} (32). In the absence PopZ_{At}, eGFP-RepB shows a diffuse signal (32). In wild type, fluorescent tagged RepB binds to its cognate *parS_{LC}* sequence forming foci (32-33). Further, **Chapter IV** (32) showed LC is tethered at the old pole by PodJ_{At} (32). This suggests that RepB-*parS_{LC}* complex directly interacts with PodJ_{At} and PopZ_{At} to maintain in place the LC.

As indicated in **Chapter IV** (32), pAT shows a specific pattern of localization compared to LC or CC (32). Early in the cell cycle, pAT is at the old pole and prior to replication it moves away from the old pole (32-33). Post replication, one pAT copy moves back to the

old pole, while the other copy migrates to the growth pole (32-33). Therefore, pAT might require PopZ_{At} and PodJ_{At} to be tethered at the growth pole and old pole, respectively. In agreement with this hypothesis, **Chapter V** reported a diffuse signal for eGFP-RepB_{AT} in the absence of PopZ_{At} or PodJ_{At}. In wild type, fluorescent tagged RepB_{At} binds to its cognate *parS*_{At} prompting the formation of fluorescent foci (32-33). Future experiments should monitor the dynamic localization pattern of pAT in the absence of PopZ_{At} or PodJ_{At}. **Chapter IV** (32) described that pTi localizes at numerous places throughout the cell (32). This localization pattern was obtained by fusing RepB_{Ti} with eGFP (eGFP-RepB_{Ti}). However, recent chromatin immunoprecipitation sequencing (Chip-seq) experiments revealed the existence of a *parS*_{Ti} site within *repB*_{Ti} (33). This apparent problem was circumvented by modifying the *parS*_{Ti} on the fluorescent reporter (33). By using this approach, Ren et al (2021) observed that pTi localizes as one or two polar foci (33). Therefore, by analogy to the CC and LC, the pTi replicons may also require PodJ_{At} and PopZ_{At} for its segregation.

Early in the *Caulobacter* cell cycle, ParA forms a gradient by randomly associating to DNA in the presence of ATP and then it relocates to the new pole whilst hydrolyzing ATP, that is directly stimulated by ParB-*parS* complex (39-41). In the so called “DNA relay-model”, chromosome segregation is mediated by the dynamics of several ParA-DNA complexes that act in sequence to transiently tether the ParB-*parS* complex (40, 42-43). Is the localization pattern of *Agrobacterium* ParA (ParA_{At}) compatible with the DNA relay-model? Probably yes, as ParA_{At} seems to relocate from the old cell compartment to the growth pole as the cell elongates. Indeed, **Chapter V** described that ParA_{At}, forms a large

dense patch (LDP) in a large region of the old pole compartment in the shortest cells and a gradient with the strongest accumulation at or near the growth pole in the longest cells. The presented insights in this thesis indicate that *Agrobacterium* polar growth cell cycle requires different structures and cell identity factors with distinct functional roles when compared to *Caulobacter* dispersed growth cell cycle. Illustrating these differences provide new opportunities to design specific antimicrobial therapies against pathogens that exhibit polar growth, such as *Mycobacterium tuberculosis* or *Brucella abortus* (25, 44).

Acknowledgments.

I thank Prof. Patricia Zambryski and John Zupan at the Department of Plant and Microbial Biology at University of California, Berkeley, and Steven Ruzin and Denise Schichnes at the College of Natural Resources Biological Imaging Facility at University of California, Berkeley, for assistance with the cell imaging. Fig. 3. was generated in the P.Z. laboratory. Research in the P.Z. laboratory was supported by National Science Foundation Grant MCB-0923840. I thank Prof. Holger Lill, Dirk Bald and Hojjat Ghasemi at Department of Molecular and Cell Biology at Vrije University Amsterdam for assistance with membrane protein purification. Figs. 1 and 2 were generated in the D.B laboratory. I thank Prof. Patricia Zambryski at the Department of Plant and Microbial Biology at University of California, Berkeley and Prof. Holger Lill at Department of Molecular and Cell Biology at Vrije University Amsterdam for the insightful and critical reading of this discussion. I received fellowship support from Secretaría Nacional de Educación Superior, Ciencia, Tecnología, e Innovación, Ecuador.

References

1. L. Shapiro, H. H. McAdams, R. Losick, Generating and exploiting polarity in bacteria. *Science*. **298**, 1942–1946 (2002).
2. L. Shapiro, H. H. McAdams, R. Losick, Why and how bacteria localize proteins. *Science*. **326**, 1225–1228 (2009).
3. K. Lasker, T. H. Mann, L. Shapiro, An intracellular compass spatially coordinates cell cycle modules in *Caulobacter crescentus*. *Curr. Opin. Microbiol.* **33**, 131–139 (2016).
4. L. Garaldine, C. Jacobs-Wagner, How do bacteria localize proteins to the cell pole? *J Cell Sci* **127** (2014).
5. W. Zhao, *et al.*, A circuit of protein-protein regulatory interactions enables polarity establishment in a bacterium. *BioRxiv*. (2018).
6. Z. Hu, A. Mukherjee, S. Pichoff, J. Lutkenhaus, The MinC component of the division site selection system in *Escherichia coli* interacts with FtsZ to prevent polymerization. *PNAS* **96**, 14819–14824 (1999).
7. M. Thanbichler, L. Shapiro, MipZ, a Spatial Regulator Coordinating Chromosome Segregation with Cell Division in *Caulobacter*. *Cell* **125**, 147–162 (2006).
8. C. Zhang, W. Zhao, S. W. Duvall, K. A. Kowallis, W. S. Childers, Regulation of a bacterial histidine kinase by a phase separating scaffolding protein. *BioRxiv* (2021).
9. W. Zhao, *et al.*, Scaffold-scaffold interactions regulate cell polarity in a bacterium. *BioRxiv*. (2020).
10. A. M. Randich, D. T. Kysela, C. Morlot, Y. V Brun, Origin of a Core Bacterial Gene via Co-option and Detoxification of a Phage Lysin. *Curr Biol* **29**, 1634–1646 (2019).
11. T. A. Cameron, J. R. Zupan, P. C. Zambryski, The essential features and modes of bacterial polar growth. *Trends Microbiol.* **23**, 347–353 (2015).
12. P. H. Viollier, N. Sternheim, L. Shapiro, Identification of a localization factor for the polar positioning of bacterial structural and regulatory proteins. *PNAS* **99**, 13831–13836 (2002).
13. A. J. Hinz, D. E. Larson, C. S. Smith, Y. V. Brun, The *Caulobacter crescentus* polar organelle development protein PodJ is differentially localized and is required for polar targeting of the PleC development regulator. *Mol. Microbiol.* **47**, 929–941 (2003).
14. J. C. Chen, *et al.*, Cytokinesis signals truncation of the PodJ polarity factor by a cell cycle-regulated protease. *EMBO J.* **25**, 377–386 (2006).
15. J. C. Chen, P. H. Viollier, L. Shapiro, A membrane metalloprotease participates in the sequential degradation of a *Caulobacter* polarity determinant. *Mol. Microbiol.* **55**, 1085–1103 (2005).
16. R. Grangeon, J. R. Zupan, J. Anderson-furgeson, P. C. Zambryski, PopZ identifies the new pole, and PodJ identifies the old pole during polar growth in *Agrobacterium tumefaciens*. *PNAS*. **112**, 1166–11671 (2015).
17. T. A. Cameron, J. Anderson-Furgeson, J. R. Zupan, J. J. Zik, P. C. Zambryski, Peptidoglycan synthesis machinery in *Agrobacterium tumefaciens* during unipolar growth and cell division. *mBio*. **5** (2014).
18. J. R. Zupan, R. Grangeon, J. S. Robalino-Espinosa, N. Garnica, P. Zambryski, GROWTH POLE RING protein forms a 200-nm-diameter ring structure essential

- for polar growth and rod shape in *Agrobacterium tumefaciens*. *PNAS*. **116**, 10962–10967 (2019).
19. J. Zupan, Z. Guo, T. Biddle, P. Zambryski, *Agrobacterium tumefaciens* Growth Pole Ring Protein: C terminus and internal apolipoprotein homologous domains are essential for function and subcellular localization. *mBio*. **12** (2021).
 20. H. Lam, W. B. Schofield, C. Jacobs-Wagner, A landmark protein essential for establishing and perpetuating the polarity of a bacterial cell. *Cell* **124**, 1011–1023 (2006).
 21. E. Huitema, S. Pritchard, D. Matteson, S. K. Radhakrishnan, P. H. Viollier, Bacterial birth scar proteins mark future flagellum assembly site. *Cell* **124**, 1025–1037 (2006).
 22. M. C. Phillips, New insights into the determination of HDL structure by apolipoproteins. *J. Lipid Res.* **54**, 2034–2048 (2013).
 23. Y. Ding, *et al.*, Identification of the major functional proteins of prokaryotic lipid droplets. *J. Lipid Res.* **53**, 399–411 (2012).
 24. K. Matsumoto, H. Hara, I. Fishov, E. Mileyskoykaya, V. Norris, The membrane: Transertion as an organizing principle in membrane heterogeneity. *Front. Microbiol.*, 1 (2015).
 25. P. J. B. Brown, *et al.*, Polar growth in the Alphaproteobacterial order Rhizobiales. *PNAS*. **109**, 1697–1701 (2012).
 26. E. Kuru, *et al.*, In situ probing of newly synthesized peptidoglycan in live bacteria with fluorescent D-amino acids. *Angew. Chem. Int. Ed. Engl.* **51**, 12519–12523 (2012).
 27. H. M. Ehrle, *et al.*, Polar Organizing Protein PopZ is required for chromosome segregation in *Agrobacterium tumefaciens*. *J. Bacteriol.* **199** (2017).
 28. M. Howell, *et al.*, Absence of the Polar Organizing Protein PopZ Results in Reduced and Asymmetric Cell Division in *Agrobacterium tumefaciens*. *J. Bacteriol.* **199** (2017).
 29. R. Grangeon, J. Zupan, Y. Jeon, P. C. Zambryski, Loss of PopZ At activity in *Agrobacterium tumefaciens* by deletion or depletion leads to multiple growth poles. *mBio*. **8** (2017).
 30. J. C. Anderson-furgeson, J. R. Zupan, R. Grangeon, P. C. Zambryski, Loss of PodJ in *Agrobacterium tumefaciens* leads to ectopic polar growth, branching, and reduced cell division. *J. Bacteriol.* **198**, 1883–1891 (2016).
 31. M. Howell, *et al.*, *Agrobacterium tumefaciens* divisome proteins regulate the transition from polar growth to cell division. *Mol. Microbiol.* **111**, 1074–1092 (2019).
 32. J. S. Robalino-Espinosa, J. R. Zupan, A. Chavez-Arroyo, P. Zambryski, Segregation of four *Agrobacterium tumefaciens* replicons during polar growth: PopZ and PodJ control segregation of essential replicons. *PNAS* **117**, 26366–26373 (2020).
 33. Z. Ren, *et al.*, Conformation and dynamic interactions of the multipartite genome in *Agrobacterium tumefaciens*. *PNAS*. **119** (2022).
 34. L. S. Kahng, L. Shapiro, Polar Localization of Replicon Origins in the Multipartite Genomes of *Agrobacterium tumefaciens* and *Sinorhizobium meliloti*. *J. Bacteriol.* **185**, 3384–3391 (2003).
 35. G. R. Bowman, *et al.*, A Polymeric protein anchors the chromosomal origin/ParB

- complex at a bacterial cell pole. *Cell* **134**, 945–955 (2008).
36. G. Ebersbach, A. Briegel, G. J. Jensen, C. Jacobs-Wagner, A self-associating protein critical for chromosome attachment, division, and polar organization in *Caulobacter*. *Cell* **134**, 956–968 (2008).
 37. G. B, *et al.*, Genome sequence of the plant pathogen and biotechnology agent *Agrobacterium tumefaciens* C58. *Science (80-.)*. **294**, 2323–2328 (2001).
 38. D. W. Wood, *et al.*, The genome of the natural genetic engineer *Agrobacterium tumefaciens* C58. *Science (80-.)*. **294**, 2317–2324 (2001).
 39. B. E. Funnell, ParB Partition Proteins: Complex Formation and Spreading at Bacterial and Plasmid Centromeres. *Front. Mol. Biosci.* **3** (2016).
 40. H. C. Lim, *et al.*, Evidence for a DNA-relay mechanism in ParABS-mediated chromosome segregation. *Elife* **23** (2014).
 41. J. L. Ptacin, *et al.*, A spindle-like apparatus guides bacterial chromosome segregation. *Nat. Cell Biol.* **12**, 791–798 (2010).
 42. P. A. Wiggins, K. C. Cheveralls, J. S. Martin, R. Lintner, J. Kondev, Strong intranucleoid interactions organize the *Escherichia coli* chromosome into a nucleoid filament. *PNAS* **107**, 4991–4995 (2010).
 43. I. V Surovtsev, M. Campos, C. Jacobs-Wagner, DNA-relay mechanism is sufficient to explain ParA-dependent intracellular transport and patterning of single and multiple cargos. *PNAS* **113**, 7268–7276 (2016).
 44. N. R. Thanky, D. B. Young, B. D. Robertson, Unusual features of the cell cycle in mycobacteria: Polar-restricted growth and the snapping-model of cell division. *Tuberc.* **87**, 231–236 (2007).

Summary

Acknowledgment

Curriculum vitae

Publication list

Summary.

Caulobacter crescentus and *Agrobacterium tumefaciens* display different growth modes. Indeed, *Caulobacter* elongates through dispersed growth, whereas *Agrobacterium* elongates through single polar growth. In this thesis, “*Studies of cell identity factors reveal their role in cell differentiation, polar growth and DNA segregation*”, I studied cell pole identity factors of *Caulobacter* and *Agrobacterium*. I observed that, 1) the subcellular accumulation of a swarmer pole determinant is inhibited by a stalked pole determinant in *Caulobacter*; that 2) a previously uncharacterized *Agrobacterium* protein, with little amino acid sequence identity to a land mark protein of *Caulobacter*, forms at the growth pole a striking hexameric ring required for polar growth; that 3) the four *Agrobacterium* genetic elements exhibit different timing of replication and segregation, and that specific old pole and growth pole markers are critically required for the segregation of the two essential replicons of *Agrobacterium*; and that 4) the localization of an ATPase protein, likely required for DNA segregation in *Agrobacterium*, requires rod shape morphology dependent on two specific growth pole markers. These insights indicate that polar growth cell cycle requires different structures and cell identity factors with distinct functional roles when compared to dispersed growth cell cycle.

Acknowledgment.

These past years have been incredible, all full of science and friends, who were extremely generous and gentle. I thank Prof. Holger Lill and Dirk Bald at Vrije Universiteit Amsterdam for the admission to the PhD program allowing me to explore my research interests in the States and The Netherlands; for giving me the opportunity to perform research on membrane protein biochemistry, support and guidance. I also thank Hojjat Ghasemi Goojani for the introduction to the lab in Amsterdam. I thank Henk Hakvoort and Gregory Koningstein at Vrije Universiteit Amsterdam for technical support. I deeply thank Prof. Patricia Zambryski and John Zupan at UC Berkeley for the admission to the Zambryski lab as a visiting PhD student allowing me to learn about polar growth cell cycle in *Agrobacterium tumefaciens*, also for the incredible mentoring, guidance and support. The bulk of this thesis was performed in P.Z laboratory under the supervision of Prof. Patricia Zambryski. I thank Steven Ruzin and Denise Schichnes at UC Berkeley for assistance with fluorescent imaging. I also thank Romain Grangeon for the introduction to the lab in Berkeley. I thank Prof. Lucy Shapiro at Stanford University for the admission to the Shapiro lab as visiting PhD student allowing me to learn about *Caulobacter crescentus* cell cycle, also for guidance and support. I thank Tom Mann for the introduction to the lab at Stanford. I thank Virginia Kalogeraki, Rogerio Lourenco, Saumya Saurabh, Darshan Pathak at Stanford University for training. I thank Todd Galitz at Stanford University for technical assistance. I also thank Joseph Chen at San Francisco State University for the insightful, critical reading, discussions and edits of chapter II. I thank Conrad Woldringh at University of Amsterdam for his precious friendship and teaching me bacterial physiology for so many years. I thank my family for their love and

support. I dedicate this thesis to my father and to the resilience of my mother. Finally, I thank fellowship Secretaría Nacional de Educación Superior, Ciencia, Tecnología, e Innovación, Ecuador for the fellowship support.

Curriculum vitae.

I was born on April 27, 1979 in Quito, Ecuador. I majored in biotechnology and minored in chemistry at Universidad San Francisco de Quito, Ecuador on 2005. After a post baccalaureate research internship on molecular epidemiology at the Institute of Microbiology of Universidad San Francisco de Quito, I obtained a scholarship of the Netherlands fellowship program to perform Masters studies on Biomolecular Sciences at Vrije Universiteit Amsterdam. During my Masters studies, I obtained experience on biogenesis of membrane proteins of *Neisseria meningitidis* at Utrecht University under the supervision Martine Bos, and on *Escherichia coli* cell cycle at the University of Amsterdam under the supervision of Bart van den Berg van Saparoea. I graduated with a Masters degree in 2009, and returned to my home country to teach biomolecular sciences at Universidad Internacional del Ecuador, Escuela Politécnica de Ejercito and Universidad de las Américas. After obtaining a scholarship of my home country, I started my PhD on 2016 as an external student at Vrije Universiteit Amsterdam to study the cell cycle in alpha-proteobacteria. On August 2016, I joined Prof. Lucy Shapiro lab at Stanford University to study *Caulobacter crescentus* cell cycle and, August 2017, I joined Prof. Patricia Zambryski lab at UC Berkeley to study *Agrobacterium tumefaciens* cell cycle. On August 2021, I returned to Amsterdam and joined the group of Dirk Bald at Vrije Universiteit Amsterdam to study membrane protein biochemistry.

Publication list

J. R. Zupan, R. Grangeon, **J. S. Robalino-Espinosa**, N. Garnica, P. Zambryski, GROWTH POLE RING protein forms a 200-nm-diameter ring structure essential for polar growth and rod shape in *Agrobacterium tumefaciens*. *PNAS*. **116**, 10962–10967 (2019).

J. S. Robalino-Espinosa, J. R. Zupan, A. Chavez-Arroyo, P. Zambryski, Segregation of four *Agrobacterium tumefaciens* replicons during polar growth: PopZ and PodJ control segregation of essential replicons. *PNAS* **117**, 26366–26373 (2020).

Robalino Espinosa JS, J. S. (2010). Divisome dynamics and interactions of the murein precursor lipid I synthetase MraY in *E. coli*. [poster presentation]. EURO-INTAFAR. Poitiers, France.